Aus dem Adolf-Butenandt-Institut
Lehrstuhl für Stoffwechselbiochemie
im Biomedizinischen Centrum (BMC)
der Ludwig-Maximilians-Universität München
Vorstand: Prof. Dr. rer. nat. Dr. h. c. Christian Haass

An *in vitro* and *in vivo* study on the function of Signal Peptide Peptidase-Like 2c and 3

Dissertation
zum Erwerb des Doktorgrades der Naturwissenschaften
an der Medizinischen Fakultät der Ludwig-Maximilians-Universität zu München

vorgelegt von
Alkmini Papadopoulou
aus Thessaloniki, Greece

2019

Mit Genehmigung der Medizinischen Fakultät der Universität München

Betreuerin: Prof. Dr. rer. nat. Regina Fluhrer
Zweitgutachterin: Prof. Martha Merrow, PhD
Dekan: Prof. Dr. med. dent. Reinhard Hickel
Prüfungsdatum: 27.09.2019

Eidesstattliche Versicherung/Affidavit

Ich erkläre hiermit an Eides statt, dass ich die vorliegende Dissertation mit dem Thema "An *in vitro* and *in vivo* study on the function of Signal Peptide Peptidase-Like 2c and 3" selbständig verfasst, mich außer der angegebenen keiner weiteren Hilfsmittel bedient und alle Erkenntnisse, die aus dem Schrifttum ganz oder annähernd übernommen sind, als solche kenntlich gemacht und nach ihrer Herkunft unter Bezeichnung der Fundstelle einzeln nachgewiesen habe. Ich erkläre des Weiteren, dass die hier vorgelegte Dissertation nicht in gleicher oder in ähnlicher Form bei einer anderen Stelle zur Erlangung eines akademischen Grades eingereicht wurde.

I hereby confirm that the submitted dissertation entitled "An *in vitro* and *in vivo* study on the function of Signal Peptide Peptidase-Like 2c and 3" is the result of my own work and that I have only used sources or materials listed and specified in the dissertation. Where the work of others has been quoted or reproduced, the source is always given. I further declare that the submitted dissertation or parts thereof have not been presented as part of an examination degree to any other university.

München, den 15. April 2019

Unterschrift Alkmini Papadopoulou

"Believe you can and you're halfway there."
Theodore Roosevelt

Publications of the thesis

Papadopoulou, A. A., Muller, S. A., Mentrup, T., Shmueli, M. D., Niemeyer, J., Haug-Kroper, M., von Blume, J., Mayerhofer, A., Feederle, R., Schroder, B., Lichtenthaler, S. F. and Fluhrer, R. (2019). "Signal Peptide Peptidase-Like 2c (SPPL2c) impairs vesicular transport and cleavage of SNARE proteins." EMBO Rep 20(3).

Niemeyer, J., Mentrup, T., Heidasch, R., Muller, S. A., Biswas, U., Meyer, R., **Papadopoulou, A. A.**, Dederer, V., Haug-Kroper, M., Adamski, V., Lullmann-Rauch, R., Bergmann, M., Mayerhofer, A., Saftig, P., Wennemuth, G., Jessberger, R., Fluhrer, R., Lichtenthaler, S. F., Lemberg, M. K. and Schroder, B. (2019). "The intramembrane protease SPPL2c promotes male germ cell development by cleaving phospholamban." EMBO Rep 20(3).

Contents

List of Figures

List of Tables

Summary

Perfect synthesis and function of proteins is needed for optimal survival of an organism. Specific protein functions are dictated not only by the amino acid sequence of a protein but also from other factors, including post-translational modifications such as glycosylation, and the localisation of a protein. The hydrolysation of a protein's peptide bonds is termed proteolysis and is performed by proteases. The purpose of proteolysis can vary from activation to degradation of a protein. Although in most cases proteolysis occurs in a hydrophilic environment, a specific subtype of proteases called intramembrane proteases, is capable of hydrolysing peptide bonds in the hydrophobic environment of a cellular membrane. This ability makes these proteases, that are polytopic membrane proteins, both very interesting and quite hard to study.

Signal-Peptide-Peptidase (SPP) and Signal-Peptide-Peptidase-Like proteins (SPPLs) are a family of intramembrane proteases that compirse a conserved active site located in a GxGD motif. Hence, SPP and SPPLs are members of the GxGD family of intramembrane proteases together with the presenilins, which are well studied due to their crucial role in the pathology of Alzheimer's disease. Five members compose the SPP/SPPL family in mammals, SPP, SPPL2a, SPPL2b, SPPL2c, and SPPL3, with generally a few less members being present in different organisms. From the five members, SPPL3 and especially SPPL2c were the least understood until recently.

For SPPL3, it was shown previously that it has the ability to process full-length glycosidases and glycosyltransferases *in vitro* and *in vivo*, leading to a reduction of glycosylation of cellular glycoproteins. In the first part of this study, the amino acid sequence of two SPPL3 substrates, N-acetylglucosaminyltransferase V (GnTV) and exostosin-like glycosyltransferase 3 (EXTL3), is analysed by introducing mutations to identify amino acids crucial for recognition and cleavage by SPPL3. Within the transmembrane (TM) domain (TMD) of GnTV, the presence of two glycines in a GxxxG motif appears to play a role for cleavage, and further destabilisation of the TM α-helix by introducing a proline at either glycine site increases processing by SPPL3, however not all results for this motif are consistent. Mutating the amino acids surrounding the previously identified cleavage site of GnTV and a similar location on the EXTL3 sequence causes a shift to a SPPL3-independent cleavage for both substrates. The protease responsible for the cleavage of the mutants remains elusive.

The second part of the study focuses on the *in vivo* function of SPPL3 initially through the analysis of a SPPL3 deficient mouse line. SPPL3 knockout is only supported in a mixed background mouse line. Apart from some deficits in the mating of knockout mice and a reduced motor activity present in old knockout mice ($>$12 months), the main phenotype observed is a severe reduction in the adipose tissue of the SPPL3 deficient mice. To analyse

this phenotype further, SPPL3 knockout mouse embryonic stem cells (SPPL3 KO ESCs) were generated with the CRISPR/Cas9 system and were then differentiated to adipocytes *in vitro*. The results from the ESCs follow the same tendencies as observed in the mice with a very low number of adipose cells at the end of the differentiation period for the SPPL3 KO ESCs compared to control cells, suggesting involvement of SPPL3 in the formation and/or function of mature adipocytes.

The last part of this study focuses on the purpose of the least understood member of the family, SPPL2c. Since its discovery, SPPL2c was considered a pseudoprotease due to the lack of substrates *in vitro*, while protein levels could not be detected *in vivo*. After successfully demonstrating that SPPL2c is indeed expressed *in vivo* in the testis of humans and mice, this study effectively identifies and validates physiological substrates of SPPL2c (Niemeyer et al. 2019, Papadopoulou et al. 2019). It also demonstrates that SPPL2c can affect vesicular trafficking and holds a physiological role in the maturation of spermatozoa.

Taken together, this study focuses on two members of the SPP/SPPL family, SPPL3 and SPPL2c, and analyses them both *in vivo* and *in vitro* revealing new characteristics and physiological implications of the proteases. The knowledge this work provides is important not only in the context of these two proteins, but also for the general understanding of the mechanism and purpose of intramembrane proteolysis.

Zusammenfassung

Die optimale Funktion von Proteinen ist für das bestmögliche Überleben eines Organismus entscheidend. Spezifische Funktionen werden nicht nur durch die Aminosäuresequenz eines Proteins definiert, sondern auch durch verschiedene andere Faktoren wie Glykosylierung und subzelluläre Lokalisierung des Proteins. Außerdem regulieren proteolytische Spaltungen diverse physiologische Prozesse und steuern beispielsweise durch Aktivierung und Abbau die Funktionen von Proteinen.

Proteolyse bezeichnet die Hydrolyse der Peptidbindungen eines Proteins. Enzyme, die diese Reaktion katalysieren, werden als Proteasen bezeichnet. Obwohl Proteolyse bevorzugt in hydrophilen Umgebungen stattfindet, kann ein spezifischer Subtyp von Proteasen, die Intramembranproteasen, Peptidbindungen innerhalb einer Zellmembran hydrolysieren. Das macht diese polytopischen Intramembranproteasen sehr interessant, aber auch schwer zu untersuchen.

Die Signal-Peptid-Peptidase (SPP) und Signal-Peptid-Peptidase-like Proteine (SPPLs) bilden eine Intramembranprotease-Familie. Das aktive Zentrum, das durch ein GxGD-Motiv charakterisiert ist, ist innerhalb dieser und der Presenilin-Familie hoch konserviert. Die Presinilin-Familie ist aufgrund ihrer entscheidenden Rolle in der Pathologie der Alzheimer-Krankheit gut untersucht und bildet zusammen mit den SPP/SPPL-Proteasen die Klasse der GxGD-Intramembran-Aspartyl-Proteasen. Die SPP/SPPL-Familie umfasst in Säugetieren die fünf Mitglieder SPP, SPPL2a, SPPL2b, SPPL2c und SPPL3. SPPL3 und vor allem SPPL2c sind die bis dato am wenigsten untersuchten Mitglieder dieser Protease-Familie. Für SPPL3 konnte gezeigt werden, dass es die Fähigkeit besitzt, Glykosidasen und Glykosyltransferasen *in vitro* und *in vivo* zu hydrolysieren, was zu einer reduzierten Protein-Glykosylierung führt. Im ersten Teil dieser Studie wird versucht durch gezielte Mutation der Aminosäuresequenz von zwei bekannten SPPL3-Substraten, N-Acetylglukosaminyltransferase V (GnTV) und Exostosin-like-Glycosyltransferase 3 (EXTL3), das für die Prozessierung durch SPPL3 entscheidenden Erkennungsmotiv zu identifizieren. Die beiden Glyzine innerhalb eines GxxxG-Motiv in der Transmembrandomäne (TMD) von GnTV scheinen eine wichtige Rolle für seine Spaltung zu spielen. Insbesondere eine Destabilisierung der α-Helix in der TMD durch den Austausch eines Glyzins gegen ein Prolin beschleunigt die Prozessierung von GnTV durch SPPL3. Umgekehrt führt in einigen Fällen aber auch die Stabilisierung der Helix in diesem Bereich zu einer beschleunigten Prozessierung von GnTV, sodass sich derzeit kein schlüssiges Gesamtbild ergibt. Mutationen im Bereich der zuvor identifizierten SPPL3-Spaltstelle von GnTV, sowie an einer vergleichbaren Stelle in der EXTL3-Sequenz, führen zu einer SPPL3-unabhängigen Spaltung beider Substrate. Die Protease, die für die Spaltung dieser Mutanten verantwortlich ist, konnte bisher nicht

identifiziert werden.

Der zweite Teil dieser Studie konzentriert sich auf die Analyse einer Sppl3-defizienten Mauslinie zur Aufklärung der *in vivo*-Funktion von SPPL3. Überlebensfähige Tiere mit einem SPPL3-Knockout konnten ausschließlich in einer Mauslinie mit gemischtem genetischen Hintergrund generiert werden. Diese SPPL3-defizienten Tiere zeigen neben einer reduzierten Geburtenrate und verringerter motorischer Aktivität, die insbesondere in älteren Tieren ($>$ 12 Monate) beobachtet wird eine starke Reduktion des Fettgewebes. Zur weiteren Analyse dieses Phänotyps wurden SPPL3-defiziente embryonale Maus-Stammzellen (ESC) mit Hilfe des CRISPR/Cas9-Systems generiert und anschließend zu Adipozyten differenziert. Am Ende der Differenzierungsperiode wird im Vergleich zu Kontrollzellen eine verringerte Anzahl von Adipozyten in SPPL3-Knockout ESC beobachtet. Diese Beobachtung legt nahe, dass SPPL3 an der Bildung und Funktion gereifter Adipozyten beteiligt ist.

Der letzte Teil dieser Studie konzentriert sich auf die Funktion des am wenigsten untersuchten Familienmitglieds SPPL2c. Seit seiner Entdeckung wurde aufgrund des fehlenden Nachweises von Substraten und Proteinexpression angenommen, dass SPPL2c eine Pseudoprotease ist. Nach dem erfolgreichen Nachweis, dass das SPPL2c Protein tatsächlich *in vivo* in menschlichen und murinen Hoden exprimiert wird, werden in dieser Studie physiologische Substrate von SPPL2c identifiziert und validiert. Es wird außerdem nachgewiesen, dass SPPL2c den vesikulären Transport beeinflussen kann und unter physiologischen Bedingungen an der Reifung von Spermatozoen beteiligt ist (Niemeyer et al. 2019, Papadopoulou et al. 2019).

Zusammengefasst konzentriert sich diese Studie auf zwei Mitglieder der SPP/SPPL-Familie, SPPL3 und SPPL2c, und analysiert diese sowohl *in vivo* als auch *in vitro*. Dabei werden neue Eigenschaften und physiologische Funktionen der Proteasen beschrieben. Das neu gewonnene Wissen ist nicht nur im Zusammenhang mit diesen beiden Proteinen wichtig, sondern auch für das allgemeine Verständnis des Mechanismus und der Funktion der Intramembranproteolyse.

1. Introduction

Life comes in a multicompartmental, highly organised form, where every single aspect of each process needs to be finely tuned and function "on-spot" in order to achieve what we refer to as "healthy/physiological" conditions. Proteins are the main building blocks of organisms, where the majority of these processes depends upon. It is now very well documented that small changes in a protein's expression pattern or function have detrimental results in the overall prosperity of an organism. Cystic fibrosis, breast cancer and Alzheimer's disease (AD) are just a few examples of severe pathologies that can be caused by altered expression or function of a single protein (Cruts et al. 1996, King et al. 2003, Tang and Gershon 2003, Lim et al. 2017). There are about 19.000 protein-coding genes in humans (Ezkurdia et al. 2014) and 24.000 in mice (MGI statistics). Despite the importance of proteins in the successful operation of an organism, so far only a small fraction of these proteins has been studied in detail.

The goal of the current thesis is to shed more light into the role and function of two proteins, signal peptide peptidase-like 3 (SPPL3) and signal peptide peptidase-like 2c (SPPL2c), both members of the same family of intramembrane proteases. For SPPL3, it has been shown that through intramembrane proteolysis, it can regulate sensitive cellular functions, such as protein glycosylation (Voss et al. 2014a, Kuhn et al. 2015). However, its cleavage mechanism and the *in vivo* relevance of its function remain to be discovered. Regarding SPPL2c, there is a vast lack of knowledge as it was considered a pseudogene for the past 10 years (Golde et al. 2009).

1.1 Protein glycosylation

The function of proteins is not controlled just by their amino acid sequence and structure. Post-translational modifications, proteolytic processing and the localisation of a protein within the cell/organism all play important roles in the final functionality of a protein. A large number of cellular proteins are glycosylated; these are predominantly transmembrane and secreted proteins, but also cytosolic proteins can be glycosylated (Moremen et al. 2012). The addition of carbohydrate moieties to a protein, i.e. glycosylation, is found in all kingdoms of

life and the complexity of the glycans seems proportionate to the complexity of the organism. Environmental conditions and development are known to affect and alter the glycosylation pattern of cells and organisms (Moremen et al. 2012).

Glycans are attached to proteins for a number of purposes, from contributing to and controlling protein folding and function, to cell-cell recognition and communication. There are more than 700 proteins involved in the formation and attachment of more than 7000 different glycan structures (Moremen et al. 2012). The importance of a precise regulation of this procedure can easily be observed *in vivo*, since a number of animal models are available with defective glycosylation that present with very severe phenotypes (reviewed in (Hennet 2012)). Additionally, altered glycosylation has been linked to a number of severe pathologies (Varki and Freeze 2009), such as cancer (reviewed in (Stowell et al. 2015, Cheng and Oon 2018)) and AD (reviewed in (Schedin-Weiss et al. 2014)).

The two major forms of glycosylation are named according to the linkage formed between the protein and the glycans. Attachment of glycans to the side chains of luminal asparagine residues in an N-glycosidic amide linkage is termed N-glycosylation. O-glycosylation characterises the O-glycosidic linkage of glycans to serine or threonine residues (Moremen et al. 2012).

1.1.1 Glycan-modifying enzymes

All procedures regarding the attachment and rearranging of glycans are initiated within the endoplasmic reticulum (ER) and then advanced in the *medial*- and *trans*-Golgi network (TGN) by approximately 200 different enzymes. Their purpose is to extend existing glycan structures, which they recognise as their substrates, by adding sugars from nucleotide- or lipid-linked activated donors. Specific glycosidases and glycosyltransferases are responsible for every alteration and they compete amongst them for their substrates. This competition for overlapping substrates together with the number of enzymes and activated sugar donors available is responsible for the characteristic final glycan pattern of a cell (Moremen et al.

2012). Most of these enzymes are type-II TM proteins with a long C-terminal ectodomain harbouring their catalytic site and a rather short N-terminal cytoplasmic domain (Varki et al. 2009).

It has been known since many years that the catalytic site-containing ectodomain of glycosidases and glycosyltransferases is secreted (Lammers and Jamieson 1989, Paulson and Colley 1989). This secretion negatively regulates the function of these enzymes since despite retaining their active catalytic site in the cleaved form, they can no longer glycosylate proteins, most likely due to the lack of substrates and sugar donors outside the Golgi stacks (Paulson and Colley 1989, Varki et al. 2009). Consequently, regulation of the cleavage of these enzymes can play a key role in controlling their function thus, quickly and effectively altering the glycan patterns of a cell. Since 2014, we know that one of the main proteases involved in the secretion of the glycosylating enzymes is SPPL3 (Voss et al. 2014a, Kuhn et al. 2015). What still remains to be discovered is under what conditions this process is activated/deactivated and what is the exact mechanism of substrate recognition for this cleavage by SPPL3.

1.1.1.1 N-acetylglucosaminyltransferases

N-acetylglucosaminyltransferase V (GnTV) is encoded by the gene *MGAT5* and is the best-studied substrate of SPPL3. As suggested by its name, GnTV belongs to the family of N-acetylglucosaminyltransferases (GnTs) that are responsible for N-acetylglucosamine (GlcNAc) branching during the formation of complex N-glycans, and are located in the Golgi (Schachter 2000).

The initial 14-sugar long ($Glc_3Man_9GlcNAc_2$) N-glycan is synthesized on a lipid anchor in the ER and is then transferred and linked to an asparagine through a GlcNAc. The receiving asparagine needs to be within an Asn-x-Ser/Thr acceptor sequence, where the x amino acid cannot be a proline. This sugar already contains the $Man_3GlcNAc_2$ core that is common in all three types of N-glycans: high mannose, complex and hybrid glycans (Moremen et al. 2012). For non-ER

resident glycoproteins, this initial high-mannose glycan is trimmed both before leaving the ER and after arriving to the Golgi, before it can be further processed in the Golgi (Bieberich 2014). GnTs are responsible for attaching GlcNAc in β-linkage to the different mannose positions on trimmed N-glycans present in the Golgi. GnTI generates $GlcNAcMan_5GlcNAc_2$ that can give rise to hybrid N-glycans by having more GlcNAc attached to it by GnTIII and GnTIV. Alternatively, the trimmed N-glycan has two additional mannose molecules removed by Golgi α-mannosidase II (α-Man II) resulting to $GlcNAcMan_3GlcNAc_2$, which can then be further processed by GnTII, GnTIV and GnTV, giving rise to complex N-glycans (Schachter 2000) (Fig. 1.1). From this point on, hybrid and complex N-glycans can join the rest of O-glycans and glycolipids to undergo additional modifications within the Golgi including fucosylation and sialyation of their terminal GlcNAc residues (Stanley and Cummings 2009, Stanley et al. 2009).

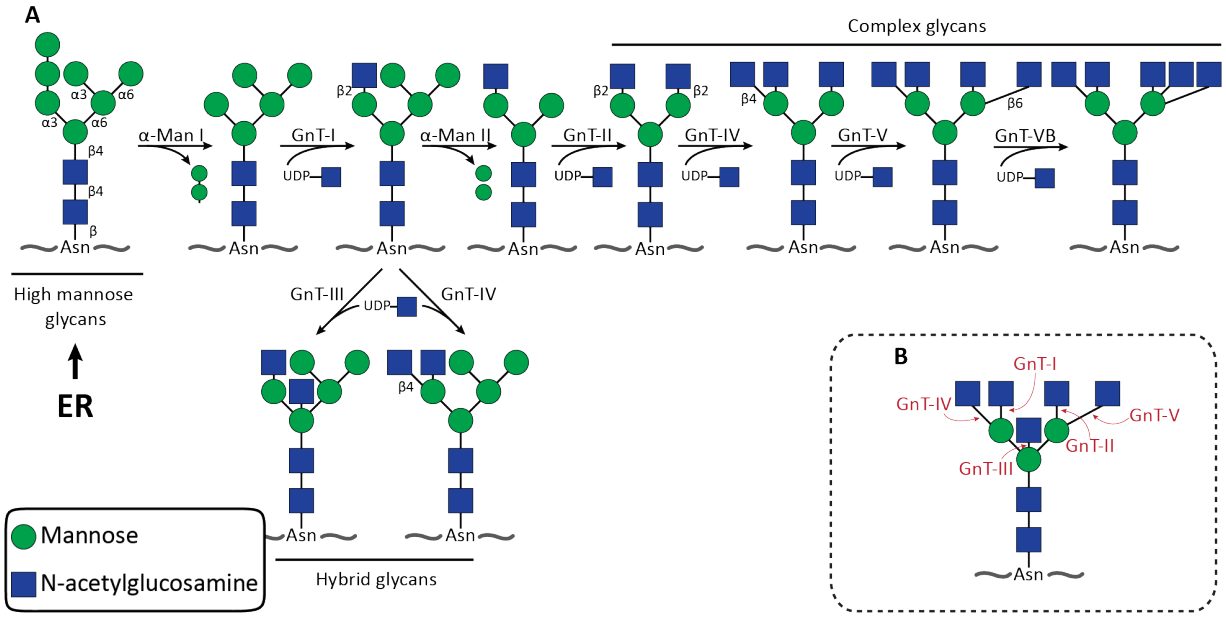

Fig. 1.1: N-glycosylation A. GlcNAc branching. Already trimmed high mannose glycans arrive to the Golgi from the ER, where they are further trimmed by α-mannosidase I and II (α-Man I, α-Man II). N-acetylglucosaminyltransferases I-VB (GnT-I – GnT-VB) can act in a relatively sequential manner adding GlcNAc to different mannose positions forming hybrid and complex N-glycans. **B.** Depiction of a complex N-glycan indicating which GnT is responsible for the respective connection.

The function of GnTV *in vivo* has so far been connected to both physiological and pathological processes. Results obtained from *Mgat5* deficient mice indicate that this glucosyltransferase is involved with tissue and skin renewal, fat storage and response to nutrient conditions (Cheung

et al. 2007, Miyoshi et al. 2012). Pathologically, increased GnTV expression is detected in early stages of most cancers and is connected to cancer growth and metastasis through enhanced signaling of growth factors (Miyoshi et al. 2012, Drake et al. 2015). GnTV expression negatively correlates with patient survival in specific types of cancer such as renal cancer (Liu et al. 2015), while positively correlates in other types such as thyroid and liver cancer (Miyoshi et al. 2012). Recent studies are trying to target GnTV in an effort to treat cancer (Nagae et al. 2018).

1.1.2 Proteoglycans

Proteoglycans are formed from one core protein that has covalently attached one or more molecules of glycosaminoglycan chains. Disaccharide molecules that consist of one amino sugar and one uronic acid or galactose molecule are the building blocks of the linear polysaccharides called glycosaminoglycans (GAGs). Some of these approximately 80 sugar long residues are chondroitin sulfate, keratan sulfate, heparan sulfate and others. Despite the limited amount of core proteins detected in nature, proteoglycans are ubiquitously expressed and can be found in the plasma membrane, the extracellular matrix and secretory granules. The variation of proteoglycans is very high due to the different chains available that can be used in different combinations, numbers and positions and that can also be differentially sulfated (Varki 2008). As with glycosylation, numerous enzymes are involved to ensure the correct synthesis of GAGs. The synthesis of chondroitin and heparan sulfate starts with a common path when a xylosyltransferase (XYLT1 or XYLT2) links xylose to a serine residue of the core protein using UDP-xylose as a donor. The GAG chain is prolonged by addition of two galactose residues by a β4-galactosyltransferase (B4GALT1, B4GALT7, etc.) and a β3-galactosyltransferase (B3GALT6, etc.), followed by β3-glucuronosyltransferase (B3GAT3) adding a glucuronic acid. Heparan sulfates separate from the chondroitin when exostosin-like glycosyltransferase 3 (EXTL3) adds the first GlcNAc residue to the growing GAG chain of heparan sulfates (Varki 2008) (Fig. 1.2).

Interestingly, SPPL3 has been shown to cleave numerous of the enzymes involved in the

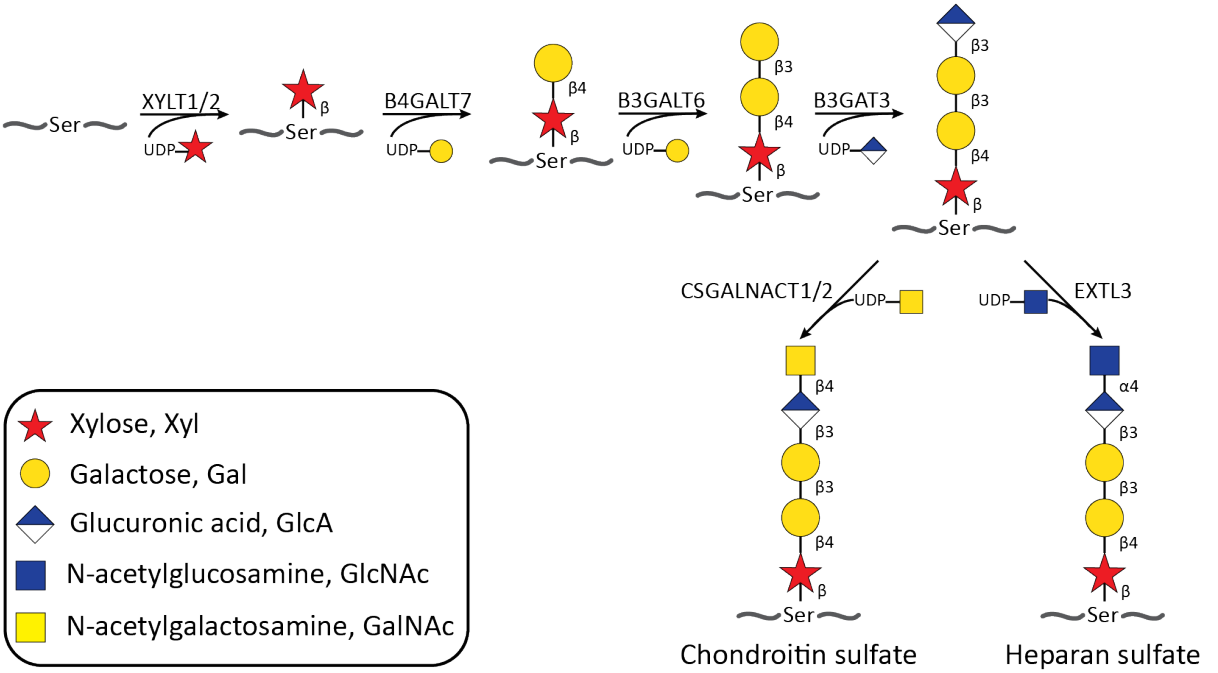

Fig. 1.2: Biosynthesis of chondroitin and heparan sulfate. First a xylose and subsequently two residues of galactose are covalently attached to the serine of a core protein that has a glycine attached to its carboxy side. After addition of the GlcA, the two sulfates are separated by the addition of the first hexosamine (GlcNAc for heparan or GalNAc for chondroitin) (Varki et al. 2017).

synthesis of heparan sulfate including XYLT2, B4GALT1, B4GALT5, B4GALT7, B3GALT6 and EXTL3 (Kuhn et al. 2015). This could be of high importance given the ubiquitous expression of heparan sulfate proteoglycans (HSPGs) in invertebrates and vertebrates. HSPGs are shown to have a strategical role in cell signaling and the interactions between a cell and its environment (Gallagher and Hampson 1984, Hook et al. 1984), thus affecting key functions of the organism, such as cell growth, development (Lin 2004).

1.1.3 Lectins

Initially discovered in plants at the end of the 19th century, lectins are now known to exist in all forms of life, from viruses and bacteria to animals. Lectins are carbohydrate-binding molecules that can specifically bind to sugars and simple or complex glycan structures of glycoproteins. The structures identified by the lectins include N-glycans and O-glycans amongst others. The recognition takes place through specific pockets present on lectins that recognise specific structures at the end of the glycan chains (Varki 2008).

The use of lectins in science started due to their ability to distinguish between the different blood types during the Second World War. Since then, the scientific use of lectins has progressed a lot and has become much more detailed and sensitive. Lectins can nowadays be used in multiple techniques, such as blotting, chromatography, histochemistry and even in lectin microarrays, requiring minimal amount of sample. They can be used not only to detect microorganisms, but also to analyse the precise glycosylation fingerprint of a selected sample (Hendrickson and Zherdev 2018). Such information can be used to identify which glycan structures are more or less present in certain conditions and thus, which glycosyltransferases are more or less active.

1.2 Vesicular trafficking

For posttranslational modifications, such as glycosylation, to take place but also to ensure proper function of all cellular processes, each protein needs to localise at the right place at the right time. This becomes more complicated when one takes into account that a common characteristic of all eukaryotic cells is the presence of membrane formed organelles that compartmentalise and make the cell a functioning unit. For a cell to produce and secrete a protein, a number of these organelles need to function sequentially forming the "secretory pathway". Proteins that are destined for this pathway enter first through the ER and then pass through the Golgi, before reaching the plasma membrane (PM) or other structures like the lysosomes. The high degree of membrane-derived compartmentalisation creates the need for a guided trafficking system. This will take the proteins through the necessary organelles to ensure that protein synthesis is followed by post-translational modifications, like glycosylation, before each protein can reach its final destination and fulfil its function, either within or outside the cell. The main mean of transport between these various organelles is termed vesicular trafficking and consists of small membrane vesicles that transport cargo proteins along the secretory pathway (Lee et al. 2004a, Gomez-Navarro and Miller 2016, Wang et al.

2017).

Small vesicles are formed from a donor membrane, then translocate towards the target organelle where they tether to the membrane before fusing with it (Lee et al. 2004a, Gomez-Navarro and Miller 2016, Wang et al. 2017). The first step of this process, vesicle formation, is performed by cytoplasmic coat proteins that localise to the donor membrane. Different coat proteins are found along the secretory pathway and their role also extends to selecting some of the vesicle cargo by identifying and interacting with the cytoplasmic domains of the cargo proteins, which carry specific signals (Lee et al. 2004a). The coat proteins at the first part of the secretory pathway include the COPI and COPII coatomer complexes that function in the retrograde and anterograde trafficking between the ER and Golgi, respectively (Fig. 1.3). Another abundant coat protein is clathrin, which localises further along the secretory pathway and mediates trafficking between TGN, endosomes, lysosomes and PM (Lee et al. 2004a). The trafficking between ER and Golgi has been studied for years and a number of mechanisms have been discovered to exist in order to ensure the trafficking of the correct proteins (reviewed in (Lee et al. 2004a)). In principle, only fully folded proteins can access COPII vesicles and leave the ER. At the same time COPI vesicles primarily ensure the return of ER-resident proteins from the Golgi (Lee et al. 2004a). The ER-Golgi intermediate compartment (ERGIC) is located between the ER and the Golgi and has evolved in metazoan as an intermediate quality control and cargo-sorting step in the secretory pathway (Fig. 1.3) (Hanna et al. 2018).

The transit of the vesicles is mediated by use of the cytoskeleton and proteins, such as dynactin and kinesin II, that facilitate the binding and movement of the vesicles along the microtubules (Deacon et al. 2003). The Rab family of GTPases plays a crucial role in vesicular transport by regulating the recruitment of different protein complexes required for each step of the process (Hutagalung and Novick 2011). When the vesicle approaches the correct membrane, it is tethered by long coiled-coil tethering proteins, such as myosin-shaped

molecule p115, and large multiprotein tethering complexes. Tethering proteins also facilitate the formation of soluble NSF (N-ethylmaleimide-sensitive factor) attachment protein receptor (SNARE) complexes that mediate the fusion of membranes (Appenzeller-Herzog and Hauri 2006).

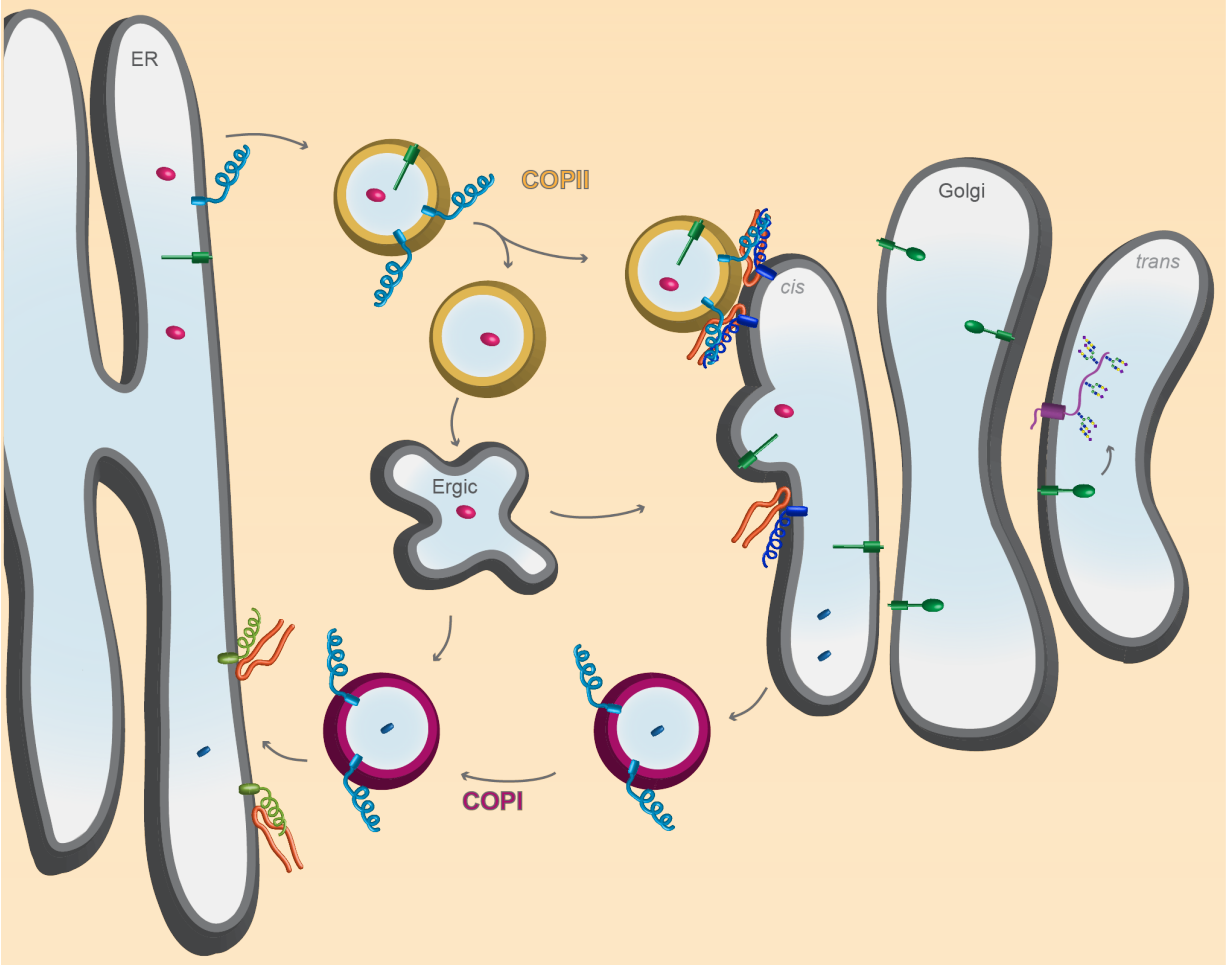

Fig. 1.3: Vesicular trafficking. COPII vesicles (yellow) transport correctly folded soluble (pink) and TM proteins (dark green) from the ER to the Golgi. TM proteins, such as glycosyltransferases (dark green), mature within the Golgi and are then ready to perform their function. Glycosyltransferases, for example, are responsible for the glycosylation of glycoproteins (purple) in the *trans*-Golgi. SNARE proteins, including syntaxins (dark blue & light green), VAMPs (light blue) and SNAP25 (orange) participate in the specific fusion of the vesicles and different combinations of SNAREs are found in different paths of the secretory pathway. COPI vesicles (aubergine) are responsible for the retrograde transport.

SNARE proteins were discovered and identified as mediators of membrane fusion already in 1988 (Trimble et al. 1988, Jahn and Scheller 2006). The great majority of SNARE proteins share the same tail-anchored type-II transmembrane orientation (type-IV) (Fig. 1.4) and all of them comprise at least one SNARE motif at their N-terminal domain. Proteins of the

SNAP25 family do not have a transmembrane domain and comprise two SNARE motives per protein. The SNARE motif faces the cytosol and consists of a conserved 60-70 amino acid-long strand that facilitates the formation of a coiled-coil (Teng et al. 2001, Bonifacino and Glick 2004, Wang et al. 2017).

The formation of tetrameric SNARE-motif complexes from proteins of the opposing membranes are required for membrane fusion. The four SNARE motives in most cases derive from three proteins, two of them having one SNARE motif and one protein with two SNARE motives. Typically, three of these SNARE motives belong to SNARE proteins localised on the target-membrane (t-SNAREs) and they form a coiled-coil formation with one vesicle-membrane SNARE (v-SNARE). This tetrameric SNARE complex is characterised as *trans* while the proteins are on opposing membranes and it becomes a *cis* complex following the membrane fusion (Bonifacino and Glick 2004). In order to recycle the SNAREs, the *cis* complex needs to dissociate with the help of NSF and the soluble NSF attachment protein (SNAP) and then the v-SNAREs are returned to the donor compartment (Fig. 1.3) (Jahn and Scheller 2006).

So far, there have been over 38 SNARE proteins identified in mammalian cells (Wang et al. 2017) and their categorization in v- and t-SNAREs does not always match their localisation on the membranes. Notably, each SNARE motif possesses either a conserved glutamine (Q) or a conserved arginine (R), which can be used for a more precise categorisation. The heterotetrameric SNARE complexes are composed by one R-SNARE, corresponding mostly to the v-SNARE, and three Q-SNAREs (Qa-, Qb- and Qc-SNAREs), which usually correspond to the t-SNAREs (Jahn and Scheller 2006). The three main components of a SNARE complex are the syntaxins, the vesicle associated membrane proteins (VAMPs) and the 25-kD synaptosomal-associated protein SNAP-25. As the name suggests, VAMPs are mainly on the vesicles and represent the R-SNAREs. Syntaxins and SNAP-25 are at the target membrane with syntaxins being the Qa-SNAREs. SNAP-25 represents the small number of SNAREs that

lack a TMD and comprise two SNARE motives, the Qb- and Qc- (Jahn and Scheller 2006). Different vesicles along the secretory pathway require diverse combinations of SNARE proteins for successful fusion to the target membrane. The combinations depend on the subcellular compartments from where the vesicle originates, on where it is targeted and on the cargo of the vesicles.

1.3 Shedding and Intramembrane Proteolysis

Proteolysis refers to the hydrolysis of peptide bonds leading to the breakdown of proteins. This process can have two purposes, one is to regulate the function of a protein as a post-translational modification and the other is to degrade a protein so it can be removed and/or recycled. The cellular enzymes that catalyse the peptide bonds are referred to as proteases. Although in the past it was thought that peptide bonds can only be degraded in hydrophilic conditions, and thus not within the transmembrane span of membrane proteins, the concept of intramembrane proteolysis is now well accepted (Steiner et al. 2008). The processing of membrane substrates can also serve different roles, from activation, maturation and secretion of proteins to simply their degradation and removal from the membrane. As proteolytic cleavage is an irreversible process, precision of cleavage and tight regulation of proteases are extremely important. In fact, deregulation of intramembrane proteolysis has been linked to severe and complex diseases such as rheumatoid arthritis, Alzheimer's disease (AD), Parkinson's disease and others (Langosch et al. 2015).

An organism harbours a variety of essential membrane proteins and the vast majority of them undergo shedding of their ectodomain by proteases named "sheddases". In some of those cases, the ectodomain is secreted from the cell following the cleavage, in which scenario the sheddase is actually a "secretase". Most commonly, shedded substrates are processed within the luminal juxtamembrane domain, close to the TMD, by "canonical sheddases". Prominent canonical-sheddases include β-site of APP cleaving enzyme 1 and 2 (BACE 1 and 2), a disintegrin and

metalloproteinase (ADAM) family and site-1 protease (S1P) (Lichtenthaler et al. 2018).

Numerous of the membrane proteins, either full-length or shedded, have been also identified as substrates of intramembrane cleaving proteases (I-CLIPs), since the recognition of this phenomenon in the 1990s. Certain I-CLIPs, such as the rhomboids and SPPL3, can directly cleave full-length substrates that span the membrane one or multiple times and comprise long ectodomains (Fig. 1.4). These I-CLIPs are named "non-canonical sheddases" because the cleavage occurs at the membrane border or within the TMD of the substrate. Other I-CLIPs, such as the presenilins, are only capable of cleaving substrates with extremely short ectodomain, and substrates with long ectodomain are only processed after removal of their ectodomain (Lichtenthaler et al. 2011, Voss et al. 2013). In this last scenario, I-CLIPs participate in a two-step process termed regulated intramembrane proteolysis (Lichtenthaler et al. 2018).

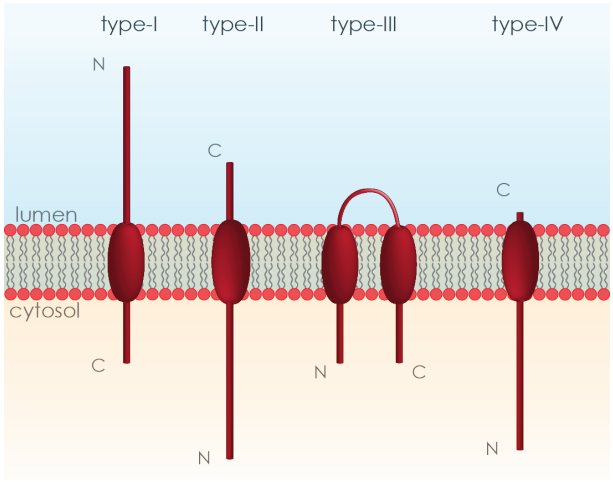

Fig. 1.4: Types of transmembrane proteins. Depending on the orientation of the N- and C-termini, single-pass TM proteins are either considered type-I or -II. Different I-CLIPs have different preferences, with γ-secretase for example cleaving only type-I substrates, while SPP/SPPLs type-II. Type-III TM proteins can be turned into both type-I & II via cleavage of the loop, while type IV have practically no ectodomain and are C-terminally tail-anchored.

1.3.1 Regulated intramembrane proteolysis

This specific type of intramembrane proteolysis was first identified and described in 2000 by Brown et al. It was named regulated intramembrane proteolysis (RIP) due to the double processing of the transmembrane substrate in two sequential proteolytic steps. Since its identification, RIP has been the subject of numerous studies and reviews. RIP is conserved throughout evolution from single- to multi-cellular organisms and is thought to play a dual role as initiator of signalling and in the degradation of membrane proteins. Under normal conditions, RIP has a crucial role in numerous physiological processes, such as the

development of the embryo and the functionality of the immune and the nervous systems. Moreover, deregulation of RIP can lead to pathological conditions, such as leukaemia and AD (Brown et al. 2000, Lichtenthaler et al. 2011).

Substrates of RIP are both single- and multi-pass TM proteins (Lichtenthaler et al. 2011). The first cleavage occurs within the luminal domain of the substrate and in close proximity to the TMD. It can either lead to a release of the soluble ectodomain, in case of a single span TM protein or to the breakage of a loop in a multi-span TM protein. This step is often referred to as "ectodomain shedding" due to the shortening of the luminal part of the protein via the removal of a large part of the substrate's ectodomain. The second cleavage occurs within the TMD of the substrate and results in the secretion of a small extracellular peptide and the release of the intracellular domain (ICD) in the cytosol (Fig. 1.5). The second cleavage tends to depend on the initial cleavage, making ectodomain shedding the rate-limiting factor in this process (Lichtenthaler et al. 2011).

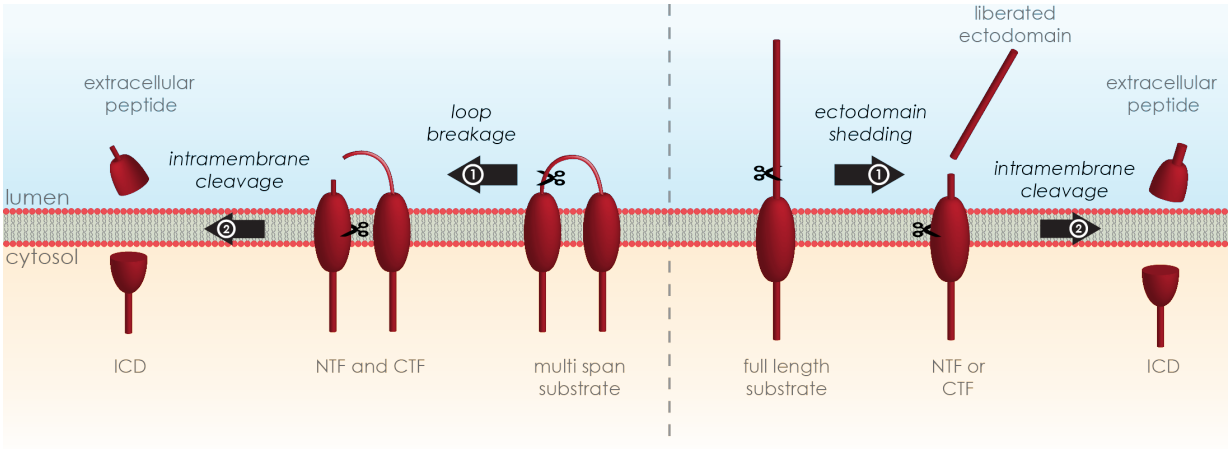

Fig. 1.5: Regulated Intramembrane Proteolysis. A multi-pass (left of the dotted line) or a single-pass (right of the dotted line) transmembrane protein can undergo RIP. In the first step (1), a "sheddase" either breaks the loop or releases the substrate's ectodomain. The N-terminal (NTF) or C-terminal (CTF) fragment that is left tethered to the membrane serves as the substrate for the second proteolytic step (2). During this step, an I-CLIP cleaves the substrate within the TMD releasing an extracellular peptide and an intracellular domain (ICD).

Different families of proteases perform the two distinct cleavages. In most cases, "canonical sheddases" are responsible for the removal of the ectodomain and depending on the orientation of the TM protein, they either leave behind a C-terminal fragment (CTF), for

type-I proteins, or an N-terminal fragment (NTF) for type-II proteins (Fig. 1.4). Some of these membrane-tethered and membrane-spanning canonical sheddases are characterized as metalloproteinases due to the requirement of a metal ion, Zn^{2+}, at their active site to ensure an active state (Edwards et al. 2008, Muller et al. 2016). For some substrates, the initial cleavage can also be performed by "non-canonical sheddases" (Lichtenthaler et al. 2018).
The CTF or NTF, that is left spanning the membrane after the shedding step, serves as the substrate for the second cleavage. This time the substrate is cleaved within the TMD by I-CLIPs. This cleavage is facilitated by the active site of the protease being most likely in a structural cavity with access to aquatic environment, thus allowing the entering of water and ions to create a microenvironment favourable to hydrolysis (Wolfe 2013).

1.3.2 Intramembrane-cleaving proteases

All I-CLIPs are multipass transmembrane proteins and their entire active site is located within their transmembrane segments. This characteristic allows them to cleave their substrates within or very close to the membrane domain. Intramembrane proteases are classified in four categories, depending on the respective mechanism of catalysis: metalloproteases, serine proteases, glutamyl proteases and aspartyl proteases (Wolfe 2009, Manolaridis et al. 2013). To the current state of knowledge, evidence suggests that all proteases belonging to these protease classes except γ-secretase, process their substrates without requiring cofactors (Langosch et al. 2015).

1.3.2.1 Metallo-intramembrane proteases

The class of metallo-intramembrane proteases is represented in mammals by the site-2-protease (S2P) (Fig. 1.6) that requires binding of a Zn^{2+} ion to its active site. Their purpose is to activate membrane-bound proteins by releasing the active fragment from its membrane anchor (Rawson et al. 1997, Feng et al. 2007). S2P can affect the cholesterol homeostasis via cleavage of sterol regulatory element-binding protein 2 (SREBP2), a well-studied transcription factor and long-known substrate of S2P (Hua et al. 1995, Kroos and Akiyama 2013). Other known

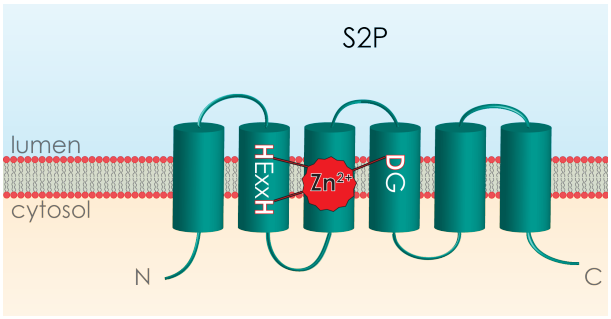

Fig. 1.6: Site-2-Protease. The protease consists of six TMDs. The Zn^{2+} ion responsible for the catalytic activity of this metalloprotease is coordinated from the histidine 54 and 58 in the **H**Exx**H** motif in TMD2 and the asparagine 148 in the **D**G motif in TMD4 (Sun et al. 2016).

S2P substrates include activating transcription factor 6 (ATF6) and old astrocyte specifically induced substance (OASIS). Both of these proteins are transcription factors that are released and activated by S2P as a response to ER-unfolded protein stress (Ye et al. 2000b, Murakami et al. 2006). One common characteristic of S2P substrates is that they require initial cleavage by S1P before they can be processed by S2P, although the exact reason remains speculative (Sun et al. 2016).

1.3.2.2 Serine intramembrane proteases

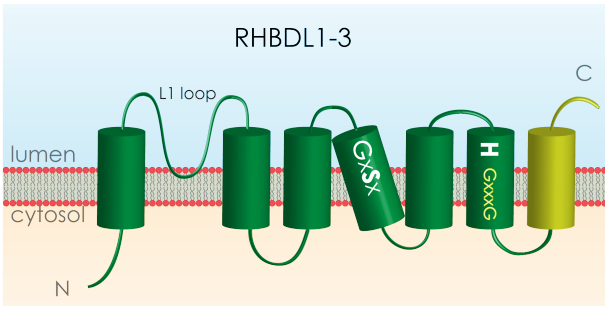

Fig. 1.7: RHBDL1-3 RHBDL4 consists of six core TMDs (green) and RHBDL1-3 have additionally a seventh TMD (lime). The active site consists of the serine (S) in TMD 4 and the histidine (H) in TMD 6.The L1 loop is conserved in all active rhomboid proteases and is thought to participate in substrate binding. The GxxxG motif in TMD 6 is conserved along the whole superfamily and is thought to help stabilise the protein (Ticha et al. 2018).

Initially discovered in *Drosophila melanogaster* due to its crucial role in the epidermal growth factor receptor signalling (EGFR) (Lee et al. 2001, Urban et al. 2001, Urban et al. 2002), the rhomboid family of serine proteases is almost ubiquitously found in all organisms (Koonin et al. 2003). Four rhomboid-like proteins are located in the mammalian secretory pathway, rhomboid "secretases" RHBDL1, 2, 3 and 4 (Lemberg and Freeman 2007) (Fig. 1.7), and one inside the mammalian mitochondria, PARL (Strisovsky 2016). A number of substrates have been identified for the mammalian rhomboids including thrombomodulin, EGF and EGFR. They have been linked to physiological functions, such as the unfolded protein response via the endoplasmic-reticulum-associated-protein-response (ERAD), but also to pathological conditions such as type-2 diabetes and Parkinson's disease (Urban 2006, Urban 2016).

Rhomboid proteases are very well understood biophysically (Urban 2016) and one peculiarity of this family of I-CLIPs lies on the fact that rhomboid proteases, in contrast to many other intramembrane proteases, can cleave full-length substrates and do not strictly depend on regulation by shedding. Therefore, rhomboids have been described to act as sheddases (Bergbold and Lemberg 2013, Urban 2016).

1.3.2.3 Glutamyl intramembrane proteases

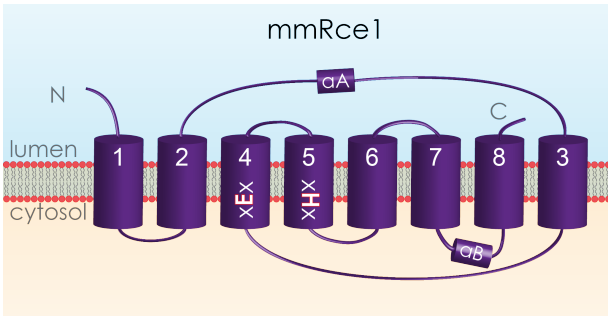

Fig. 1.8: Rce1 Glutamyl protease Rce1 consists of eight TM α-helices and two peripheral α-helices (αA and αB). Four of its TMDs (TMDs 1-3, 8) are on the outer side of the protein structure, while the other four (TMDs 4-7) are in the inner part of the structure. The conserved active site is formed by a catalytic dyad comprising a glutamine (E) in TMD4 and a histidine (H) in TMD5 (Manolaridis et al. 2013, Sun et al. 2016).

Glutamyl proteases are represented by the Ras converting enzyme (Rce1) (Fig. 1.8). Although the protein has been known since 1997 (Boyartchuk et al. 1997), it was not until 2013 that its function and structure were better understood (Manolaridis et al. 2013). Rce1 is found in both prokaryotic and eukaryotic organisms and is able to cleave CaaX-type prenyl proteins at their carboxy-side. The substrates of Rce1 hold key positions in a variety of pathological situations varying from cancer to infectious disease mortality, so efforts have been put lately to increase the understanding of Rce1 and to control its activity (Hampton et al. 2018).

1.3.2.4 Aspartyl intramembrane proteases

The importance of all I-CLIPs goes beyond doubt, however, aspartyl intramembrane proteases have known increasing popularity in research over the past two decades. In 1995, it was discovered that presenilins, founding members of this family, play a crucial role in the development of Alzheimer's disease (AD) pathology (Levy-Lahad et al. 1995a, Levy-Lahad et al. 1995b, Rogaev et al. 1995, Sherrington et al. 1995, Cruts et al. 1996), although their function remained elusive until 1998 (De Strooper et al. 1998).

The presenilin family comprises the active site of the γ-secretase complex (Steiner et al.

2000) and consists of two members in mammals, presenilin 1 (PS1) and presenilin 2 (PS2). Sequence database analyses, as well as biochemical methods, revealed the existence of five presenilin homologues that complete this class of proteases in mammals: signal peptide peptidase (SPP) and signal peptide peptidase-like 2a (SPPL2a), 2b (SPPL2b), 2c (SPPL2c) and 3 (SPPL3) (Grigorenko et al. 2002, Ponting et al. 2002, Weihofen et al. 2002). These five proteases form the SPP/SPPL family of aspartyl proteases.

As the name "aspartyl" indicates, these I-CLIPs comprise two aspartic acids (D) at their catalytic active site. All 7 members of this protease class consist of 9 TMDs and are also referred to as GxGD proteases because one of the aspartic acids of the active site is always located within a conserved GxG**D** motif in TMD 7. The second aspartate is located within a conserved Y**D** motif in TMD 6. Mutagenesis of either of the two aspartic acids is sufficient to inactivate these proteases (Steiner et al. 1999, Wolfe et al. 1999, Weihofen et al. 2002, Fluhrer et al. 2006, Friedmann et al. 2006, Kirkin et al. 2007, Voss et al. 2012, Voss et al. 2014a). Additionally, all aspartyl proteases feature a conserved PAL motif in TMD 9 (Fig. 1.9, 1.11-1.15) (Grigorenko et al. 2002, Ponting et al. 2002, Weihofen et al. 2002). Mutations of any of the three amino acids comprising the PAL motif (proline, alanine, and leucine) in presenilin and SPP affects their proteolytic ability suggesting this sequence is also critical for the function of the proteases (Tomita et al. 2001, Wang et al. 2004b, Wang et al. 2006, Voss et al. 2013).

However, presenilins and SPP/SPPLs can be considered as two separate subfamilies since despite their similarities they are also divided by some significant differences. The predicted membrane topology of the 9 TMDs is inverted between the two groups, with PSs having the N-termini in the cytosol and the C-termini in the lumen, while SPP/SPPLs have the N-termini in the lumen and the C-termini in the cytosol (Friedmann et al. 2004a, Nyborg et al. 2004). This means that their active sites are also inverted and can possibly account for the distinction in the substrates of these GxGD proteases. Presenilins cleave exclusively type-I

oriented TM proteins, releasing the N-terminus of the protein as soluble ectodomain in the lumen/extracellular space and a C-terminal ICD. SPP/SPPLs cleave only type-II TM proteins releasing a C-terminal peptide (C-peptide) in the lumen/extracellular space and an N-terminal ICD (Fig. 1.4, 1.5) (Voss et al. 2013, Mentrup et al. 2017a). Finally, while presenilins need the formation of the γ-secretase complex and favour endoproteolysis to be active, SPP/SPPLs have most likely no such requirements (Weihofen et al. 2002, Edbauer et al. 2003).

1.3.2.4.1 Presenilins

Either of the two mammalian presenilins, PS1 and PS2, together with three more proteins can form the γ-secretase heterotetrameric complex. Multi-pass membrane protein anterior pharynx defective-1 (APH-1), single-pass glycoprotein nicastrin and double-pass membrane protein presenilin enhancer-2 (PEN-2) were all found to associate with presenilins and are indispensable for a functioning γ-secretase complex (Haass 2004, Wolfe 2013) (Fig. 1.9).
Following the assembly of the complex, presenilin is autocatalytically endoproteolysed in the cytoplasmic loop between TMD 6 and 7. This leads to the formation of a NTF and a CTF, each of which contains one of the two aspartic acids forming the active site (Wolfe et al. 1999, Fukumori et al. 2010). The two subunits of presenilin are closely interacting with each other, forming a physically and catalytically stable complex as a heterodimer (Capell et al. 1998).
It took 10 years from their discovery (Levy-Lahad et al. 1995a, Levy-Lahad et al. 1995b, Rogaev et al. 1995, Sherrington et al. 1995, Cruts et al. 1996) to clarify the topology of PS1. We now consider this the "typical" 9-TMD topology of the GxGD proteases (Fig. 1.9) (Laudon et al. 2005, Oh and Turner 2005). It took another 10 years to achieve an atomic structure of human γ-secretase (Bai et al. 2015a, Bai et al. 2015b). The fact that all four subunits of γ-secretase are needed for an active protease, points to distinct and important roles for each subunit and these roles have been studied over the years (Kimberly et al. 2003, Takasugi et al. 2003). PS provides the active centre of the protease with the two aspartic

acids in TMD 6 and 7. Already in 1999, it was shown that mutating one of these aspartates to alanines almost completely inhibits the proteolytic activity of the gamma secretase complex (Steiner et al. 1999, Wolfe et al. 1999). PEN-2 is not only essential for the proteolytic activity of the protease, but also for the endoproteolytic cleavage of PS and the stabilisation of the deriving CTF and NTF (Capell et al. 1998, Prokop et al. 2004, Bai et al. 2015a). APH-1, comprises seven TMDs and is believed to act as a connecting subunit, keeping nicastrin, PS NTF and PS CTF together through the presence of a GxxxG motif (Lee et al. 2004b). Nicastrin, finally, has only one TMD but is equipped with a very large and heavily glycosylated ectodomain, which would enable it to act as the gatekeeper of the complex responsible for selective recognition of substrates with a short ectodomain (Shah et al. 2005) (Fig. 1.9).

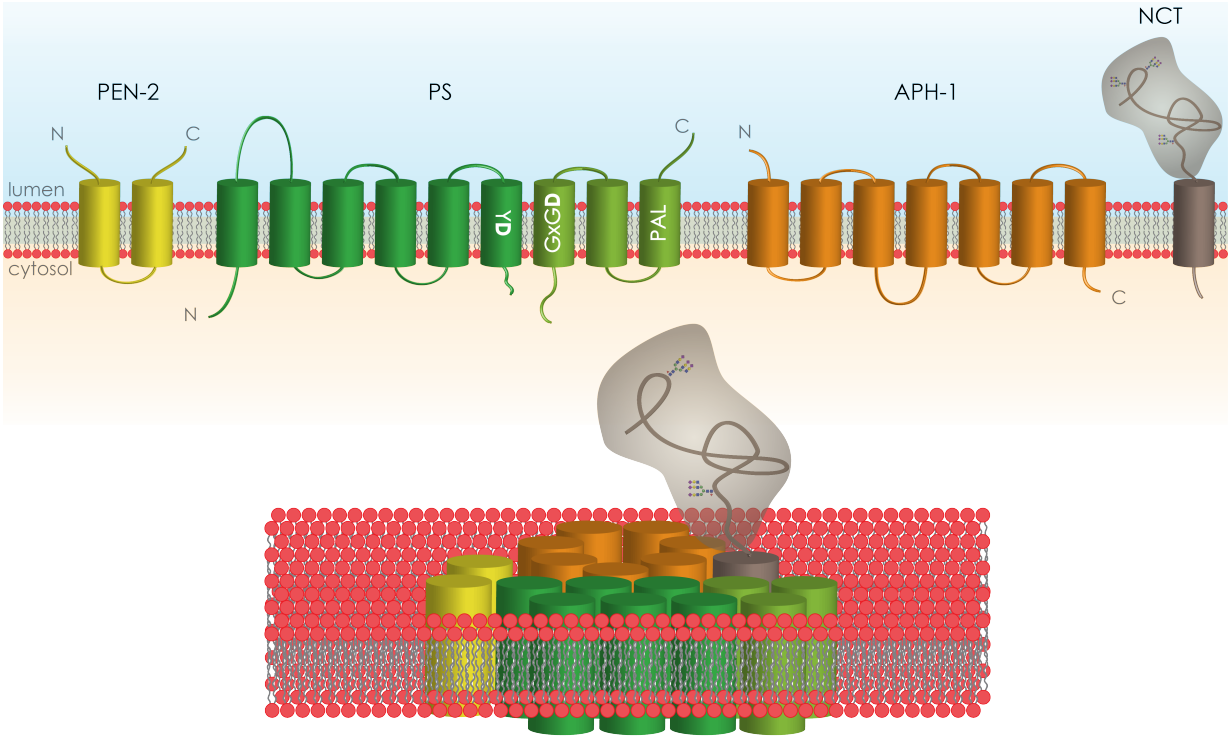

Fig. 1.9: γ-secretase complex. The complex consists of four proteins, PEN-2 (yellow), presenilin (green), APH-1 (orange) and nicastrin (brown, NCT). Presenilin is autocatalytically endoproteolysed giving rise to two pieces, the NTF (dark green) and the CTF (light green). The two catalytic aspartates (D) are located within the conserved motifs Y**D** and GxG**D** in TMD 6 and 7. The interactions between the different members of the complex suggest an arrangement on the membrane as depicted below. PEN-2 interacts with the PS NTF, while nicastrin interacts with Aph-1. The PS NTF can interact with the PS CTF, which also interacts with Nicastrin/Aph-1 (Fukumori et al. 2010, Wolfe 2013). Lipid bilayer is depicted in red and grey.

The discovery of presenilins came through studying cases of early-onset familial Alzheimer's

disease (FAD) and detecting mutations in the genes *PSEN1* and *PSEN2*, which code for PS1 and PS2, respectively (Levy-Lahad et al. 1995a, Levy-Lahad et al. 1995b, Rogaev et al. 1995, Sherrington et al. 1995, Cruts et al. 1996). AD is a severe neurodegenerative disease and its pathophysiology is characterized by a significant loss of both neurons and synapses in the affected brain. Hallmarks of the disease's pathogenesis are the deposition of amyloid-beta (Aβ) plaques in the brain, which are aggregates of Aβ peptides, and the appearance of neurofibrillary tangles of hyperphosphorylated tau (Huang and Mucke 2012). The generation of Aβ peptides through proteolytic processing of the amyloid precursor protein (APP) is considered the trigger that eventually leads to neuronal cell death through a cascade of events. Presenilins were discovered to hold a key role in the processing of APP (Selkoe 1991, Hardy and Higgins 1992, Hardy and Selkoe 2002, Haass 2004, Haass and Selkoe 2007, Lichtenthaler et al. 2011).

APP was one of the first three proteins ever identified to undergo RIP, already in 1999 (Brown et al. 2000), and although the physiological function of APP remains unknown, a lot of effort has been devoted in understanding its processing (Fig. 1.10). As a type-I TM protein, APP first undergoes shedding of the ectodomain generating soluble APP (sAPP) and a CTF. This CTF is then cleaved inside the membrane by γ-secretase (Hardy and Selkoe 2002, Haass 2004, Haass and Selkoe 2007).

Despite the recognition of some additional enzymes, the first cleavage of APP is mainly performed by two different sheddases, ADAM10 and BACE1 (Lichtenthaler et al. 2018). Each of the two sheddases prefers a distinct cleavage site and this can already partially determine the generation or not of toxic Aβ peptides (Lichtenthaler et al. 2011). When APP ectodomain is shedded by an "α-secretase" (Esch et al. 1990), mainly ADAM10 (Kuhn et al. 2010), this is considered as "non-amyloidogenic processing". It takes place closer to the membrane and gives rise to longer soluble APPα (sAPPα) and the shorter CTFα (83 amino acids). Processing of CTFα by γ-secretase does not release Aβ into the extracellular space

but p3 (Lichtenthaler et al. 2011). p3 is a significantly smaller peptide, less hydrophobic and less prone to aggregation compared to Aβ, so it practically lacks the disease-causing attributes of the Aβ (Dulin et al. 2008). On the other hand, shedding of APP by BACE1, a "β-secretase", releases the shorter sAPPβ in the extracellular space and leaves the longer CTFβ bound to the membrane. This 99-amino acid long CTF (C-99) is further processed by γ-secretase giving rise to Aβ, making this the "amyloidogenic" processing of APP (Selkoe 1991, Hardy and Higgins 1992, Haass and Selkoe 2007, Wolfe 2013). In both scenarios there is also the release of an APP-ICD (AICD) inside the cell, which gets rapidly degraded (Fig. 1.10) (Lichtenthaler et al. 2011). Despite the fact that AICD is suggested to have transcriptional functions similarly to the Notch ICD, no solid evidence exist so far to confirm this hypothesis (Schettini et al. 2010, Bukhari et al. 2017).

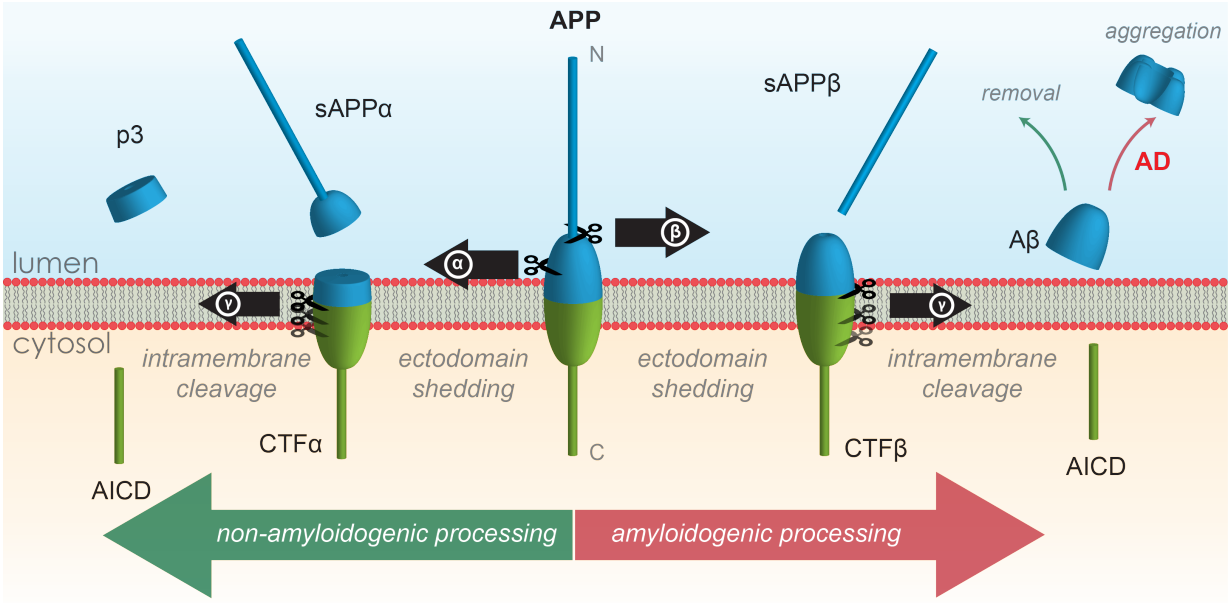

Fig. 1.10: Processing of APP. There are two possible processing pathways. Depicted on the left is the non-amyloidogenic processing that cannot lead to an amyloid pathology, on the right, the amyloidogenic processing that produces Aβ. In the cases of Alzheimer's disease (AD) Aβ aggregates and forms plaques. The first cleavage can be performed by either an "α-secretase" or a "β-secretase" and this determines the processing pathway. The second cleavage takes place intramembranously and is performed by γ-secretase.

A key point in the "amyloidogenic processing" is the sequential cleavage of C-99 by γ-secretase that can give rise to Aβ peptides of different lengths, mostly varying between 37 and 43 amino acids. While the shorter Aβ species are less prone to aggregation and less toxic

for the organism, the longer, more hydrophobic species (Aβ42, 43) tend to aggregate and are considered the most neurotoxic (Haass and Selkoe 2007, Holtzman et al. 2011, Lichtenthaler et al. 2011, Saito et al. 2011). Mutations causing FAD can be found predominantly in the *PSEN1* gene, but also in the *PSEN2* and *APP* genes (Levy-Lahad et al. 1995a, Levy-Lahad et al. 1995b, Rogaev et al. 1995, Sherrington et al. 1995, Cruts et al. 1996). The mutations in the proteases show an increased production of Aβ42 and Aβ43 without necessarily increasing the total amount of Aβ (Scheuner et al. 1996, Kretner et al. 2016). These findings demonstrate that differential processing of C-99 by γ-secretase can either prevent or cause the disease. This makes γ-secretase a very attractive pharmaceutical target for treatment and prevention of AD by modulation or inhibition of its function. Unfortunately though, none of the so-far tested treatments can specifically target the processing of APP by γ-secretase without affecting the processing of the other γ-secretase substrates.

To date, an increasing number of physiological γ-secretase substrates have emerged, such as N-cadherins, CD44, low density lipoprotein receptor, Nectin-1 and others (Hemming et al. 2008, Haapasalo and Kovacs 2011, Wolfe 2013, Muller et al. 2016). However, the most prominent of these γ-secretase substrates, responsible for the great majority of adverse effects observed upon γ-secretase-targeted treatment are the Notch receptors. The Notch signalling pathway is involved in cell-to-cell communication and plays a crucial role in cell-fate and differentiation both during development and in the adult organism (reviewed in (Bray 2016)). Notch was found to undergo RIP at the same time as APP (Brown et al. 2000) and further research has shown how important the fine-tuning of this process is. Lack of functional γ-secretase in mice can recapitulate the severe developmental effects observed in transgenic Notch-deficient mice (Wong et al. 1997, Li et al. 2003, Serneels et al. 2005, Bammens et al. 2011). Another example of Notch's importance is the case of Semagacestat, a γ-secretase inhibitor that aimed to reduce Aβ production and made it to phase-III clinical trials but had to be terminated due to effects of chronic Notch inhibition leading to increased incidents of skin

cancer (De Strooper 2014).

1.3.2.4.2 Signal Peptide Peptidase

SPP was initially discovered and named due to its ability to remove the signal peptides that remain embedded in the ER membrane after their separation from the protein they are guiding by Signal Peptidase (SP) (Weihofen et al. 2000). The removal of the signal peptides falls into the category of RIP as the substrates are first cleaved by SP and then the intramembrane cleavage occurs (Fig. 1.11A).

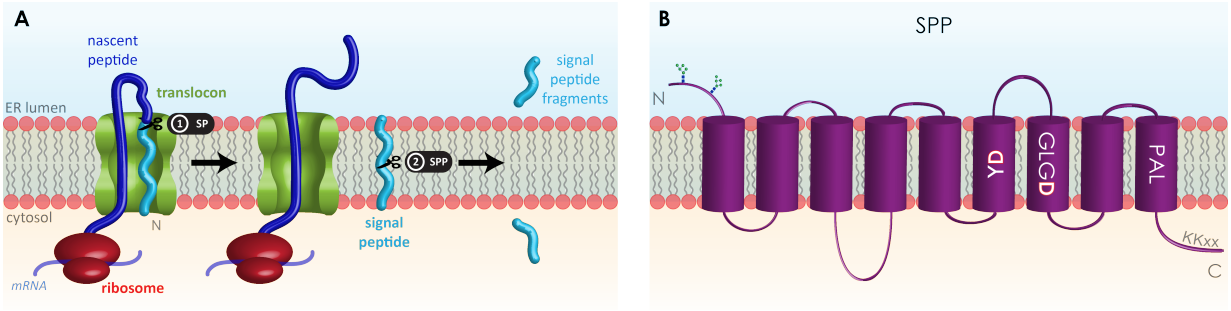

Fig. 1.11: SPP and SPP-mediated signal peptide cleavage. A. SP performs the first cleavage (1) removing the signal peptide (light blue) of nascent secretory proteins (dark blue) synthesised at the ER translocon. The liberated signal peptides are then endoproteolysed within their transmembrane domain by SPP (2). **B.** SPP shares the nine TMD topology characteristic of GxGD proteases, the two aspartic acids Y**D** and GLG**D** and the conserved PAL motif. It also has two presumed N-glycosylation sites at its N-terminus and an ER retention signal at the C-terminus.

In 2002, SPP was identified as a "presenilin-type aspartic protease" and since then it is known to belong to the family of the GxGD-aspartyl proteases (Weihofen et al. 2002). In concordance with the rest of the family members, SPP has nine TMDs and two aspartic acids at its active centre. Additionally, it is glycosylated and it has an ER-retention signal at its C-terminus (Weihofen et al. 2002) (Fig. 1.11B). Due to its expression pattern, it was assumed since early on that it holds a key role in the development of metazoan and especially their nervous system (Urny et al. 2003). Moving from drosophila to zebrafish to mice, the deficiency of SPP always causes a severe phenotype including neuronal cell death and embryonic/larval lethality (Casso et al. 2005, Krawitz et al. 2005, Voss et al. 2013, Aizawa et al. 2016, Mentrup et al. 2017a). A variety of signal peptides from a number of proteins fall within the preferences of SPP. Prolactin signal peptide cleavage was one of the first followed in detail (Martoglio et al. 1997)

and was later attributed to SPP (Weihofen et al. 2000, Weihofen et al. 2002). In some cases, the cleavage of these peptides aims solely in facilitating their removal from the ER membrane and proteosomal degradation (Kilic et al. 2010), while in other cases it serves the removal of potentially toxic peptides from the cell (Wu and Chang 2004). SPP can also be involved in immunosurveillance by generating peptides for the major histocompatibility complex (MHC) class I either in collaboration with signal peptidase from MHC class I-signal peptides (Lemberg et al. 2001) and from non-MHC-signal peptides (El Hage et al. 2008), or independently of signal peptidase, directly from multipass TM proteins (Oliveira et al. 2013).

Despite what the name signal peptide peptidase suggests, SPP is also capable of cleaving a variety of non-signal peptides. Through a proteomic approach, certain C-terminally tail anchored type-II oriented (type-IV) TM proteins (Fig. 1.4) were identified as SPP substrates. As these substrates have either an extremely short or practically no extracellular domain, the cleavage by SPP does not require initial shedding and these substrates do not undergo RIP but direct intramembrane cleavage. Among the substrates identified were cytochrome B5A (CYB5A), ribosome-associated membrane protein 4 (RAMP4) and heme-oxygenase-1 (HO-1) (Boname et al. 2014). SPP-dependent HO-1 cleavage proved of crucial importance for the nuclear translocation of HO-1, which in turn increases the tumorigenicity of HeLa cells via boosting their proliferatory and migratory abilities, proving that SPP can indeed have a regulatory role (Hsu et al. 2015, Mentrup et al. 2017a).

SPP was also found capable of cleaving the X-box binding protein 1 (XBP1u). What makes this discovery interesting is that in contrast to the cleavage of signal peptides, shedding of the 59 amino acid long ectodomain is not required in this case prior to the intramembrane cleavage. Although a 59 amino acid-long ectodomain might be considered short enough to allow direct intramembrane cleavage, as seen for γ-secretase (Struhl and Adachi 2000) and SPPL2b (Martin et al. 2009), there is also another possibility. The interaction of SPP with Derlin-1, a catalytically inactive homologue of the rhomboids, observed under certain conditions

could play a role in the recognition of XBP1u's ectodomain (Chen et al. 2014). This study by Chen et al, clearly indicates that SPP is involved in the ERAD, since cleavage of XBP1u by SPP initiates its ERAD and also releases its splice variant, XBP1s, from their heterodimer to induce the unfolded protein response (UPR) (Chen et al. 2014, Mentrup et al. 2017b). This procedure is not limited to metazoan as the SPP-yeast orthologue Ypf1 has also been linked to ERAD by a novel regulatory pathway (Avci et al. 2014).

1.3.2.4.3 Signal Peptide Peptidase-Like 2 subfamily

The SPPL2 subfamily is less conserved throughout evolution than SPP or SPPL3 (Voss et al. 2013). Drosophilas appear to completely lack SPPL2s, since they have only two members of the SPP/SPPL family that resemble mostly SPP (Casso et al. 2005) and SPPL3 (Casso et al. 2012). The SPPL2 subfamily consists of only one member in zebrafish (Krawitz et al. 2005), and just in mammals 3 different family members exist, SPPL2a, SPPL2b and SPPL2c (Grigorenko et al. 2002, Ponting et al. 2002, Weihofen et al. 2002, Voss et al. 2013). All three members possess an N-terminal signal sequence and a long glycosylated N-terminal extracellular domain, in addition to the nine TMDs (Friedmann et al. 2004a). The level of understanding of these proteases decreases from SPPL2a, where some *in vivo* functions are known, to SPPL2b, where the cleavage mechanism has been investigated *in vitro*, to lastly SPPL2c, which so far is not a proved active protease.

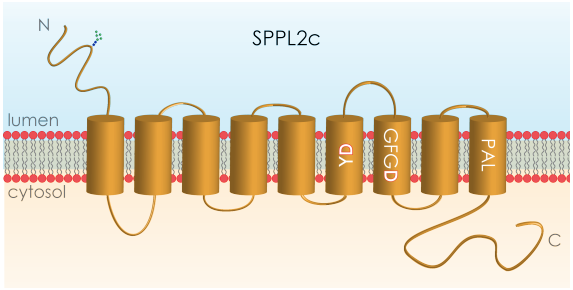

Fig. 1.12: Signal Peptide Peptidase-Like 2c. SPPL2c shares the same membrane topology and active site as the other SPP/SPPLs, the two aspartic acids Y**D** and GFG**D** and the conserved PAL motif. It also has one presumed N-glycosylation site at its N-terminus.

Although the *SPPL2C* gene can potentially give rise to a proteolytically active protease (Fig. 1.12) (Friedmann et al. 2004a), SPPL2c remains an orphan protease with no substrates assigned to it so far. *SPPL2C*'s polymorphism through evolution together with its intronless structure has made it a candidate pseudoprotease (Golde et al. 2009). To this point, all knowledge regarding

the SPPL2 subfamily derives from the other two proteases, SPPL2a and SPPL2b (Fig. 1.13A, B) (Voss et al. 2013, Mentrup et al. 2017a).

A number of "canonical" RIP substrates have been identified *in vitro* for SPPL2a and SPPL2b, such as tumour necrosis factor α (TNFα) (Fluhrer et al. 2006, Friedmann et al. 2006), Fas ligand (FasL) (Kirkin et al. 2007), integral membrane protein 2B (ITM2B) (Martin et al. 2008) and cluster of differentiation 74 (CD74) (Beisner et al. 2013, Bergmann et al. 2013, Schneppenheim et al. 2013). All of these substrates first undergo shedding of their ectodomain by ADAM 10 or 17, or by lysosomal proteases and then cleavage within the TMD by SPPL2a or SPPL2b (Mentrup et al. 2017a). Apart from the type-II TM proteins mentioned above, also proteins with two TMDs can be cleaved by SPPL2a/b after opening of the loop by a different protease, such is the case for the foamy virus envelope protein (FVenv) (Voss et al. 2012) and for neuregulin 1 type III (NRG1 type III) (Fleck et al. 2016).

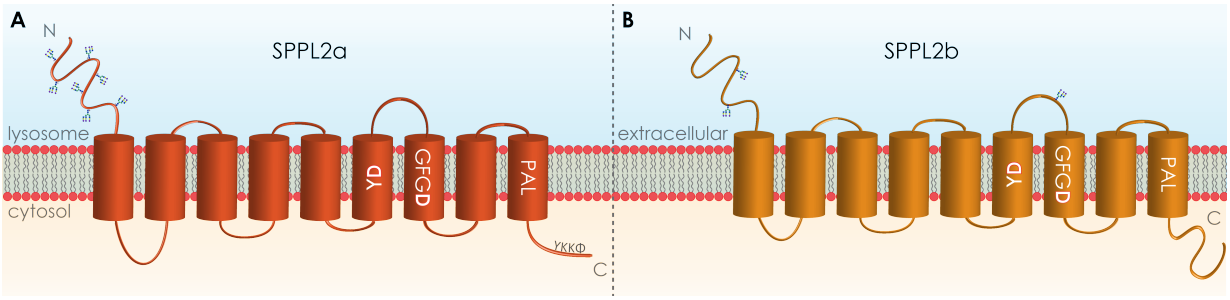

Fig. 1.13: Signal Peptide Peptidase-Like 2a and 2b. A. SPPL2a has the typical GxGD characteristics with 9 TMDs, two aspartic acids within a Y**D** and GFG**D** motif, and the conserved PAL motif. It also has numerous N-glycosylation sites at its N-terminus and a lysosomal sorting signal at its C-terminus. **B.** As the other members of the SPP/SPPLs, SPPL2b has two aspartic acids embedded in a Y**D** and GFG**D** motif, and the conserved PAL motif. It also has N-glycosylation sites at its N-terminus and in the loop between TMD 6 and 7.

The purpose of the SPPL2a/b cleavage can differ from "simple" removal of the leftover membrane fragment, to induction of signalling either by the release of the ICD or the secretion of the extracellular peptide. In the case of the *in vivo* cleavage of CD74, it appears that both purposes are served (Beisner et al. 2013, Bergmann et al. 2013, Schneppenheim et al. 2013, Schneppenheim et al. 2014a, Mentrup et al. 2015). The CD74 ICD is assumed to have functions within the nucleus where it translocates after its liberation by SPPL2a (Mentrup et al. 2015). Additionally, SPPL2a deficiency leads to an accumulation of CD74 NTF in B-

lymphocytes of SPPL2a$^{-/-}$ mice (Beisner et al. 2013, Bergmann et al. 2013, Schneppenheim et al. 2013). This accumulation not only disturbs intracellular trafficking (Schneppenheim et al. 2013), but it also increases the expression of pro-apoptotic genes via the PI3K/Akt signalling (Huttl et al. 2015). The splenic B cell maturation is halted under these conditions but it can improve with additional CD74 deficiency (Beisner et al. 2013, Schneppenheim et al. 2013) demonstrating the importance of the removal of the CD74 NTF.

Some of the substrates discovered *in vitro*, like TNFα (Fluhrer et al. 2006, Friedmann et al. 2006), ITM2B (Martin et al. 2008) and NRG1 type III (Fleck et al. 2016) are cleaved by both proteases, however, there are also some protease-specific substrates. For instance, FasL is cleaved only by SPPL2a, while the transferrin receptor 1 (TfR1) is only cleaved by SPPL2b (Zahn et al. 2013). Interestingly, only cleavage by SPPL2a has been confirmed *in vivo* , while the physiological function of SPPL2b remains elusive (Mentrup et al. 2017a). Functionally, the cleavage of CD74 by SPPL2a *in vivo* is the only well-understood process and it seems conserved in both mice and humans (Beisner et al. 2013, Bergmann et al. 2013, Schneppenheim et al. 2013, Schneppenheim et al. 2014a). However, evidence supports non-redundant functions for the two proteases. First, the proteases localise differentially within the cell with SPPL2a being predominantly found in the lysosomes and late endosomes, while SPPL2b localises mainly to the cell membrane (Friedmann et al. 2006, Behnke et al. 2011). Second, there is a differential expression in tissues *in vivo*, while SPPL2a is ubiquitously expressed; SPPL2b is predominantly expressed in the central nervous system (CNS), bone marrow and the lymphoid glands (Schneppenheim et al. 2014b). *In vivo* data regarding the function of SPPL2b would be needed to clarify further the point of non-redundancy.

1.3.2.4.4 Signal Peptide Peptidase-Like 3

Even though SPPL3 was initially believed to be a redundant protease with functions similar to SPP (Krawitz et al. 2005, Nyborg et al. 2006), today we know that this is not the case and a number of SPPL3 substrates have been reported ((Voss et al. 2012, Voss et al. 2014a,

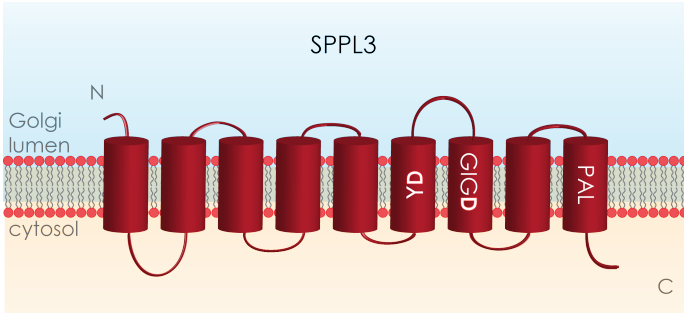

Fig. 1.14: Signal Peptide Peptidase-Like 3. SPPL3 is the smallest member of the family and it does not have any glycosylation sites. It has the two aspartic acids in TMD 6 and 7, Y**D** and GIG**D**, and the conserved PAL motif in TMD 9.

Kuhn et al. 2015), reviewed in (Mentrup et al. 2017a)). SPPL3 is the smallest member of the SPP/SPPLs, it lacks the N-terminal signal peptide and is the only non-glycosylated member of this family (Fig. 1.14) (Friedmann et al. 2004a). It possesses the nine TMD topology characteristic of all GxGD proteases (Friedmann et al. 2004a) and its proteolytic activity was finally proven in 2012, when Voss et al. showed in a cell culture model system that the FVenv is a substrate of proteolytically active SPPL3 (Voss et al. 2012).

Together with the identification of the first substrate, two very interesting characteristics of SPPL3 became apparent. First, SPPL3 activity cannot be inhibited by typical GxGD protease inhibitors, such as DAPT or 1,3-di-(N-carboxybenzoyl-L-leucyl-L-leucyl)-amino acetone ((Z-LL)$_2$-ketone). Second, no ectodomain shedding of the substrate was required prior to SPPL3 cleavage, since SPPL3 was capable of processing full length FVenv, a hairpin type-III TM protein, at the C-terminal of the first TMD, which adopts a type-II orientation (Voss et al. 2012). The function of SPPL3 as a "type-II sheddase" was confirmed by two more studies demonstrating that SPPL3 can cleave numerous full-length substrates at a close proximity to the border between the TM and the extracellular domain (Voss et al. 2014a, Kuhn et al. 2015). In contrast to SPP, that was shown to have sheddase abilities only under specific circumstances (Chen et al. 2014), SPPL3 exclusively acts as a sheddase.

In compliance with the high conservation of *SPPL3* through evolution suggesting an important physiological function for this aspartyl protease, Voss et al. showed in 2014 that SPPL3 is capable of regulating cellular N-glycosylation through shedding and secretion of glycan modifying enzymes (Voss et al. 2014a). A year later, these results were reinforced with

the use of a new proteomic method named SPECS, for secretome protein enrichment with click sugars. Using this technique, the secretome of cells overexpressing or lacking SPPL3 was compared to that of control cells in regards to the amount of secreted ectodomains of membrane proteins. All type-II TM proteins the ectodomains of which were significantly increased in SPPL3 overexpression and/or decreased in absence of SPPL3 were considered as potential substrates. Most of the confirmed substrates are involved in the complex N- and O-glycosylation and the glycosaminoglycan biosynthesis (Kuhn et al. 2015).

SPPL3 can cleave the ectodomain of Golgi-resident glycosidases and glycosyltransferases, such as GnTV and EXTL3, leading to the secretion of their active-site containing domain in a soluble form. Processing of these enzymes by SPPL3 leads to a decrease of their intracellular levels. Secreted glycosidases and glycosyltransferases are considered deactivated due to their reliance on sugar donors in order to function, these donors are known to be present within the ER and the Golgi but not in the extracellular space (Paulson and Colley 1989, Freeze and Elbein 2009, Varki et al. 2009). Thus, increased amount of SPPL3 causes a reduction in glycosyltransferases and a hypoglycosylation phenotype, while decreased presence of SPPL3 leads to an accumulation of glycosyltransferases and a hyperglycosylation phenotype (Fig. 1.15) (Voss et al. 2014a, Kuhn et al. 2015, Mentrup et al. 2017a). A large number of glycoproteins can be affected by changes in the SPPL3 expression and these results have been confirmed *in vivo* (Voss et al. 2014a).

Despite the crucial role of SPPL3 in cellular glycosylation, $SPPL3^{-/-}$ mice are viable; however, this is true only on a mixed background of C57Bl6/129S5. The mice are characterised by mild growth-related phenotypic anomalies and reduced reproduction (Tang et al. 2010). As SPPL3 is ubiquitously expressed, a hyperglycosylation phenotype is observed on glycoproteins from all analysed organs (Voss et al. 2014a). Various other studies have also touched on other phenotypic characteristics of the SPPL3 knockout mice, apart from the reproduction difficulties. From the initial generation of this mouse line, a phenotype of reduced natural killer (NK) cells was observed by Tang et al. and was later confirmed in the doctoral thesis of

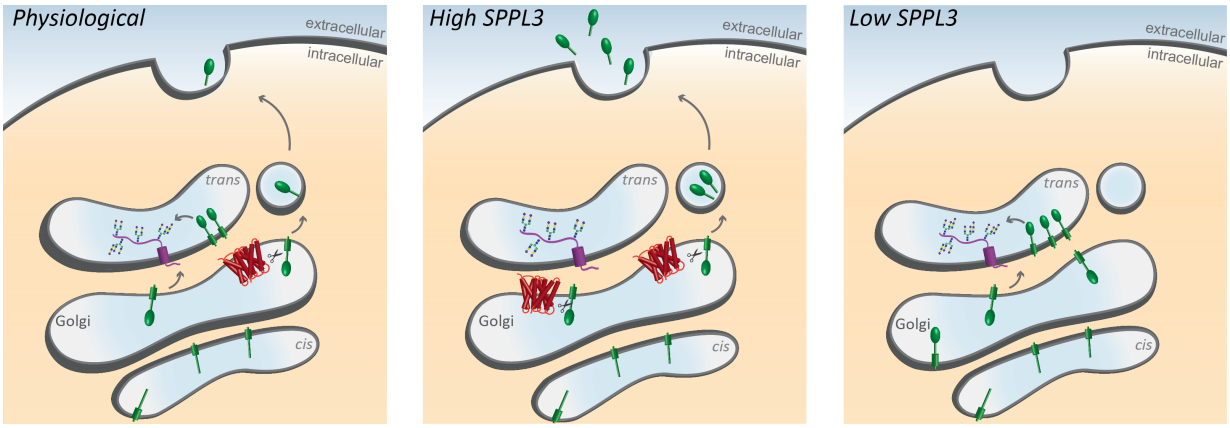

Fig. 1.15: Physiological function of SPPL3. SPPL3 (red) is located in the Golgi where glycosidases and glycosyltransferases (green) undergo maturation while moving from the *cis*- to the *trans*-Golgi. The mature glycosylation enzymes add glycans on glycoproteins (purple) in the *trans*-Golgi. SPPL3 can shed and remove the active site of these enzymes, which then is secreted in the extracellular space. The physiological balance can be disturbed both by high and low levels of SPP3 leading either to reduction of enzymes and hypoglycosylation or accumulation of enzymes and hyperglycosylation, respectively. The differences in glycosylation are depicted through the complexity of the glycan branches. Adapted from (Voss et al. 2014a)

Matthias Voss (Tang et al. 2010, Voss et al. 2014b). More effort has been placed recently in the underlying mechanism of this reduction and a targeted SPPL3-knockdown mouse model was used. SPPL3 deficiency in the hematopoietic system causes a cell autonomous decrease in maturation efficiency of NK cells and a decrease in clearance of MHC class I-deficient tumours (Hamblet et al. 2016). Although this phenotype appears to be dependent on the proteolytic ability of SPPL3, since it cannot be rescued by proteolytically inactive SPPL3, the substrates responsible for this effect remain elusive (Hamblet et al. 2016). As NK cells are linked to the growth of tumours, SPPL3 might indeed play a role in tumorigenicity as some single nucleotide polymorphisms (SNPs) in the coding region of *SPPL3* have recently been linked to breast cancer as a risk factor (Noh et al. 2015).

Despite the increased insight into the substrate spectrum of SPPL3 and the initial understanding of its *in vivo* function, many gaps remain regarding both the regulation of SPPL3 expression and the mechanism of substrate recognition and cleavage.

1.3.3 Substrate Requirements

One question that arose early on within the context of intramembrane cleavage and still lingers is how these proteases recognise and cleave their substrates. The active sites of

proteases are known to almost exclusively bind to β-strand conformations, however all I-CLIP substrates consist of transmembrane α-helices. Based on this knowledge, intrinsic instability of the substrate's α-helix surrounding the cleavage site is believed to be a key feature for the determination of a substrate (Tyndall et al. 2005, Madala et al. 2010).

Different proteases have more or less strict substrate requirements. Rhomboids (1.3.2.2) have some of the most specific requirements from their substrates. In 2007, it was discovered that helical instability is not the only common feature shared by rhomboid substrates (Akiyama and Maegawa 2007). Comparing cleavage sites and other key characteristics of a physiological bacterial substrate revealed the requirement for both a hydrophobic TMD and a six-amino acid long linear sequence, termed "recognition motif". P1, N-terminally of the cleavage site, commonly requires a small amino acid, while P4 and P2', N- and C-terminally of the cleavage site, respectively, often require large hydrophobic amino acids (Strisovsky et al. 2009, Strisovsky 2017). Structural visualisation of protease-inhibitor complexes have allowed for a better understanding of the various interactions (Zoll et al. 2014, Cho et al. 2016). However, not all rhomboids share the exact same "recognition motif", and some of them have additional requirements (Strisovsky 2017). This would explain the differences in the substrate spectra (Strisovsky 2016). Despite the existence of a "recognition motif", there is still some flexibility in their selection of rhomboid substrates, as non-substrates can also be cleaved upon chemical alteration of the membrane composition or destabilisation of the α-helix of the TMD through mutagenesis (Moin and Urban 2012, Urban and Moin 2014).

Regarding the substrate requirements of SPP, it appears that relatively short but not necessarily shedded ectodomains can be recognised and cleaved by SPP, as seen for XBP1u (Avci et al. 2014). Interestingly however, the importance of α-helix destabilising amino acids within the TMD and in close proximity to the cleavage site was demonstrated when the C-peptide release of the ceramide synthase Trh4 was studied (Oliveira et al. 2013). These data are in accordance with similar observations regarding SPPL2b (Martin et al. 2008,

Martin et al. 2009).

As with SPP (Oliveira et al. 2013), substrate analysis by introduction of mutations in the TMD of Bri2 for SPPL2b (Martin et al. 2009, Fluhrer et al. 2012) or CD74 for SPPL2a (Huttl et al. 2016) revealed that even though none of the substrate's TM regions is absolutely crucial for the cleavage, removal of α-helix breaking sequences from within the TMD reduces cleavage efficiency (Mentrup et al. 2017a).

2. Aims of Study

The main goal of this study is to deepen our understanding of SPPL3 and SPPL2c in particular, and of the GxGD-type aspartyl protease family in general.

As the first physiological substrates of SPPL3 have already been identified and validated in previous studies (Voss et al. 2014a, Kuhn et al. 2015), the first aim is to analyse the substrate requirements of SPPL3 by mutating amino acids in key positions of selected substrates.

The second focus of this study is the physiological role of SPPL3 *in vivo*. To this end, a SPPL3-deficient mouse line (Tang et al. 2010) will be analysed for phenotypical anomalies. Furthermore, the potential mechanism underlying these characteristics will be studied.

The last part of this study is devoted on the last orphan protease of this family, SPPL2c. Using a cell culture and a murine model it will be investigated whether SPPL2c is indeed a pseudoprotease as believed or whether it actually has a catalytic ability. If SPPL2c is indeed an active protease with physiological substrates, efforts will concentrate on identifying the physiological function of this protease.

3. Materials and Methods

3.1 Materials

3.1.1 Instruments, consumables and reagents

Centrifuges Heraeus Pico, Heraeus Frisco 17, 21, Megafuge 40R, Biological Safety Cabinet Safe2020 and cell culture incubator Heraeus from Thermo Fisher (Waltham, USA). ThermomixerC and Research plus pipettes from Eppendorf (Hamburg, DE). Accu-jet pro pipette boy from Brand (Wertheim, DE). SDS Gel electrophoresis and western blotting equipment by Biorad (California, USA). Agarose electrophoresis from Peq Lab (Erlangen, DE). 1.5, 2, 15ml, 50 ml reaction tubes, 2, 5, 10, 25 ml pipettes, and pipette tips from Starstedt (Nuembrecht, DE). PCR Mastercycler by Eppendorf and 7500 Fast Real-Time PCR System by Applied Biosystems (California, USA). Special instruments, consumables and reagents will be mentioned when applicable.

Table 3.1: List of chemical reagents

Chemical	Company
1kb Plus DNA Ladder	Invitrogen
Acetic Acid	Merck
Acrylamide/Bis 40% 29:1	BioRad
Acrylamide/Bis 40% 37.5:1	Invitrogen
Agarose	Invitrogen
APS (10%)	Merck
Brilliant Blue R	Sigma
Bromphenolblue	Fluka
BSA	Uptima
$CaCl_2$	Merck
DDM	Calbiochem
DMSO	Roth
dNTP	Roche
DTT	Biomol
EDTA	Merck
EGTA	Serva

Chemical	Company
EtOH	Merck
GelRed	Biotium
Glucose	Merck
Glycerine	Merck
Glycine	Biomol
Hepes	Biomol
Tropix® I-Block	Applied Biosystems
Isopropanol	Merck
KCH_3COO	Sigma
KCl	Merck
$KH_2PO_4 \cdot H_2O$	Merck
$Mg(CH_3COO)_2$	Fluka
$Na_2HPO_4 \cdot 2H_2O$	Merck
NaCl	Roth
$NaHCO_3$	Merck
NaOH	Merck
Orange G	Sigma
Pierce™ ECL Western Blotting Substrate & Plus	Thermo Fisher
PI-Mix	Sigma
SDS	Serva
See Blue Plus 2 Standard	Invitrogen
Sucrose	Sigma
TEMED	Roth
Tris	Biomol
Triton X100	Merck
Tween20	Merck
Westar Supernova	Cyanagen
β-mercaptoethanol	Sigma

3.1.2 Plasmids

pcDNA3.1 Hygro(+) was purchased from Invitrogen, as well as pcDNA4/TO/myc-his A used for SPPL3 WT and D/A. pcDNA4/TO A used for the SPPL2c constructs was purchased from

Thermo Fisher. The pCMV-Cas9-GFP plasmids were purchased from Sigma Aldrich (St. Louis, USA).

3.1.3 cDNA constructs

The coding sequence of human *SPPL3* (isoform 2), *SPPL3* D271A, human *SPPL2C* (isoform A) and *SPPL2C* D448A in the original plasmid were kindly provided by Bruno Martoglio. These sequences were later C-terminally HA-tagged (AYPYDVPDYA) and cloned into pcDNA4/TO in the laboratory of Regina Fluhrer. The human GnTV coding sequence (gene name *MGAT5*) (OCABo5050G0617D/100061790) and the human *EXTL3* (IMAGE ID 4131101/IRAu33 E12 (M13F)) were obtained from Source BioScience (Nottingham, UK). An N-terminal Flag (DYKDDDDK) epitope tag after the initiating methionine residue and a C-terminal in-frame V5 (GKPIPNPLLGLDST) epitope tag (Flag-GnTV-V5) were added to both cDNAs.

3.1.4 Cell lines

Table 3.2: cDNA constructs established in this study for stable and transient transfections. The name of each construct includes the plasmid used, the tags, the cDNA and the restriction enzymes used for subcloning.

cDNA Constructs	
pcDNA3.1Hygro(+)-KpnI-Flag-GnTVWT-V5-XhoI	pcDNA3.1Hygro(+)-KpnI-Flag-GnTVG22A-V5-XhoI
pcDNA3.1Hygro(+)-KpnI-Flag-GnTVG26A-V5-XhoI	pcDNA3.1Hygro(+)-KpnI-Flag-GnTVG22,26A-V5-XhoI
pcDNA3.1Hygro(+)-KpnI-Flag-GnTVG22L-V5-XhoI	pcDNA3.1Hygro(+)-KpnI-Flag-GnTVG26L-V5-XhoI
pcDNA3.1Hygro(+)-KpnI-Flag-GnTVG22,26L-V5-XhoI	pcDNA3.1Hygro(+)-KpnI-Flag-GnTVG22P-V5-XhoI
pcDNA3.1Hygro(+)-KpnI-Flag-GnTVG26P-V5-XhoI	pcDNA3.1Hygro(+)-KpnI-Flag-GnTVG22,26P-V5-XhoI
pcDNA3.1Hygro(+)-KpnI-Flag-GnTVM27A-V5-XhoI	pcDNA3.1Hygro(+)-KpnI-Flag-GnTVM28A-V5-XhoI
pcDNA3.1Hygro(+)-KpnI-Flag-GnTVL29A-V5-XhoI	pcDNA3.1Hygro(+)-KpnI-Flag-GnTVL30A-V5-XhoI
pcDNA3.1Hygro(+)-KpnI-Flag-GnTVH31A-V5-XhoI	pcDNA3.1Hygro(+)-KpnI-Flag-GnTVF32A-V5-XhoI
pcDNA3.1Hygro(+)-KpnI-Flag-GnTVMM27AA-V5-XhoI	pcDNA3.1Hygro(+)-KpnI-Flag-GnTVLH30AA-V5-XhoI
pcDNA3.1Hygro(+)-KpnI-Flag-GnTVH31L-V5-XhoI	pcDNA3.1Hygro(+)-KpnI-Flag-GnTVH31R-V5-XhoI
pcDNA3.1Hygro(+)-KpnI-Flag-GnTVH31D-V5-XhoI	pcDNA3.1Hygro(+)-HindIII-Flag-EXTL3WT-V5-XhoI
pcDNA3.1Hygro(+)-HindIII-Flag-EXTL3H48A-V5-XhoI	pcDNA3.1Hygro(+)-HindIII-Flag-EXTL3H48L-V5-XhoI
pcDNA3.1Hygro(+)-HindIII-Flag-EXTL3H48R-V5-XhoI	pcDNA3.1Hygro(+)-HindIII-Flag-EXTL3H48D-V5-XhoI

All cell lines used are included in the table below with their name, genetic alterations, specific antibiotic resistances and the source that provided them.

Table 3.3: Cell lines used in this study. Genetic alterations include stably transfected plasmids or genetic modifications with the CRISPR/Cas9 system. Antibiotic resistance required for culturing the cells and source are also mentioned in the table.

Cell line name	Genetic alteration	Antibiotic Resistance	Source
T-Rex™-293 (TR)	pcDNA™6/TR	Blasticidin	Invitrogen Cat. No. R710-07
TR-GnTV WT	pcDNA™6/TR pcDNA3.1Hygro(+)-Flag-GnTV-V5	Blasticidin Hygromycin	Current Study
TR-GnTV AG	pcDNA™6/TR pcDNA3.1Hygro(+)-Flag-GnTV-G22A-V5	Blasticidin Hygromycin	Current Study
TR-GnTV GA	pcDNA™6/TR pcDNA3.1Hygro(+)-Flag-GnTV-G26A-V5	Blasticidin Hygromycin	Current Study
TR-GnTV AA	pcDNA™6/TR pcDNA3.1Hygro(+)-Flag-GnTV-G22A,G26A-V5	Blasticidin Hygromycin	Current Study
TR-GnTV M27A	pcDNA™6/TR pcDNA3.1Hygro(+)-Flag-GnTV-M27A-V5	Blasticidin Hygromycin	Current Study
TR-GnTV L30A	pcDNA™6/TR pcDNA3.1Hygro(+)-Flag-GnTV-L30A-V5	Blasticidin Hygromycin	Current Study
TR-GnTV H31A	pcDNA™6/TR pcDNA3.1Hygro(+)-Flag-GnTV-H31A-V5	Blasticidin Hygromycin	Current Study
TR-GnTV F32A	pcDNA™6/TR pcDNA3.1Hygro(+)-Flag-GnTV-F32A-V5	Blasticidin Hygromycin	Current Study
TR-EXTL3 WT	pcDNA™6/TR pcDNA3.1Hygro(+)-Flag-EXTL3-V5	Blasticidin Hygromycin	Current Study
TR-EXTL3 H48A	pcDNA™6/TR pcDNA3.1Hygro(+)-Flag-EXTL3-H48A-V5	Blasticidin Hygromycin	Current Study
TR SPPL2c WT	pcDNA™6/TR pcDNA4/TO-SPPL2cWT-HA	Blasticidin Zeocin	Martina Haug-Kröper
TR SPPL2c D/A	pcDNA™6/TR pcDNA4/TO-SPPL2cD448A-HA	Blasticidin Zeocin	Martina Haug-Kröper
TR SPPL2c WT GnTV WT	pcDNA™6/TR pcDNA4/TO-SPPL2cWT-HA pcDNA3.1Hygro(+)-Flag-GnTV-V5	Blasticidin Zeocin Hygromycin	Current Study
TR SPPL2c D/A GnTV WT	pcDNA™6/TR pcDNA4/TO-SPPL2cD448A-HA pcDNA3.1Hygro(+)-Flag-GnTV-V5	Blasticidin Zeocin Hygromycin	Current Study

Cell line name	Genetic alteration	Antibiotic Resistance	Source
TR SPPL3 WT	pcDNA^{TM}6/TR pcDNA4/TO-SPPL3WT-HA	Blasticidin Zeocin	Voss et al, 2012 LMU Munich
TR SPPL3 D/A	pcDNA^{TM}6/TR pcDNA4/TO-SPPL3D271A-HA	Blasticidin Zeocin	Voss et al, 2012 LMU Munich
TR SPPL3 KO clone 11	pCMV-Cas9-GFP gRNA2 *hSPPL3*	Blasticidin	Current Study
TR SPPL3 WT GnTV WT	pcDNA^{TM}6/TR pcDNA4/TO-SPPL3WT-HA pcDNA3.1Hygro(+)-Flag-GnTV-V5	Blasticidin Zeocin Hygromycin	Current Study
E14TG2a (ES WT)	——	——	ATCC CRL 2255
E14TG2a clone 27 (ES 27)	pCMV-Cas9-GFP gRNA1 *mSppl3*	——	Current Study
E14TG2a clone 38 (ES 38)	pCMV-Cas9-GFP gRNA2 *mSppl3*	——	Current Study
E14TG2a clone 40 (ES 40)	pCMV-Cas9-GFP gRNA2 *mSppl3*	——	Current Study

3.1.5 Mouse lines

B6;129S5-Sppl3Gt(OST279815)Lex/Mmucd mice have been generated by Lexicon Pharmaceuticals (The Woodlands, USA) and Genentech (San Francisco, USA) and are made available for research purposes. They were obtained through the Mutant Mouse Regional Resource Centre (MMRRC) at the University of California at Davis (USA). The 129S6/SvEv mice used for the back crossing were purchased from Taconic (Ejby, DK). The mice were crossed back for 10 generations. The SPPL2c transgenic mice, as well as their wild-type littermates, were kindly provided Dr. Bernd Schröder and are described in detail in Niemeyer et al. 2019.

3.1.6 Antibodies

All primary and secondary antibodies used for Western Blotting were diluted in 1 x PBS supplemented with 2% (w/v) Tropix I-Block^{TM} and 0.5% (v/v) Tween 20. All primary and

secondary antibodies used for immunofluorescence (IF) were diluted in 1 x PBS supplemented with 5% BSA.

Table 3.4: Primary antibodies used in this study. The table contains the antigen (h=human, m=mouse). The host indicates the species of origin and the specific type of the antibody is mentioned (mAb=monoclonal antibody, pAb=polyclonal antibody). Commercial and scientific sources are mentioned, as well as clone when available. Each method the antibody was used is indicated, WB = Western Blot, IH = Immunohistochemistry, IF = Immunofluorescence, as well as the dilution used for each method. DSHB=Developmental Studies Hybridoma Bank

Antigen	host & type	Source	Clone	Method	Dilution
B4GALT1	mouse, mIgG2b	R&D Systems	MAB 3609	WB	1:1000
Cab-45	rabbit, pAb	Dr. von Blume	—	IH IF	1:500 1:300
Calnexin	rabbit, pAb	Enzo	—	WB IF	1:3000 1:100
EXTL3	mouse, mAb	Santa Cruz	G-5	WB	1:500
Giantin	mouse, mIgG1	Enzo	ALX-804-600	IF	1:1000
GM130	rabbit mAb	Abcam	EP892Y	IF	1:50
GnT-V	mouse, mIgG2A	R&D Systems	706824	WB	1:1000
Membrin	mouse, mIgG1	Thermo Fisher	4HAD6	WB	1:500
GRP78 BiP	rabbit, pAb	Abcam	—	IF	1:1000
hLamp2	mouse, mAb	DSHB	H4B4	WB	1:500
hSPPL2a	mouse, mAb	Dr. Feederle	6E9	WB	1:20
hSPPL2c	mouse, IgG2a/k	Dr. Feederle	1A1	WB	1:10
mSPPL2c	rabbit, pAb	Dr. Schröder	—	WB	1:500
Nicastrin	rabbit, pAb	Sigma-Aldrich	N1660	WB	1:10000
OGFOD3	goat, pAb	Santa Cruz	F-19	WB	1:200
SPP	rat, mAb	Dr. Feederle	5H7	WB	1:10
SPPL3	mouse, mAb	Dr. Feederle	7F9	WB	1:10
Syntaxin 18	mouse, mIgG2b	Santa Cruz	10	WB	1:200
Syntaxin 5	mouse, mIgG1	Santa Cruz	B-8	WB IF	1:1000 1:50
Syntaxin 6	rabbit, mAb	Cell Signaling	C34B2	WB	1:2000
Syntaxin 8	mouse, mIgG1	Santa Cruz	A-9	WB	1:100
TGN46	sheep, pAb	Acris	AP32693PU	IF	1:300

Antigen	host & type	Source	Clone	Method	Dilution
TMEM 192	rabbit, pAb	Dr. Schröder	—	WB	1:1000
V5 tag (mono)	mouse, mIgG2A	Life Technologies	R960-25	WB IF	1:2000 1:400
V5 tag (poly)	rabbit, pAb	Millipore	AB3792	WB IF	1:5000 1:500
VAMP8	rabbit, mAb	Abcam	—	WB	1:10000
VAPA	rabbit, mAb	Abcam	—	WB	1:10000
VAPB	rabbit, pAb	Abcam	—	WB	1:500
β-actin	mouse, IgG2a	Sigma	A5316	WB	1:2000

Table 3.5: Secondary antibodies used in this study. The table contains the target organism as well as the host where the antibody was raised. Coupling indicates the detection mechanism, HRP = Horseradish peroxidase-conjugated, Alexa = Fluorescent dye. Commercial sources are mentioned, as well as the method the antibody was used is indicated, WB = Western Blot, IF = Immunofluorescence, and the dilution used for each method.

Target organism	Host	Coupling	Source	Method	Dilution
mouse	goat	Alexa 555	Thermo Fisher	IF	1:400
rabbit	goat	Alexa 488	Thermo Fisher	IF	1:400
mouse	donkey	Alexa 555	Thermo Fisher	IF	1:400
sheep	donkey	Alexa 568	Thermo Fisher	IF	1:400
mouse	goat	HRP	Promega	WB	1:10.000-15.000
rat	goat	HRP	Millipore	WB	1:10.000
rabbit	goat	HRP	Promega	WB	1:20.000
goat	donkey	HRP	Santa Cruz	WB	1:10.000

3.1.7 Small-interfering RNAs

Small interfering RNAs were used for transient knockdown of protein expression in T-Rex™-293 cells. All siRNAs were purchased from Dharmacon (Lafayette, USA) and are from the siGENOME SMARTpool siRNA line. They were all applied at a final concentration of 20 nM using Lipofectamine™ RNAiMAX according to the manufacturer's instructions (Thermo Fisher, Waltham, USA). siRNAs were diluted in 4 parts RNA-free water (Qiagen) and one part

5xRNA buffer (GE Healthcare, Illinois, US).

Table 3.6: Small interfering RNAs. The table contains the target protein and the catalogue number of each siRNA used in this study.

Name	Catalogue number
siGENOME Non-Targeting siRNA Pool 1	D-001206-13
SMARTpool siGENOME Human GORS2 siRNA	M-010980-02
SMARTpool siGENOME Human SPPL3 siRNA	M-006042-02
SMARTpool siGENOME Human SPPL2a siRNA	M-006040-01
SMARTpool siGENOME Human SPP siRNA	M-005896-02
SMARTpool siGENOME Human STX18 siRNA	M-020624-00
SMARTpool siGENOME Human STX5 siRNA	M-017768-01
SMARTpool siGENOME Human STX8 siRNA	M-019873-02
SMARTpool siGENOME Human VAMP8 siRNA	M-013503-01
SMARTpool siGENOME Human VAPA siRNA	M-021382-01
SMARTpool siGENOME Human VAPB siRNA	M-017795-00

3.1.8 Kits and Enzymes

All kits used in this study are commercially available and were always used according to the manufacturer's instructions.

Table 3.7: Commercially available kits. The company the kits were obtained from and the purpose of use are indicated.

Kit name	Company	Purpose
Amaxa™ P4 Primary Cell 4D Nucleofector	Lonza	Embryonic Stem cell transfection
BCA Assay Solutions	Interchim	Protein quantification
Go Taq polymerase	Promega	Genotyping & other PCRs
High Capacity cDNA Reverse Transcription Kit	Applied Biosystems	Reverse Transcription
Lipofectamine™ 2000	Thermo Fisher	cDNA transient & stable transfection
Lipofectamine™ RNAiMAX	Thermo Fisher	siRNA transient transfection
NucleoSpin® & NucleoBond®	Mackerey & Nagel	Plasmid purification
Pfu Turbo Polymerase	Agilent technologies	High Fidelity PCRs
Protease Inhibitor mix (PI mix)	Sigma Aldrich	Protein isolations (1:500)

Kit name	Company	Purpose
Pwo polymerase	PEQLAB	Construct PCRs
Quick-RNA™ Mini Prep Plus Kit	Zymo Research	mRNA extraction
T4 ligase	Thermo Fisher	Ligation of DNA

3.1.9 Cell Culture media and antibiotics

A series of different media were used depending on the characteristics of each cell line and the purpose of the experiments. The base media for all T-Rex™-293 cells was DMEM GlutaMAX™ (Thermo Fisher, Waltham, USA). Stem cells were always cultured in Stempan E14 GMEM from PAN Biotech (Aidenbach, DE) in presence of ESGRO® mLIF Medium Supplement by Millipore. All solutions used in cell culture were sterilised either by autoclave or by sterile filtration. Autoclaving was done at 120°C and 1.2 bar for 20 min.

Table 3.8: Cell culture media and supplements. Media and supplements used in cell culture for this study.

Name	Company
Blasticidin	Life Technologies
DMEM GlutaMAX™I	Life Technologies
Doxycycline	Carl Roth
ESGRO® mLIF Medium	Millipore
Fetal Bovine serum (FBS)	Sigma Aldrich
Hygromycin	Life Technologies
L-Glutamine (L-Gln)	Life Technologies
OptiMEM®I + GlutaMAX™I	Life Technologies
Penicillin/streptomycin (P/S)	Life Technologies
Poly-L-lysine	Sigma
Stempan E14 GMEM	PAN Biotech
Trypsin (0.05%) -EDTA (1x)	Life Technologies
Zeocin	Life Technologies

Table 3.9: Specific Media Composition. Composition and purpose of use of all cell culture media used in this study.

Name	Composition	Purpose
Antibiotic free medium - Doxycycline (ABF + Dox)	DMEM GlutaMAX 10% v/v FCS 1 µg/ml Doxycycline	Induction of SPPLs expression
Antibiotic free medium (ABF)	DMEM GlutaMAX 10 % v/v FCS	Experiment conditions Transfection
Basic Medium	DMEM GlutaMAX 10 % v/v FCS 1% v/v P/S 1% L-Gln	Short term culture and resuspension
Blast Hygromycin Medium (B/H)	DMEM GlutaMAX 10 % v/v FCS 1% v/v P/S 1% L-Gln 5 µg/ml Blasticidin 100 µg/ml Hygromycin	Culture of stably transfected TR cells
Blast Medium	DMEM GlutaMAX 10 % v/v FCS 1% v/v P/S 1% L-Gln 5 µg/ml Blasticidin	Culture of TR cells
Blast Zeocin Hygromycin Medium (B/Z/H)	DMEM GlutaMAX 10 % v/v FCS 1% v/v P/S 1% L-Gln 5 µg/ml Blasticidin 200 µg/ml Zeocin 100 µg/ml Hygromycin	Culture of stably transfected inducible TR cells

Name	Composition	Purpose
Blast Zeocin Medium (B/Z)	DMEM GlutaMAX 10 % v/v FCS 1% v/v P/S 1% L-Gln 5 µg/ml Blasticidin 200 µg/ml Zeocin	Culture of inducible TR cells
E14 - LIF	Stempan E14 GMEM	Basis for differentiation of ES cells
E14 + LIF	Stempan E14 GMEM 60µl mLIF Medium	Culture of Stem cells

3.1.10 Buffers

When no dilution media is mentioned, double-distilled water was used. Protease inhibitor mix (PI mix) was always added freshly to the buffer shortly prior to use.

Table 3.10: Buffers used in this analysis. List of buffers that were not commercially acquired with the specific composition and "purpose".

Name	Composition	Purpose & Comments
4% (w/v) PFA (100 ml)	4 g PFA (Sigma) 80 ml PBS (ca. 60°C) stir 1 M NaOH until clear filter, cool and adjust pH 6.9 (HCl) a.d. 100 ml with PBS	Fixation of cells for IF (-20°C, 4°C after dilution to 1x)
$CaCl_2$ buffer	50 mM $CaCl_2$ 10 mM Tris pH 8.0	Obtaining heat shock-competent cells
DNA sample buffer (10x)	100 mM Tris pH 9.0 10 mM EDTA 50% (v/v) glycerol 0.5% (w/v) Orange G	Preparation of DNA samples for agarose electrophoresis

Name	Composition	Purpose & Comments
gDNA Lysis Buffer (1L)	5 ml 2M Tris-HCl pH 7.5 20 ml 0.5M EDTA 2 ml 5M NaCl 5 g sarcosyl (N-lauryl sarcosine) 10 µg/ml Proteinase K (before use)	Isolation of genomic DNA
gDNA precipitation Buffer (10 ml, slurry)	0.3 ml 5M NaCl 9.7 ml 100% EtOH	Isolation of genomic DNA (prepare fresh)
I-Block solution	2% (w/v) I-Block™ (life technologies) 0.1% (v/v) Tween 20 in PBS	Antibody dilution, PVDF membrane blocking
LB agar plates	LB medium 15 g/l agar autoclaved at 120°C at 1.2 bar 20 min 100 µg/ml ampicillin or spectinomycin	Growth of *E.coli* transformations
LB medium	1% (w/v) bactotrypton 0.5% (w/v) yeast extract 1% (w/v) NaCl	Bacteria growth
Lower Tris (4x)	1.5 M Tris 0.4% (w/v) SDS, pH 8.8	Gel electrophoresis (4°C)
Mass Spec Lysis Buffer	150 mM NaCl 50 mM TrisHCl pH 7.5 2 mM EDTA 1% Triton X-100	Dissolving membrane pellets for Mass Spec (4°C)
Mowiol	6.0 g glycerol 2.4 g Mowiol 4-88 (Carl Roth) 12.0 ml 0.2 M Tris x HCl pH 8.5 6.0 ml double-distilled water 25 mg/ml DABCO (Carl Roth)	Fixing of coverslips for IF (-20°C, heat prior to use)

Name	Composition	Purpose & Comments
Organ-lysis buffer	5 mM Tris x HCl, pH 7.4 250 mM sucrose 5 mM EGTA, PI mix 1:500	Homogenisation of tissue and whole organs (4°C)
PBS (10x)	140 mM NaCl 10 mM Na_2HPO_4 1.75 mM KH_2PO_4 pH 7.4	Multiple uses
Running buffer	25 mM Tris 200 mM Glycine 0.1 (w/v) SDS	Gel electrophoresis (4°C)
Sample buffer (5x) – diluted 2.5 times for sample buffer (2x)	50% (v/v) glycerol 7.5% (w/v) SDS 7.5% (w/v) DTT bromophenol blue (traces) dissolved in 4x upper Tris buffer	denature proteins and charge them negatively in preparation of WB (-20°C -> RT) (heat prior to use)
STE-Buffer	250mM sucrose 5mM Tris pH 7 1mM EGTA PI mix 1:500	Opening cells for Mass Spectrometry (4°C)
STEN Buffer	50 mM Tris pH 7.5 150 mM NaCl 2 mM EDTA 1% NP-40 PI mix 1:500	Lysis of cells for Lectin array (4°C)
Stripping buffer	62.5 mM Tris x HCl pH 6.7 2% (w/v) SDS 0.7% (v/v) β-mercaptoethanol	Removal of primary and secondary Ab from PVDF

Name	Composition	Purpose & Comments
TAE buffer (50x)	40 mM Tris pH 8.0 20 mM $Na(CH_3COO)_2$ 2 mM EDTA	Agarose gel electrophoresis
TBE Buffer (10x) 1L	108 g Tris 55 g Boric Acid 40 ml 0.5 M Na_2EDTA pH 8.0	Agarose gel electrophoresis <500 base pairs
TBS-T	50 mM Tris 150 mM NaCl 0.05% (v/v) Tween 20 pH 7.6	Washing of PVDF membranes
Transfer buffer	25 mM Tris 200 mM glycine	Electroblotting
Upper Tris (4x)	0.5 M Tris 0.8% (w/v) SDS pH 6.8	Gel electrophoresis (4°C)
Hypotonic buffer	10 mM Tris pH 7.6 1 mM EDTA 1 mM EGTA, pH 7.6 PI mix 1:500	Opening of cells (4°C)
Membrane lysis buffer/ Basic Buffer	40 mM Tris pH 7.8 40 mM KCH_3COO 1.6 mM $Mg(CH_3COO)_2$ 100 mM sucrose 0.8 mM DTT PI mix 1:500	Solubilisation of membranes for WB (4°C)
Tail lysis buffer	100 mM Tris, pH 8.5 5 mM EDTA 0.2% (w/v) SDS 200 mM NaCl proteinase K (100 µg/ml, Roche)	proteinase K is freshly added

3.1.11 Acrylamide gels

Two types of acrylamide gels were used in this study. One type was used for protein analysis and the other type to analyse DNA as it gives a very precise running behaviour depending on the matching of the double-stranded DNA and it is sensitive enough to detect mismatched base pairs.

Table 3.11: Acrylamide gels composition for protein analysis. Three different percentages of acrylamide were used depending on the molecular weight of the protein in question.

	Running gel (8%)	Running gel (10%)	Running gel (12%)	Stacking gel
H_2O	4.4 mL	4 mL	3.6 mL	3.25 mL
Acrylamide/Bis 37.5:1	1.6 mL	2 mL	2.4 mL	0.5 mL
Lower Tris	2 mL	2 mL	2 mL	-
Upper Tris	-	-	-	1.25 mL
TEMED	15 µl	15 µl	15 µl	15 µl
APS (10%)	15 µl	15 µl	15 µl	15 µl

Table 3.12: Acrylamide gels composition for DNA analysis. Only 8% Polyacrylamide gels were used to analyse 50-400 bp DNA size. In this gel the front is at 45bp.

	Running gel (8%)
H_2O	8.4 mL
Acrylamide/Bis 29:1	2.4 mL
10 x TBE	1.2 mL
TEMED	10 µl
APS (10%)	200 µl

3.2 Methods

3.2.1 Molecular Cloning

3.2.1.1 DNA Amplification by PCR

DNA was amplified by PCR when new DNA was received in the lab or when the DNA stocks were running low. Additionally, this technique was used to add tags, restriction enzyme sequences, signal sequences etc. to the construct.

For the PCR, 5-10 ng of clonal DNA were used together with 0.5 µM forward and reverse primer, 400 µM dNTPs, 5 µl 10x Buffer, 1 µl Pwo-PoI polymerase and 39 µl H_2O.

Table 3.13: PCR Program. *Steps 2-4 were repeated 30 times.

PCR Program		
1	5 min	95°C
2	30 sec*	95°C
3	1 min*	55°C
4	4 min/kb*	68°C
5	10 min	68°C
6	∞	10°C

3.2.1.2 Transferring of cDNA to desired vector

Commercially purchased DNA required transferring to an appropriate vector for subsequent use in human cells. To this end, the following steps were taken.

3.2.1.2.1 Digestion

The insert DNA and the plasmid were digested with the same restriction enzymes that were predefined and their restriction sites were cloned into the construct. Digestion was performed at 37°C for 2-4 hours. The restriction endonucleases were obtained from commercial sources (Thermo Fisher or NEB).

Table 3.14: DNA Digestion. List of all the components required for digestion of insert DNA and a vector. x+y=30

Vector's DNA 2 µg **Construct's DNA 5-10 µg**	x µl
Buffer matching enzymes	3 µl
Enzyme 1	1 µl
Enzyme 2	1 µl
H2O a.d. 30 µl	y µl

3.2.1.2.2 Ligation

The digested DNA samples were run on an agarose gel and the band depicting the expected nucleotide length was cut out and eluted from the gel. The two complementary samples were then ligated for 2 hours at RT or overnight at 4°C or 14-18 hrs at 14°C. A control ligation was also done in absence of the insert. 10 µl of the ligated samples were used to transform 100 µl *E.coli* (3.2.1.4).

Table 3.15: Ligation of plasmids.

	Control	Probe
cleaved vector	2 µl	2 µl
Insert	—	15 µl
T4 ligase buffer 10x	2 µl	2 µl
T4 ligase	1 µl	1 µl
H2O ad. 20 µl	15 µl	—

3.2.1.3 Quick Change

This technique was used to introduce mutations into existing plasmids. Up to 7 nucleotides can be changed with this technique at once. Primers for Quick change were designed using the online software by Agilent Technologies (http://www.genomics.agilent.com/primerDesignProgram.jsp) and purchased by Sigma Aldrich, or Thermo Fisher when primer size exceeded 120 nucleotides.

After the PCR, 1µl of DpnI enzyme per reaction was added for 1.5h at 37°C to degrade the

original template. 10 µl of each reaction when then used to transform 50 µl of *E.coli* (3.2.1.4).

Table 3.16: PCR mix for Quick Change. List of all components of the Quick Change PCR.

PCR Mix	
Template	10 ng (i.e. 1µl of 1µl/µg diluted 1:100)
Primer fw	(125 ng, 1 µl of 10 µM)
Primer rv	(125 ng, 1 µl of 10 µM)
dNTP Mix (Roche, 10 mM)	2 µl
Buffer (10x)	5 µl
Pfu Turbo (Agilent)	1 µl
ddH_2O	39 µl

Table 3.17: PCR program for Quick Change Program used on the PCR machine. *Steps 2-4 were repeated 16 times.

PCR Program QUICK		
1	1 min	95°C
2	30 sec*	95°C
3	30 sec*	55°C
4	2 min/kb*	68°C
5	20 min	68°C
6	∞	10°C

3.2.1.4 Competent cells DH5α and transformation

Heat shock-competent cells were obtained as follows. Overnight culture of *E. coli* DH5α was diluted in fresh LB medium and incubated at 37°C and 250 rpm until it reached an OD_{600} of 0.5. Bacteria were then centrifuged at 1500 g at 4°C for 5 min. The pellet was resuspended in ice-cold $CaCl_2$ buffer and left on ice for 30 min. After another round of centrifugation, the cells were resuspended in 1 ml $CaCl_2$ buffer and aliquots were stored at -80°C.

For transformation, 50-100 µl competent cells were thawed on ice for 10 min and mixed with bacterial plasmids, 10 µl for a ligation reaction, 1 µl for a site-directed mutagenesis reaction or 50 ng of intact plasmid. The cells were then incubated on ice for another 10 min and the mixture

was incubated at 42°C for 2 min and instantly chilled on ice for 2 more min. 1 ml of sterile LB medium was added and samples were shaken at 37°C for 1 h. The mixture was then spun down at 2500 rpm for 2 min and the pellet was resuspended in 80 µl fresh LB-medium, before being either plated on LB agar plates or used to inoculate sterile LB medium. In either case, media were supplemented with the antibiotic according to the plasmid to select for transformed cells.

3.2.1.5 Agarose gel electrophoresis

DNA plasmids and fragments were analysed by submerged agarose gel electrophoresis (SAGE). Samples for analysis were mixed 1:4 with DNA sample buffer and separated using either 1 x TAE-buffered or TBE-buffered gels containing 1 to 2 % (w/v) agarose and 0.2 µg/ml GelRed depending on the base-pair length. Commercially available 1kb Plus DNA ladder was used to assess the length of the DNA under UV illumination. When further processing was required, DNA fragments of the expected size were cut from the gel and eluted using the NucleoSpin Gel and PCR clean-up kit according to the manufacturer's instructions.

3.2.1.6 Plasmid preparation

Plasmids were isolated from bacterial cultures shaken overnight at 37°C, 200 rpm using commercially available kits according to the manufacturer's instructions (Macherey-Nagel). DNA concentration was determined using a UV-Vis NanoPhotometer (Implen, Munich, Germany) and was adjusted commonly to 1 µg/µl using autoclaved H_2O.

3.2.1.7 Sequencing

Empty plasmids were sequenced prior to use. Plasmids containing the desired constructs were sequenced to confirm the presence of the constructs and the absence of unwanted mutations. DNA of stem cells CRISPR clones were also sequenced to confirm mutations. All DNA was sequenced by Eurofins Genomics (Ebersberg, DE) and prepared for sequencing according to their standards. Sequence information was obtained by Sanger sequencing using standard sequencing primers or, alternatively, internal, pre ordered, sequencing primers, for longer constructs. Sequence analysis was performed using the CLC Main Workbench, v6.9.

3.2.2 Cell Culture

3.2.2.1 T-Rex™-293

3.2.2.1.1 TR Culturing

All cells were cultivated in water-jacket incubators in a humidified atmosphere containing 5% (v/v) CO_2. All treatment of cells in culture was done under luminar flow hoods. Under non-experimental conditions, the cells were cultured in the presence of appropriate antibiotics listed in table 3.3 in the media mentioned in table 3.9. Cells were split every 3-4 days to a dilution that would ensure reaching confluency by the next splitting day. Trypsin-EDTA was used to detach the cells and was either neutralised by the FCS present in the media or the cells were centrifuged 5 min x 1000 rpm and resuspended in absence of trypsin.

When plated for experiments, all additives except FCS were removed from the culture medium (ABF +/- Dox). Poly-L-Lysine (100 µg/ml in 1xPBS) was used for coating the cell culture plates used in experiments (1 hour of coating followed by 3 washes with 1xPBS).

3.2.2.1.2 TR Transfection

Cells were plated the day before and kept in ABF medium at a 60-80% confluency. Transient cDNA transfections were achieved using Lipofectamine™ 2000 according to the manufacturer's instructions; no selection by antibiotic was performed. For one well of a 6-well plate, 6 µl Lipofectamine were preincubated in 250 µl OptiMEM (solution A) and 1.5 µg DNA in 250 µl OptiMEM (solution B) for 5 min at room temperature (RT). Then solutions A and B were mixed and incubated for further 5 min at RT before being added to the well. 24 hours later the media was changed removing the Lipofectamine. For a 6-cm plate 8 µl Lipofectamine were used in 500 µl OptiMEM (A) and 2 µg DNA in 500 µl OptiMEM (B).

For transient knockdown, cells were plated either the day before or the same day. The cells were transfected with siGENOME SMARTpool siRNA from Dharmacon (table 3.6) at a final concentration of 20 nM using Lipofectamine™ RNAiMAX according to the manufacturer's

instructions. For one well of a 6-well plate, 250µl OptiMEM with 8 µl LipoRNAiMAX and 2 µl siRNA were used, the mixture was incubated for 10 min before being added to the well. For a 6-cm and an 8-cm plate 12 µl LipoRNAiMAX and 4 µl siRNA were used. After 24 hours, the media was exchanged with fresh media.

For some experiments that required both DNA and siRNA transfections, cells were treated on experimental day 1 with the siRNA and on experimental day 2 or 3 with the cDNA depending on their confluency.

3.2.2.1.3 TR Cell line generation

SPPL2c and SPPL2c D448A expressing cells were generated by stably transfecting the respective cDNAs into doxycycline-inducible TR cells and keeping the cells in the presence of zeocin. Single cell clones with desirable expressions were selected after analysis of the expression by immune blotting. TR cells expressing SPPL3 with a C-terminal HA-tag under a doxycycline inducible promoter were generated similarly and have been described previously (Voss et al. 2014b). Expression of the SPPL-proteases was induced by 1 µg/ml of doxycycline in the culture medium (ABF +/- Dox) for at least 48 hours, unless differently indicated.

Cells stably expressing cDNA constructs (such as Flag-GnTV-V5, table 3.3) were generated by transfecting the respective plasmid using Lipofectamine^{TM} 2000 according to the manufacturer's instructions. Four days after transfection, cells were selected by addition of 100 µg/ml hygromycin to the culture medium and were kept in this medium to ensure continuous expression of the protein.

3.2.2.1.4 Inhibitor Treatment

Cells were treated with inhibitors in 2 ml media in 6-well plates. PI mix 4.5 µl, Roche inhibitors 4.5 µl, Bafilomycin 30 nM, E64 50 µM, EDTA 2 mM, Pepstatin 1 µM, X-Merc 1 µM, Epoxomycin 1 µM, Caspase3 30 µM and MG132 10 µm final concentration, for 24 hours before being collected.

3.2.2.1.5 Generation of SPPL3 knockout HEK293 via CRISPR/Cas9

The TR cells were used for this method and the knockout was done according to the 2013 publication by Ran et al. (Ran et al. 2013).

3.2.2.1.5.1 Transfection and single-cell sorting

The HEK293 cells were transfected with the pCMV-Cas9-GFP gRNA plasmids (Sigma, table 3.2) as described above (3.2.2.1.2). One day after transfection, the GFP expression was checked using an LSM 710 Zeiss Observer Z.1 confocal microscope to confirm the transfection's success. A day later, the cells were subjected to single cell-sorting at the FACS sorting facility of the Helmholtz Centre (Munich, DE) using a BD FACSAria^{TM} III. The cells were sorted into 96-well plates, two plates of cells with high GFP expression and two plates with low GFP expression for each of the two gRNAs used. The single cell colonies that survived (about 20%) were allowed to grow sufficiently before being passaged progressively to bigger plates (24-wells, 12 wells, 6-wells). At the 6-well stage, each clone was frozen and protein, as well as DNA were collected to assess the success of the genetic modification. The clones were analysed progressively.

3.2.2.1.5.2 Protein analysis of single cells clones by Western Blot

The proteins from the single cell clones were extracted (as described in 3.2.3) and the expression levels of SPPL3 for each of the clones were analysed by Western Blotting (3.2.4). Only the clones that showed no remaining SPPL3 expression in this step were further subjected to analysis of their genomic DNA.

3.2.2.1.5.3 Genomic DNA analysis

For the extraction of the genomic DNA (gDNA), cells were span down at 3500 rpm for 5 min, washed two times with 1xPBS, resuspended in 500 µl of gDNA Lysis buffer and placed in -80°C for 1 hour. After thawing, 1.5 ml of gDNA precipitation buffer was added to each tube and incubated for 30 min at RT. Samples were spun down at 13500 rpm for 15 min at 4°C and washed with 1 ml 70% EtOH. After another 5 min centrifugation at max speed the wash buffer was removed and the pellets were dried before being resuspended in 100 µl of TE buffer. 1

µl of DNA was used for the PCR amplification. All of the clones and 3-4 WT samples were included in the analysis.

In order to ensure the specific amplification of only the required part of the genetic material, as this is a crucial step for the efficiency of the analysis, nested PCR was performed with two sets of primers for each gRNA. The first pair amplified a region 700-1000 base pairs, while the second pair amplified 200-400 base pairs.

Table 3.18: PCR primers for nested PCR of gRNA targets on DNA of *SPPL3* in HEK293 cells. List of all forward and reverse primers for "outer" and "inner" nested PCR of both target sites.

human gRNA 1 1st PCR	**Sequence (5'->3')**	**Length**	**Start**	**Stop**	**Tm**	**GC%**
Forward primer	TCAAAGACTCTCTCCTTAACC	21	120810510	120810530	54.32	42.86
Reverse primer	ATGCAGGCTTTACCTCATC	19	120811308	120811290	54.92	47.37
Product length	799 bp					
human gRNA 1 2nd PCR	**Sequence (5'->3')**	**Length**	**Start**	**Stop**	**Tm**	**GC%**
Forward primer	GTTTTGGTACCAGCACTTTC	20	120810729	120810748	55.1	45
Reverse primer	AAGCTCCATTAGGACTCACT	20	120810943	120810924	55.54	45
Product length	215 bp					
human gRNA 2 1st PCR	**Sequence (5'->3')**	**Length**	**Start**	**Stop**	**Tm**	**GC%**
Forward primer	TCCTGTGTACTTGCCAATTT	20	120768637	120768656	55.15	40
Reverse primer	ATGAAAGGGGGTGCTATCTA	20	120769424	120769405	55.26	45
Product length	788 bp					
human gRNA 2 2nd PCR	**Sequence (5'->3')**	**Length**	**Start**	**Stop**	**Tm**	**GC%**
Forward primer	GTACGACTTTTCAGCAAACA	20	120768770	120768789	54.5	40
Reverse primer	AATTGCAAACTCTGTGAAGG	20	120769154	120769135	54.39	40
Product length	385 bp					

All the clones that had showed no SPPL3 expression on the protein level were sent for

sequencing (3.2.1.7).

3.2.2.2 E14TG2a mouse Stem Cells (ES cells, ESCs)

3.2.2.2.1 ESCs Culturing

ESCs were cultivated in water-jacket incubators in a humidified atmosphere containing 5% (v/v) CO_2. All treatment of cells was done under luminar flow hoods and contaminations with other cell lines were strictly avoided. All solutions used in cell culture were sterilised either by autoclaving or sterile filtration. To inhibit differentiation, cells were grown in the presence of mouse leukaemia inhibitory factor (mLIF). Cells were split every 2-3 days to a dilution that would ensure reaching a maximum of 80% confluency by the next passage to avoid differentiation. Cells were grown in special flasks (Starstedt) that allow attachment of cells and help the formation of colonies. Trypsin-EDTA was used to detach the cells and was either neutralised by the FCS present in the media or the cells were centrifuged 5 min x 1000 rpm and resuspended in absence of trypsin. Cells were exchanged after approx. 50 passages.

3.2.2.2.2 Generation of SPPL3 knockout ESCs via CRISPR/Cas9

The principle of this method was done according to the 2013 publication by Ran et al. (Ran et al. 2013).

3.2.2.2.2.1 Transfection and single-cell sorting

Low passage ESCs were transfected with the pCMV-Cas9-GFP gRNA plasmids (Sigma, table 3.2) using the P4 Primary Cell 4D-Nucleofector™ X Kit (Lonza) 100 µl format and a 4D-Nucleofector™ (Lonza), according to manufacturer's instructions. Following the transfection, cells were seeded as usual and one day later, the GFP expression was checked using an LSM 710 Zeiss Observer Z.1 confocal microscope to confirm the transfection's success. Two days after transfection the cells were subjected to single cell-sorting at the FACS sorting facility of the Helmholtz Centre (Munich, DE) using a BD FACSAria™ III. ESCs were sorted into 96-well plates. For each of the two gRNAs used, 2 plates of cells with high GFP expression and 2 plates with low GFP expression were sorted. The cells were kept always under the presence of

LIF. The single cell colonies that survived (50%) were allowed to grow sufficiently before being passaged progressively to bigger plates (24-wells, 12 wells, 6 wells). At the 6-well stage, each clone was frozen and protein as well as DNA were collected to assess the success of the genetic modification. The clones were analysed progressively.

3.2.2.2.2.2 Genomic DNA analysis

The genomic DNA of the cells was isolated and analysed as described in 3.2.2.1.5.3. The primers for this analysis were designed in the same principle as before.

Table 3.19: PCR primers for nested PCR of gRNA targets on DNA of *Sppl3* in ESCs. List of all forward and reverse primers for "outer" and "inner" nested PCR of both target sites.

mouse gRNA 1 1st PCR	**Sequence (5'->3')**	**Length**	**Start**	**Stop**	**Tm**	**GC%**
Forward primer	GGTGAGAGAGATGTGGTTTT	20	115061202	115061221	54.98	45
Reverse Primer	TCCCAGATAAACTCTGCTTC	20	115062057	115062038	54.46	45
Product length	856 bp					
mouse gRNA 1 2nd PCR	**Sequence (5'->3')**	**Length**	**Start**	**Stop**	**Tm**	**GC%**
Forward primer	CTGTCCGAGTATCTTTGGTT	20	115061418	115061437	54.8	45
Reverse primer	ATGCTTCCTCTATCTGCAAC	20	115061687	115061668	55.22	45
Product length	270 bp					
mouse gRNA 2 1st PCR	**Sequence (5'->3')**	**Length**	**Start**	**Stop**	**Tm**	**GC%**
Forward primer	TCTCTGATGACCTGTTACCT	20	115082037	115082056	54.87	45
Reverse primer	AGCTGTGATTAGCTGTCAATA	21	115082763	115082743	54.74	38.1
Product length	727 bp					
mouse gRNA 2 2nd PCR	**Sequence (5'->3')**	**Length**	**Start**	**Stop**	**Tm**	**GC%**
Forward primer	TTAGGTGACATCAGTGCATC	20	115082090	115082109	55.17	45
Reverse primer	ATGGCATGGCACATACATTA	20	115082399	115082399	55.14	40
Product length	310 bp					

Part of the sample from the second PCR was loaded on a 1.5% agarose in TBE to confirm the amplification of a single band. After the agarose gel analysis, the samples were denatured and reannealed either on their own, or in combination with the DNA from WT ESCs.

Table 3.20: Denaturing and reannealing sample composition

Self reannealing	Reannealing with WT
2 µl 2nd PCR product	1.5µl 2nd PCR product + 1.5 µl WT PCR
2 µl T7 Buffer	2 µl T7 Buffer
16 µl H_2O	15 µl H_2O

Table 3.21: Denaturing and reannealing PCR program

Denature/Reannealing PCR program	
95°C	2 min
-2°C/s to 85°C	—
-0.1°C/s to 25°C	—
16°C	∞

Following the reannealing, 15µl of each sample were mixed with 4µl DNA loading buffer and were loaded on DNA Acrylamide gels. The gels were run for 4-5 h in 1 x TBE at 30 Volt and subsequently were incubated for 30 min in TBE with 0.2 µg/ml GelRed. Commercially available 1kb Plus DNA ladder was used to assess the length of the DNA under UV illumination and a picture of each blot was taken.

With this method, homozygous dsDNA runs as a single band, while mismatched DNA runs as multiple bands. The clones that had different DNA from the WT (mismatch in the reannealing with the WT) but were homozygous (single band at the self-reannealing) were selected. These clones were sequenced (3.2.1.7) and three clones with early stop codons were selected.

3.2.2.2.3 Differentiation of Stem cells to Adipocytes

Wildtype and knockout stem cells were differentiated to adipocytes following the protocol

from Cuaranta-Monroy et al. (Cuaranta-Monroy et al. 2014). In brief, cells were cultured in "hanging drops" (2000 cells/drop, 20 µl) for two days without LIF to prom the formation of embryonic bodies (EBs). On day 2, the EBs from one 15 cm plate were transferred in one well of a 6-well gelatin-coated plate. On days 3-5, the cells were daily treated with fresh media containing 1 µM retinoic acid (RA) and 12.5 µg/ml ascorbic acid (AsA). On day 6, the RA was removed and on days 7-11, the cells were given daily fresh media containing 0.5 µM Rosiglitazone, 0.5 µg/ml Insulin, 3 nM T3 hormone and 12.5 µg/ml AsA. On day 12, the cells were dispersed with trypsin and split into different wells in media containing 0.5 µg/ml Insulin, 3 nM T3 hormone to serve experimental purposes. Some cells were plated on poly-lysine coated cover slips for Oil Red stainings (Abcam). On day 13, 0.5 µM Rosiglitazone and 12.5 µg/ml AsA were added on the cells. From day 15 to 20, the media was changed every second day and contained 0.5 µM IBMX, 0.1 µM Dexamethasone, 20 µg/ml Insulin, 0.5 µM Rosiglitazone, 0.06 mM Indomethacin and 12.5 µg/ml AsA. On day 21 and 24, the media was changed to media containing 20 µg/ml Insulin, 0.5 µM Rosiglitazone, 12.5 µg/ml AsA and 3 nM T3 hormone. On day 27, the adipocyte cultures were evaluated. Oil Red staining was performed according to the manufacturer's instructions.

3.2.3 Protein Extraction/Preparation

To extract and further analyse the majority of intracellular proteins, cells were washed with fresh ice cold 1xPBS and harvested on ice. The cells were pelleted by 5 min centrifugation at 4°C and 3500 rpm. The supernatant was removed and the cells were lysed using ice-cold STEN buffer without BSA, 100 µl or 300µl were used for 6-well plates or 6 cm plates, respectively. Samples were resuspended and incubated on ice for 30 min, the cell debris was removed by centrifugation at 17000 g at 4°C for 30 min. BCA assay was used to determine the total protein concentration in the cell lysates, and inconsistencies between sample-concentrations were normalized appropriately.

For analysis of TM proteins, cellular membranes were isolated. To this end, cell pellets were

collected as before and resuspended in hypotonic buffer by pipetting and incubated on ice for 10 min. Cells were lysed with a 23-gauge needle (10-15 times) and centrifuged at 5000 rpm at 4°C for 5 min, to remove cell debris and nuclei. The supernatant was transferred to a fresh tube and centrifuged at 13000 rpm at 4°C for 45 min. The final membrane pellet was resuspended with membrane lysis buffer.

For analysis of secreted proteins, conditioned media was collected after 24-48 hours incubation and centrifuged at 17.000 g at 4°C for 20 minutes to remove any cell debris and dead cells. Subsequently, samples were most commonly directly mixed 4:1 with 5x sample buffer and heated at 65°C for 10 minutes before being subjected to gel electrophoresis (SDS-PAGE). For the detection of secreted endogenous proteins, the supernatant was TCA precipitated (3.2.3.1).

3.2.3.1 Trichloroacetic acid precipitation

For this procedure, cells were cultured in absence of FCS for 24 hours to avoid precipitation of albumin during trichloroacetic acid (TCA) precipitation. 800 µl of conditioned media were mixed with 200 µl freshly prepared aqueous 100% (w/v) TCA and incubated for 1 h on ice. Samples were centrifuged at 13000 rpm at 4°C for 30 min and the pellets were washed twice with ice-cold acetone (-20°C). The samples were dried and the precipitated proteins were resuspended in 2x sample buffer. Judging by the colour of the samples, the pH was adjusted by adding 1-3 µl of 1M Tris x HCl, pH 7.8. The samples were incubated at 65°C for 10 min and stored at -20°C.

3.2.4 Electrophoresis/Immunoblotting

Proteins from lysates, membrane preparations, conditioned media or TCA-precipitations were separated by SDS-polyacrylamide (SDS-PAGE) gels. The amount of total protein loaded varied (5-40 µg) and depended on the abundance of the protein in question. The proteins were separated on an acrylamide gel. To determine the percentage of the SDS-gel, the molecular weight of the protein in question was taken into account. The gels were run at 70 Volt until the proteins surpassed the stacking gel and then at 120V until the required end point. 10 µl of See Blue Plus protein ladder were used for estimating the apparent molecular

weight of the proteins.

The proteins were transferred onto polyvinylidene fluoride (PVDF) membranes (PVDF; immobilon P transfer membrane, 0.45 µm pore width; Millipore) by wet transfer using transfer buffer, 400 mAmp/chamber for 1 hour. The PVDF membranes were activated for 1 min in isopropanol, then washed for 1 min in destilled water and then incubated in transfer buffer until use.

Following the transfer, membranes were incubated in blocking solution at RT for 30 min to 1 h before being incubated with the primary antibody overnight at 4°C. Membranes were washed three times for 15 min with TBS-T and then incubated with the secondary, HRP-conjugated antibodies for 1h at RT. All antibodies were diluted in 1xPBS supplemented with 2% (w/v) Tropix® I-Block™ and 0.5% (v/v) Tween 20. The membranes were washed again three times for 15 min with TBS-T and then the proteins were visualized using enhanced chemiluminescence technique (ECL) Pierce™ ECL Western Blotting Substrate (Thermo Fisher) or Westar Supernova (Cyanagen, Bologna, Italy) for increased sensitivity, and detected on Super RX-N X-ray films (Fuji, Tokyo, Japan) with Cawomat 2000IR developer. Developed films were scanned with an Epson Perfection V700 PHOTO scanner (Epson, Suwa, Japan). For quantification, proteins were detected using the Pierce™ ECL Plus Western Blotting Substrate (Thermo Fisher). The chemiluminescence signals of at least three independent experiments were measured with a CCD camera-based imaging system (ImageQuant LAS-4000 Fuji Film). The intensity values were obtained using the software Multi Gauge v3.0. In case the same membrane needed to be detected by another antibody, primary and secondary antibodies were removed from the membranes by incubation in stripping buffer at 50°C for 30 min. The membrane was then extensively washed with TBS-T and the immunodetection procedure was repeated starting from the initial blocking step.

3.2.5 Quantitative Real-Time PCR

Cells and tissues were carefully collected to avoid trans-contaminations between the samples. The samples were stored in DNA/RNA shield (Zymo Research, Freiburg, DE) at -80°C until analysis. Total cellular RNA was isolated from cells using Quick-RNA^{TM} Mini Prep Plus Kit RNA (Zymo Research) and the concentrations were determined by UV-Vis spectroscopy. mRNA samples were stored at -80°C. Equal amounts of RNA (2-5 µg) were reverse-transcribed with the High Capacity reverse transcription kit (Applied Biosystems) according to the manufacturer's instructions and cDNA products were stored at -20°C. Quantitative real-time PCR was performed using 2x TaqMan master mix (Applied Biosystems) and pre-designed FAM-labelled 20x TaqMan probes targeting SPPL3 (Applied Biosystems (Cat. Hs00293370-m1)) and VIC-labelled probes targeting GAPDH ((Applied Biosystems) (Cat. Hs02786624-g1)) mRNAs. Reactions were performed with a 7500 Fast Real-Time PCR System (Applied Biosystems). Signals were normalised to levels of GAPDH mRNA and relative mRNA levels were calculated with the ΔΔCT method. For the Stx8 qPCR, UPL assay system from Roche was used by Torben Mentrup. The housekeeping gene used was Tuba1a (fw: 5'-CTGGAACCCACGGTCATC-3', rv: 5'-GTGGCCACGA GCATAGTTATT-3'). The Stx8 primers were (fw: 5'-ATGACCTTGTCACCCGAGAG-3', rv: 5'-CTTTGCTTCTTCGCTCATCA).

3.2.6 Animals

Mice were kept at specific pathogen-free conditions at the Centre for Stroke and Dementia Research, Munich, Germany.

3.2.6.1 Genotyping

Mouse genotyping was conducted on genomic DNA isolated from ear or tail clips, tissue samples were kept in -20°C until isolation. Each sample was agitated at 55°C for 4-16 hours in 500 µl tail lysis buffer and debris was removed by centrifugation at 13000 rpm for 5 min. For DNA

precipitation from the clear supernatant, 400 µl isopropanol were added to each sample, mixed well and centrifuged at 13000 rpm at 4°C for 20 min. The pellet (not visible) was washed with 70% (v/v) ice-cold ethanol and dried at 55°C. The DNA was resuspended in 200 µl sterile water and incubated at 55°C for 1 h. Following the isolation, samples were kept at 4°C.

Table 3.22: Primers for genotyping the *Sppl3* KO mouse lines. The first PCR only gives rise to product when there is a WT allele present. The second PCR recognises the presence of the genetrap. If both PCRs give a band then the mouse is heterozygous, while if only one of the two gives a band the mouse is either WT or KO.

WT allele – 1st PCR	**Sequence (5'->3')**
p95-Fw-Wt-mouse-Papadopoulou	GCAGGCATCTGCAGAACTCATG
p96-Rv-Wt-mouse-Papadopoulou	GCCGTGACACAGCAAGTGCA
Product length	440
Genetrap – 2nd PCR	**Sequence (5'->3')**
p97-fw-genetrap-mouse-Papadopoulou	AAATGGCGTTACTTAAGCTAGCTTGC
p98-rw-genetrap-mouse-Papadopoulou	AAACCTTTACTAGGGAGAGGCGTCA
Product length	220

Different quantities of each primer were used to avoid unspecific bands (table 3.24). A common, "touch-down", PCR program (table 3.23) was used for both PCRs and both negative and positive controls were always included in the analysis. The PCR products were separated on a 1.5% Agarose in 1xTAE.

Table 3.23: PCR program for genotyping. The same PCR program was used for the genotyping of both alleles.

Genotyping PCR program		
94°C	10 min	
94°C 68°C 72°C	30 sec 30 sec 45 sec	Decrease 1°C/cycle x 10
94°C 58°C 72°C	15 sec 30 sec 45 sec	Repeat 25-30 cycles
72°C	5 min	
10°C	∞	

Table 3.24: PCR mix for genotyping. The mix for each PCR differed in the primer amount to ensure specificity.

Template 1 µl	**WT allele**	**Genetrap**
Forward primer (10 µM)	0.25 µl	0.5 µl
Reverse Primer (10 µM)	0.25 µl	0.5 µl
5x Green Buffer	5 µl	5 µl
dNTPs	0.5 µl	0.5 µl
Taq Polymerase	0.5 µl	0.5 µl
ddH_2O	17.5 µl	17 µl

3.2.6.2 Rotarod Performance Test

The mice were analysed in groups of littermates containing wildtype, heterozygous and knockout animals. Each group was brought into the rotarod room 15 min before the start of the test to acclimatise to the environment. The rotarod was set on a stable speed of 3 rpm and the mice were placed on the rotating beam. When all mice were stable on the beam the speed increase was activated going from 3 to 30 rpm in 480 sec (8 min). The time in sec the mice were walking on the rotarod from the beginning of the acceleration period was measured. Every time a mouse fell, the timer was automatically stopped. Each group of mice had no training session but three trials per session and 15 minutes of break between each of the trials.

3.2.6.3 Metabolic cages

Mice were individually housed for five days in metabolic cages from Tecniplast (Buggiate, Italy). Mice were provided with a house, dry food and water. The food and water were weighed at the beginning of each day before and after supplementing the mice with fresh food and water. The faeces and urine of the mice were collected daily and separately by the structure of the cage. After the five days period the mice were placed back in the original cages.

3.2.7 Tissue Homogenates from mouse and human samples

For homogenisation of tissue and organs from mice and humans, the same protocol was used. Organs analysed include brain, heart, liver, kidney, testis, muscle and others. The organs were removed from the mouse *post mortem* and snap frozen in liquid nitrogen. Human testis samples

were previously described (Mayer et al. 2016). The patients had granted written Informed Consent, for the scientific use of the samples and the Ethical Committee (Ethikkommission, Technische Universität München, Fakultät für Medizin, München, project number 5158/11) has approved the study. All relevant guidelines and regulations were followed in the experimental procedures. All samples were kept in -80°C until analysis.

Organs (100-250 mg) were thawed on ice and were homogenized in ice cold organ-lysis buffer using a Wheaton tissue grinder (Thermo Fisher) and 23G needles. Samples were first centrifuged at 500 g, 4°C for 5 min to remove big remains and then the supernatant was subjected to further centrifugation at 100.000 g, 4°C for 60 minutes. Pellets were resuspended in organ-lysis buffer containing 2% (v/v) Triton X-100 to solubilise the cell membranes and incubated for 30 min on ice. To remove cell debris, samples were centrifuged at 17000 g, 4°C for 30 min and the supernatants were used for protein quantification by BCA and further analysis by immunoblot.

3.2.8 Immunostaining and Confocal Imaging

This technique was used for visualising localisation of intracellular proteins, and shape and condition of intracellular organelles. Cells were seeded at low confluency (30%) on 15mm Poly-L-Lysine-coated coverslips and where indicated, treated with siGENOME siRNA during seeding (3.2.2.1.2). All cells used for the imaging were stably transfected with cDNA plasmids. On day 3, the media was removed from the cells and they were washed with filtrated PBS one time before being fixated for 20 min at RT, under luminal flow, in 4% paraformaldehyde (PFA) in PBS. Following fixation, cells were washed three times with PBS and were permeabilized using 5% (w/v) BSA supplemented with 0.2% (v/v) Triton X-100 and 0.5% (w/v) SDS for 5 min. Unspecific binding was blocked at RT with 5% (w/v) BSA for one hour. After blocking, cells were incubated with primary antibodies diluted in 5% (w/v) BSA for 16-20 hours at 4°C, taking care that the samples would not dry. After extensive washing (6 times with 1xPBS), the cells were incubated with secondary antibodies diluted 1:400 in 5% (w/v) BSA for one hour at RT. Cells were washed another 6 times with 1xPBS and in order to visualise the nuclei,

incubated for 5 min with 1:10000 4,6-Diamidin-2-phenylindol (DAPI, 5µg/mL) solution at RT. The coverslips were loaded onto glass plates facing down using Mowiol mounting media and left to dry overnight avoiding direct lighting. Pictures were taken using a LSM 710 Zeiss Observer Z.1 confocal microscope with a 40x-60x oil lens, and 1-2x optical zoom. Airy Unit (AU) 1 was preferred when possible and AU2 was used when necessary. The intensity of the pictures was increased for visualization purposes with the ZEN lite 2011 program. Scale bars were inserted using the same software.

3.2.9 Histological analysis

Histological analysis of murine testis was performed by our collaborator Artur Mayerhofer. The samples were fixed by immersion in Bouin's solution and were embedded in paraffin according to standard procedures. The paraffin sections were immunohistologically stained using the ABC System (Vector Laboratories, California, USA) and diaminobenzidine as peroxidase substrate. Anti-Cab45 was the only antibody utilized in this analysis in 1:500 dilution. To control for unspecific binding, rabbit polyclonal control IgG (BioLegend) was used as a negative control. Hematoxylin was used to visualize the nuclei. Images were taken with a Zeiss Axiovert microscope equipped with an Insight Camera (18.2 Color Mosaik) and Spot advanced software 4.6 (SPOT Imaging Solutions, Sterling Heights, MI, USA). For the quantifications, 14 images were used, each containing one stage VII/VIII seminiferous tubule. These stages were selected because they are characterized by two generations of spermatids and can be reliably recognized in immuno-stained sections (also by the presence of residual bodies (Meistrich and Hess 2013)). Three equally sized squares were positioned randomly around each seminiferous tubule and the pre-acrosomal resembling structures within each square were counted. The average of the three squares was assigned to each tubule.

3.2.10 Mass Spectrometry

Mass Spectrometry analysis was performed by our collaborator Stephan Müller. Cells were harvested and centrifuged at 1000 rpm for 5 min at 4°C, the cell pellets were resuspended in STE-Buffer and lysed with a 27-gauge needle. Samples were centrifuged for 10 min at 800 g to remove cell nuclei, then 10 min at 15000 g to remove mitochondria and finally ultracentrifuged for 1 hour 100.000 g to pellet the membranes. The membrane pellets were washed two times with 100 mM Na_2CO_3 and centrifuged for 30 min at 100.000 g after each wash. The cleaned pellets from membrane preparations were dissolved in lysis buffer and the protein concentration was calculated using the Pierce 660nm protein assay (Thermo Fisher Scientific, US). 15 µg of protein were subjected to proteolytic digestion with trypsin and LysC (Promega, Germany) using the filter-aided sample preparation (FASP) with Vivacon centrifugal concentrators (30 kDa cut-off, Sartorius, Germany) according to published protocol (Wisniewski et al. 2009). The peptides were enriched and desalted using a stop and go extraction with self-packed C18 Tips (3M Empore, US) (Rappsilber et al. 2003). Eluted peptides were then dried by vacuum centrifugation and dissolved in 20 µl 0.1% formic acid. Finally, the peptides were analysed on an Easy nLC 1000 nanoHPLC (Thermo Scientific, US), coupled online via a Nanospray Flex Ion Source (Thermo Scientific, US) equipped with a PRSO-V1 column oven (Sonation, Germany) to a Q-Exactive mass spectrometer (Thermo Scientific, US). 1.3 µg of peptides were separated on an in-house packed C18 column (30 cm x 75 µm ID, ReproSil-Pur 120 C18-AQ, 1.9 µm, Dr. Maisch GmbH, Germany) using a binary gradient of water (A) and acetonitrile (B) supplemented with 0.1% formic acid (0 min., 2% B; 3:30 min., 5% B; 137:30 min., 25% B; 168:30 min., 35% B; 182:30 min., 60% B) at 50°C column temperature. Data dependent acquisition method was used and full mass spectrometric scans were acquired at a resolution of 70,000 (m/z range: 300-1400, AGC target: 3E+6). The ten most intense peptide ions per full MS scan were chosen for peptide fragmentation (resolution: 17,500, isolation width: 2.0 m/z, AGC target: 1E+5, NCE: 25%). A dynamic exclusion of 120 sec was used for peptide

fragmentation.

Data was analysed with the software Maxquant (maxquant.org, Max-Planck Institute Munich) version 1.5.5.1 (Cox et al. 2014). The acquired data was compared against a reviewed fasta database of *Homo sapiens* from UniProt including protein isoforms (downloaded: August 8th 2017, 42219 entries). The defined protease was trypsin with two missed cleavages allowed for the database search. The option "first search" was used to recalibrate the peptide masses within a window of 20 ppm. For the main search peptide and the peptide fragment, mass tolerances were set to 4.5 and 20 ppm, respectively. Carbamidomethylation of cysteine was defined as static modification. Acetylation of the protein's N-terminal, as well as oxidation of methionine were set as variable modifications. The false discovery rate (FDR) for both peptides and proteins was adjusted to smaller than 1%. At least two ratio counts of razor peptides were required for label free quantification (LFQ). Only unique peptides and razor were used for quantification. For the data analysis, the software Perseus (version 1.5.8.5) was used. The protein LFQ intensities were log2 transformed and a two-sided student's t test was applied to evaluate the significance of proteins with changed abundance. Finally, a permutation based false discovery rate estimation was also used (Tusher et al. 2001).

3.2.11 Pathway Analysis

Using the online STRING 10.5 (https://string-db.org/) program a bioinformatic analysis of the SPPL2c candidate substrates that were identified through the mass spectrometric approach was performed. All potential type II and type IV TM proteins were uploaded to the programme and the possible interaction networks were visualised. Using the function "More" of STRING 10.5, potential SPPL2c substrates that were missed by the proteomic analysis were identified.

3.2.12 Lectin chip microarray (LecChip)

Lectin analysis was performed by our collaborator Merav Shmueli on spermatozoa collected from the SPPL2c transgenic mice by Torben Mentrup and Johannes Niemeyer. Mature

spermatozoa of SPPL2c knockout and wildtype mice were recovered from the cauda epididymides (n = 4 per group) as described in (Niemeyer et al. 2019) and were used for lectin chip microarray analysis (LecChip). Samples were lysed in STEN-Buffer, incubated on ice for 30 min, centrifuged at 10000 g for 10 min and brought to a protein concentration of 0.05 mg/ml in TBS. Reagent Cy3 NHS ester (PA13101, GE Healthcare Life Sciences), dissolved in dimethyl sulfoxide, was added at a final concentration of 0.05 mg/ml for 1 hour at RT. Excess reactive reagent was inactivated with free lysine (final concentration, 0.05 mM; L5501, Sigma-Aldrich). Probing Solution (provided by the manufacturer) was used to wash three times the LecChip (GlycoTechnica Ltd.), and to add the Cy3-labeled sperm lysates (1 µg/ml) (n = 4 per group) to the wells (100 µl per well). Samples were incubated overnight at 18°C and the following day the LecChip was washed 30 min with TBS and 30 min with double-distilled water. An InnoScan 710 Microarray scanner (Innopsys) was used to scan the LecChip and the results were analysed with CLIQS Array Professional software (TotalLab). In total, 45 lectin intensities were measured per sample. All samples had an average Pearson correlation coefficient calculated at 0.98 and above. Lectin intensities were log2 transformed and a two-sided student's t test was used to evaluate the significance of lectin binding with changed abundancy.

3.2.13 Statistical analyses

All statistical analyses concerning WB quantification and the count of preacrosomal structures were conducted with GraphPad Prism 7 (Graphpad, La Jolla, USA) and details are indicated in the respective figure legends. In general, at least three biological replicates were performed for statistical analysis. Values that had to be transformed to ratios to allow an equal comparison and visualisation were then transform to log2 for the statistical analysis. For comparison of 2 groups with equal size simple unpaired, two-tailed student's t test was used. If the 2 groups were not of equal size, a Welch's t test was used. If more than two groups were being compared to the same control data set, multiple unpaired, two-tailed t tests were performed and then

corrected by the Holm-Šídák method. For the mouse data with multiple measurements per mouse and per genotype, a 2-way ANOVA test with Sidak multiple corrections was used. The significance threshold was set with *p $<$ 0.05, **p $<$ 0.01 and ***p$<$0.001.

4. Substrate requirements of SPPL3

A wide variety of SPPL3 substrates have been identified in the past few years and the vast majority of them are implicated in glycosylation being either glycosidases or glycosyltransferases, such as N-acetylglucosaminyl-transferase V (GnTV) and exostosin-like glycosyltransferase 3 (EXTL3) (Voss et al. 2014a, Kuhn et al. 2015). In all cases, SPPL3 is capable of cleaving the full length substrate and the cleavage site has been analysed for GnTV (Voss et al. 2014a, Kuhn et al. 2015). The aim of this part is to understand the substrate requiremnets of SPPL3 in more detail and to this end, point mutations were generated on the substrates to identify amino acid residues important for intramembrane proteolysis. Such strategy has been successfully employed in the past to define a consensus cleavage site of rhomboid I-CLIPs (Strisovsky et al. 2009) and the sequence requirements of Bri2 for SPPL2b cleavage (Fluhrer et al. 2012).

4.1 Results

4.1.1 Impact of the GxxxG sequence of GnTV on cleavage by SPPL3

The best-characterised SPPL3 substrate is GnTV and it was chosen as the first target for mutagenesis. Analysing the amino acid sequence of GnTV, the first area of interest was found within the TMD and consists of two glycines that are separated by 3 amino acids (**G**FIW**G**), we refer to this sequence as GxxxG (Fig. 4.1). A similar GxxxG sequence is also present in Bri2 (**G**VIL**G**), a substrate of SPPL2a/b, but was found not to be of importance for the cleavage of Bri2 by SPPL2b (Fluhrer et al. 2012).

Glycines have the ability to slightly destabilise an α-helix when located within the TMD. To test their importance as α-helix destabilising residues, a series of mutants that would either increase or decrease the α-helical stability at the respective position were generated. Alanines (A) are capable of stabilising an α-helix, although they function more effectively outside of the membrane. Leucines (L) are the most effective α-helix stabilisers within the boundaries of the TMD. In contrast, prolines (P) are the strongest α-helix-destabilising amino acids within the TMD. All three amino acids were used and either replaced one of the glycines from GxxxG

motif at a time or both simultaneously (Fig. 4.1). Based on proteases preference to bind on more open structures, like β-strands, to perform cleavage, it is expected that a looser α-helix would constitute a more favourable substrate (Tyndall et al. 2005, Madala et al. 2010).

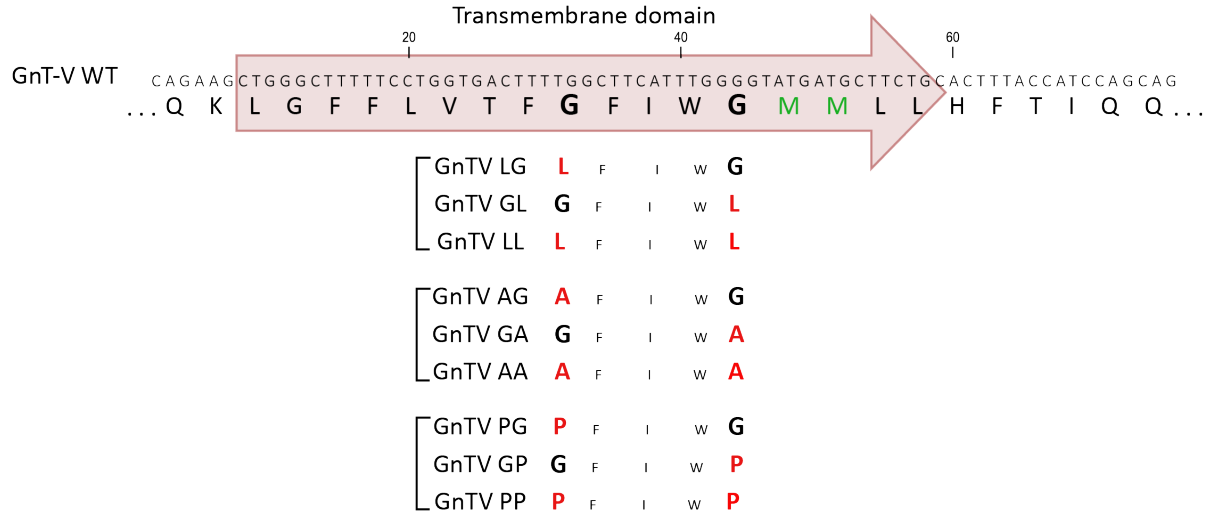

Fig. 4.1: GnTV GxxxG mutants. The amino acid sequence of a part of GnTV is depicted together with the respective nucleotides triplets of the mRNA. The predicted TMD is annotated within the red arrow, which also depicts the N- to C-terminal orientation of the protein. The α-helix destabilizing glycines are marked in bold G. Below the sequence of GnTV the respective amino acid sequences of the three sets of mutations are shown. The mutated amino acids are marked in red.

4.1.1.1 Effect of GxxxG mutants on GnTV shedding

To assess cleavage of wildtype GnTV (GnTV WT) and its mutants, double-tagged variants of all substrate constructs were expressed in T-Rex^{TM}-293 (HEK293) cells. These cells have an endogenous expression of SPPL3 that efficiently cleaves GnTV. Using the N-terminal Flag-tag, only full length GnTV is detected, while with the C-terminal V5 tag both the full length (FL) and the secreted, soluble GnTV (sGnTV) are detected. However, the sGnTV is detected in the supernatant of the cells, while the FL only within the cells (Fig. 4.2).

Certain glycine mutations of the GxxxG sequence affected the ratio of secreted sGnTV compared to full length GnTV. More specifically, for the glycine to alanine mutations, only one alanine at a time was not enough to significantly reduce secretion. However, simultaneously mutating both glycines to alanines induced a small (30%) but statistically significant decrease in the secretion of sGnTV (Fig. 4.3A). Although mutation of the first glycine in the GxxxG to leucine had the

expected effect (LG mutant) and significantly decreased the secretion of sGnTV, mutating the second glycine (GL mutant), or both at the same time, notably and significantly increased the shedding of GnTV (Fig. 4.3B).

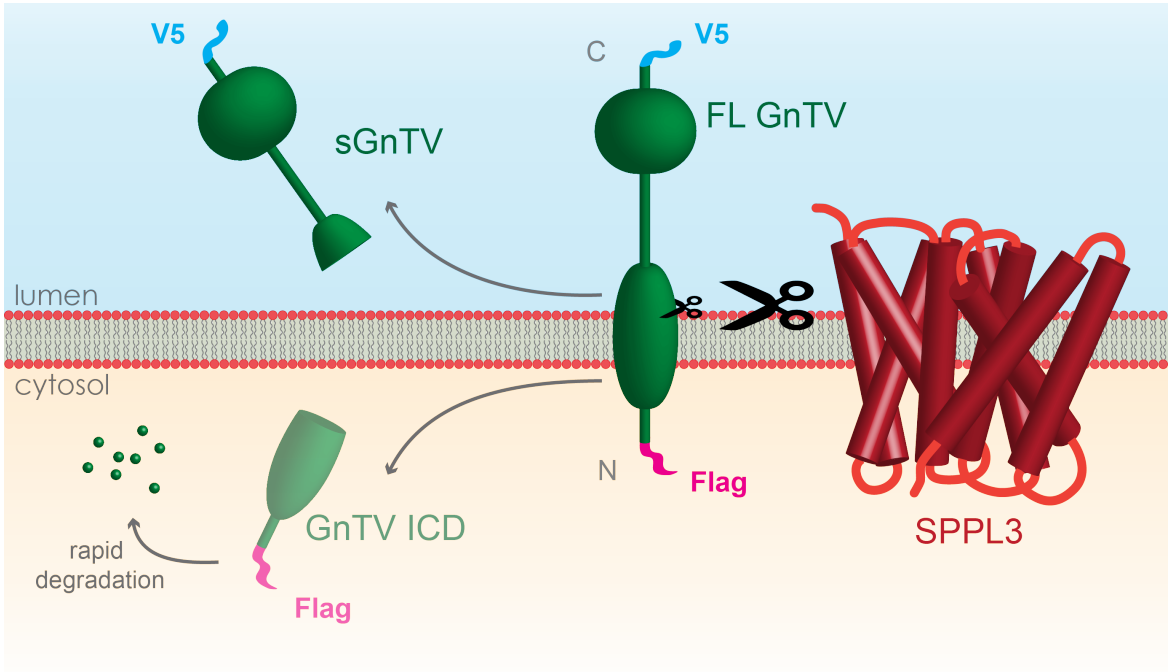

Fig. 4.2: Cleavage of double-tagged GnTV. Ectopically expressed GnTV is tagged with a Flag tag on the N-terminus and a V5 tag on the C-terminus. Full-length GnTV (FL GnTV) can be detected by both tags in cell lysates. Cleavage by SPPL3 leads to the release of soluble GnTV (sGnTV) that can be detected only with the V5 tag in conditioned media. The GnTV ICD is very small in size (4kDa) and gets rapidly degraded making it thus, non-detectable.

Lastly, introducing an α-helix-destabilising proline instead of one glycine (PG, GP mutants) significantly increased the cleavage of GnTV. This is in accordance with data suggesting that less stable α-helices make for better substrates of intramembrane proteases. Also in the case of proline substitutions, the two glycine-positions have a noticeable difference in the intensity of the effect they cause, with the position closer to the cleavage site appearing more crucial, still they both show the same tendency to increase shedding (Fig. 4.3C). However, inserting two prolines simultaneously into the TMD of GnTV strongly interferes with the expression and maturation of the protein, as can be seen by the lack of mature GnTV in the lysates (Fig. 4.3C). Therefore, no quantification or assessment of the double P mutants was possible.

To analyse whether introducing the mutations on the substrate might affect the intracellular

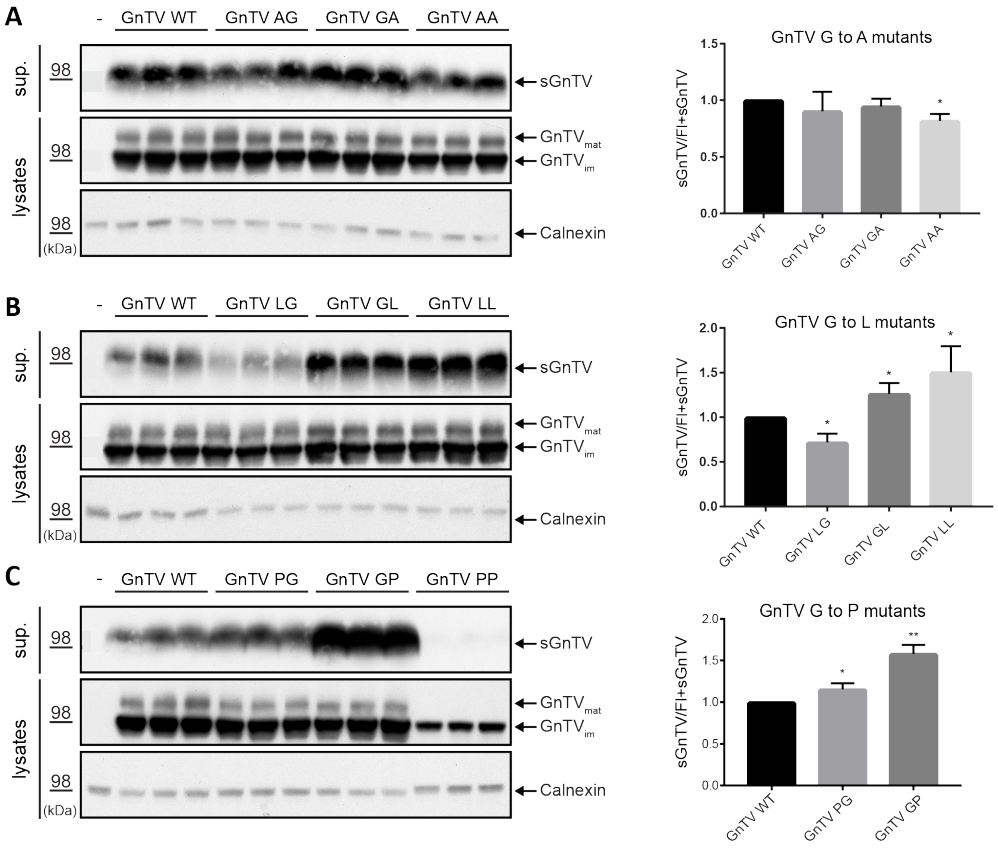

Fig. 4.3: Cleavage of GnTV GxxxG mutants. A-C. Western blots depicting ectopically expressed WT GnTV and mutants of the GxxxG motif in HEK293 cells. Secretion of soluble GnTV (sGnTV) is visible in the supernatant (sup.) while the full length GnTV is detected in the lysates by V5 monoclonal antibody. Calnexin was used as a loading control. For quantifications, sGnTV was compared to the amount of full-length GnTV (FL GnTV), including mature ($GnTV_{mat}$) and immature ($GnTV_{im}$) GnTV. The secretion of WT GnTV was set to 1. Three biological replicates are depicted in the bar graphs (mean + SD). Multiple unpaired, two-tailed t tests with Holm-Sidak multiple comparisons correction *$p<0.05$, **$p<0.01$.

localisation of GnTV, ectopically expressed wildtype GnTV and all three G to A mutants were visualised by immunofluorescence via the V5 tag in HEK293 cells. As GnTV is expected to localise predominantly in the Golgi, the Golgi protein Giantin was used as a marker. GnTV WT and all three mutants tested were found to share similar staining patterns and colocalised primarily with Giantin (Fig. 4.4). This suggests that SPPL3 should still be able to catalytically process mutant GnTV, as both protease and substrate localise in the Golgi. Due to technical limitations, the localisation of the other mutants was not analysed so far but is assumed to follow the patterns of WT GnTV, as is the case for the G to A mutants.

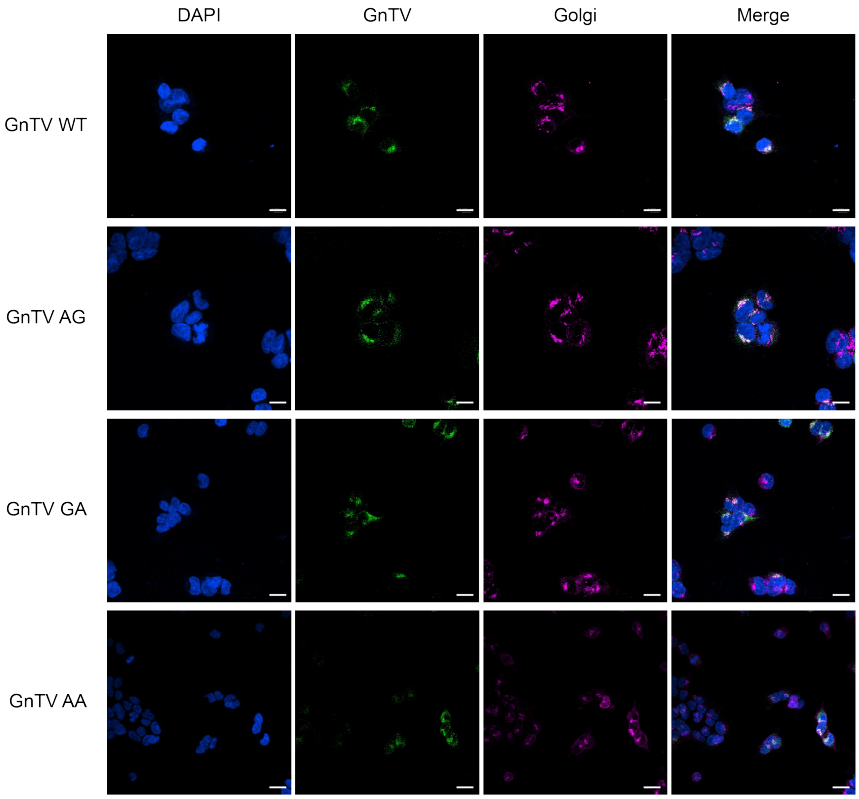

Fig. 4.4: Immunofluorescent stainings of GnTV GxxxG to A mutants. Ectopically expressed WT and mutated GnTV was visualized using the anti-V5 antibody. The Golgi was stained using the anti-Giantin antibody. All GnTV mutants tested appear to predominantly colocalise with the Golgi marker, similarly to WT GnTV. Scale bar 5 µm.

4.1.2 Impact of GnTV cleavage site on cleavage by SPPL3

The second evident area of interest in GnTV is the cleavage site (MMLLHF) that was identified by analysing the cleavage of a truncated tagged GnTV by MALDI-TOF mass spectrometry (Voss et al. 2014a). Primary and secondary cleavage sites were identified by this technique and were later confirmed (Kuhn et al. 2015). Interestingly, TNFα, a substrate of SPPL2a/b, also shares a similar sequence at its cleavage site comprising LLHF. To analyse the contribution of this site to substrate recognition and cleavage, all amino acids surrounding the cleavage sites were mutated to alanine, one at a time or in pairs. The aim was to assess whether a more stable α-helix around the cleavage site would decrease shedding of GnTV by SPPL3 or whether a specific amino acid is crucial for the processing (Fig. 4.5).

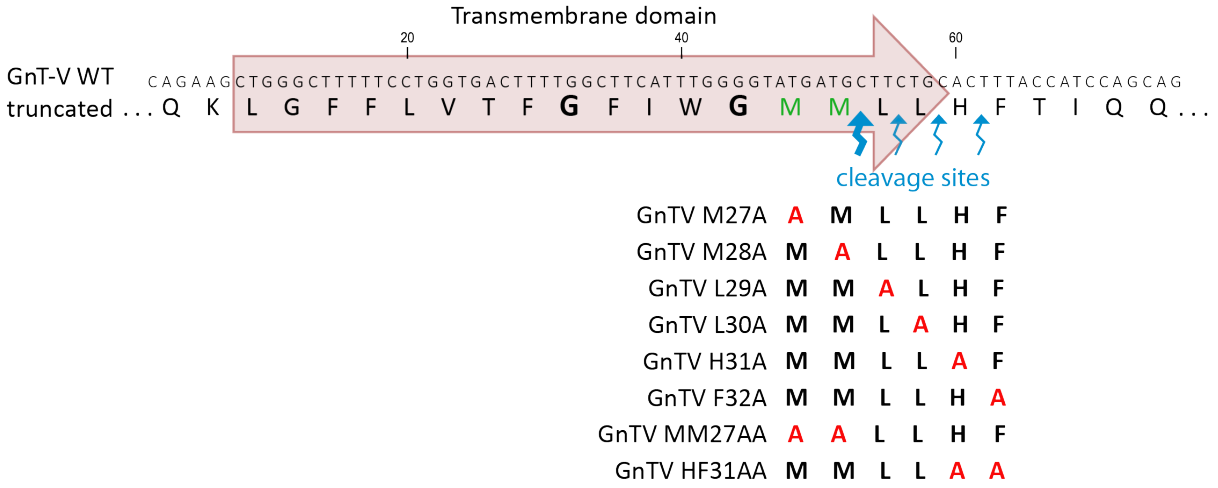

Fig. 4.5: GnTV cleavage site mutants. The nucleotide and amino acid sequence of GnTV is depicted as in Fig. 4.1. The cleavage sites of GnTV by SPPL3 are marked by the blue arrows, while the primary cleavage site is marked with a thicker line. Underneath all initially tested mutations for this site are listed in red.

4.1.2.1 Effect of cleavage site mutants on GnTV Shedding

The effect of the mutations on the cleavage of GnTV was assessed as before (compare Fig. 4.3). Although some of the mutations did not strongly alter the shedding rate of GnTV, three mutations (M27A, L30A and F32A) showed an increase of shedding and one mutation (H31A) a decrease (Fig. 4.6).

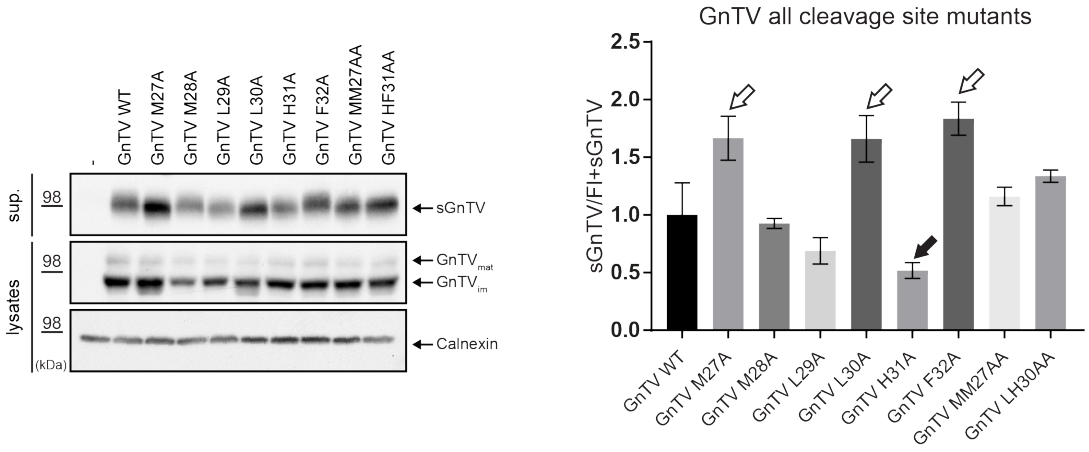

Fig. 4.6: Processing of GnTV cleavage site mutants. Western blots depicting ectopically expressed WT GnTV and GnTV cleavage site mutants in HEK293 cells. Secretion of soluble GnTV (sGnTV) is detected in the supernatant (sup.) while the full length GnTV in the lysates. Calnexin was used as a loading control. For quantifications, sGnTV was compared to the amount of full-length GnTV (FL GnTV), including mature ($GnTV_{mat}$) and immature ($GnTV_{im}$) GnTV. The secretion of WT GnTV was set to 1. Open arrows point to increased mutants while the filled arrow marks the decreased mutant. Two biological replicates are depicted in the bar graphs (mean +/- SD), no significance testing performed.

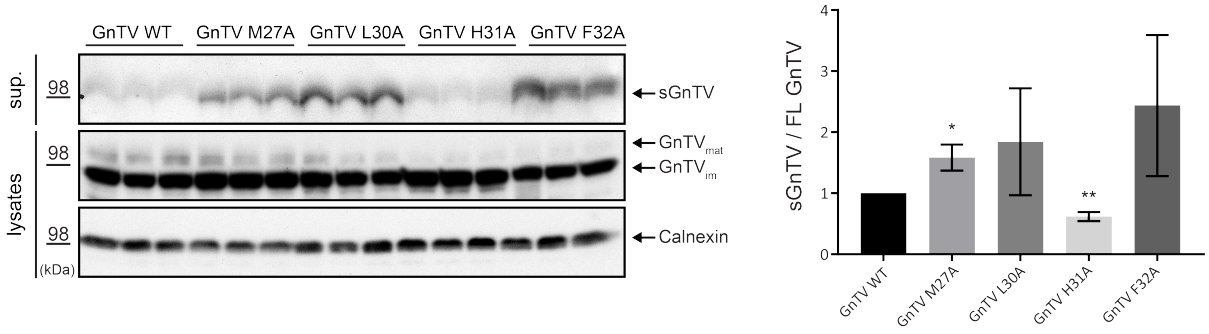

Fig. 4.7: Selection of GnTV cleavage site mutants. Western blots depicting ectopically expressed WT GnTV and selected mutants of the cleavage site in three technical replicates in HEK 293 cells. Calnexin was used as a loading control. For the quantifications, sGnTV was compared to the amount of full-length GnTV (FL GnTV), including mature ($GnTV_{mat}$) and immature ($GnTV_{im}$) GnTV in three biological replicates for each mutant. The secretion of WT GnTV was set to 1 (mean +/- SD). Multiple unpaired, two-tailed t tests with Holm-Sidak correction *$p<0.05$, **$p<0.01$.

These mutants were further analysed and were all found to be altered with the GnTV H31A mutant being the only significantly less secreted (Fig. 4.7). The localisation of all four mutants with altered processivity was visualised by immunofluorescence, as before, and appeared unaffected by the mutations (Fig. 4.8). Both the Golgi and the ER were indicatively stained to compare the localisations.

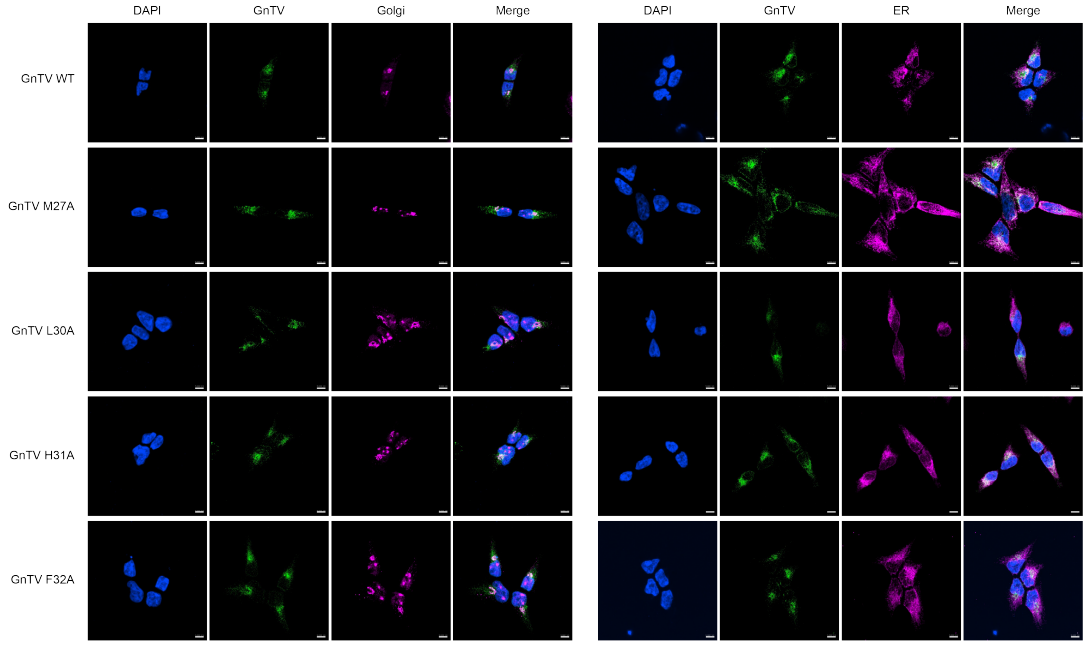

Fig. 4.8: Immunofluorescent stainings of GnTV cleavage site mutants. Anti-V5 monoclonal antibody was used to visualise ectopically expressed WT and mutated GnTV. The Golgi was stained using the anti-GM130 antibody and the ER using an anti-BIP antibody. All GnTV mutants appear to colocalise predominantly with the Golgi marker, similarly to WT GnTV. Scale bar 5 µm.

4.1.2.2 Importance of histidine at the border of the substrate's TMD

The histidine in position 31 of GnTV is of interest not only because it is the only position that significantly decreased GnTV shedding when mutated to an alanine, but also because of its positive charge. What made this histidine at the border of the TMD even more intriguing is the fact that EXTL3, another confirmed SPPL3 substrate (Kuhn et al. 2015), also has a histidine close to the border of its TMD, where the cleavage site of SPPL3 was predicted.

In order to analyse the role of this amino acid in the shedding of GnTV in more detail, both substrates were further mutated using either a different positively charged amino acid (arginine, R), a negatively charged amino acid (aspartic acid, D), or an α-helix stabilising neutral amino acid (leucine, L) (Fig. 4.9).

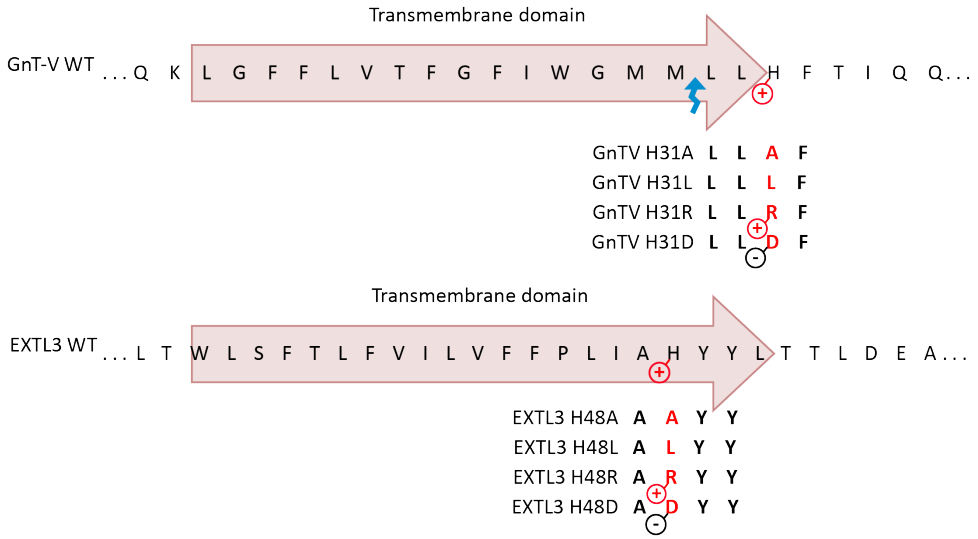

Fig. 4.9: GnTV and EXTL3 histidine mutants. The amino acid sequences of a part of GnTV and EXTL3 are depicted. In both sequences, the predicted TMD is marked by a red arrow, which also points the N- to C-terminal direction. The histidine mutated in both substrates is marked by its positive charge. Underneath each WT protein, there is a list of all histidine mutations in red and the charge of the amino acids is marked when present.

The results from the GnTV to some degree matched our expectations. Alanine and leucine are predicted to stabilise the TM α-helix of GnTV and both decreased the secretion of sGnTV in a statistically significant manner (Fig. 4.10). However, both mutations decreased the secretion of GnTV only by a small fraction (20-30%), indicating that the histidine facilitates cleavage but is not a prerequisite.

In contrast, both the negatively charged aspartic acid and the positively charged arginine significantly increased processing of GnTV (Fig. 4.10).

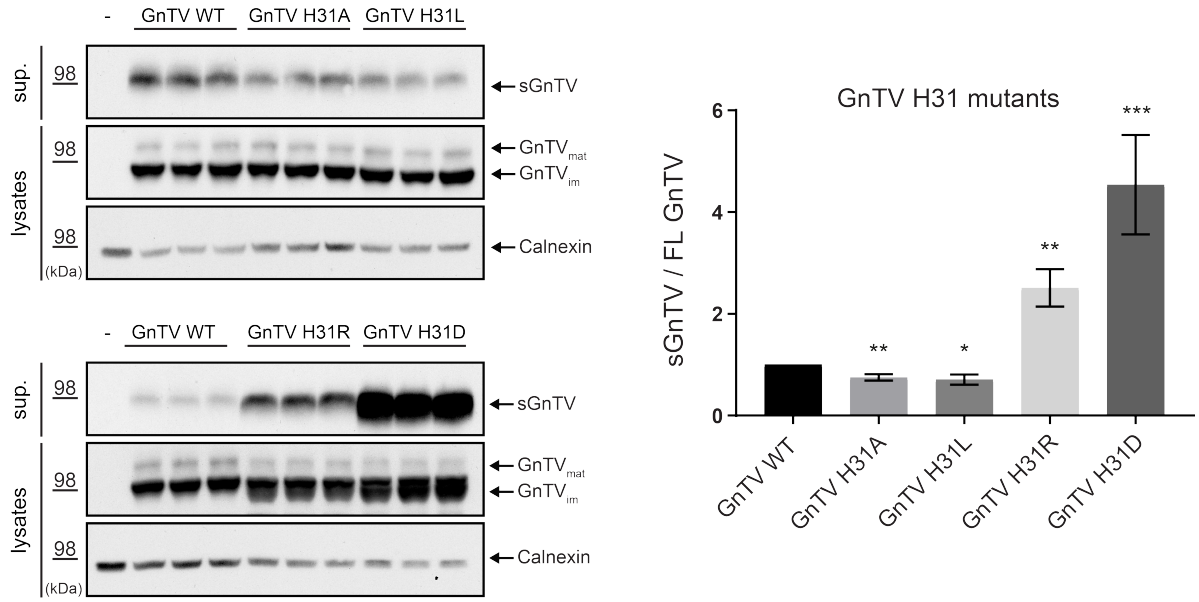

Fig. 4.10: Processing of GnTV H31 mutants. Western blots depicting ectopically expressed WT GnTV and mutants of histidine 31 in HEK 293 cells show the level of soluble GnTV (sGnTV) in the supernatant (sup.) and the full-length GnTV in the cell in three technical replicates. Calnexin was used as a loading control. For quantifications, sGnTV was compared to the total amount of full-length GnTV (FL GnTV), including mature ($GnTV_{mat}$) and immature ($GnTV_{im}$) GnTV. The secretion of WT GnTV was set to 1. Three biological replicates are depicted in the bar graph (mean +/- SD). Multiple unpaired, two-tailed t tests with Holm-Sidak correction *$p<0.05$, **$p<0.01$, ***$p<0.001$.

Unexpectedly, the results on EXTL3 did not follow the exact same tendencies as for GnTV. While mutating the histidine to leucine did not significantly alter the cleavage of EXTL3, mutating the histidine to alanine strongly increased the secretion of EXTL3 (Fig. 4.11). This observation is counter intuitive and further testing was used to control whether this increase of EXTL3 secretion is dependent on SPPL3 (4.1.3.1).

Mutation of the histidine into a different positive amino acid, arginine, significantly decreased ETXL3 secretion. Mutating the histidine to the negatively charged aspartic acid significantly increased shedding (Fig. 4.11).

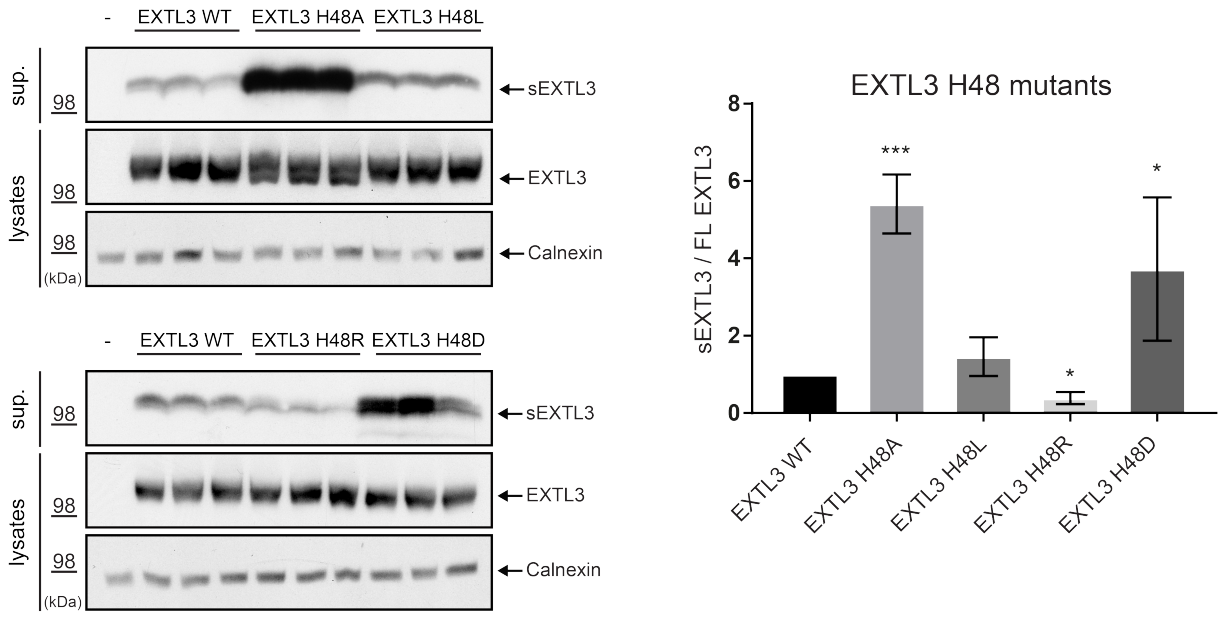

Fig. 4.11: Processing of EXTL3 H48 mutants. Western blots depicting ectopically expressed WT EXTL3 and mutants of histidine 48 in HEK 293 cells show the level of soluble EXTL3 (sEXTL3) in the supernatant (sup.) and the full-length EXTL3 in the lysates in three technical replicates. Calnexin was used as a loading control. For quantifications, the amount of sEXTL3 was compared to the amount of intracellular full-length EXTL3. The secretion of WT EXTL3 was set to 1. Three biological replicates are depicted in the bar graph (mean +/- SD). Multiple unpaired, two-tailed t tests with Holm-Sidak correction *$p<0.05$, ***$p<0.001$

4.1.3 Ability of SPPL3 to process the GnTV and EXTL3 mutants

In order to confirm that SPPL3 is the major protease responsible for the cleavage of the GnTV and EXTL3 mutants, we analysed whether processing of the mutants decreases in absence of SPPL3. To this end, the CRISPR/Cas9 genome editing technique was used to generate a HEK293 SPPL3 KO cell line. Two different, commercially available guide RNAs (gRNA1 and gRNA2) were used to target the *SPPL3* gene as described in 3.2.2.1.5. gRNA1 gave rise to only heterozygously mutated single cells clones, but gRNA2 gave rise to three clones with identical homozygous mutations that lead to an early stop codon in the mRNA. They were all characterised by the insertion of one nucleotide (T) at the targeted site (Fig. 4.12A) that led to an early stop codon in the mRNA (Fig. 4.12B) and no detectable SPPL3 levels in western blotting (Fig. 4.12C). Clone 11 was chosen for further experiments.

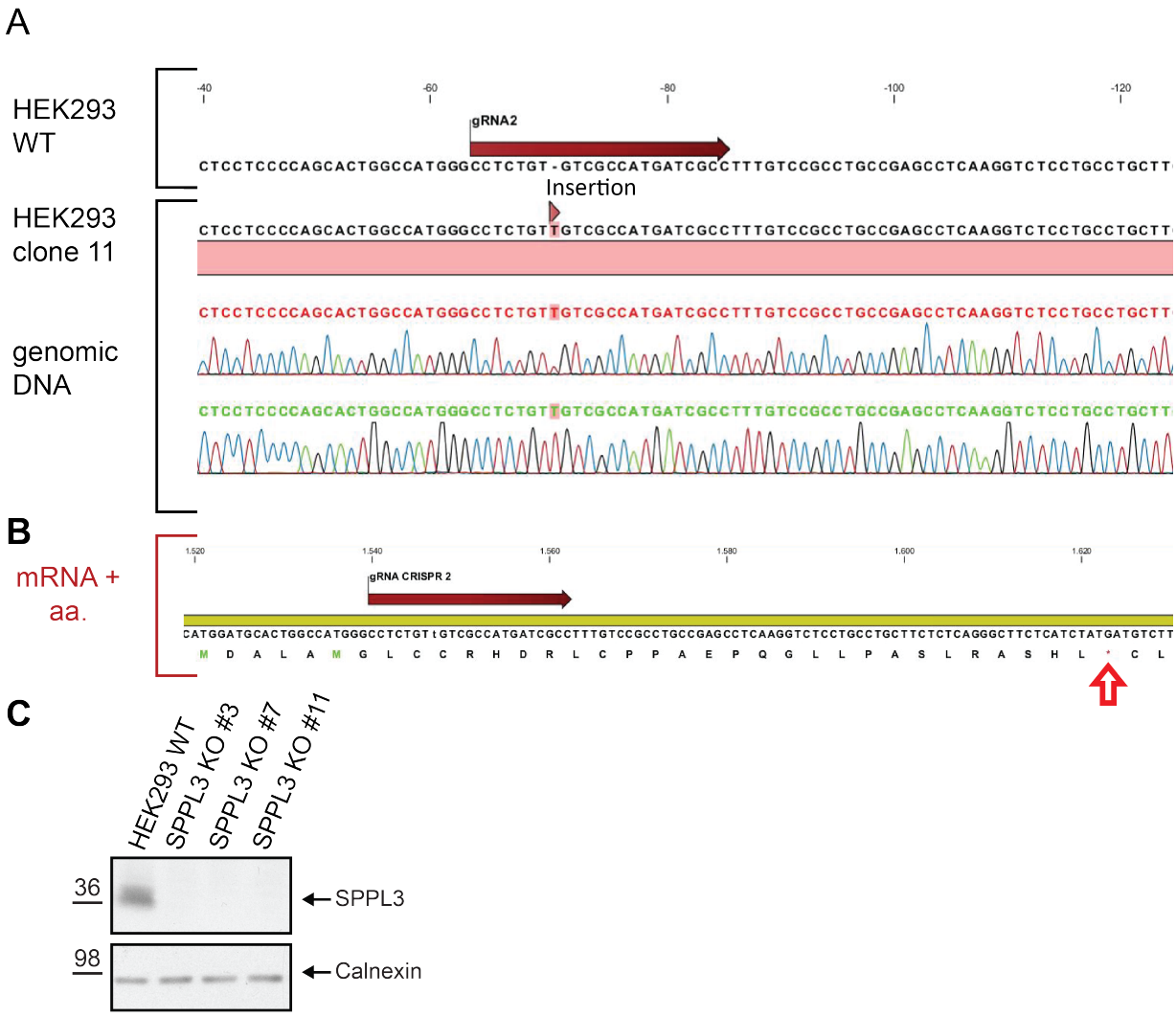

Fig. 4.12: HEK293 SPPL3 knockout (KO) cell line. A. Comparison of the wildtype human *SPPL3* genomic DNA with KO clone 11 is depicted confirming the presence of homozygous insertion of a thymidine, highlighted in red. **B.** mRNA sequence of clone 11 with the thymidine insertion and the amino acid sequence resulting from this nucleotide sequence. An early stop-codon is generated as indicated by a red arrow. **C.** Western blot analysis of control HEK293 cells and the three clones deriving from the CRISPR/Cas9 treatment, showing the absence of SPPL3 protein expression. Calnexin was used as a loading control.

Control HEK293 cells and HEK293 SPPL3 KO cells were transiently transfected with the WT substrates and the mutants, and the shedding efficiency was compared between the two cell lines. Regarding the GxxxG mutants, although WT GnTV appears to be the most consistently decreased substrate, all mutants are also significantly less secreted in absence of SPPL3 suggesting that they are all at least partly processed by SPPL3 (Fig. 4.13).

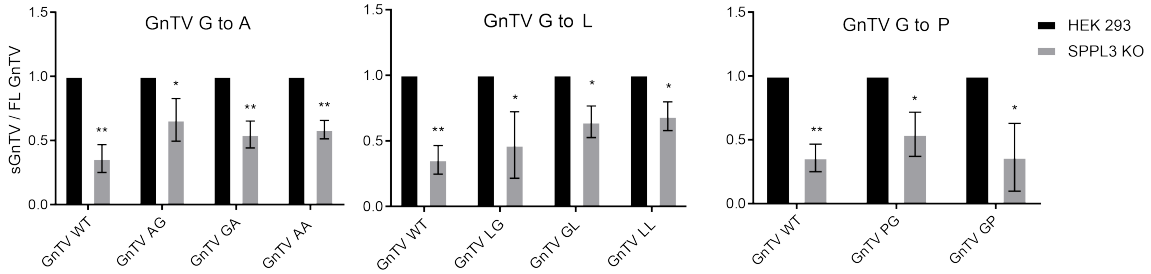

Fig. 4.13: Shedding of GnTV GxxxG mutants upon KO of SPPL3. Three biological replicates each consisting of three technical replicates were used for quantifications. All samples were analysed by Western Blot with Calnexin as loading control and endogenous SPPL3 expression was checked. For each construct, the amount of soluble GnTV (sGnTV) was compared to the total amount of full-length GnTV in the cells (as in Fig. 4.3). The secretion of GnTV for the control HEK293 cells was set to 1. Mean +/- SD, unpaired, two-tailed t tests *p<0.05, **p<0.01.

Regarding the cleavage site mutants of GnTV and EXTL3, the results upon SPPL3 KO are more unexpected, as it appears that a number of mutants are in fact only affected to a minor effect by the lack of SPPL3 expression. Apart of EXTL3 H48L, the levels of which are decreased to similarly to WT EXTL3, all other substrates appear to be cleaved by one or more additional proteases to different extents (Fig. 4.14). Some substrates, like GnTV H31A, H31L and EXTL3 H48D are partially but not consistently decreased. Meanwhile, other mutants such as GnTV H31D and EXTL3 H48A remain unaffected by the lack of SPPL3. Efforts to identify which protease is responsible for the secretion of these mutants were concentrated on the analysis of the cleavage of EXTL3 H48A, as the cleavage of this mutant was increased by several fold (Fig. 4.11).

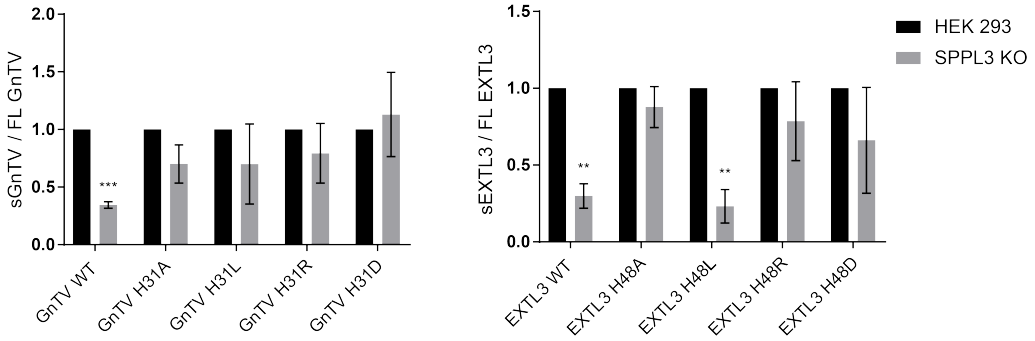

Fig. 4.14: Shedding of histidine mutants of GnTV and EXTL3 upon KO of SPPL3. Three biological replicates each consisting of three technical replicates were used for quantifications. All samples were analysed by Western Blot with Calnexin as loading control and endogenous SPPL3 expression was checked. For each construct, the amount of soluble substrate (sGnTV or sEXTL3) was compared to the total amount of full-length GnTV or EXTL3 in the cells (as in Fig. 4.10 and 4.11). The secretion of GnTV or EXTL3 for the control HEK293 cells was set to 1. Mean +/- SD, unpaired, two-tailed t test, *p<0.05, **p<0.01, ***p<0.001.

4.1.3.1 Analysis of EXTL3 H48A cleavage

Treating HEK293 cells stably and ectopically expressing either EXTL3 WT or EXTL3 H48A with either control siRNA or siRNA targeting SPPL3, confirms that the cleavage of EXTL3 H48A is not catalysed by SPPL3. While secretion of EXTL3 WT is significantly decreased upon SPPL3 knockdown, the secretion of the H48A mutant remains unaffected as expected from the previous results (Fig. 4.15A).

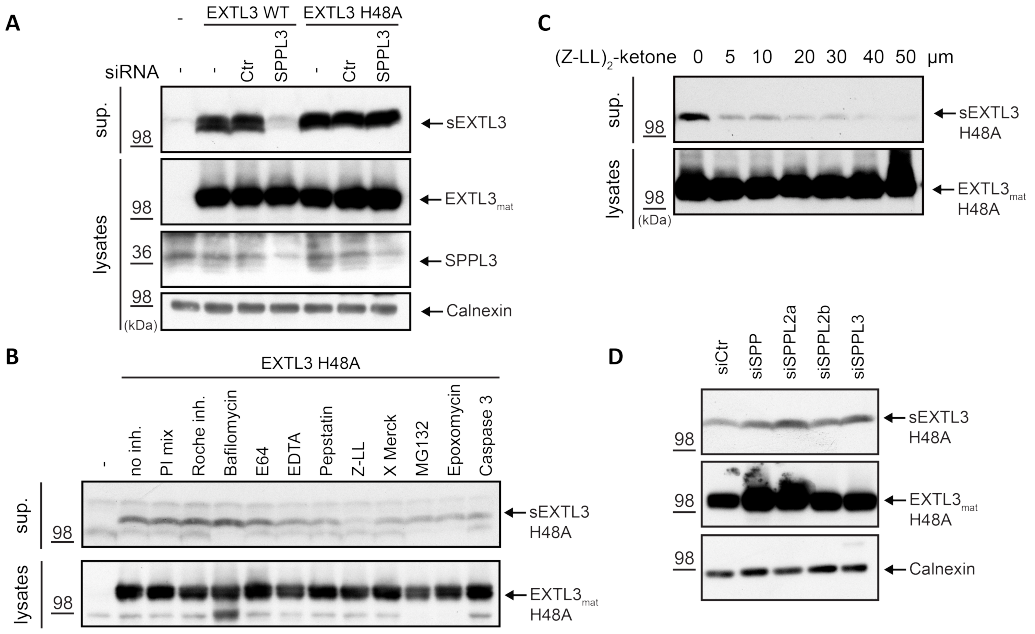

Fig. 4.15: Cleavage of EXTL3 H48A is SPPL3-independent and can be inhibited by (Z-LL)$_2$-ketone. **A.** Western blots of ectopically expressed EXTL3 WT and H48A mutant in HEK293 cells. Levels of soluble EXTL3 (sEXTL3) in the supernatant and the full-length EXTL3 in the lysate are depicted. Cells were treated with control siRNA (Ctr) and SPPL3 targeting siRNA as indicated, secretion of EXTL3 H48A remained unaffected. SPPL3 levels serve as a knockdown control and Calnexin as loading control. **B.** HEK293 cells ectopically expressing EXTL3 H48A were treated with different inhibitors as indicated. Only (Z-LL)$_2$-ketone treatment (Z-LL) shows a decrease in EXTL3 H48A secretion. **C.** HEK293 cells ectopically expressing EXTL3 H48A were treated with increasing concentrations of (Z-LL)$_2$-ketone as indicated, secretion of sEXTL3 H48A was reduced in a dose-dependent manner. **D.** Western blots of ectopically expressed EXTL3 H48A mutant in HEK293 cells treated with siRNA to specifically reduce the expression of the indicated SPP/SPPL-family members. None of the siRNAs had an effect on the secretion of EXTL3. Calnexin was used as a loading control.

Trying to determine which protease is responsible for the shedding of EXTL3 H48A, a variety of inhibitors was tested including bafilomycin, E64, EDTA, pepstatin, MG132, Epoxomycin, caspase 3, but only 1,3-di-(Ncarboxybenzoyl-L-leucyl-L-leucyl) amino acetone ((Z-LL)$_2$-ketone) affected EXTL3 H48A secretion (Fig. 4.15B). (Z-LL)$_2$-ketone reduced secretion of EXTL3 H48A in a dose-dependent manner showing strong inhibition from a low dose (Fig. 4.15C).

This inhibitor is known to inhibit SPP and SPPL2a/b, however knockdown of any of the three proteases by specific siRNA did not affect secretion of EXTL3 H48A (Fig. 4.15D). Further testing will be needed to identify the protease responsible for this cleavage.

4.2 Discussion

This study demonstrates that SPPL3 substrate cleavage is sensitive to single amino acid mutations in the predicted TMD and juxtamembrane domain (JMD) of the substrate. However, despite the fact that such mutations can increase or reduce the cleavage of the substrates by SPPL3, no specific region or amino acid has been found so far to be indispensable for substrate processing. In other words, it was so far impossible to turn a SPPL3 substrate into a non-substrate.

The cleavage mechanism of intramembrane cleaving proteases is a subject of numerous studies (Ye et al. 2000a, Lemberg and Martoglio 2002, Lemberg et al. 2005, Martin et al. 2008, Martin et al. 2009, Fukumori et al. 2010, Fluhrer et al. 2012, Zoll et al. 2014, Huttl et al. 2016). This is not only because intramembrane cleaving proteases are involved in numerous physiological and pathological processes, but mainly because they seem not to follow the "rules" of classical proteolysis. "Classical" proteolysis is considered to take place under hydrophilic conditions and is catalysed by soluble proteases. Under these conditions, it has been shown that in order for substrates to be processed they need to present their cleavage site as an extended β-strand conformation for the protease to bind and cleave (Tyndall et al. 2005). At the same time, α-helical structures are well "protected" from the proteases (Madala et al. 2010). However, intramembrane cleaving proteases are not only capable of cleaving their substrates in a hydrophobic environment, but it is well accepted that the TMDs of the substrates adapt an energetically favourable, α-helical conformation within the lipid bilayer (Popot and Engelman 2000). Due to proteases requirement for a β-strand to bind to their substrates, it is presumed that in most cases, in order to facilitate processing by intramembrane proteases, the substrates' TMDs need to have a lower α-helical-content than would be normally expected for a TM region. Lowering the α-helical stability can be achieved through the presence of α-helix-destabilizing amino acids, glycine, proline, aspragine and

serine (Li and Deber 1994, Madala et al. 2010). Results in favor of this hypothesis have already been published regarding SPPL2b, SPP, S2P and rhomboids (Ye et al. 2000a, Lemberg and Martoglio 2002, Urban and Freeman 2003, Akiyama and Maegawa 2007, Fluhrer et al. 2012).

The model substrate of SPPL3 chosen in this study, GnTV, comprises two α-helix-destabilising glycines within its TMD (Fig. 4.1). It is interesting to point that the arrangement of these glycines is in a "GxxxG" motif, which has previously been seen in a SPPL2b substrate (Bri2) and in numerous γ-secretase substrates, including the best-studied substrate, APP (Eggert et al. 2009, Fluhrer et al. 2012, Sykes et al. 2012). The GxxxG motif within the TMD has been shown for APP to facilitate dimerization of TMDs (Munter et al. 2007), so far however, there have been no indications suggesting the dimerization of GnTV through this motif or a preference of SPPL3 towards cleaving homodimeric substrates. Bearing that in mind, only the α-helix-destabilising properties of the glycine were taken under consideration.

Reducing the α-helical-capacity of GnTV's TMD even further by mutating either of the two glycines to prolines does indeed increase the secretion of GnTV (Fig. 4.1, 4.3C). However, exchanging both glycines to prolines impaired the maturation and consequently the secretion of GnTV. The double proline mutant is most likely degraded due to high destabilisation of the construct's TMD caused by the prolines. As only fully matured GnTV is cleaved by SPPL3, the cleavage of the GnTV PP mutant is practically absent (Fig. 4.3C) and was thus, not taken into consideration.

Interestingly, the results deriving from stabilisation of the TM α-helix by mutating the glycines to alanines or leucines are variable and do not all appear to completely agree with the hypothesis of reducing cleavability of the substrate. The effect of the alanines appears to be as expected, but only very mild and only simultaneous mutation of both glycines induces a small (15-20%) but significant reduction on GnTV secretion (Fig. 4.3A).

The α-helix stabilisation achieved by alanine is inferior to that achieved by leucine, which would imply that the glycine to leucine mutants should show a more striking decrease in GnTV shedding. While mutation of the first glycine to leucine achieves a significant 30% reduction of GnTV secretion, mutating the glycine in the second position causes an increase of secretion by 20%. Even more unexpectedly, mutating both glycines to leucines simultaneously does not balance-out their contribution but further increases GnTV secretion by 50% in total (Fig. 4.3B). Leucines are expected to form a perfect α-helix within the TMD so our initial hypothesis that stabilisation of the α-helix would hinder shedding seems incomplete.

CD spectroscopy of Bri2 substrate in lipid vesicles had shown that the glycines within the GxxxG motif, as well as one further C-terminally glycine, were not important for α-helix-destabilisation and cleavage of Bri2 by SPPL2b. However, a glycine at the N-terminus of Bri2's TMD (G60) was responsible for the destabilization of the α-helix and determined the cleavability of the substrate (Fluhrer et al. 2012). It is possible that like for Bri2, the two glycines in position 22 and 26 of GnTV do not have such a strong effect in the α-helical conformation of the TMD. The GnTV TMD also contains an additional glycine in position 15, however, this is only the second amino acid of GnTV's predicted TMD, as opposed to the glycine G60 of Bri2 that holds position 6 within the Bri2 TMD (Fig. 4.1). GnTV's G15 was thought less likely to affect cleavage by SPPL3 and was thus omitted from the analysis so far. A CD spectroscopy study of the conformation of GnTV's TMD along with mutations of G15 could provide crucial information in determining which of the glycines are responsible for the helical instability of the TMD.

Another hypothesis is connected to SPPL3's resemblance of the rhomboids, given its ability to cleave full-length substrates without requiring previous shedding of the ectodomain (Voss et al. 2014a). Similarly to rhomboids, SPPL3 might also need to recognise a rigid α-helix at one part of the substrate (recognition site), in order to cleave at the cleavage site at a different part of the substrate (Strisovsky et al. 2009). So far, there have been no indications, for the

existence of a "consensus" sequence in SPPL3 substrates, however it would still be possible that SPPL3 follows some of the rules related to rhomboid cleavage.

Although this hypothesis would not agree with the increased shedding observed upon destabilisation of the α-helix with prolines, it is very well imaginable that the shedding of the proline and the leucine mutants takes place at a different cleavage site. Following the idea of a potential shift of the cleavage site in some of the mutants, GnTV already contains a LxxxL motif in its TMD (L14, L18), as does also EXTL3 (Fig. 4.9). It may be possible that SPPL3 can recognise the LxxxL motif and cleave about 15 amino acids C-terminally of this motif. By replacing the two glycines with leucines, a new LxxxL site is created that could potentially shift SPPL3 cleavage towards the juxtamembrane region where the conditions are more hydrophilic and could account for an increased shedding. Mass spectrometry analysis could be used in order to analyse the cleavage sites of mutated GnTV similarly to the analysis performed by Kuhn et al. (Kuhn et al. 2015). For the cleavage of APP by γ-secretase, it is known that mutations in the TMD of APP close to presenilin's cleavage site can be a cause of FAD. The exact way these mutations can affect the processing by the protease is not fully understood but it appears that they can shift the sequential cleavage of C99 to a more pathological product line (Chavez-Gutierrez et al. 2012, Weggen and Beher 2012).

Intracellular stainings of the G to A mutants suggest that their localisation has not changed compared to WT GnTV (Fig. 4.4). Despite the localisation of the other mutants not having been analysed yet, the shedding of WT GnTV, as well as all the GxxxG mutants is significantly decreased in SPPL3 KO cells (Fig. 4.13). All these data together suggest that SPPL3 is still capable of cleaving these substrates to a great extent. Since SPPL3 is capable of cleaving a wide variety of glycosidases and glycosyltransferases, complete lack of this processing would have a detrimental effect on the organism. Thus, it is expected that other proteases are also capable of cleaving these substrates, though possibly to a lesser extent. It has already been shown for instance for some sialyltransferases that BACE1 is capable of

cleaving these enzymes leading to their secretion (Kitazume et al. 2005, Kitazume et al. 2006, Kuhn et al. 2012). Due to this, the remaining secretion of GnTV upon SPPL3 KO is not surprising and can most likely be attributed to another protease. However, the preference of each protease for the substrate might be affected by slight changes in the amino acid sequence like those introduced in this study. Interestingly, the G to L mutants that behaved most unexpectedly in regards to their shedding (GL and LL, Fig. 4.3) seem to be less sensitive to the SPPL3 absence (Fig. 4.13).

Another important part of the amino acid sequence of a substrate is the cleavage site. For rhomboids, extensive analysis has shown that these proteases have numerous preferences regarding the cleavage site. These preferences include the cleavage taking place directly after a small amino acid (position P1), while being flanked on both sides (P4 and P2') by large hydrophobic amino acids (Akiyama and Maegawa 2007). For γ-secretase, it is seen that the size of the amino acids surrounding the cleavage site is of importance as they might interfere with the fitting of the substrate in the enzyme's pockets. Such interferences can shift the product line of Aβ (Bolduc et al. 2016). To explore such possibilities regarding SPPL3, mutations were designed surrounding the cleavage site that has been previously identified (Voss et al. 2014a) (Fig. 4.5). Remarkably, the sequence -LLHF-, directly C-terminally of GnTV's cleavage site, is shared between GnTV and TNFα, a substrate of SPPL2a/b (Fluhrer et al. 2006).

However, the majority of the mutations introduced in GnTV either do not alter shedding or cause an increase in shedding. It is interesting to note that the running behaviour of sGnTV of the different cleavage-site mutants is altered (Fig. 4.6). This could be attributed either to changes in the glycosylation of GnTV mutants or to shifting of the cleavage site for the mutants resulting to a longer or shorter soluble peptide. Efforts to determine the exact cleavage site of the mutants have not been fruitful so far and this point would need to be further investigated. Only one position (H31, P3') appears to have a negative correlation with

the processing of GnTV (Fig. 4.6, 4.7). Taking into account that histidine is most likely charged at the pH of the Golgi and that EXTL3, another substrate of SPPL3 of which the cleavage site is still unknown, also has a histidine in a similar part of the TMD, further experiments were focused on that amino acid. To this end, additional mutations were designed to explore the effect of charge and α-helical-stability at this position. To assess the role of charge, a different positively charged amino acid was introduced (arginine, R), as well as a negatively charged (aspartic acid, D). In order to stabilise the α-helix around the cleavage point an alanine or a leucine was introduced (Fig. 4.9).

Mutating the histidine at the border of the GnTV TMD to alanine or leucine should increase the α-helical-stability and maybe extend the TMD. Although the initial hypothesis was that the histidine could play the same role in both substrates, the results of the mutations on GnTV and EXTL3 appear quite different (Fig. 4.10, 4.11). Alanine and leucine both significantly decrease cleavage of GnTV as it would be expected by a more rigid α-helix at the cleavage site, however they only cause a 30% decrease (Fig. 4.10). On the contrary, the leucine mutation has no effect on EXTL3 secretion, while the alanine mutation increases shedding of EXTL3 by 6-fold. Exchanging histidine for a different positively charged amino acid, arginine, causes a non-significant increase in cleavage of GnTV but a significant decrease in EXTL3 cleavage. However, what these two substrates seem to have in common is that cleavage of both is increased when the positive charge is replaced by a negatively charged aspartic acid (Fig. 4.10, 4.11). It is important to note here that the TMD neither of GnTV nor of EXTL3 have been properly investigated. All assumptions for the exact location of the histidine within the two TMDs are based on predictions and could be problematic. If the location of the histidine in the TMD significantly differs for the two substrates, it could account for the differences we see on the processing of the mutants.

Although, the subcellular localisation of the alanine mutants of GnTV does not seem to change (Fig. 4.8), interestingly, secretion of all but one of the mutations targeting the

cleavage site in both substrates appeared to be less dependent on SPPL3 than the secretion of both WT substrates (Fig. 4.14). In the search for the protease responsible for cleaving the mutants, EXTL3 H48A was further analysed.

Shedding of EXTL3 H48A appears to be SPPL3-independent but sensitive to treatment with $(Z\text{-}LL)_2$-ketone (Fig. 4.15A-C). It is known that this inhibitor targets substrate processing by SPP, SPPL2a and SPPL2b, but has no effect on SPPL3 or γ-secretase (Mentrup et al. 2017b). Efforts to identify the protease responsible for the cleavage have been not successful so far, as knockdown of SPP or SPPL2a or SPPL2b did not seem to have any effect on the cleavage of EXTL3 H48A (Fig. 4.15D).

Further work will be needed to determine the responsible protease and a wide range of inhibitors, as well as rhomboid inhibitors might help determine the mysterious protease. Identifying the cleavage site of EXTL3 WT and possibly of all the mutants would prove of great help for better interpreting these results.

The fact that the results of all these mutations do not seem to come to a strong conclusion most probably points to the lack of specific substrate requirements and a consensus-sequence in SPPL3 substrates. Instead, small changes affecting the α-helical-stability can make a substrate more or less efficiently cleaved without, however, turning it into a "non-substrate". Two main obstacles exist currently that prohibit us from better understanding how SPPL3 selects its substrates. The first is the lack of an *in vitro* assay, such as the one existing for γ-secretase (Edbauer et al. 2003), that would eliminate effects of other proteases and missorting of substrates. The second is the absence of a SPPL3 non-substrate that could be used to compare differences and similarities between the two proteins as has been done for the SPPL2b substrate Bri2 and the non-substrate Bri3 (Martin et al. 2009).

Our understanding of substrate selectivity of intramembrane proteases is far from complete. Even proteases like rhomboids that have numerous prerequisites and substrate requirements, are capable of cleaving theoretical "non-substrates" when the membrane properties are altered

(Moin and Urban 2012, Urban and Moin 2014). Regarding SPPL3, all data so far point to numerous different factors being involved in the substrate specificity without any of them proving indispensable. Only with further analyses, will we get closer to deciphering substrate recognition.

5. Indications for SPPL3 *in vivo* function

To understand thoroughly the SPP/SPPL family in general and SPPL3 in particular, it is fundamental to study the physiological function of these proteases. This has already been done extensively for SPPL2a, which was shown to have a role in B lymphocyte development and, hence, is a possible target to tackle some autoimmune disorders (Beisner et al. 2013, Bergmann et al. 2013, Schneppenheim et al. 2013, Schneppenheim et al. 2014a, Schneppenheim et al. 2014b, Mentrup et al. 2017b).

5.1 Results

5.1.1 Reproduction of SPPL3 deficient mice

The SPPL3 deficient mouse line was previously established by insertion of a genetrap between exons 6 and 7 of *Sppl3*, causing the absence of SPPL3 transcripts and protein in the homozygous knockout mice ($SPPL3^{-/-}$) (Tang et al. 2010). These mice were generated in a mixed background of C57BL/6J and 129S5/SvEvBrd (B6;129S5). Infertility was observed for male $SPPL3^{-/-}$ mice in the initial analysis (Tang et al. 2010).

5.1.1.1 Reproduction of mixed genetic background SPPL3 deficient mice

Further analysis of B6;129S5 SPPL3 deficient mice over the course of several matings (n=8 litters) between heterozygous ($SPPL3^{+/-}$) and knockout ($SPPL3^{-/-}$) mice, did not confirm infertility of male knockout mice. The litter size was in average 8.4 pups per litter, however 3.3 pups were in average born dead in each litter. The Mendelian ratios of the alive progeny of these matings were analysed and were found to be altered. According to the Mendelian principles, mating between a +/- animal and a -/- animal should give a 50:50 ratio

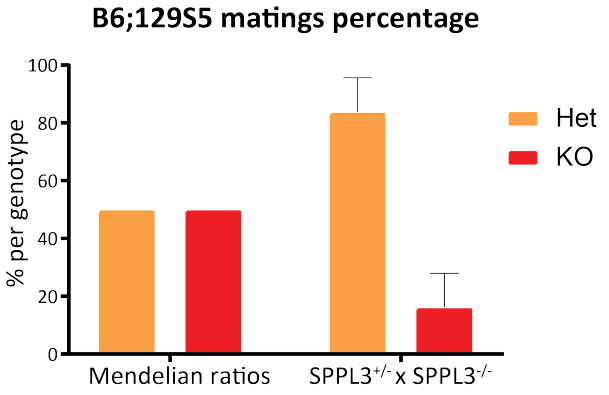

Fig. 5.1: Matings of SPPL3 deficient mice in a mixed background. Graph depicting the results of mating an SPPL3 heterozygous mouse ($SPPL3^{+/-}$) with an SPPL3 KO mouse ($SPPL3^{-/-}$) from the mixed B6;129S5 background, n=8 litters. On the left side are the expected Mendelian ratios and on the right side the ratios that resulted after analysing the litters. Orange bars depict heterozygous mice and red the knockout.

of +/- and -/- offspring. However, in the case of SPPL3 deficient mice, only 20% of the offspring where knockout ($SPPL3^{-/-}$), while 80% were heterozygous ($SPPL3^{+/-}$) (Fig. 5.1).

5.1.1.2 Reproduction of pure genetic background SPPL3 deficient mice

The B6;129S5 SPPL3 deficient mouse line was also crossed back over 10 generations to C57BL/6J (Voss 2014) and to 126S6 background (129S5 is not available anymore). The matings of SPPL3 heterozygous C57BL/6J mice were analysed. The average number of pups per litter of n=18 litters were 6.1 and in average 1.5 were born dead. According to Mendelian ratios, mating of two heterozygous animals (+/- x +/-) should give a ratio of 25:50:25 of wildtype (+/+), heterozygous (+/-) and knockout (-/-) animals, respectively. However, the progenies from $SPPL3^{+/-}$ C57BL/6J litters consisted of 30-35% wildtype mice, 60-65% heterozygous and only approximately 5% stillborn knockout mice (Fig. 5.2). In the 129S6 background, some knockout animals survived after birth the number is extremely low and still require further analysis (data not shown).

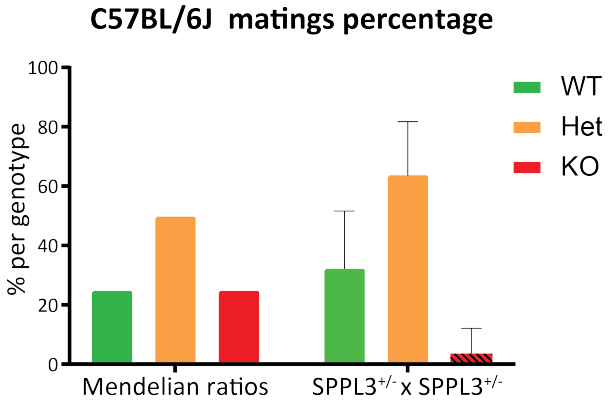

Fig. 5.2: Matings of SPPL3 heterozygous C57BL/6J mice. Matings of SPPL3 heterozygous C57BL/6J mice. Graph depicting the results of mating two SPPL3 heterozygous mice ($SPPL3^{+/-}$) of the pure C57BL/6J background, n=18 litters. On the left side, the expected Mendelian ratios are depicted and on the right side the actual ratios that resulted after analysing the litters. Green bars depict wildtype mice, orange heterozygous and red knockout. The red bar with the black lines symbolizes KO pups that were found dead shortly after birth.

5.1.2 SPPL3 deficient mice are characterised by a reduced weight phenotype

Already following the initial characterisation of SPPL3 deficient mice by Tang et al., it was observed that both male and female knockout animals displayed delays in their growth characterised by reduced weight and size compared to their wildtype littermates (Tang et al. 2010). To investigate this point, the growth of wildtype and knockout littermates was

followed by regular weighing between the ages of 8 and 40 weeks. Separate groups consisting of either males or females were weighed weekly, however, due to technical limitations, breeding ratios and dropouts of some animals due to disease etc, the numbers of animals measured for each time point/gender/genotype vary from 2 to 7. Nevertheless, the vast majority of measurements for wildtype and knockout animals included 3 or more mice allowing for statistical calculations. Both male and female SPPL3 knockout animals demonstrated reduced

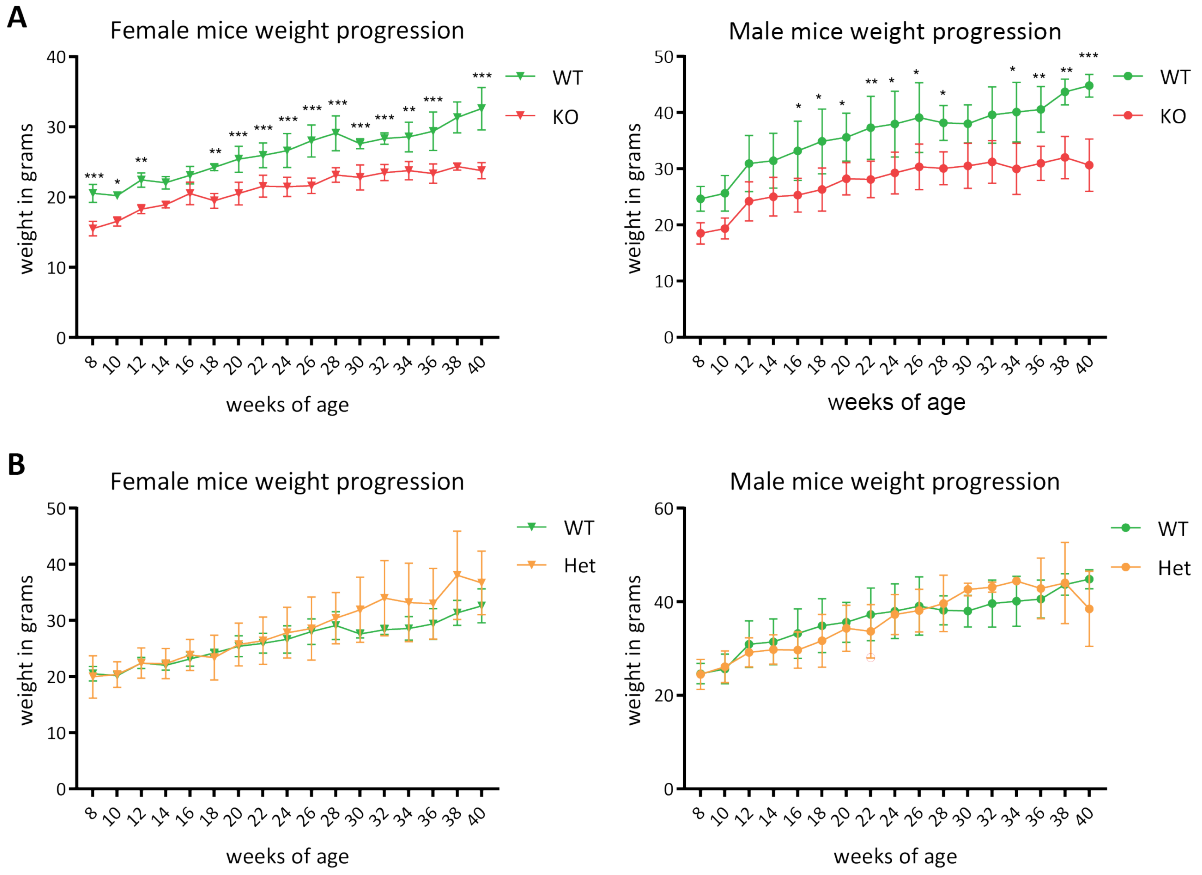

Fig. 5.3: Weight progression of SPPL3 deficient mice and littermates. A. Graph depicting the weights of SPPL3 KO mice (red) and wildtype littermates (green) for both female and male mice (left and right, respectively). The weight was measured biweekly and the n numbers varied from n=2-8 for each gender. 2-way ANOVA test with multiple comparisons and Sidak correction was used to calculate the statistics of time points with $n \geq 3$, *$p<0.05$, **$p<0.01$ ***$p<0.001$ **B.** Graphs depicting the same WT mice as in A but comparing them to the measurements from heterozygous mice (orange).

weight at the initial measurement at an age of 8 weeks compared to their wildtype littermates. This difference in weight appeared to increase with age, as the wildtype animals continued gaining weight up to the end of the measurement period (40 weeks of age), while the

knockout littermates stopped gaining weight between 24 and 30 weeks of age (Fig. 5.3 A). The reduced weight phenotype had a complete penetrance, as all the knockout animals were smaller and lighter than their littermates. Additionally, the phenotype remained consistent following embryo-transfer to a new animal facility. The weight of heterozygous animals tended to be between that of wildtype and knockout littermates. All over, heterozygous animals were never as thin as the knockout mice, but overweighed the wildtype in some cases (Fig. 5.3 B).

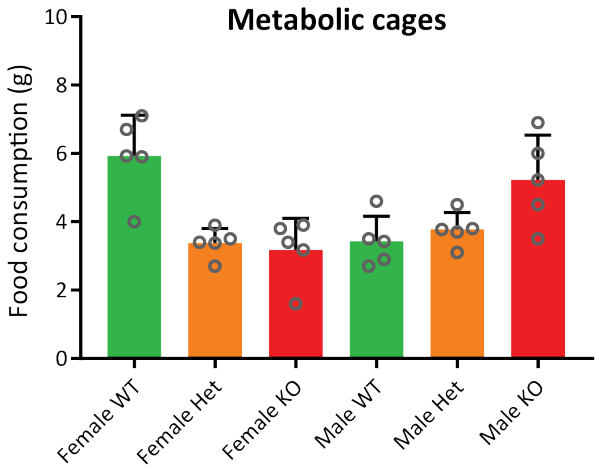

Fig. 5.4: Food consumption of mice during metabolic cage measurements. All mice were placed in the cages on day 1 until day 5 and the remaining food was measured at the beginning and end of each day (24h). The average daily consumption is depicted in this graph (Mean +SD) of the four days measured.

In order to determine whether the reduced weight of the wildtype was due to a decreased appetite and food consumption, metabolic cages were used. Food and water intake, as well as secretions of two knockout mice were followed for five days in metabolic cages, together with heterozygous and wildtype littermate controls. During this period, the knockout animals did not consume significantly different amounts of food than their littermate controls (Fig. 5.4) and secretions were in a similar range between all mice (data not shown).

5.1.2.1 SPPL3 deficient mice have reduced adipose tissue

To unravel the reason for the reduced weight phenotype of the SPPL3 deficient mice more precisely, it is important to understand whether it is caused by an overall smaller size of the mouse or by reduction of a specific tissue/organ. Visual inspection of the mice during sacrifice for organ collection revealed reduced adipose tissue in at least three adipose deposits. In knockout mice, visceral fat was severely reduced to almost non-existant, subcutaneous fat was almost absent and the adipose layer surrounding the kidneys and the genitals was greatly reduced compared to wildtype mice (data not shown). Prompted by these observations, further

tissue analysis was planned for these mice.

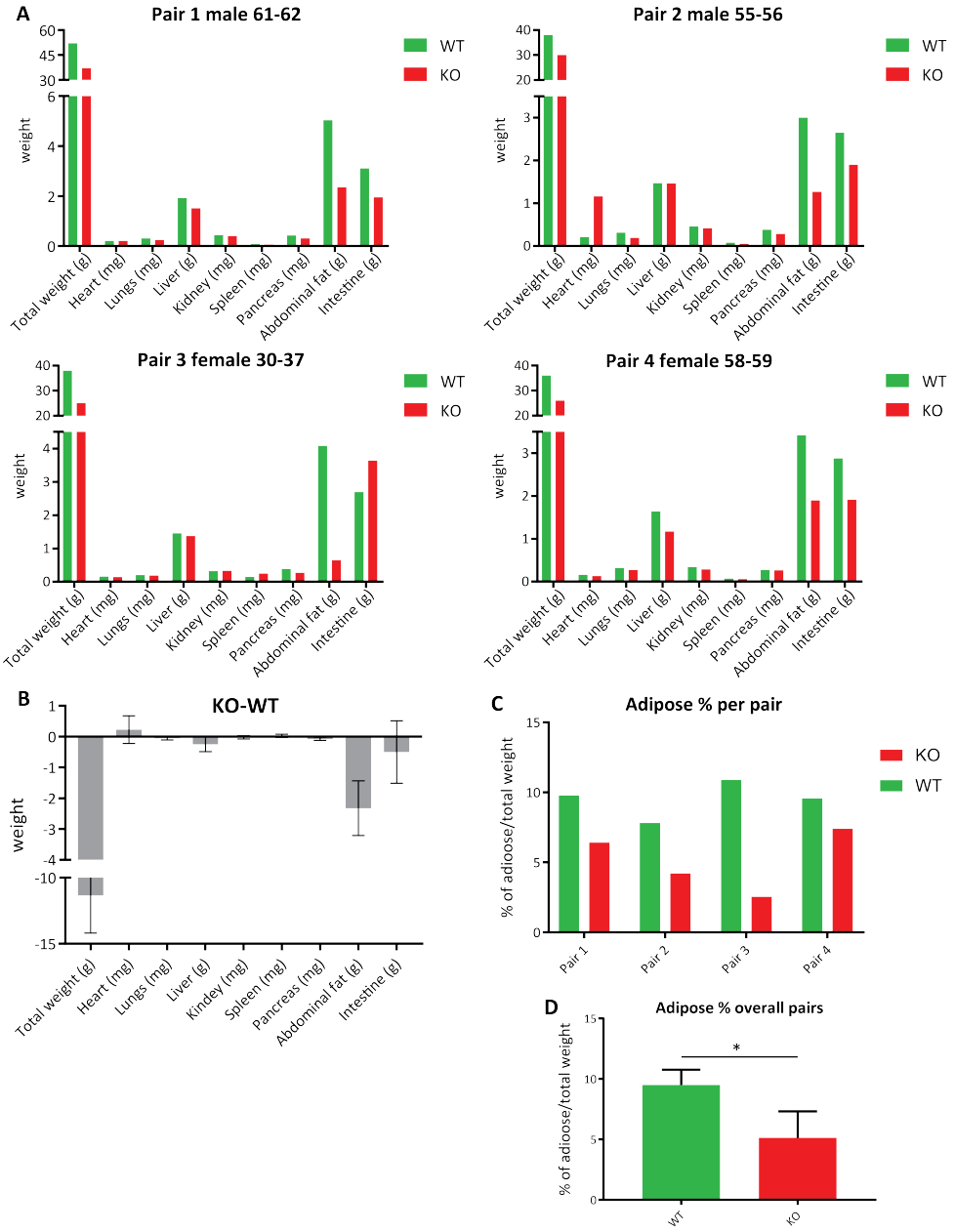

Fig. 5.5: Detailed analysis of body weight of SPPL3 deficient mice and littermate controls. A. Four graphs depicting the results of the total weight and organ weight from 4 pairs of age and gender matched littermate mice. Each organ's weight is depicted in either g or mg, as indicated. **B.** The weight difference for each organ/tissue was calculated for each mouse pair and the mean value +/- SD for all pairs is depicted. **C.** The percentage of adipose fat was calculated compared to the total weight for each mouse and is depicted per pair. **D.** The mean of "adipose to total weight" percentage was calculated per genotype, mean + SD. Unpaired, two-tailed t test, *p<0.05, n=4 WT and 4 KO. WTs are depicted in green and KOs in red.

To this end, 4 pairs of age and gender matched mice were analysed at the Veterinary Clinic of Munich by Dr. Nadja Herbach. Each pair consisted of one wildtype and one knockout mouse

from the same litter. The mice were approximately one year of age when they were analysed. The total weight of the mice was analysed, as well as the specific weight of a number of organs, namely abdominal fat, intestines, liver, kidneys, spleen, pancreas, heart and lungs. The graphs depict all measurements for each mouse in the matched pairs (Fig. 5.5 A).

In all four pairs, regardless of age or gender, the KO mouse is clearly weighing less than the wildtype littermate. Interestingly, the most notable difference in weight between each pair was mainly due to reduced abdominal fat, while other organs such as kidneys, spleen and heart were not reduced in size. This observation became more apparent when the difference in weight for each organ/tissue was calculated between each pair of mice (KO-WT) and the mean of all those differences is depicted in Fig. 5.5 B (mean +/- SD). It is clear that the only tissue that is consistently and significantly decreased in the knockout mice is the abdominal adipose tissue. In order to confirm that the reduction in adipose tissue is not solely due to a smaller mouse size, the percentage of fat was calculated for each mouse compared to the total body weight of that mouse (Fig. 5.5 C). The "adipose to total weight" percentage of each mouse was taken into account when calculating the average for each genotype. There is a significant difference between wildtype and knockout mice, with the knockout mice having significantly less adipose tissue even when the total weight is taken into consideration (Fig. 5.5 D). All results from these measurements point to an effect of SPPL3 on the generation and/or storage of adipose tissue.

5.1.3 Generation of SPPL3 knockout Stem Cells Lines

Due to the troublesome breeding of the SPPL3 deficient mice and the complexity of studying the accumulation of adipose tissue in the mouse, we considered establishing an SPPL3 knockout stem cell line as a useful tool for further investigation. For this purpose, E14 stem cells (ESCs) were used and were subjected to CRISPR/Cas9 genome editing. Using two commercially available gRNA constructs, three single cell knockout clones that completely lack SPPL3 expression were successfully generated. The first gRNA targeted the second exon

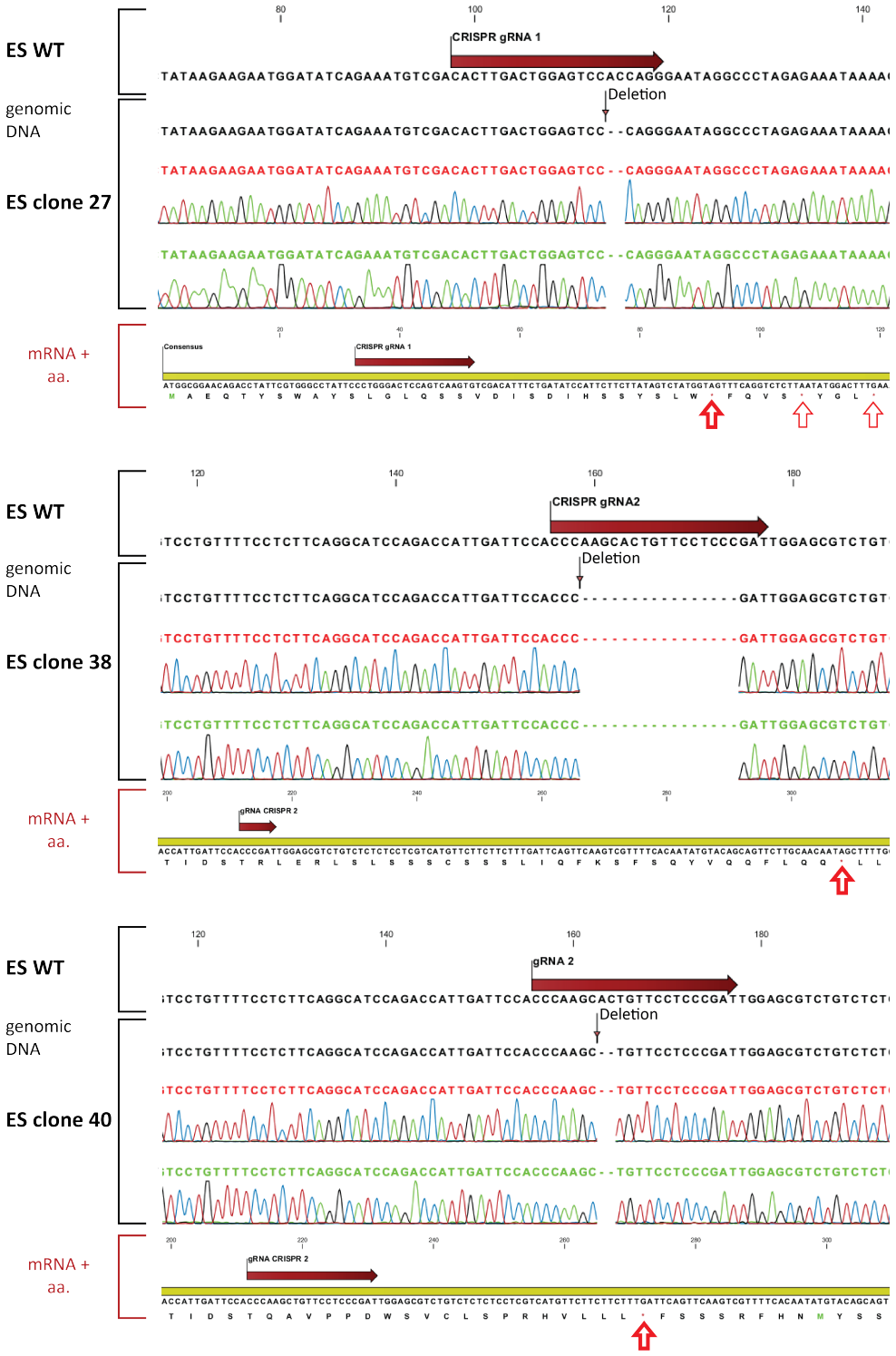

Fig. 5.6: Genomic, mRNA and amino acid sequence of SPPL3 KO stem cells. Three different SPPL3 knockout (KO) stem cells clones are shown. For each clone first the comparison of the wildtype mouse *Sppl3* genomic DNA with that of the KO clone is depicted confirming the presence of homozygous mutations. Below, for each clone the mRNA sequence following the deletions and the amino acid sequence it would code for is given. In all three clones, an early stop-codon is generated as indicated by red arrows.

of *Sppl3* and the second gRNA targeted exon 3. Following single cell sorting and analysis of the genome of a number of clones, three SPPL3 KO clones were selected (3.2.2.2.2). One clone was treated with gRNA1 (27), while two clones were treated with gRNA2 (38, 40). All three clones had homozygous deletions close to the binding position of the gRNA and in all cases, these deletions lead to an early stop codon in the SPPL3 mRNA (Fig. 5.6).

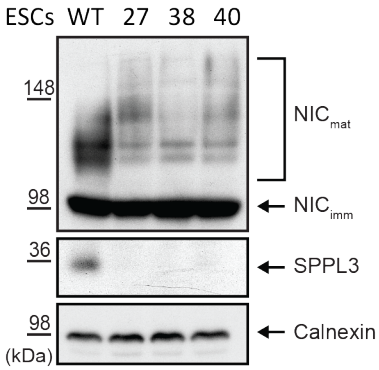

Fig. 5.7: Nicastrin glycosylation in SPPL3 KO ESCs. As expected, protein levels of SPPL3 are only detectable in the WT ESCs. The upper blot depicts both mature and immature Nicastrin. Calnexin was used as a loading control.

Similar to MEF cells, ES cells can handle the absence of SPPL3 without any visible difficulties and appear morphologically similar to their wildtype source (data not shown). Western Blot analysis of the SPPL3 protein levels confirmed the absence of the protein in all three clones compared to the WT ESCs (Fig. 5.7). As mentioned before (1.3.2.4.4), SPPL3 is capable of reducing active glycosidases and glycosyltransferases within the cell via proteolytic removal of their active site. According to that, a hyperglycosylation of certain glycoproteins is expected in SPPL3 KO ESCs. Indeed, the glycoprotein Nicastrin is hyperglycosylated in the KO cells compared to the control, confirming a reduction in SPPL3 levels (Fig. 5.7).

5.1.3.1 Differentiation of ESCs to adipocytes

Following the protocol published by Cuaranta-Monroy et al. (Cuaranta-Monroy et al. 2014), stem cells were differentiated to adipocytes over a period of 27 days. Due to the complexity of this procedure, only the wildtype and one KO clone (27) were used. Stem cells cultured to confluency were treated with a variety of growth factors and reagents including ascorbic acid, retinoic acid, dexamethasone, insulin and others (3.2.2.2.3). Light microscopy and Oil Red Stainings were used to assess the success of differentiation. With light microscopy, colonies of adipocytes were identified based on their gross morphology (Fig. 5.8 A). Oil Red stains the lipid content of adipocytes, while at the same time the cell nuclei were stained blue by hematoxylin

(Fig. 5.8 B). Both techniques showed a severely reduced number and size of adipocytic colonies in the KO cells compared to the WT controls (Fig. 5.8). However, despite the reduced number and size of colonies, the size of the adipocytic cells appeared similar in both WT and KO ESCs.

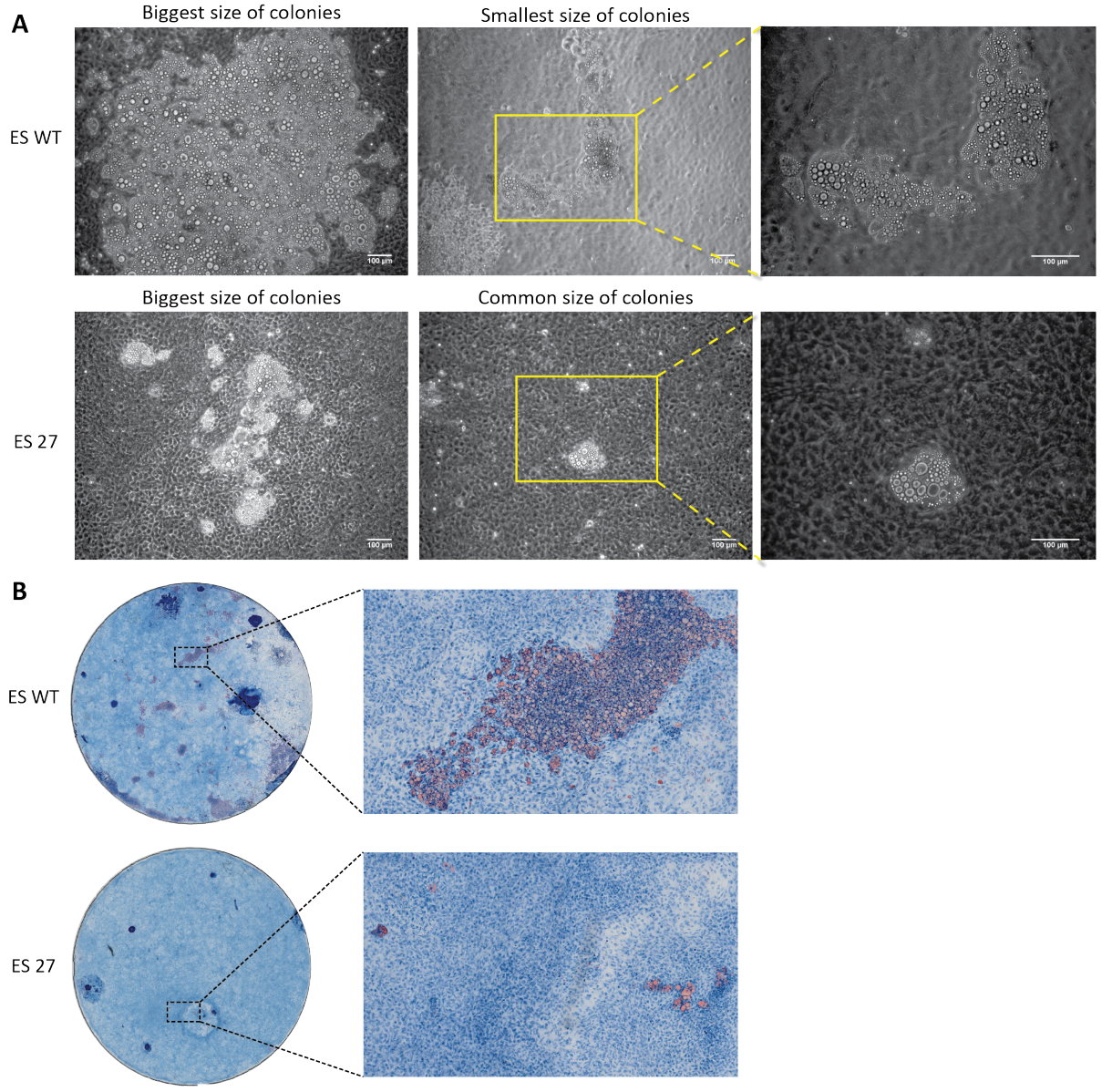

Fig. 5.8: Differentiation of ESCs to adipocytes. **A.** Wildtype stem cells (ES WT) and SPPL3 knockout stem cell clone 27 (ES 27) were differentiated to adipocytes for 27 days and then visualised by light microscopy. On the left hand side some of the biggest colonies are shown for each cell line, in the middle the smallest WT and average ES 27 colonies and on the right, a higher magnification is included. **B.** Oil Red Staining of the differentiated cells. On the left side one cover slip for each cell line of 1cm diameter is depicted and on the right a higher magnification of a selected area with adipocytes. Red staining is indicative for the present of adipocytes due to the staining of their lipids.

5.1.4 SPPL3 deficient mice demonstrate age-dependent motor deficiency

The motor coordination abilities of SPPL3 deficient mice were compared to that of wildtype and heterozygous littermate controls with the use of a Rotarod Performance Test. The ability and endurance of the mice was tested while walking on a rotating beam, the rotation speed of which was steadily increasing with time. The time each mouse spends on the beam before falling is indicative of the balance, grip strength and motor coordination of the mouse. Untrained mice had three-four sessions, each consisting of three trials for each littermate group, with 15 minutes of break in between (3.2.6.2).

Due to breeding limitations, only a small number of mice was available for participating in this study. Two different age groups were tested, one consisting of mice that were older than one year at the time of the first session (55 weeks) and one consisting of mice that were 5-6 months old at the first session. Each group, comprised one mouse of each gender and each genotype, however, one mouse was not willing to participate in the test and was excluded. Looking at the average of all sessions for each mouse, it is clear that in the older mice, the knockout animals have an overall weaker performance compared to their heterozygous and wildtype littermates (Fig. 5.9 A). The same analysis of the younger mice revealed a very high variation in the performance of all mice and especially the knockout animals (Fig. 5.9 B).

The performance of each mouse in each of the sessions was also analysed to observe any learning abilities or physical deterioration. The results of the old mice indicate that although the knockout animals in both genders were the weakest performers, there was some ability to learn and improve their performance similarly to the wildtype (Fig. 5.9 C). Regarding the group of younger mice, the performance of all three genotypes, but especially of the knockout seems to be deteriorating as they approach one year of life, to levels similar to the older mice (Fig. 5.9 D).

Despite the fact that the n numbers in the rotarod analysis are extremely low, one additional phenotypic characterisation that supports a motor deficiency is the hindlimb clasping response. The mice were gently lifted by their tails and their response to spread or clasp their hind legs was observed for 10 seconds. A grade of 0 was given for completely stretched legs, if one limb showed tendencies to clasp for more than 5 sec it was graded with 1, if both limbs were retracted for more than 5 sec it was marked with 2 and if both limbs were completely retracted and clasping for more than 5 sec it was ranked a 3 (Guyenet et al. 2010). Wildtype and heterozygous animals were always graded with 0, while knockout animals had an average of 2.5 scoring always between 2 and 3.

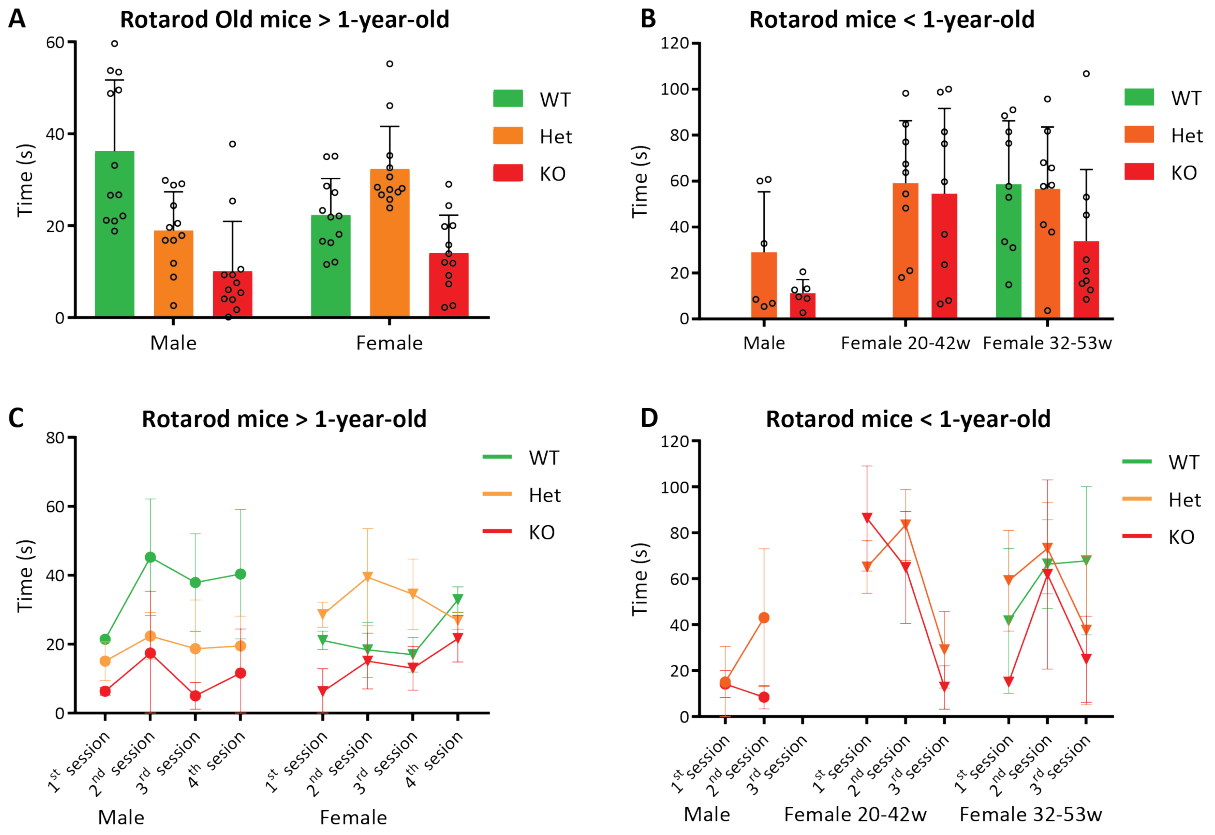

Fig. 5.9: Rotarod performance test. A, B. Graphs depicting the average performance of SPPL3 deficient mice and their littermates in the rotarod test measured in seconds. Graph A summarises mice above 1 year of age at the first session, while in B mice under one year of age at the first session are shown. The bars depict the mean of all trials +/- SD, while the single performances are visualized by circles **C, D.** Graphs depicting the average of three trials for each session for each mouse +/- SD. Wildtype mice are always depicted in green, heterozygous in orange and knockout in red.

5.2 Discussion

Despite the lack of *SPPL3* homologues in single-cell organisms, all multi-cellular organisms comprise an *SPPL3* homologue. Even more interestingly, the degree of conservation in the amino acid sequence of *SPPL3* between the various organisms suggests SPPL3 must have a crucial physiological role (Voss et al. 2013). Presence of an almost identical protein in all metazoan suggests its necessity for the successful survival and reproduction of the organism.

In agreement with these indications, the SPPL3 deficient mouse line that was created in a mixed B6;129S5 background, fails to reproduce with Mendelian ratios. In contrast to a previous study where infertility of male SPPL3$^{-/-}$ mice was reported (Tang et al. 2010), we found both male and female knockout mice capable of breeding but with an increased mortality rate in the pups. However, the percentage of knockout progeny when mating a knockout and a heterozygous animal is 20% instead of the expected 50% (Fig. 5.1). Even more striking is the effect of the SPPL3 deficiency in a pure genetic background. B6;129S5 SPPL3$^{-/-}$ mice are not viable (Fig. 5.2).

It was previously postulated that the C57BL/6 background might be less capable to adjust to the lack of SPPL3 due to the mouse line's inbreeding factor. At the same time, it was thought that the 129S5 background might harbour protective characteristics, so this could explain why the SPPL3 deficient mice survive in a mixed background (Voss 2014). Following this notion, the B6;129S5 mouse line was crossed for 10 generations with 129S6 mice (successor of 129S5 mouse line that is no longer available). Analysis of this mouse line is ongoing only for approximately 6 months and only two SPPL3$^{-/-}$ mice have arisen from the matings indicating a persistent phenotype with progeny numbers too low to investigate the phenotype in depth (data not shown).

Based on the current results, it appears that SPPL3 deficiency can be best tolerated only in a mixed background and in order to achieve more in depth analysis of the phenotype in a

reproducible background, a conditional knockout mouse line is needed. The observation that a protein deficiency can be differently tolerated based on the genetic background of the mouse line has been seen before. However, what makes it more interesting is that background dependency is often seen in mouse-lines with complex N-glycosylation deficiencies. Such background dependent phenotype severity is seen for instance in both *Mgat2* and *Mgat5* deficient mice (Wang et al. 2001, Dennis et al. 2002, Lee et al. 2012).

It has been already shown and also further investigated in this study that SPPL3 can cleave glycosyltransferases reducing their activity inside the cell (Voss et al. 2014a, Kuhn et al. 2015). A previous study, has already shown that SPPL3 absence *in vivo* reproduces the effects observed in cells and causes hyperglycosylation of glycoproteins due to reduced shedding, and thus accumulation of active glycan-modifying enzymes (Voss et al. 2014a). Given this connection between GnTV (encoded by *Mgat5*) and SPPL3, SPPL3 deficiency would be expected to mimic an over-expression model of GnTV and other glycosyltransferases, and not the knockout *in vivo* models.

However, one characteristic that is common in both SPPL3 and *Mgat5* deficient mice is the lack of soluble GnTV, due to the lack of cleavage in absence of SPPL3 and due to the complete lack of GnTV, respectively. The presence of soluble glycosyltransferases in bodily fluids is already known since the early 1980s (Beyer et al. 1981) and it was soon understood that they derive via proteolytic cleavage of the membrane spanning intracellular forms (Lammers and Jamieson 1989, Paulson and Colley 1989). It has also been shown that proteolytic release of glycosyltransferases is a dynamic process that can take place as a response to certain stimuli. For instance, conditions that cause hepatopathological liver inflammation induce the release of soluble ST6GalI in the acute response stage (Kitazume et al. 2009). Despite these results suggesting specific functions of soluble glycosyltransferases, it remains unclear what these functions really are (Saito et al. 2002, Varki et al. 2009). A possible explanation why the SPPL3 deficient mice mimic parts of the phenotype of the

Mgat5 deficient mice would be the disturbance of the function of secreted GnTV, which in turn accounts for some of the phenotype similarities observed. Alternatively, it is known that a very tight regulation of glycosylation is required for optimal function of the organism. Possibly, the disruption of a glycoprotein's function either by hyper- or hypo-glycosylation, could lead to the same phenotype *in vivo*. However, rigorous experimentation will be needed to discover possible connections between these two mouse models.

In C57BL/6 background, very few SPPL3 deficient mice surpass the embryonic stages and even those were found dead shortly after birth (Fig. 5.2). The small size of the litters suggests that embryo resorption takes place during pregnancy. Efforts to analyse the reason of embryonic/post-natal death of SPPL3 deficient mice remain so far unsuccessful due to the high variability in the stage that miscarriage or death occurs.

The physical abilities of the SPPL3 deficient mice also seem to be affected and they deteriorate with aging. Trembling and peculiarities during walking were often observed (data not shown). This prompted us to use a rotarod performance test and also assess the hindlimb clasping tendency of the knockout mice. Hindlimb clasping is a marker of motor neuron deficiency and cerebellar ataxia (Chou et al. 2008) and while the wildtype mice had consistently a score of zero, knockout mice had an average of 2.5 according to a published scoring system (Guyenet et al. 2010) (5.1.6). Their performances on the rotarod were more variable and a higher n-number will be needed to analyse this phenotype in depth, however, a tendency for knockout animals to perform more poorly especially at an older age was observed (Fig. 5.9). It is unclear if the reason is of neurological or a musculature source. For *Mgat5* deficient mice, reduced muscle satellite cells, osteogenic activity and an early aging phenotype has been reported. If we assume there is some connection between these two deficiencies, this could also explain why the SPPL3 deficient mice look and perform better at a younger age and deteriorate faster with age (Cheung et al. 2007).

The most reproducible characteristic observed in all SPPL3$^{-/-}$ mice regardless of gender, age

or animal facility is their reduced weight phenotype. Both male and female mice have a consistently lower body weight as compared to wildtype animals of the same age. Regular weighing has revealed that the difference is already present shortly after birth and tends to increase with age (Fig. 5.3A). Heterozygous animals of the same age seem unaffected by the lack of one SPPL3 allele as their weight is comparable to that of WT mice and sometimes exceeds it (Fig. 5.3B). Analysis of different tissues and organs in wildtype and knockout mice revealed that although most organs were of comparable size, abdominal fat was significantly reduced in all knockout animals (Fig. 5.5A, B). To correct for a potential smaller body size of the knockout mice, the percentage of abdominal fat compared to the total mouse weight was calculated. Even considering this, the knockout animals had approximately one third to half the percentage of abdominal fat of the wildtype (Fig. 5.5C).

One point that needs further investigation and was only briefly addressed in this study is whether the reason for the reduced weight is behavioural. To answer the question whether the knockout animals consume less food than the wildtype, six mice (one of each genotype for each gender) were placed in metabolic cages for five days, however, the knockout mice did not appear to consume less food than their littermates (Fig. 5.4). To confirm these results, the metabolic cage experiment should be repeated with a higher n-number and additionally the energy consumptions in form of exercise could be taken into account. Interestingly, GnTV knockout mice are also characterised by a lean phenotype, however it only appears after a high-fat diet, as they are resistant to weight gain (Cheung et al. 2007).

The defective reproduction of SPPL3 deficient mice poses as an obstacle for the further analysis of the reduced adipose phenotype of the mice and for discovering the molecular mechanism behind this phenotype. To this end, we opted for a simpler but at the same time very potent tool to further study this aspect. Using the CRISPR/Cas9 technology, SPPL3 deficient embryonic stem cell lines were generated (Fig. 5.6). All three single cell clones that were generated kept the hyperglycosylation phenotype that has already been seen in cells

(HEK293, MEF) and in mice (Fig. 5.7) (Voss et al. 2014a).

Following existing protocols, wildtype and one SPPL3 deficient ES cell line were differentiated into adipocytes (Cuaranta-Monroy et al. 2014). It was clear in both the size and the number of colonies that the knockout cells differentiated less efficiently than the wildtype cells (Fig. 5.8). These results are very exciting because similarly to the phenotype observed in SPPL3$^{-/-}$ mice, adipose cells are not completely absent, but their number is strongly decreased compared to control cells. Although these results are very interesting as they would perfectly mimic the *in vivo* phenotype, they need to be considered with caution since they remain preliminary. Additional repetitions including the other ES clones would be needed to confirm the results and exclude off-target effects of the genetic manipulation. Another point that needs to be further investigated is whether the differentiation into adipocytes is *per se* failing or whether adipocytes are formed but are not capable of storing lipids and were thus, not stained by the Oil Red staining (Fig. 5.8B). This could be analysed by checking the expression of various differentiation markers as performed in Cuaranta-Monroy et al. 2014.

As ES cells are pluripotent and can be differentiated into numerous cells lines, it would be of value to investigate their differentiation efficiency into other cell lines. Cell types from all three embryonic germ layers could be tried. As adipocytes derive from the mesodermal germ layer, another cell type that can be easily tried from the same layer are cardiomyocytes (van den Berg et al. 2016). For the ectoderm, neuronal cells would be a feasible option (Wongpaiboonwattana and Stavridis 2015) and for the endoderm, hepatocytes (Zhou et al. 2010). These experiments could help us understand if SPPL3 holds a key role specifically in adipocyte formation or if there is a general mechanism and differentiation deficiency.

Over a decade ago, the effect of adipose-specific knockout of raptor was analysed *in vivo* (Polak et al. 2008). An adipose-specific knockdown of raptor was used in Polak et al. study as mice lacking raptor in all tissues die during embryonic stages (Guertin et al. 2006). Raptor is an indispensable component of the mammalian target of rapamycin complex 1 (mTORC1),

which in turn holds a crucial role in cell growth and metabolism. mTORC1 also has a central role in development and aging, participating at the same time in the pathology of various diseases such as cancer, diabetes and obesity. mTORC1 is a protein kinase that phosphorylates numerous other proteins as its substrates. mTORC1 is controlled by "external" factors such as insulin, nutrients, growth factors, amino acids and others (Ben-Sahra and Manning 2017).

The decrease in adipocyte differentiation efficiency reported in Polak et al. highly resembles the results obtained from the ES cell differentiation (Fig. 5.8). Additionally, raptor$^{ad-/-}$ mice display a lean body phenotype with reduced adipose levels that is very similar to that of SPPL3$^{-/-}$ mice (Fig. 5.3, 5.5) (Polak et al. 2008). It would be very interesting to investigate whether metabolic changes observed in the raptor$^{ad-/-}$ mice, like increased mitochondrial respiration, also hold true for the SPPL3 deficiency. Furthermore, unpublished data from AG Fluhrer that are not part of this study suggest that physiological SPPL3 levels in HEK293 cells can also be regulated by metabolic cues present in the cell culture media, so a further connection between mTORC1 and SPPL3 might exist. Given the ability of mTOR to affect also other functions, such as muscle mass and aging, it seems crucial to investigate a potential link between SPPL3 and the mTOR pathway.

In summary, SPPL3 deficiency *in vivo* can only be tolerated in a mixed background, without ever reaching Mendelian ratios in reproduction. In contrast, SPPL3$^{-/-}$ mice display numerous phenotypes, the most penetrant of which is the reduced presence of adipose tissue. SPPL3 knockout ES cells are being used to mimic the adipose phenotype in a simple model system. Next step would be to establish connections with potent pathways that could mechanistically explain this phenotype.

6. SPPL2c impairs vesicular trafficking

Despite the accumulation of knowledge regarding SPP, SPPL2a, SPPL2b and SPPL3, and the fact that the SPP/SPPL family has been discovered in 2002 (Grigorenko et al. 2002, Ponting et al. 2002, Weihofen et al. 2002), the understanding of SPPL2c has not progressed through the years. Analysis of the glycosylation of ectopically expressed SPPL2c in HEK293 cells points to the protease being localised in the ER or early Golgi (Friedmann et al. 2004a). However, in spite of the detection of SPPL2c mRNA in a variety of tissues in the past (Friedmann et al. 2004a), no endogenous protein levels of SPPL2c have been detected so far, pointing to a possible false positive result due to the lack of introns in the *SPPL2C* gene. The lack of endogenous protein expression and the absence of SPPL2c substrates need to be addressed in order to increase our understanding of this protease.

6.1 Results

6.1.1 *SPPL2C* is not a pseudogene

SPPL2C has been believed since its discovery to be a pseudoprotease and a pseudogene lacking any functional expression (Golde et al. 2009, Voss et al. 2013). However, analysis of testis samples from humans and mice revealed SPPL2c protein expression (Fig. 6.1A), while SPPL2c protein levels were only detected in testis and not detected in brain, kidney, spleen, or liver of Black6 mice (Fig. 6.1B). The specific expression suggests of a functional role of SPPL2c in testis. However, the lack of any identified substrate remained an obstacle in determining whether SPPL2c is a catalytically active protease and discovering its physiological function.

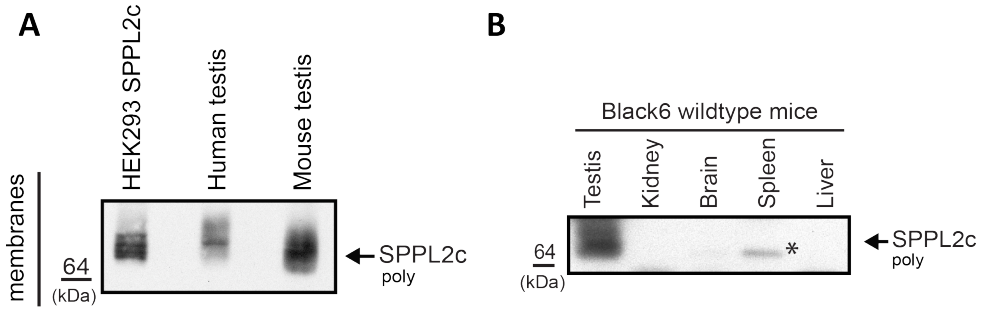

Fig. 6.1: SPPL2c is expressed in testis from human and mice. A. Western blot of membrane preparations from HEK293 inducibly expressing SPPL2c, human and mouse testicular tissue. 2 µg of membrane preparation is loaded for each of the organs and 0.04 µg of HEK293 cell lysate. **B.** Western blot of membrane preparations from five different organs of WT Black6 mice, same amounts of protein were loaded, 10 µg. The asterisk points an unspecific band.

6.1.2 Mass Spectrometric analysis of SPPL2c expressing HEK293 cells

To identify potential SPPL2c substrates, protein label-free quantification (LFQ) mass spectrometric analysis was used. T-Rex^{TM}-293 (HEK293) cells that stably express SPPL2c under a doxycycline-inducible promoter were compared to control cells with no SPPL2c expression. 4841 proteins were identified in membrane preparations of each condition by at least two peptides. 3726 of those proteins were quantified relatively based on at least three of the six biological replicates of control and SPPL2c expressing cells. These proteins were subjected to statistical analysis and 917 were altered with a p-value less than 0.05. Finally, following the false discovery rate (FDR) correction for multiple hypotheses, 451 proteins were found significantly altered. The changes in the abundance of proteins under the two conditions are depicted in a volcano plot (Fig. 6.2). As expected, SPPL2c is the most predominantly increased protein of all, confirming the successful overexpression of the protein in those cells. Considering that intramembrane cleavage of a substrate, in most cases, leads to its release from the membrane, any potential SPPL2c substrates are expected to be decreased upon protease overexpression in membrane preparations. SPP/SPPLs are known to cleave TM proteins with type-II (and type-IV in the case of SPP) orientation (1.3.2.4.2-4). For this reason, only the 25 decreased type-II and type-IV TM proteins were considered as potential

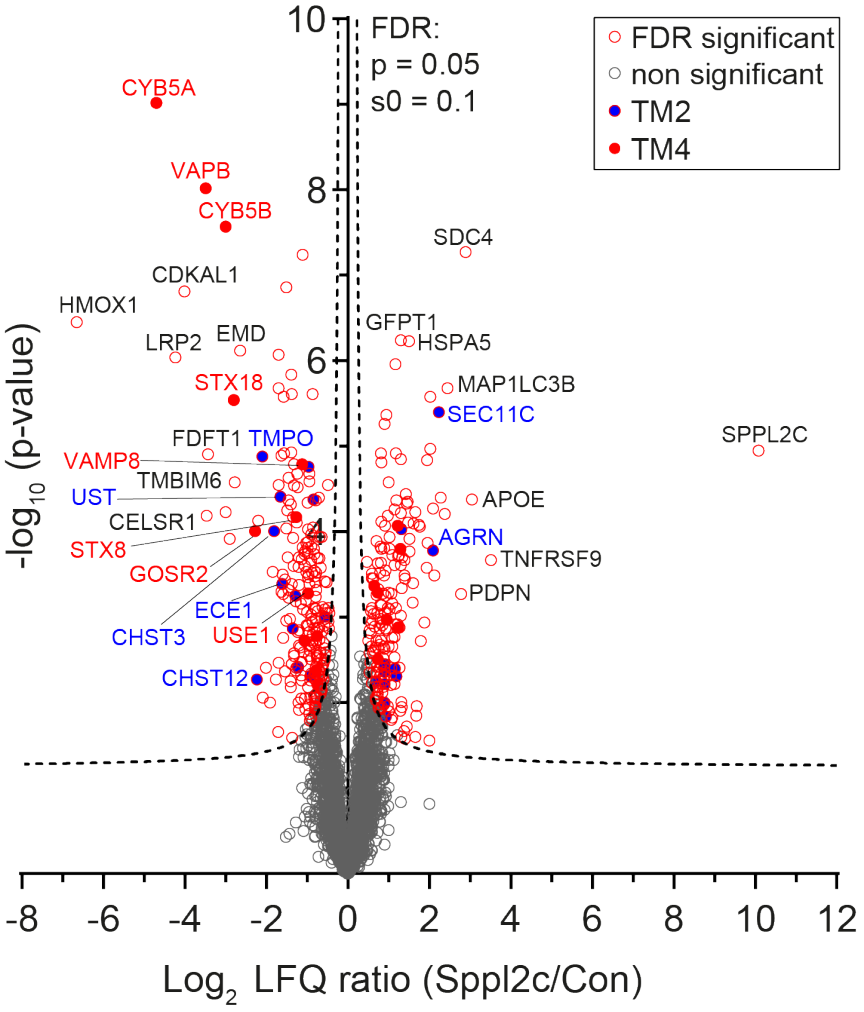

Fig. 6.2: Volcano plot of proteome analysis of SPPL2c expressing HEK293 cells. The negative log10 of the p-value (y-axis) is plotted versus the log2 LFQ ratio of SPPL2c overexpressing and control cells (x-axis) of each identified protein. A permutation based FDR correction for multiple hypotheses was applied ($p = 0.05$; $s0 = 0.1$; dashed line). Grey open circles indicate non-significantly altered proteins in SPPL2c expressing cells, red open and filled circles indicate significantly altered proteins after FDR correction. Filled red circles with red labels indicate type-IV membrane proteins and filled blue circles with red rim and blue labels indicate type II proteins altered in SPPL2c expressing cells. On the right hand side of the graph, the proteins that were increased in the samples expressing SPPL2c are depicted and on the left hand side the decreased proteins.

SPPL2c substrates (table 6.1). Regarding the orientation of the proteins, the Uniprot annotations were taken into account. Two of the most strongly decreased proteins, cytochrome b5 type A and B, were not annotated as either type-II or type-IV on Uniprot but were included in the analysis since they appear to have a similar structure to type-IV TM proteins.

Table 6.1: Significantly decreased type-II and type-IV TM proteins upon SPPL2c ectopic expression in HEK293 cells. Proteins are sorted based on their fold change and are manually annotated as type-II or -IV according to their Uniprot profile. Proteins that have already been linked to SPPL3 as substrates in previous studies are marked in bold (Voss et al. 2014a, Kuhn et al. 2015). Proteins involved in glycoprotein homeostasis are labelled in italics.

UniProt Accession	Protein name	Gene name	Type-II	Type-IV	Ratio (Sppl2c vs. Con)	Log2 (Sppl2c vs. Con)	p-value
P00167	Cytochrome b5	CYB5A	0	1*	0.04	-4.69	9.65E-10
O95292	Vesicle-associated membrane protein-associated protein B/C	VAPB	0	1	0.09	-3.48	9.58E-09
O43169	Cytochrome b5 type B	CYB5B	0	1*	0.13	-2.99	2.67E-08
Q9P2W9	Syntaxin 18	STX18	0	1	0.14	-2.8	2.91E-06
O14653	Golgi SNAP receptor complex member 2	GOSR2	0	1	0.21	-2.27	9.81E-05
Q9NRB3	***Carbohydrate sulfotransferase 12***	***CHST12***	***1***	***0***	***0.21***	***-2.23***	***5.36E-03***
P42167	Lamina-associated polypeptide 2, isoforms beta/gamma;	TMPO	1	0	0.24	-2.09	1.31E-05
Q7LGC8	*Carbohydrate sulfotransferase 3*	*CHST3*	*1*	*0*	*0.28*	*-1.81*	*9.84E-05*
Q9Y2C2	*Uronyl 2-sulfotransferase*	*UST*	*1*	*0*	*0.32*	*-1.65*	*3.86E-05*
P42892	**Endothelin-converting enzyme 1**	**ECE1**	**1**	**0**	**0.33**	**-1.61**	**4.06E-04**
Q9Y274	***Type 2 lactosamine alpha-2,3-sialyltransferase***	**ST3GAL6**	**1**	**0**	**0.39**	**-1.35**	**1.35E-03**
Q9NX62	*Inositol monophosphatase 3*	*IMPAD1*	*1*	*0*	*0.41*	*-1.28*	*5.60E-04*
Q9UNK0	Syntaxin-8	STX8	0	1	0.42	-1.26	6.77E-05
Q68CQ7	*Glycosyltransferase 8 domain-containing protein 1*	*GLT8D1*	*1*	*0*	*0.43*	*-1.22*	*3.90E-03*
Q9BV40	Vesicle-associated membrane protein 8	VAMP8	0	1	0.46	-1.12	1.63E-05
P14415	Sodium/potassium-transporting ATPase subunit beta-2	ATP1B2	1	0	0.48	-1.06	1.86E-03
Q9NZ43	Vesicle transport protein USE1	USE1	0	1	0.49	-1.04	1.87E-03
Q14BN4	Sarcolemmal membrane-associated protein	SLMAP	0	1	0.51	-0.97	5.22E-04
Q8TC12	Retinol dehydrogenase 11	RDH11	1	0	0.51	-0.96	1.72E-05
Q5KU26	**Collectin-12**	**COLEC12**	**1**	**0**	**0.53**	**-0.92**	**4.86E-03**
Q07075	Glutamyl aminopeptidase	ENPEP	1	0	0.56	-0.84	4.17E-05
Q9P0L0	Vesicle-associated membrane protein-associated protein A	VAPA	0	1	0.58	-0.77	4.15E-03
Q9UEU0	Vesicle transport through interaction with t-SNAREs homolog 1B	VTI1B	0	1	0.59	-0.75	1.66E-03
Q8N5Y8	*Mono [ADP-ribose] polymerase PARP16*	*PARP16*	*0*	*1*	*0.6*	*-0.74*	*6.10E-03*
Q8NAT1	*Protein O-linked-mannose beta-1,4-N-acetylglucosaminyltransferase 2*	POMGNT2	1	0	0.68	-0.56	9.83E-04

6.1.3 Pathway analysis of SPPL2c candidate substrates

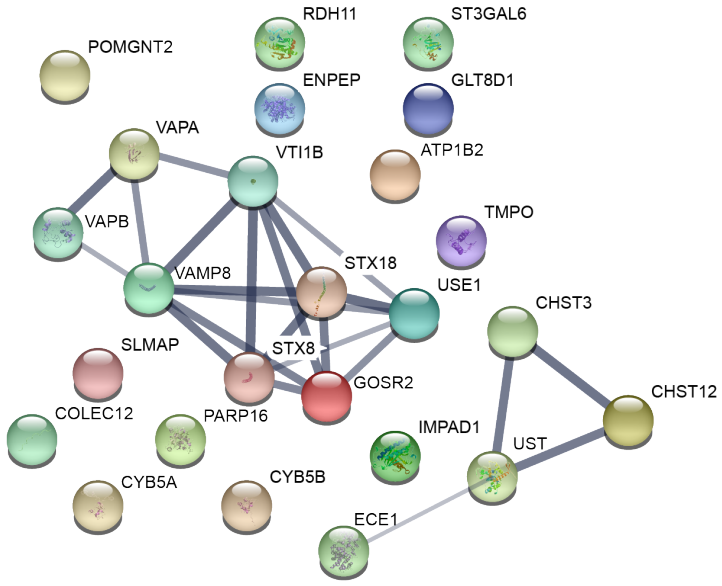

Fig. 6.3: Pathway analysis of SPPL2c candidate substrates. The online STRING 10.5 software (https://string-db.org/) was used to demonstrate possible networks of type-II and type-IV membrane proteins significantly decreased in the proteomic analysis following overexpression of SPPL2c (see Table 1). Each candidate substrate is represented by a nodule and the interactions are depicted by lines, the thickness of which indicates the degree of confidence in the prediction of the interaction.

The 25 proteins that are type-II or -IV and were decreased upon SPPL2c expression, making them potential SPPL2c substrates were uploaded to the STRING 10.5 software (https://string-db.org/) to generate a protein-protein interaction network (Fig. 6.3). This online software can link proteins based on their physical and functional associations as it draws information from a number of studies and databases. Although a number of these potential substrates do not interact with each other (eg. POMGNT2, ST3GAL6 etc.), there was a tight interaction network comprising eight single pass type-IV TM SNARE proteins with a confidence rate between 0.75 and 0.999, and an FDR of $1.01e^{-07}$ (Fig. 6.3, table 6.2). Additionally, a much smaller network consisted of four single pass type-II TM proteins with a confidence rate between 0.44 and 0.966, and an FDR of $2.6e^{-04}$ (Fig. 6.3, table 6.2).

Table 6.2: Biological pathways and processes suggested by STRING 10.5 for proteins in Table 6.1 All proteins were uploaded and then automatically sorted into interaction groups and assigned to different pathways. Listed below are the pathways identified according to either the "Kyoto Encyclopaedia of Genes or Genomes" (KEGG) or to the Biological Process of the Gene Ontology (GO) project, including the FDR.

KEGG Pathways			
pathway description	observed gene	false discovery rate	matching proteins in network
SNARE interactions in vesicular transport	5	1.01E-07	STX18,STX8,USE1,VAMP8,VTI1B
Glycosaminoglycan biosynthesis - chondroitin sulfate / dermatan sulfate	3	0.00026	CHST12,CHST3,UST

Biological Processes (GO)			
pathway description	observed genes	false discovery rate	matching proteins in network
membrane fusion	6	6.19E-05	GOSR2,STX18,STX8,VAMP8,VAPA,VTI1B
vesicle organization	6	0.000645	GOSR2,STX8,VAMP8,VAPA,VAPB,VTI1B
glycoprotein metabolic process	7	0.000784	CHST12,CHST3,POMGNT2,IMPAD1,PARP16,ST3GAL6,UST
Golgi vesicle transport	6	0.000784	GOSR2,STX18,VAMP8,VAPA,VAPB,VTI1B

6.1.4 SPPL2c is not a pseudoprotease and can cleave SNARE proteins

In order to confirm that SPPL2c has indeed a proteolytic ability, selected SNARE proteins were validated as SPPL2c substrates. To this end, the same cells as for the mass spectrometry analysis were used with the addition of cells expressing an inactive SPPL2c mutant, SPPL2c D448A (SPPL2c D/A). The vesicle-associated membrane protein-associated protein A (VAPA) and B (VAPB), the vesicle-associated membrane protein 8 (VAMP8), Syntaxin 8 and Membrin (encoded by the gene Golgi reassembly-stacking protein 2, *GOSR2*) all showed decreased levels in cells expressing SPPL2c wildtype (WT) (Fig. 6.4). This suggests that SPPL2c releases the proteins from the membrane via proteolytic cleavage, followed by degradation of the proteins causing the observed decrease in total levels. In the case of Syntaxin 18, it appears that the cleavage product is more stable than for the other substrates, which is why it is readily detectable in the Western Blot analysis as a smaller sized band. Importantly, at the same time Syntaxin 8 was also identified as a substrate of SPPL2c *in vivo* in a similar Mass Spectrometry analysis of whole testis preparations from SPPL2c$^{-/-}$ mice (Niemeyer et al. 2019). In summary, SPPL2c is able to cleave a number of SNARE proteins *in vitro*, proving for the first time that it is a catalytically active GxGD aspartyl protease.

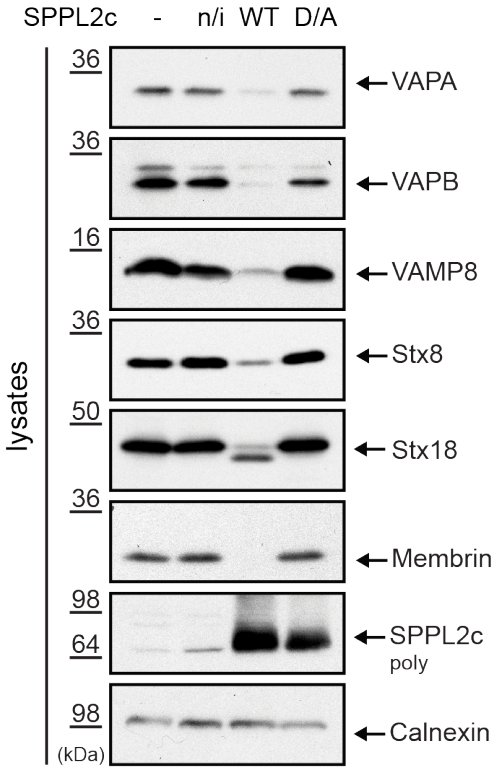

Fig. 6.4: Validation of type-IV SPPL2c substrates. Western blot of endogenous protein levels of VAPA, VAPB, VAMP8, Syntaxin 8, 18 (Stx8 & Stx18) and Membrin in HEK293 cells ectopically expressing wild type SPPL2c (SPPL2c WT) or a catalytically inactive SPPL2c (SPPL2c D/A). Non-transfected cells (-) or stably transfected but non induced SPPL2c WT cells (n/i) served as controls, expression levels of SPPL2c are depicted and Calnexin serves as loading control.

6.1.5 SPPL2c expression reduces SPPL3 protein levels

The second interaction network that was identified by STRING (3.2.11) consists of type-II TM enzymes involved in glycosaminoglycan biosynthesis (Fig. 6.3). Additionally, the levels of a number of glycosidases and glycosyltransferases were found to be affected either positively or negatively upon expression of SPP2c (table 6.3). Interestingly, some of these enzymes have been already identified as SPPL3 substrates (Voss et al. 2014a, Kuhn et al. 2015) and were found to accumulate in SPPL3$^{-/-}$ MEF cells and/or to be reduced upon SPPL3 overexpression in HEK293 cells. For this reason, the levels of endogenous SPPL3 expression in HEK293 cells that ectopically express SPPL2c were analysed.

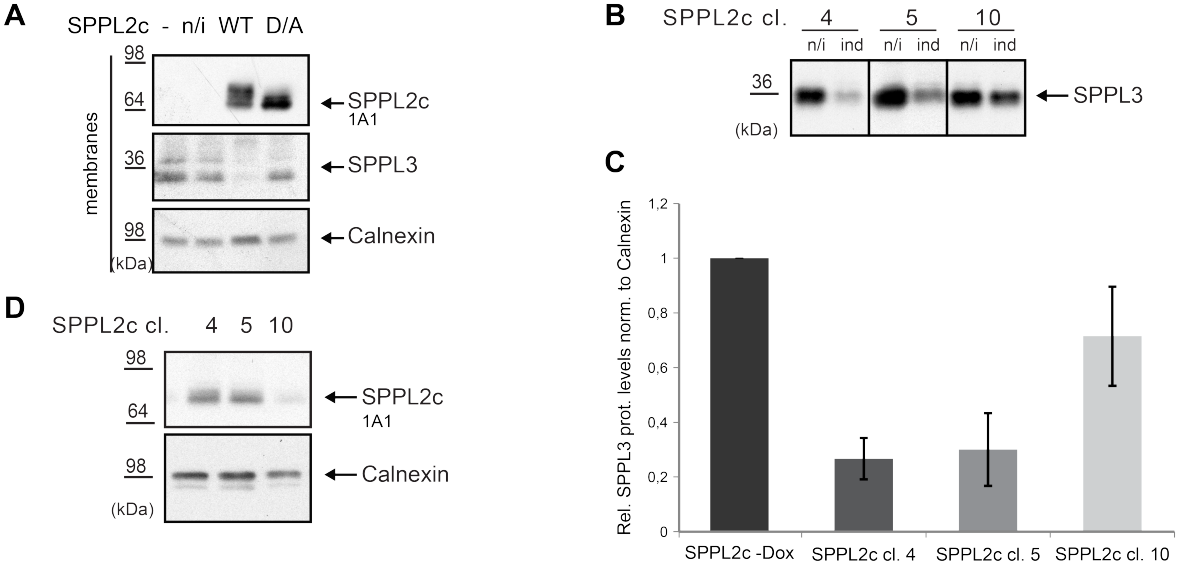

Fig. 6.5: SPPL2c reduces SPPL3 levels. A. Western blot depicting the endogenous SPPL3 levels in non-transfected cells (-), SPPL2c WT transfected but non-induced cells (n/i) and cells that inducibly express either the active (WT) or the inactive SPPL2c (D/A). **B.** The endogenous SPPL3 expression of three HEK293 clones inducibly expressing SPPL2c WT (4, 5 and 10) was analysed before (n/i) and after the induction of SPPL2c (ind.) by western blot. **C.** Quantification of three replicates for each clone of figure B. Endogenous SPPL3 protein levels were normalized to Calnexin. Depicted are the ratios of SPPL3 expression before and after induction of SPPL2c overexpression by doxycycline. SPPL3 expression of all three clones at non-induced conditions is set to 1 (SPPL2c-Dox). Mean +/- SD, n=3. **D.** Western Blot analysis depicting the ectopic SPPL2c expression of the three independent HEK293 clones under induced conditions. Calnexin served as loading control.

It was observed that catalytically active SPPL2c has the capability of reducing SPPL3 levels, while the inactive mutant SPPL2c D/A showed no such tendencies (Fig. 6.5A). To exclude the possibility of this being a clonal effect, three SPPL2c expressing cell clones were analysed (Fig. 6.5B-D). It was also observed that the decrease of SPPL3 levels seems to correlate with

the expression levels of SPPL2c, as clones with lower expression of SPPL2c have a less pronounced reduction of SPPL3 (clone 10). Other members of the SPP/SPPL family were not affected for example, SPP levels remain unchanged upon SPPL2c expression (Fig. 6.6).

Table 6.3: Glycan-modifying type-II TM proteins decreased or increased upon SPPL2c ectopic overexpression in HEK293 cells. Table includes all glycan-modifying proteins that showed a change of at least 20% upon SPPL2c expression and they are sorted according to their fold-change. Proteins that have already been linked to SPPL3 as substrates in previous studies are marked in bold (Voss et al. 2014a, Kuhn et al. 2015).

UniProt Accession	Protein name	Gene Name	Ratio (Sppl2c vs. Con)	Log2 (Sppl2c vs. Con)	p-value
Q10469	Alpha-1,6-mannosyl-glycoprotein 2-beta-N-acetylglucosaminyltransferase	MGAT2	4.74	2.24	3.98E-06
O43505	Beta-1.4-glucuronyltransferase 1	B4GAT1	2.23	1.16	3.97E-03
O60476	**Mannosyl-oligosaccharide 1.2-alpha-mannosidase IB**	**MAN1A2**	**1.88**	**0.91**	**1.01E-02**
Q8NCL4	Polypeptide N-acetylgalactosaminyltransferase 6	GALNT6	1.88	0.91	3.51E-03
Q10471	Polypeptide N-acetylgalactosaminyltransferase 2	GALNT2	1.85	0.89	1.05E-02
Q10472	Polypeptide N-acetylgalactosaminyltransferase 1	GALNT1	1.61	0.69	1.64E-02
Q9Y673	Dolichyl-phosphate beta-glucosyltransferase	ALG5	1.57	0.65	2.15E-02
Q14435	Polypeptide N-acetylgalactosaminyltransferase 3	GALNT3	1.55	0.63	2.09E-02
Q09328	**Alpha-1.6-mannosylglycoprotein 6-beta-N-acetylglucosaminyltransferase A**	**MGAT5**	**1.53**	**0.61**	**6.03E-02**
Q86SF2	N-acetylgalactosaminyltransferase 7	GALNT7	1.49	0.58	3.40E-02
Q8WVQ1	**Soluble calcium-activated nucleotidase 1**	**CANT1**	**1.49**	**0.57**	**9.43E-02**
P33908	Mannosyl-oligosaccharide 1.2-alpha-mannosidase IA	MAN1A1	1.47	0.56	9.26E-02
Q9UBQ6	**Exostosin-like 2;Processed exostosin-like 2**	**EXTL2**	**1.37**	**0.46**	**1.37E-01**
Q9UKM7	**Endoplasmic reticulum mannosyl-oligosaccharide 1.2-alpha-mannosidase**	**MAN1B1**	**1.27**	**0.35**	**3.13E-01**
O94766	Galactosylgalactosylxylosylprotein 3-beta-glucuronosyltransferase 3	B3GAT3	1.25	0.33	1.99E-01
Q9UBV7	**Beta-1.4-galactosyltransferase 7;Xylosylprotein 4-beta-galactosyltransferase**	**B4GALT7**	**1.2**	**0.26**	**3.51E-01**
O43529	**Carbohydrate sulfotransferase 10**	**CHST10**	**0.8**	**-0.32**	**3.24E-01**
Q8NBI6	Xyloside xylosyltransferase 1	XXYLT1	0.8	-0.32	1.22E-01
Q3T906	N-acetylglucosamine-1-phosphotransferase subunits alpha/beta	GNPTAB	0.78	-0.36	1.12E-01
Q7LGA3	Heparan sulfate 2-O-sulfotransferase 1	HS2ST1	0.73	-0.44	1.43E-01
O94923	D-glucuronyl C5-epimerase	GLCE	0.71	-0.5	2.66E-01
Q9NY97	N-acetyllactosaminide beta-1.3-N-acetylglucosaminyltransferase 2	B3GNT2	0.69	-0.53	1.40E-01
P52848	**Bifunctional heparan sulfate N-deacetylase/N-sulfotransferase 1**	**NDST1**	**0.69**	**-0.54**	**3.68E-02**
Q8NAT1	Protein O-linked-mannose beta-1.4-N-acetylglucosaminyltransferase 2	POMGNT2	0.68	-0.56	9.83E-04
Q4G148	Glucoside xylosyltransferase 1	GXYLT1	0.67	-0.59	1.56E-02
Q8NCH0	**Carbohydrate sulfotransferase 14**	**CHST14**	**0.65**	**-0.63**	**2.15E-02**
P15291	**Beta-1.4-galactosyltransferase 1**	**B4GALT1**	**0.63**	**-0.68**	**3.73E-02**
Q9NS00	Glycoprotein-N-acetylgalactosamine 3-beta-galactosyltransferase 1	C1GALT1	0.44	-1.19	4.23E-02
Q68CQ7	Glycosyltransferase 8 domain-containing protein 1	GLT8D1	0.43	-1.22	3.90E-03
Q9Y274	**Type 2 lactosamine alpha-2.3-sialyltransferase**	**ST3GAL6**	**0.39**	**-1.35**	**1.35E-03**
Q9Y2C2	Uronyl 2-sulfotransferase	UST	0.32	-1.65	3.86E-05
Q7LGC8	Carbohydrate sulfotransferase 3	CHST3	0.28	-1.81	9.84E-05
Q9NRB3	**Carbohydrate sulfotransferase 12**	**CHST12**	**0.21**	**-2.23**	**5.36E-03**

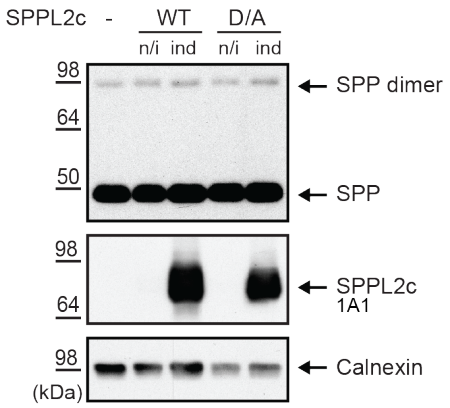

Fig. 6.6: SPP expression is not affected by SPPL2c overexpression. Western Blot analysis depicting the endogenous expression levels of SPP in control untransfected cells (-), cells overexpressing WT SPPL2c or catalytically inactive mutant, SPPL2c D/A. Stably transfected but non-induced (n/i) cells were used as controls and ectopic expression of SPPL2c WT and D/A was confirmed. Calnexin served as loading control.

Next, it was analysed whether the decrease in SPPL3 levels upon SPPL2c expression was due to an increase in the degradation of SPPL3 via the proteasome or due to a decrease in the mRNA levels of SPPL3. Neither of the possibilities seems to apply as treatment with two different proteasome inhibitors (Epoxomycin and MG132) showed no accumulation of full-length SPPL3 upon SPPL2c expression (Fig. 6.7A). Additionally, the normalised mRNA levels of SPPL3 from qPCR analysis upon induction of WT SPPL2c also showed no decrease compared to untransfected cells, non-induced controls or to cells expressing the inactive mutant of SPPL2c (D/A) (Fig. 6.7B).

Even if the reduction in SPPL3 levels would explain the accumulation of certain SPPL3 substrates upon SPPL2c expression (table 6.3), it would certainly not explain the decreased levels of some other SPPL3 substrates (table 6.1, in bold).

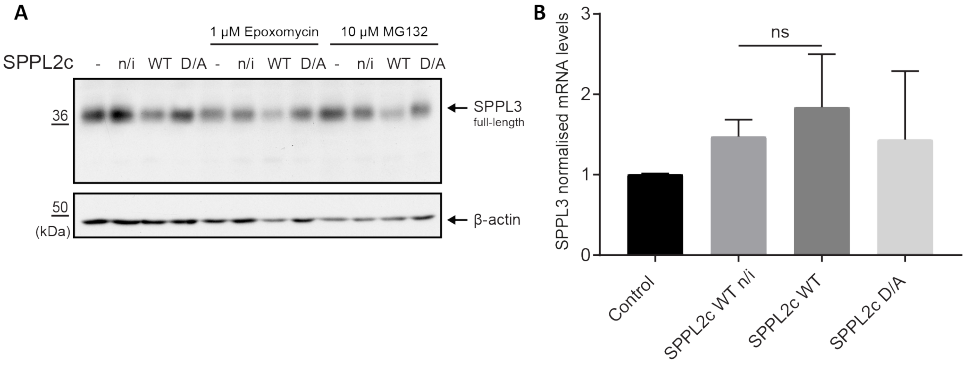

Fig. 6.7: Reduction of SPPL3 levels is not due to proteasome degradation or reduction of SPPL3 mRNA. A. The endogenous SPPL3 expression of HEK293 control cells, as well as non-induced control cells (n/i) and cells inducibly expressing SPPL2c WT or the inactive mutant D/A were analysed by western blot. Cells were either untreated or treated with proteasome inhibitors (1 µM Epoxomycin, 10 µM MG132). **B.** The mRNA levels of SPPL3 were analysed by qPCR of three biological replicates in control HEK293 cells, non-induced cells and HEK293 cells inducibly expressing WT SPPL2c or SPPL2c D/A. mRNA levels in control cells were set to 1, two sided unpaired ttest was performed ns = non-significant.

6.1.6 Substrate spectra of SPPL2c and SPPL3 do not overlap

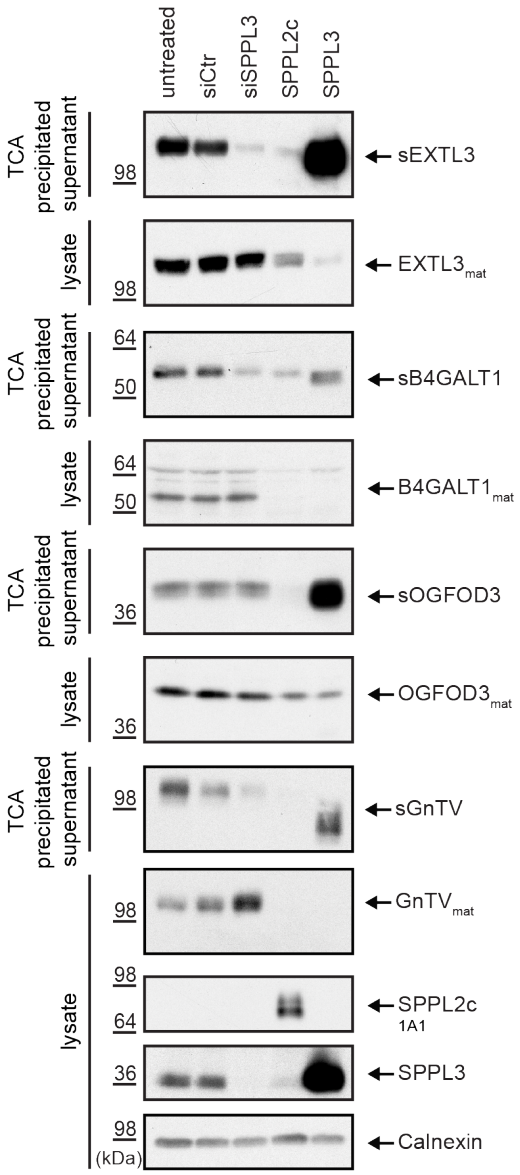

Fig. 6.8: Effect of SPPL2c on validated SPPL3 substrates. Western blot of endogenous protein levels of EXTL3, B4GALT1, OGFOD3 and GnTV in lysates of cells treated with control siRNA (siCtr) or siRNA targeting SPPL3 (siSPPL3) and cells ectopically expressing either SPPL2c or SPPL3. The secreted forms of each protein (sEXTL3, sB4GALT1, sOGFOD3, sGnTV) were also analysed in the corresponding supernatant. Endogenous and ectopic expression of SPPL3 is also analysed in the lysates, as well as the ectopic expression of SPPL2c. Calnexin was used as a loading control.

To analyse whether there is a potential overlap of the substrate spectra between SPPL2c and SPPL3, certain glycosyltransferases that have already been validated as SPPL3 substrates were chosen (Voss et al. 2014a, Kuhn et al. 2015) and it was tested if they are cleaved by SPPL2c (Fig. 6.8). Four different SPPL3 substrates were analysed: exostosin-like 3 (EXTL3), β1,4 galactosyltransferase (B4GALT1), 2-oxoglutarate and iron-dependent oxygenase domain-containing protein 3 (OGFOD3) and β1,6-N-acetylglucosaminyltransferase V (GnTV). EXTL3 levels were found unchanged according to the mass spectrometry analysis, B4GALT1 and OGFOD3 were found decreased by 40% and 30% respectively, and GnTV was found increased by approximately 50% but with a non-significant p-value of 0.06 (table 6.3). GnTV was included in the analysis because it is the best-characterised SPPL3 substrate to date (Voss et al. 2014a). The levels of SPPL3 were similarly decreased in the SPPL3 targeting siRNA treated cells (KD) as in cells ectopically expressing

SPPL2c. In both SPPL3 KD and SPPL2c expressing cells, a severe reduction in the secretion of the four substrates was observed (Fig. 6.8). However, in contrast to the SPPL3 KD cells, expression of SPPL2c causes a substantial decrease of the mature proteins within the cells (lysate).

If the reduction of SPPL3 by SPPL2c would be the only reason for reduced glycosyltransferase secretion, mature glycosyltransferases should remain stable or accumulate within the cell, similarly to the SPPL3 KD cells. However, the reduction of mature proteins is similar to that observed upon SPPL3 overexpression. So, although SPPL3 acts, as expected, like a sheddase of the four proteins analysed (Voss et al. 2014a, Kuhn et al. 2015), SPPL2c clearly has a different effect than SPPL3 on these proteins. SPPL2c does not cleave these glycosyltransferases, as observed by the lack of secretion, but also does not solely block their secretion, as observed by the lack of intracellular accumulation, demonstrating that the substrate spectra of the two proteases do not overlap. The fact that overexpression of the proteolytically inactive SPPL2c D/A has no effect on the glycosyltransferases, together with glycosyltransferases not being direct SPPL2c substrates suggests a non-direct proteolytic relation as reason for the observed phenotype.

6.1.7 SPPL2c interferes with the transport of SPPL3 substrates

It is shown that SPPL2c affects the protein levels and secretion of some SPPL3 substrates, but it is also shown this is neither via the reduction of SPPL3 levels, nor through direct cleavage of these proteins. Thus, potential mechanisms for this effect are reduced transcription of these proteins, increased degradation or altered intracellular trafficking. The last possibility appears the most plausible because it was already shown that SPPL2c can cleave certain SNARE proteins involved in transport within the secretory pathway (6.1.4). The impairment of vesicular trafficking would lead to an accumulation of glycosyltransferases in the ER/ERGIC in their immature form, however only mature endogenous glycosyltransferases can be detected by the antibodies available (Voss et al. 2014a).

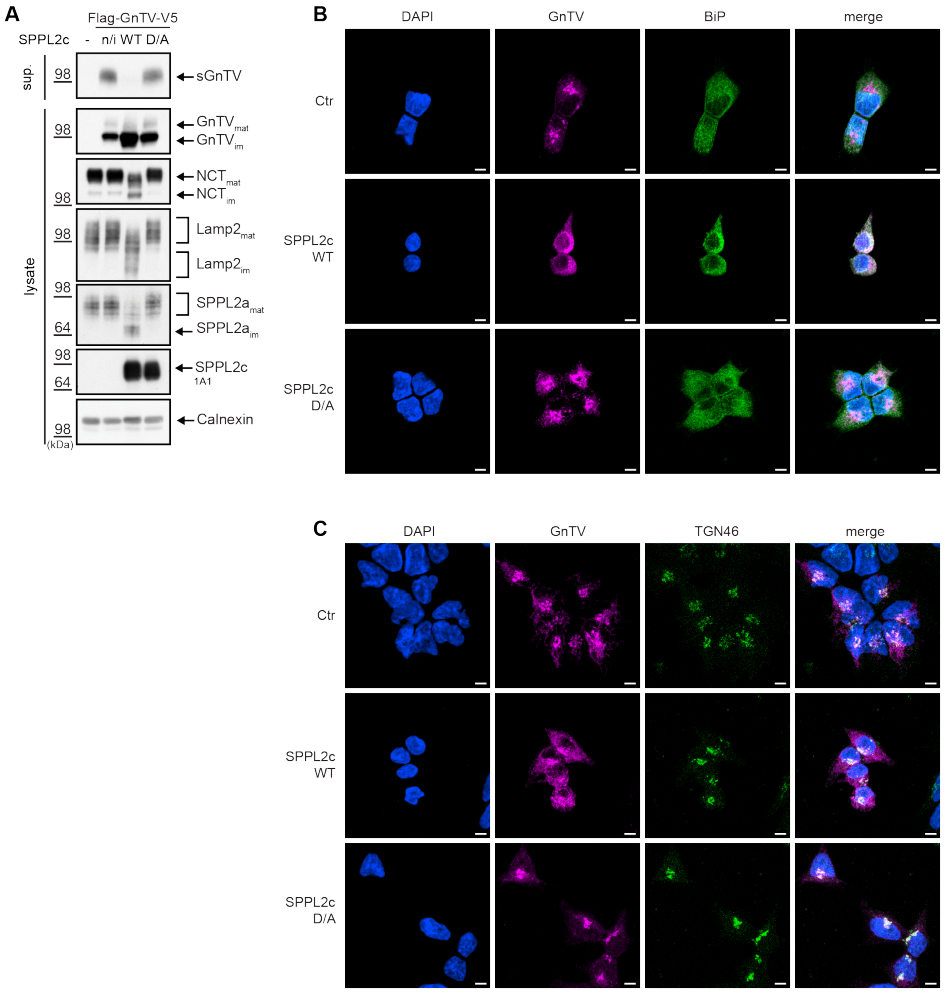

Fig. 6.9: SPPL2c inhibits GnTV trafficking and maturation. A. Western blots depicting the processing of ectopically expressed double-tagged GnTV (Flag-GnTV-V5) in lysates and conditioned media (sup.) of SPPL2c WT or SPPL2c D/A expressing cells. Non-transfected cells (-) or stably transfected but non-induced SPPL2c WT cells (n/i) served as controls. Maturation of the glycoproteins Nicastrin (NCT), Lamp2 and SPPL2a was monitored by detection of the respective mature (mat) and immature (im) version. Expression levels of the ectopically expressed SPPL2c proteases are shown and Calnexin serves as loading control. **B, C.** Immunofluorescence stainings of ectopically expressed GnTV with anti-V5 antibody either in control cells (Ctr) or in cells co-expressing either SPPL2c WT or SPPL2c D/A. The ER was stained using anti-BiP antibody (B) and the Golgi with anti-TGN46 antibody (C). Scale bar 5 µm.

As shown by Voss et.al. in 2014 (Voss et al. 2014a), the immature form of GnTV can be readily detected by western blot analysis when GnTV is expressed ectopically. Thus, proteolytically active SPPL2c (WT) or the inactive SPPL2c mutant (SPPL2c D/A) was co-expressed with N-terminally Flag- and C-terminally V5-tagged GnTV. Regarding the secretion of soluble GnTV (sGnTV), the reduction in secretion observed with the endogenous GnTV was reproduced and confirmed that only the catalytically active SPPL2c has an effect

on the glycosyltransferase. The most prominent band of ectopically expressed GnTV in the lysates is immature GnTV. An accumulation of immature GnTV can be observed only upon co-expression with SPPL2c WT (Fig. 6.9A). This accumulation is also in agreement with the results from the mass spectrometry analysis that detected an increase in cellular GnTV (table) and may be explained by impairment in the trafficking of GnTV from the ER to the Golgi. Only mature glycosyltransferases that are in the Golgi are active and can add the complex glycans to the proteins. To confirm that GnTV and other glycan modifying enzymes are indeed not reaching an active state, selected endogenous glycoproteins, like Nicastrin, lysosomal protein Lamp2 and SPPL2a were analysed. All three glycoproteins were found to be hypoglycosylated in HEK293 cells expressing SPPL2c WT, as indicated by the lower molecular weight in western blot (Fig. 6.9A). They additionally accumulate at an immature state, which most likely points to impairment of cellular trafficking affecting also their transport. To further support our theory, ectopically expressed GnTV was visualised via its V5 tag in control cells and cells expressing either active or inactive SPPL2c by immunofluorescence. Using the ER resident protein BiP or the Golgi protein TGN46 as markers, it was shown that the localisation of GnTV changes upon co-expression with WT SPPL2c. Under control conditions, GnTV was found in both the ER and Golgi, but predominantly in the latter. However, in presence of WT SPPL2c the glycosyltransferase appears to be retained in the ER. This was not observed upon expression of catalytically inactive SPPL2c D/A (Fig. 6.9B).

In conclusion, SPPL2c causes an impaired maturation of glycosyltransferases via prohibiting them from reaching the Golgi, which in turn leads to their reduced secretion and to the hypoglycosylation of various glycoproteins. These results suggest that instead of SPPL2c directly interacting and cleaving some of the SPPL3 substrates, it alters their transport through processing of SNARE proteins.

6.1.8 SNARE proteins identified by Mass Spectrometry are not responsible for GnTV trafficking

Therefore, the next step was to assess whether one of the SNARE proteins validated as SPPL2c substrates was responsible for the impaired maturation of GnTV and whether cleavage of the substrate by SPPL2c would inhibit intracellular transport of GnTV. To imitate the decrease in each SNARE's protein levels caused by SPPL2c cleavage, cells ectopically expressing GnTV were treated with targeted siRNA to mediate knockdown of each SNARE protein individually. The siRNA treatment did indeed mimic the reduction of the respective SNARE protein by SPPL2c overexpression (Fig. 6.10). Apart from the secretion of soluble GnTV and the maturation of intracellular GnTV, the glycosylation of SPPL2a as a representative glycoprotein was also analysed and all three read-outs were compared to the overexpression of SPPL2c. Only Syntaxin 18 and Membrin had a minimal effect on GnTV, slightly reducing the secretion of soluble GnTV but did not alter the maturation of cellular GnTV (Fig. 6.10E, F). SPPL2a glycosylation was slightly altered upon Syntaxin 8 knockdown, but not reaching a level comparable to the SPPL2c overexpression (Fig. 6.10D).

In conclusion, none of the proteins tested could reproduce all effects observed by SPPL2c overexpression, pointing either to a combinatory mechanism or to the existence of additional substrates that have not been identified in the mass spectrometry screen.

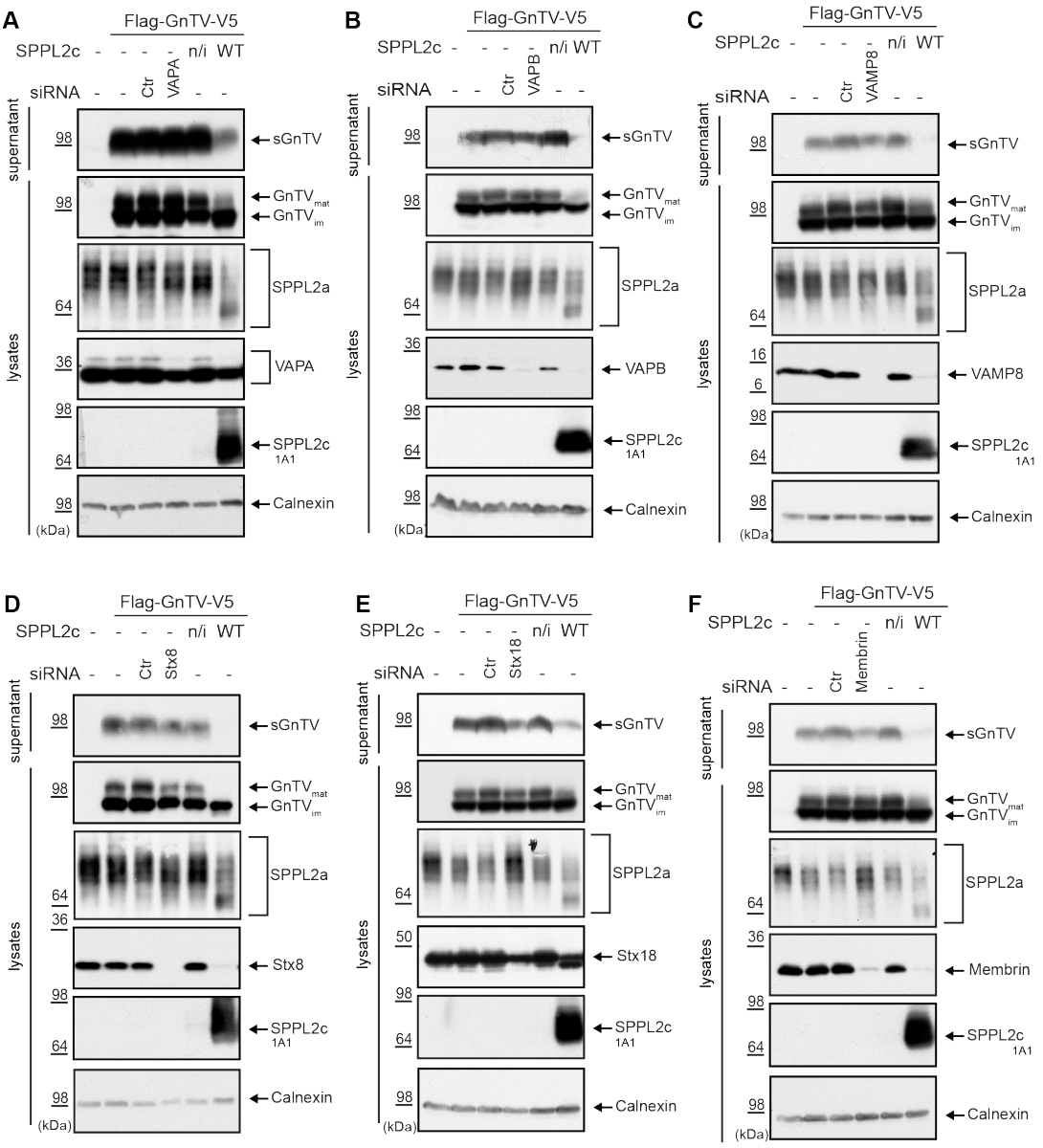

Fig. 6.10: Validated SPPL2c substrates have only minimal effects on GnTV trafficking and glycoprotein maturation. Endogenous protein levels of the validated SPPL2c substrates VAPA (**A**), VAPB (**B**), VAMP8 (**C**), Syntaxin 8 (Stx8) (**D**), Syntaxin 18 (Stx18) (**E**) and Membrin (**F**) were reduced by specific siRNAs. Non-targeting siRNA served as negative control (Ctr) and cells overexpressing SPPL2c WT were used as positive control. Non-transfected cells (-) or stably transfected but non-induced SPPL2c WT cells (n/i) served as additional controls for antibody specificity. Calnexin served as loading control and ectopic expression of SPPL2c WT was confirmed using an SPPL2c specific antibody. Western Blotting was used to follow the processing and maturation of ectopically expressed GnTV and the maturation of endogenous SPPL2a.

6.1.9 Identification of an additional SPPL2c substrate

In order to narrow down the search for additional SPPL2c substrates, the pathway analysis was used. The online software STRING 10.5 (https://string-db.org/) offers the possibility to

extend an interaction network by adding proteins that were not in the initial uploaded protein set but are known to interact closely with them. Using the "More"-function additional proteins involved in vesicular trafficking and more specifically membrane fusion were identified (Fig. 6.11A). Since proteins the trafficking of which is affected by SPPL2c are detected at a low maturation/glycosylation level, it appears that they are trapped before reaching the appropriate Golgi localisation to continue their maturation. For this reason Syntaxin 5 and Syntaxin 6 that are known for being involved in the ER to Golgi and TGN trafficking, respectively were further analysed (Rowe et al. 1998, Jung et al. 2012). Looking at the protein levels of Syntaxin 5 and 6 in lysates of cells expressing catalytically active SPPL2c compared to control cells or cells expressing inactive SPPL2c D/A, it was found that Syntaxin 6 is not a SPPL2c substrate, while Syntaxin 5 gets cleaved and produces a stable cleavage product (Fig. 6.11B).

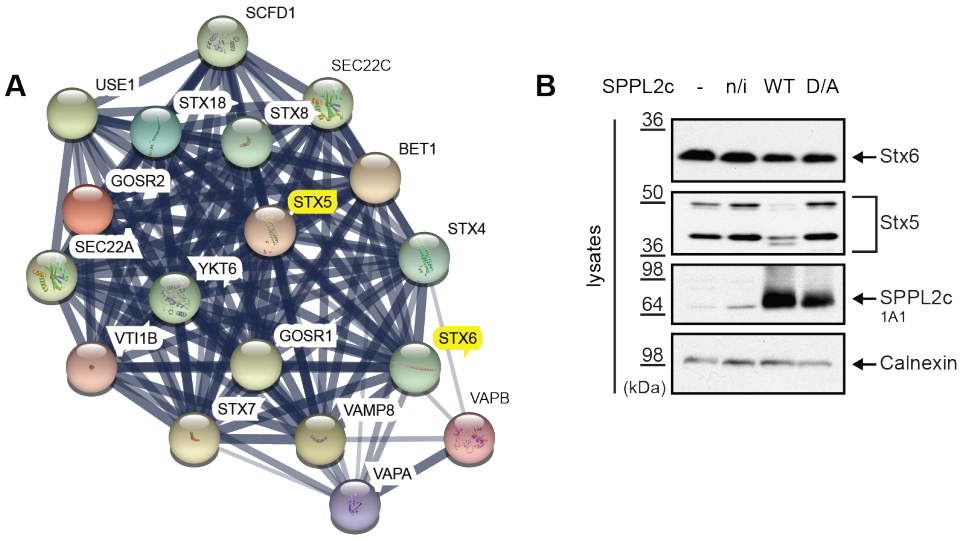

Fig. 6.11: An additional substrate of SPPL2c. A. The type-IV membrane proteins identified as candidate substrates in the proteomic analysis served as basis for extending the protein network with the function "More" of the STRING 10.5 software. Additional candidate SPPL2c substrates associated with vesicular trafficking were identified. **B.** Western Blotting of endogenous Syntaxin 5 (Stx5) and Syntaxin 6 (Stx6) levels was used to assess the processing of these candidate substrates by SPPL2c WT. Non-transfected cells (-), stably transfected but non-induced SPPL2c WT cells (n/i) and induced cells stably expressing SPPL2c D/A served as controls. Calnexin served as loading control.

6.1.10 Processing of Stx5 by SPPL2c impairs trafficking of GnTV

As before, siRNA mediated knockdown of Stx5 was used to reduce its protein levels to a similar extend as with SPPL2c expression. The HEK293-GnTV expressing cells treated with

siRNA for Stx5 convincingly mimicked the effects observed in cells expressing SPPL2c. Maturation of GnTV was reduced, immature GnTV accumulated and secretion of GnTV was blocked to a significant extent. At the same time, it became clear that Syntaxin 5 is not the only substrate responsible for the effects observed upon SPPL2c overexpression, since Nicastrin maturation and glycosylation was impaired upon Syntaxin 5 knockdown but SPPL2a glycosylation remained unaffected (Fig. 6.12).

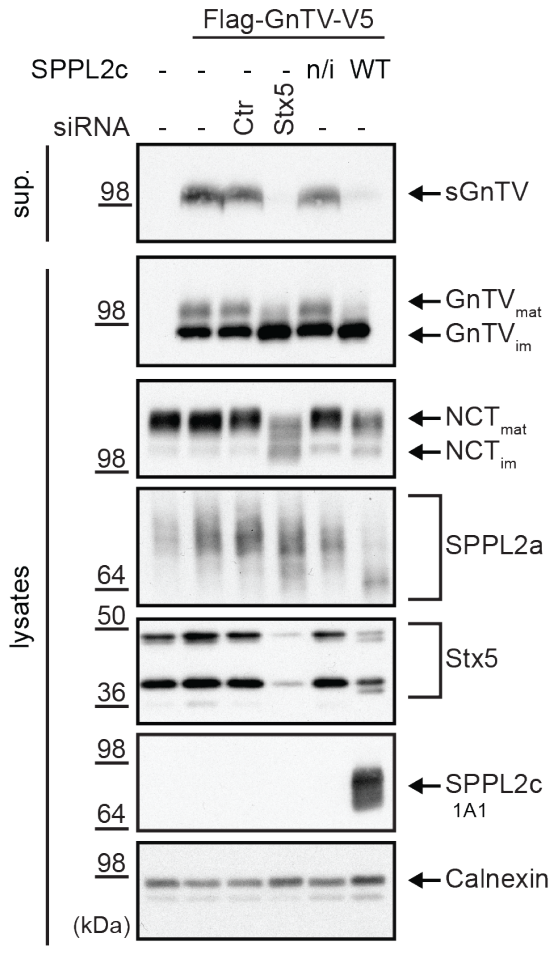

Fig. 6.12: Stx5 interferes with GnTV maturation and secretion. Western blot analysis of the processing and maturation of ectopically expressed GnTV, as well as the glycosylation of the endogenous glycoproteins Nicastrin (NCT) and SPPL2a. Protein levels of Syntaxin 5 were down regulated with specific targeting siRNA, while non-targeting siRNA (Ctr) was used as control. Ectopic expression of SPPL2c WT was confirmed. Calnexin was used as a loading control.

Total levels of Syntaxin 5 were hardly decreased upon expression of SPPL2c due to the formation of a stable cleavage product. This could explain why Syntaxin 5 was not detected as a candidate substrate in the mass spectrometry scan.

One potential mechanism, via which the cleavage of Syntaxin 5 by SPPL2c could cause the observed effect on GnTV trafficking, would be a changed localisation of Syntaxin 5. To this end, immunofluorescence stainings were performed to detect the localisation of endogenous Syntaxin 5 in control cells compared to cells expressing active (WT) or inactive (D/A) SPPL2c. Indeed, under control conditions, Syntaxin 5 localises mainly in the Golgi and expression of inactive SPPL2c D/A does not change its localisation. However, expression of catalytically active SPPL2c caused a more diffused staining of Syntaxin 5 that co-localised neither with the Golgi marker TGN, nor with the ER marker BiP (Fig. 6.13A). These data suggest that Syntaxin 5 loses its ability

to mediate membrane fusion at the *cis*-Golgi due to processing by SPPL2c and is most likely trapped in an intermediate compartment, likely in the ERGIC.

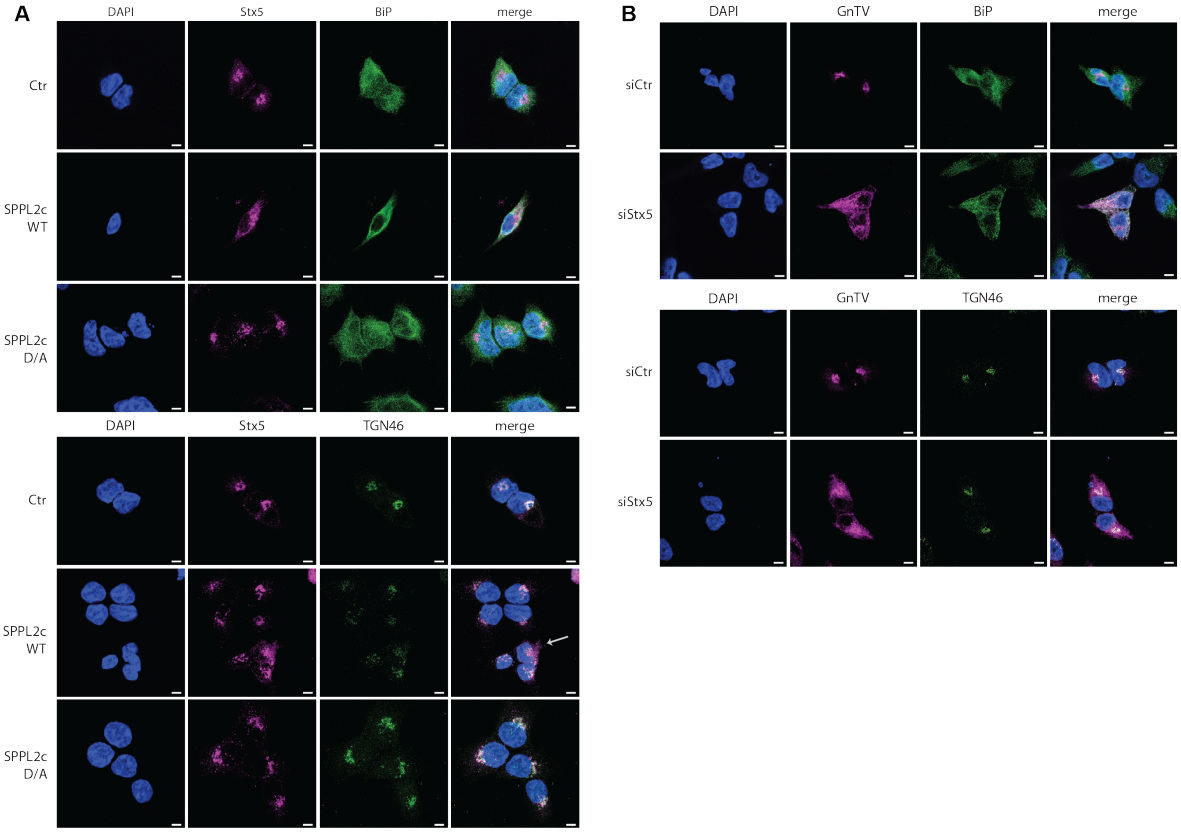

Fig. 6.13: SPPL2c alters localisation of Stx5, which in turn inhibits trafficking of GnTV. A. Endogenous Syntaxin 5 was visualized in control cells without SPPL2c expression (Ctr) and in cells overexpressing SPPL2c WT or SPPL2c D/A by immunofluorescence. BiP was used to mark the ER and TGN46 the Golgi. White arrow indicates cells with disturbed Golgi and Syntaxin 5 staining. **B.** Ectopically expressed GnTV was visualized using anti-V5 antibody in cells treated either with non-specific siRNA (siCtr) or with siRNA targeting Syntaxin 5 (siStx5). BIP was co-stained as ER marker protein and TGN46 as Golgi marker protein. Scale bar 5 µm.

Consequently, SPPL2c alters the localisation of Syntaxin 5 (Fig. 6.13A) and also clearly affects the localisation of GnTV (Fig. 6.9). In order to confirm that Syntaxin 5 is the main SPPL2c substrate the cleavage of which impairs trafficking of GnTV, immunofluorescence stainings were performed in the cells stably expressing tagged GnTV upon treatment either with control siRNA or with siRNA targeting Syntaxin 5 (Fig. 6.13B). In agreement with the previous findings, and using BiP and TGN46 to visualise the ER and the Golgi, GnTV localisation visibly shifts from more Golgi-based to more ER-based in the absence of Syntaxin 5.

Collectively, these results indicate that cleavage of Syntaxin 5 by SPPL2c causes the loss of its

SNARE function making it responsible for the hiatus in GnTV trafficking that leads to reduced maturation and shedding.

6.1.11 SPPL2c overexpression in HEK cells affects compartment structures

So far, we have shown that through cleavage of different proteins associated to vesicle trafficking, SPPL2c is capable of blocking the exchange of proteins and membranes between the ER and the Golgi. However, in order to maintain its organelle integrity, the Golgi requires a continuous exchange of vesicles with the ER (Ward et al. 2001).

For this reason the effect that prolonged SPPL2c expression would have on the integrity of ER and Golgi in HEK293 cells expressing catalytically active SPPL2c was investigated. Using different markers for ER (BiP), *cis*/*medial*-Golgi (Giantin), *trans*-Golgi (TGN46) and whole Golgi (Cab45), the effect of WT SPPL2c expression was assessed in a time-dependent manner (24 and 48 hours) and it was compared to expression of catalytically inactive SPPL2c D/A. BiP, Giantin and Cab45 were significantly mislocalised in a time-dependent manner upon expression of WT SPPL2c (Fig. 6.14). The results obtained from the immunofluorescence stainings indicate that disturbance of transport by SPPL2c is capable of disturbing the integrity of these compartments and the effect becomes stronger the longer the protease is present. TGN46 was also altered upon SPPL2c expression, however to a lesser extent. It is important to point out that although high expression of a polytopic, ER-resident, membrane protein, such as SPPL2c D/A, might be a source of ER-stress, no effect on the localisation of the organelle markers was observed upon expression of catalytically inactive SPPL2c (Fig. 6.14).

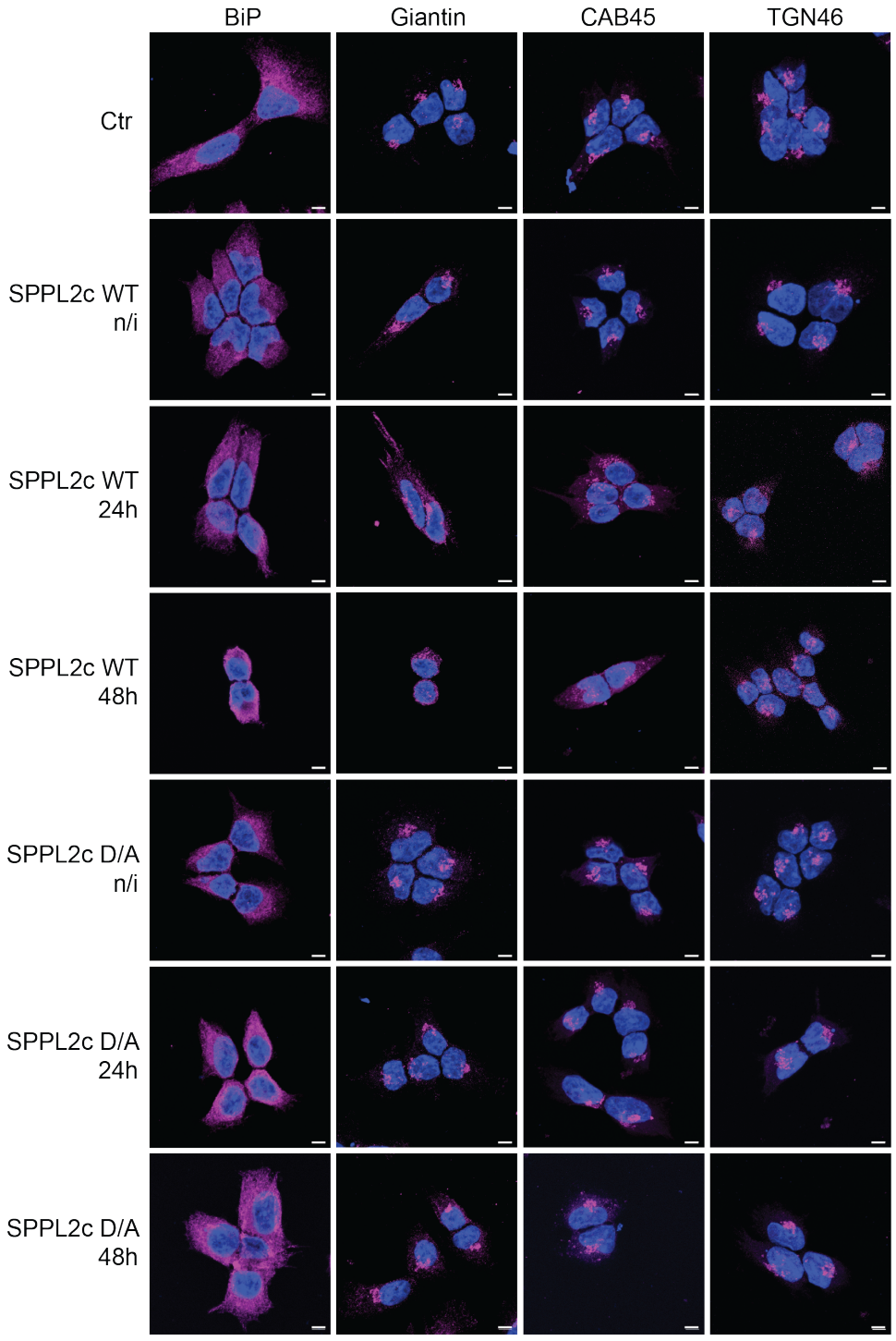

Fig. 6.14: SPPL2c disturbs the integrity of subcellular compartments. Control cells and cells with inducible expression of SPPL2c WT and the inactive mutant D/A were cultured for 72h. Expression of SPPL2c WT and D/A was either non-induced (n/i) or induced by addition of doxycycline for either 24h or 48h, as indicated. Anti-BiP antibody was used to stain the ER, anti-Giantin for the *cis*/*medial*-Golgi, anti-TGN46 for the *trans*-Golgi Network and Cab45-specific antibody for all Golgi subcompartments. Upon expression of catalytically active SPPL2c, the morphologies of ER and *cis*-Golgi were altered compared to controls. Scale bar 5µm.

6.1.12 SPPL2c has a proteolytic function *in vivo*

SPPL2c expression has only been detected in testis tissues from humans and mice (6.1.1). Through this study, we gained a better understanding of the effect that SPPL2c expression has on a cell and it has become clear that under most physiological conditions, an impairment of vesicular transport by SPPL2c would be detrimental for an organism. Analysis of maturation of the glycoproteins Nicastrin and SPPL2a in testis, kidney, brain, spleen and liver from wildtype C57BL/6 mice, revealed a hypoglycosylation and an accumulation of immature glycoproteins in testis (Fig. 6.15A). These results are in accordance to what was observed *in vitro*.

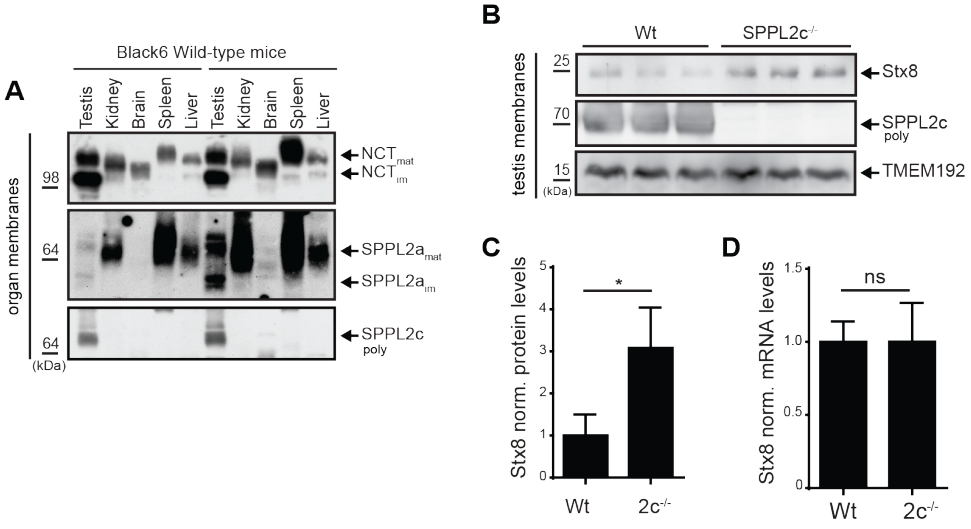

Fig. 6.15: SPPL2c retains functionality *in vivo*. A. Endogenous Nicastrin (NCT) and SPPL2a were analysed by western blot in membrane preparations from testis, kidney, brain, spleen and liver in littermate male C57BL/6 mice. Immature proteins (im) accumulate in testis compared to other tissues. SPPL2c protein is only detected in testis tissue. **B.** Analysis of Syntaxin 8 (Stx8) in whole testis from SPPL2c$^{-/-}$ mice compared to wildtype (Wt) littermates. SPPL2c is absent in the SPPL2c$^{-/-}$ mice as expected, TMEM192 serves as loading control. **C.** Quantification of Western Blot in panel B, Syntaxin 8 protein levels were normalized to those of TMEM192. Syntaxin 8 levels of wildtype mice were set to 1. Bars represent mean values of n=3 animals +/- SD, * $p<0.05$. **D.** Syntaxin 8 (Stx8) mRNA levels in testis of SPPL2c$^{-/-}$ and the wildtype mice were analysed by real-time qPCR and normalized to that of Tuba1a. Stx8 mRNA level of wildtype animals was set to 1. n=6 individual animals from two independent experiments +/- SD. For statistical analysis an unpaired Student's t-test was performed. ns = not significant. Experiments in B-D performed by Torben Mentrup.

To confirm that SPPL2c is indeed a catalytically active protease also *in vivo* that can alter vesicular trafficking, testis from SPPL2c deficient mice were analysed for accumulation of already verified SPPL2c substrates. In collaboration with Torben Mentrup and Bernd

Schröder from Dresden, an accumulation of Syntaxin 8 in whole testis membrane preparations of the SPPL2c deficient mice compared to control littermates was successfully demonstrated (Fig. 6.15B). Transcription levels of SPPL2c mRNA were not altered in the SPPL2c deficient mice, so the accumulation of Syntaxin 8 can be attributed to lack of SPPL2c processing (Fig. 6.15C-D).

6.1.13 SPPL2c supports intracellular reorganisation in maturing spermatids

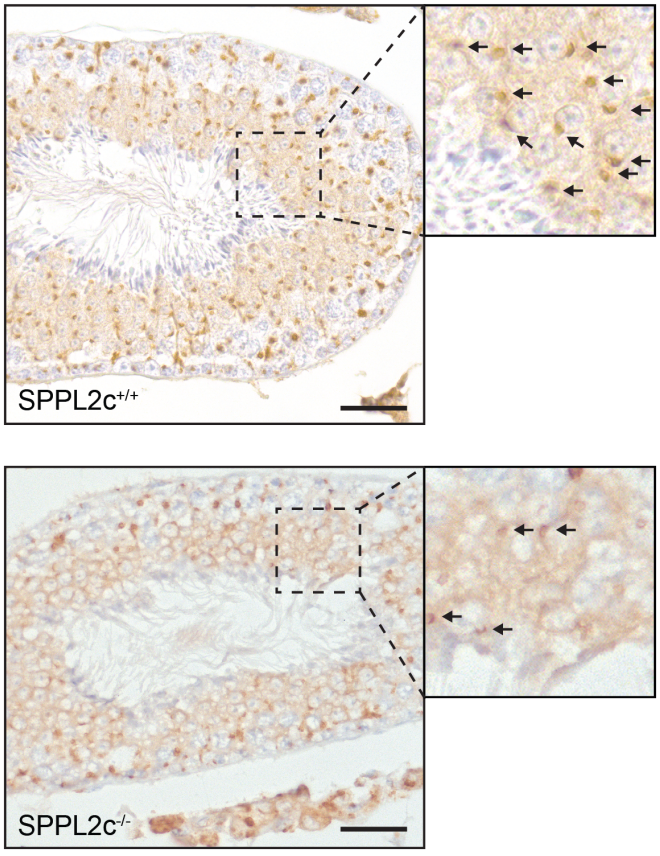

Fig. 6.16: SPPL2c interferes with the proper localisation of Cab45 in spermatids. Immunohistochemical stainings of seminiferous tubular cross-sections of SPPL2c$^{+/+}$ and SPPL2c$^{-/-}$ mice using anti-Cab45 antibody. Closer magnifications are indicated with dashed lines and black arrows mark pre-acrosomal structures. Experiment performed by Artur Mayerhofer.

The physiological expression of SPPL2c in the testis is remarkably high, only 5 µg of protein from whole testis membrane preparations of humans or mice are sufficient to detect amounts similar to 1:50 dilution of membrane preparations from cells ectopically expressing SPPL2c (Fig. 6.1). As has been shown by Niemeyer et al. 2019, SPPL2c expression *in vivo* can only be detected in a limited type of cells in the testis, the maturing spermatids. The fact that endogenous SPPL2c derives from only a limited number of cells within the testis, points to an extremely high expression of SPPL2c in these specific cells with levels similar to the HEK293 cells that homogeneously overexpress SPPL2c.

A

	Person A	Person B	Person C	Person D	Person E	Picture ID	Mouse genotype	pro acrosomic structures: Microscopic field #1	Microscopic field #2	Microscopic field #3	Average of 3 fields
Decision						36-6	SPPL2c $^{+/+}$	1	2	2	1,7
						37-5	SPPL2c $^{+/+}$	2	3	4	3,0
	wrong					37-0	SPPL2c $^{+/+}$	4	6	1	3,7
						37-1	SPPL2c $^{+/+}$	5	4	2	3,7
						36-8	SPPL2c $^{+/+}$	3	4	5	4,0
			wrong		wrong	36-7	SPPL2c $^{+/+}$	5	5	7	5,7
	wrong					35-7	SPPL2c $^{-/-}$	4	6	7	5,7
			wrong	wrong		35-6	SPPL2c $^{-/-}$	6	6	6	6,0
	wrong	wrong	wrong		wrong	36-1	SPPL2c $^{-/-}$	8	6	6	6,7
						36-3	SPPL2c $^{-/-}$	8	6	6	6,7
						35-4	SPPL2c $^{-/-}$	6	8	7	7,0
						36-2	SPPL2c $^{-/-}$	8	9	7	8,0
						36-0	SPPL2c $^{-/-}$	9	11	5	8,3
						35-9	SPPL2c $^{-/-}$	4	13	9	8,7
Correct answers	11/14	13/14	11/14	13/14	12/14						
Percentage of correct answers	79	93	79	93	86						

B

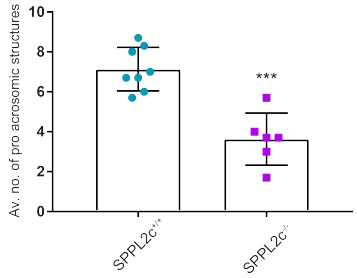

Fig. 6.17: Quantification of Cab45 stainings in seminiferous tubular cross sections. **A.** Pre-acrosomal resembling structures stained with Cab45 (Fig. 6.16, black arrows) were quantified in n=14 stage VII/VIII seminiferous tubules (n=6 SPPL2c$^{+/+}$ and n=8 SPPL2c$^{-/-}$). On the right hand side of the table, the averages of the stainings counted for each single picture as well as the single measurements of each field (microscopic fields 1-3) are depicted. The genotype of each mouse is indicated, as well as the blinded-assignment of the pictures by five independent people, accompanied by the number and percentage of correct evaluations, the wrongly guessed images are marked in red. **B.** Graph depiction of the average Cab45 stainings per image according to genotype. The average number of stainings per tubule is depicted for each genotype, mean +/- SD. Unpaired, two-sided Welch's t test. ***p<0.001 (p=0.0004)

Spermatids, the cell type that expresses SPPL2c, are one step before spermatozoa in the differentiation process of spermatogenesis. At this stage cells undergo the loss of parts of the cytosol and many organelles, including ER and Golgi, in order to form the acrosome (Berruti and Paiardi 2011). To assess the potential role of SPPL2c in this procedure, SPPL2c$^{-/-}$ mice were compared to their wildtype littermates, SPPL2c$^{+/+}$. More precisely, in a collaborative analysis, seminiferous tubular sections from these mice were stained with Cab45 and were analysed on stages VII/VIII of spermatogenesis as defined by Meistrich and Hess (Meistrich and Hess 2013). The localisation of this Golgi resident protein was severely affected by the presence or not of SPPL2c in the HEK cells (Fig. 6.14). In wildtype mice, Cab45 localised in precise and dense structures adjacent to the cell nuclei, while in SPPL2c$^{-/-}$ mice, Cab45 staining appeared more diffused and less focused on specific structures (Fig. 6.16).

To further confirm the observed differences, 14 images from both genotypes were used to quantify the average number of structures per tubule and also 5 individuals blindly evaluated the pictures regarding the genotype. Both tests gave positive results with approximately 50% reduction of the quantified dense structures in knockout animals compared to wildtype and an 86% average hit rate in the blinded assignment of genotypes (Fig. 6.17). This evidence suggests that SPPL2c is necessary in order for the compartmental reorganisation in spermatids to take place successfully.

6.1.14 The glycome fingerprint of SPPL2c$^{-/-}$ sperm is altered

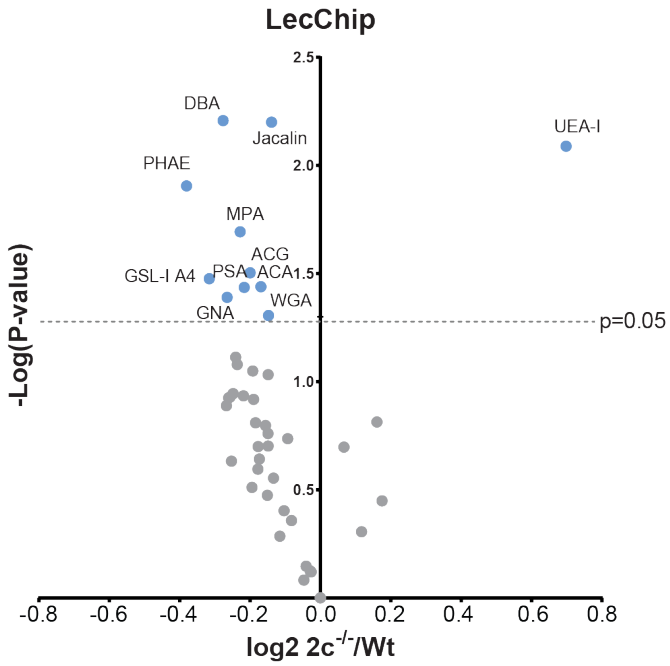

Fig. 6.18: Volcano plot of a lectin microarray analysis of sperm lysates from SPPL2c$^{-/-}$ mice compared to SPPL2c$^{+/+}$. Each circle represents one lectin, with grey circles being lectins with non-significantly changed binding affinity. Significantly altered lectins are marked in light blue, above the dashed line p-value>0.05. Lectins on the left side of the blot demonstrate reduced binding while UEA-I on the right side has increased binding in SPPL2c$^{-/-}$ spermatozoa. Experiment performed by Merav Shmueli.

The formation of the acrosome is just one of the alterations that take place during the maturation of sperm. Another characteristic of spermatozoa that plays a crucial role for successful fertilization of the ovum is the glycocalyx. This complex glycan structure covers the sperm head and holds the key for the species selectivity (Pang et al. 2011). In a collaborative analysis, we were able to analyse the glycome fingerprint of mature spermatozoa that were isolated from the cauda epididymis of SPPL2c$^{+/+}$ and SPPL2c$^{-/-}$ mice. The analysis was performed using a lectin chip microarray (LecChip) containing 45 different plant lectins. The total lysates from mature spermatozoa were analysed and the reactivity of 10 lectins was significantly reduced in the SPPL2c$^{-/-}$ sperm, while the reactivity of one lectin was increased

in the same sperm compared to the wildtype littermates (Fig. 6.18). One of the lectins that was found decreased in the SPPL2c$^{-/-}$ sperm, *Pisum sativum* (PSA), has been reported as a marker of the acrosome content (Benoff 1997). The reduction of another lectin, Wheat Germ Agglutinin (WGA), is an established marker for teratozoospermia (Benoff 1997). These data indicate that either directly or, most likely, indirectly via the disturbance of the cellular reorganisation, SPPL2c is also capable of affecting the glycan structures within and surrounding the mature sperm. Thus, lack of SPPL2c expression at the right step of sperm maturation negatively affects both the formation of the acrosome and the correct glycosylation of cellular structures.

6.2 Discussion

In this study, it is demonstrated for the first time that SPPL2c is actually an active protease, not a pseudoprotease or a pseudogene lacking any functional expression, as it was believed since its discovery (Golde et al. 2009, Voss et al. 2013). Additionally, it is shown that the GxGD-motif that characterises this family of proteins is not only functional but also indispensable also for SPPL2c, as the SPPL2c mutant D448A (SPPL2c D/A) lacks any proteolytic activity.

Microarray analysis in human tissues in the past had detected mRNA levels of SPPL2c in brain, skin, heart and testis, although no protein levels were detected (Friedmann et al. 2004a). That lack of SPPL2c protein levels created doubts concerning the mRNA results that could also be explained by contamination of the mRNA with the intronless cDNA of *SPPL2C*, which would give a false positive mRNA expression. In this analysis, we were capable to detect SPPL2c protein expression for the first time. SPPL2c expression was not detected in tissues like brain, kidney, spleen and liver, but was only detected in testis from humans and mice (Fig. 6.1). This very specific expression pattern of SPPL2c suggests that it is not a pseudoprotease but it should have a specific functional purpose.

To shed light into the function of SPPL2c, proteomic screening of HEK293 cells overexpressing ectopic SPPL2c was performed compared to control cells, lacking SPPL2c expression (Fig. 6.2). Although SPPL2c is not expressed at all in the control cells, a small amount of the protein must have been carried-over during the measurements from the SPPL2c positive cells, which at the end allows the high-fold change presented in the volcano plot. This technique allowed us to identify the first potential substrates of SPPL2c, which were narrowed down to type-II or type-IV TM proteins based on the specificity of the SPP/SPPL family (Voss et al. 2013, Mentrup et al. 2017a). Potential substrates clustered to two main pathways, vesicular trafficking and protein glycosylation (Fig. 6.3). A number of the SNARE proteins involved in vesicular trafficking through membrane fusion, were validated as SPPL2c substrates. Their processing also demonstrated the importance of the GxGD motif as catalytic site of the protease (Fig. 6.4). Additionally to those SNARE proteins that were identified as substrates via the proteomic screen (Fig. 6.3), Syntaxin 5 was also considered and identified as a substrate through the extended pathway analysis (Fig. 6.11).

SPPL2c is believed to reside in the early compartments of the secretory pathway like ER, ERGIC or even *cis*-Golgi (Friedmann et al. 2004b). Taking that into consideration, it is most likely that the cleavage of the substrates takes place within these early compartments, as all of these proteins either function in this compartment or pass-through during their maturation. The processing of these substrates seems to differ with only two of the substrates, Syntaxin 5 and 18, giving rise to stable cleavage products, while the majority of substrates show decreased protein levels but no cleavage product (Fig. 6.3, 6.11). The absence of a cleavage product suggests a rapid degradation, possibly through ERAD, which would be enhanced due to the high protein accumulation of the substrate protein in the ER upon SPPL2c expression. The presence of a stable fragment, especially in the case of Syntaxin 5, results in almost no change in the total protein levels of Syntaxin 5, which could explain why this substrate was not identified in the proteomic screen. Despite the recognition of at least seven SNARE

proteins as SPPL2c substrates in the current study, it also appears that SPPL2c has some specificity, as another SNARE protein, Syntaxin 6, was not processed by the protease (Fig. 6.11). One reason why SPPL2c maybe does not recognise Syntaxin 6 as a substrate can be that although Syntaxin 6 contains a C-terminal transmembrane domain, it has a high homology with the SNAP-25 family and is actually considered a member of that family (Jung et al. 2012). These data suggest that SPPL2c has specific substrate requirements and cleavage mechanism, as is common for other members of the SPP/SPPL family (Lemberg and Martoglio 2002, Martin et al. 2009, Fluhrer et al. 2012). Further analysis would be required to shed more light into both the mechanism of cleavage and the substrate requirements.

Cleavage of Syntaxin 5 by SPPL2c leads to a mislocalization of the SNARE protein. Following the processing, Syntaxin 5 appears incapable to properly reach the Golgi, and even the morphology of the Golgi appears to be negatively affected (Fig. 6.13A). We believe that cleavage of Syntaxin 5 in close proximity to its TMD probably leads to the release of the protein, which can no longer perform its role of triggering the specific fusion of membranes during vesicle transport (Fig. 6.19). This observation is in accordance with a study published in 1998, where it is suggested that Syntaxin 5 is not only essential for the transport of cargo from the ER to the Golgi, but also for the assembly of pre-Golgi intermediates (Rowe et al. 1998). As we already observed that cargo proteins, such as glycosidases and glycosyltransferases do not reach their final destination but are most likely retained in the ER (Fig. 6.8, 6.9), it seems very convincing that Syntaxin 5 indeed plays a role in their transport. It was successfully shown that absence of Syntaxin 5 is enough to block the maturation and secretion of GnTV, as well as decrease the glycosylation of certain glycoproteins, most probably by inhibiting GnTV from reaching the Golgi (Fig. 6.12, 6.13B). A similar effect would be expected when Syntaxin 5 can no longer mediate the transport to the Golgi because of SPPL2c expression (Fig. 6.19).

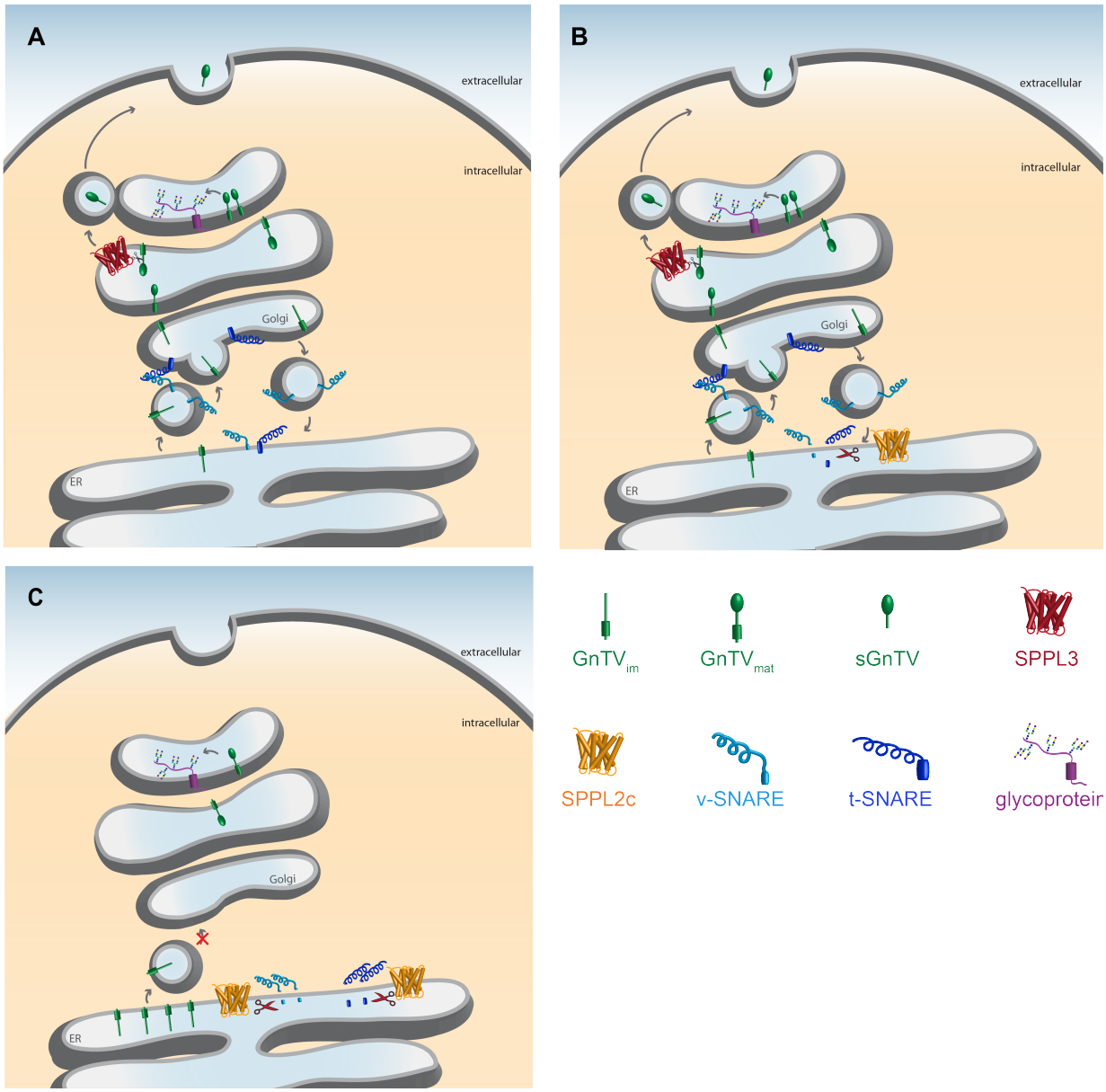

Fig. 6.19: Hypothetical model demonstrating the effect of SPPL2c expression on vesicular trafficking. A. Protein synthesis of membrane-spanning glycosyltransferases (represented here by GnTV in green) and members of the SNARE family (dark and light blue representing t- and v-SNAREs, respectively) starts on the ER and the proteins are then inserted in the ER. The glycosyltransferases are transported to the Golgi via vesicle transport and the presence of SNARE proteins is required for the vesicle fusion at its destination. These glycan-modifying enzymes move within the different compartments of the Golgi. They mature and as they make their way towards the *trans*-Golgi, they either meet SPPL3 (red) that can shed and liberate their active site, or they catalyse glycosylation of proteins (glycoprotein depicted in purple). **B.** SPPL2c expression is localised to the ER, where selective SNARE proteins are proteolytically processed. This processing leads either to the release of the SNARE proteins from the membrane and/or to their rapid degradation. Numerous SNARE proteins are processed in this step as they all pass through the ER before reaching their final destination. **C.** Cleavage of SNARE proteins impairs vesicle fusion at the *cis*-Golgi and amongst other cargo proteins, immature glycosyltransferases accumulate in the ER, while their amount in the Golgi decreases. The lack of mature glycosyltransferases leads to a decrease in protein glycosylation and at the same time, SPPL3 (red) protein levels are decreased. Decrease of SPPL3 is most likely a secondary-response effect in order to preserve the activity of the small amount of glycoproteins that have reached the Golgi.

The rest of the SPPL2c substrates that were identified in the mass spectrometry screen are not directly involved in the transport of proteins from the ER to the Golgi so it is not surprising that their cleavage by SPPL2c does not result in decreased maturation and shedding of GnTV (Fig. 6.10). However, additional phenotypes can be expected regarding the trafficking between different organelles involved in the secretory pathway. The proteins levels of VAPA, VAPB, VAMP8, Stx8, Stx18 and Membrin were all affected by SPPL2c (Fig. 6.4). Amongst other functions, VAPA can interact with Oxysterol-binding protein-related protein 3 (OSBPL3) and together they are implicated in the export of specific proteins and lipids, such as ceramide, from the ER (Wyles et al. 2002, Wyles and Ridgway 2004). Although VAPB shares a number of common functions with VAPA (Huttlin et al. 2015), it has been found to play an important role in amyotrophic lateral sclerosis through its participation in the ER UPR (Chen et al. 2010). VAMP8 (endobrevin) is thought to participate in multiple procedures, such as the fusion of late endosomes, together with Syntaxin 8 (Antonin et al. 2000), the release of granules from human platelets (Polgar et al. 2002), the fusion of lysosomes and autophagosomes (Furuta et al. 2010), and the exocytosis in the exocrine pancreas (Wang et al. 2004a). Membrin, encoded by the gene *GOSR2*, plays a role in ER to Golgi trafficking and although it is ubiquitously expressed, it seems to have a significant role especially in the nervous system (Praschberger et al. 2017). The effect of SPPL2c expression on these processes will need to be investigated in further studies.

Some of the proteins that showed significantly decreased protein levels in the proteomic screen have been previously reported as substrates of SPP (Cyb5a) (Boname et al. 2014) or SPPL3 (B4GALT1, OGFOD3) (Kuhn et al. 2015) (Fig. 6.2). Regarding the SPP substrate, it was shown that Cyb5a is not a substrate of SPPL2c (Niemeyer et al. 2019), as well as that SPP levels remain unchanged upon SPPL2c overexpression (Fig. 6.6). As this study successfully shows that SPPL2c overexpression can inhibit the transport of proteins out of the ER and into the Golgi, a plausible explanation for the increased cleavage of Cyb5a is its prolonged stay at

the ER, where also SPP resides.

Regarding SPPL3, it was apparent that endogenous protein levels were decreased proportionally to the expression of catalytically active SPPL2c (Fig. 6.5). It has been previously shown that SPPL3, which resides in the Golgi, is capable of cleaving mature glycosidases and glycosyltransferases (Voss et al. 2014a, Kuhn et al. 2015). In this context, decreased levels of SPPL3 can preserve a higher amount of glycan modifying enzymes in the Golgi, where they are active (Fig. 1.15). Since SPPL2c expression, blocks the maturation of glycan modifying enzymes and inhibits the substrates of SPPL3 from reaching their final location in the *trans*-Golgi (Fig. 6.8, 6.9), it is tempting to consider that the decrease of SPPL3 is due to a secondary effect of the SPPL2c expression and a counter-mechanism to preserve the remaining active glycan modifying enzymes (Fig. 6.19). However, so far efforts to attribute this decrease to proteasome degradation or reduced transcription levels have failed (Fig. 6.7). Thus leaving other forms of degradation and/or translational regulation as possible causes.

We have seen that SPPL2c can inhibit vesicular transport and affect the protein levels of numerous proteins, but the next aim was to understand how the expression of SPPL2c could affect the intracellular morphology of the cell. To this end, SPPL2c was overexpressed in HEK293 cells and a time-dependent fragmentation of the Golgi and collapse of the ER was observed (Fig. 6.14). The *trans*-Golgi network seems less affected by the overexpression; however, it is possible that longer expression of SPPL2c is needed for the effects to be more pronounced further down the secretory pathway.

Thus, expression of SPPL2c not only affects vesicular trafficking, glycosylation and secretion of proteins, but it can alter the whole cell structure, making expression of this protein highly restricted under healthy conditions. Indeed, expression of SPPL2c has so far only been found in the mature male reproductive system and even more specifically, only in maturing spermatids (Niemeyer et al. 2019). Mass spectrometry analysis of whole testis membrane

preparations from SPPL2c$^{-/-}$ mice compared to littermate controls also identified Stx8 as a SPPL2c substrate and its processing was validated by Western Blotting ((Niemeyer et al. 2019), Fig. 6.15B-D). Unfortunately, no accumulation of any of the other verified SPPL2c substrates was detected. This is most likely due to the very restricted expression of SPPL2c in the testis on a cellular level. While SNARE proteins are almost ubiquitously expressed, SPPL2c is exclusively found in spermatids, a small subpopulation of the testis cells. It appears logical that the accumulation of a SPPL2c substrate only in such a small population of cells would be very hard to detect in total testis lysates. Given that the two analyses were also performed in different species (human vs mouse), it is not possible to exclude that species specificity might also play a role for the substrates that do not overlap. Similar results were also obtained during the analysis of HEK293 cells overexpressing SPPL3 and MEF cells from SPPL3$^{-/-}$ mice (Kuhn et al. 2015), with the two proteomic analyses identifying few corresponding substrates and mostly singular hits.

SPPL2c expression in maturing spermatids is proving to be considerably high as whole testis membrane preparations have SPPL2c levels comparable to 1:50 dilution of the HEK293 cells (Fig. 6.1). This indicates that the overexpression system is not far off the actual *in vivo* situation and indeed, analysing the glycosylation of Nicastrin and SPPL2a in different mouse tissues, testis significantly accumulate immature glycoproteins compared to the other tissues (Fig. 6.15A). A similar hypoglycosylation is observed in the HEK293 cells upon SPPL2c overexpression (Fig. 6.9A).

Maturing spermatids are a special type of cell as they are the first haploid cells during sperm maturation. In this stage, cells undergo comprehensive reorganisation of their intracellular compartments and plasma membrane to eventually form spermatozoa (Berruti and Paiardi 2011). A key feature of mature spermatozoa is the lack of intracellular organelles, such as the Golgi and ER, but the presence of a different membrane organelle, the acrosome. Formation of the acrosome starts at the stage of spermatids through fragmentation of the Golgi into

proacrosomic granules that later fuse to form acrosomic granules that finally come to close contact with the nuclear envelope (Abou-Haila and Tulsiani 2000). Given the highly specific expression of SPPL2c in this stage, the effect of SPPL2c overexpression on the intracellular structures of HEK293 cells and the requirement for specific SNARE expression during the formation of the acrosome, it seems likely that SPPL2c is involved in this procedure. Stainings of proacrosomic structures in maturing spermatids indeed point to a defect during the formation of the acrosome in absence of SPPL2c (Fig. 6.16, 6.17). SPPL2c$^{-/-}$ mice appear to have a decreased number and/or decreased integrity of proacrosomic structures that could be attributed to problems in the formation and fusion of these granules, which possibly requires a specific pattern of SNARE protein expression.

Spermatozoa are also characterized by very specific glycosylation pattern, especially in the glycocalyx that surrounds them and ensures the species specificity while mating (Pang et al. 2011). Using a lectin microarray it was shown that the altered glycosylation patterns observed in HEK293 cells expressing SPPL2c are represented also *in vivo*. Only in this case, SPPL2c expression is required to reach the wanted glycosylation pattern and lack of it results to profound changes in the glycan fingerprint of the sperm (Fig. 6.18). A number of lectins showed reduced binding activity in the SPPL2c$^{-/-}$ sperm, amongst them also WGA that is an established marker of teratozoospermia. Other reduced lectins are considered indicative of the sperm maturation and fertility, as well as the content of the acrosome (Benoff 1997, Xin et al. 2016).

These results regarding acrosome formation and protein glycosylation, in combination with the study by Niemeyer et al. 2019 that shows altered Ca^{2+} signaling upon lack of SPPL2c could explain the decreased breeding capabilities observed in the SPPL2c$^{-/-}$ mice. However, we only hold part of the puzzle pieces, as it is not clear how SPPL2c deficiency affects reproduction and why the deficient male mice have normal litters when mated with wildtype female mice, or how SPPL2c deficiency might affect female mice. As it was shown that SPPL2c expression

starts with sexual maturity, it is possible that SPPL2c does not hold a key role but rather has a "booster function" aiming to improve the maturation of sperm. Further studies are needed to investigate other factors/mechanisms that could be the missing pieces to sperm maturation in absence of SPPL2c and the possible expression of SPPL2c in the female reproduction system.

In summary, this study shows that SPPL2c is an active aspartyl protease that can cleave numerous SNARE proteins *in vitro* and at least Syntaxin 8 *in vivo*. Cleavage of the SNARE proteins interferes with their role of mediating vesicle fusion in vesicular transport and thus, numerous cargo proteins accumulate in the early stages of the secretory pathway. This leads to a decreased maturation and secretion of glycan-modifying proteins, as well as to hypoglycosylation of glycoproteins and an alteration of compartmental structures in the cell. *In vivo*, SPPL2c is so far exclusively found in maturing spermatids in the male reproduction system and can affect fertility. It is required for optimal maturation of sperm, in regards of both glycosylation and acrosome formation. It remains to be discovered what other types of cells might be able to express SPPL2c upon very specific circumstances that might require altered Ca^{2+} signalling or intracellular reorganisation.

7. References

Abou-Haila, A. and Tulsiani, D. R. (2000). "Mammalian sperm acrosome: formation, contents, and function." Arch Biochem Biophys 379(2): 173-182.

Aizawa, S., Okamoto, T., Sugiyama, Y., Kouwaki, T., Ito, A., Suzuki, T., Ono, C., Fukuhara, T., Yamamoto, M., Okochi, M., Hiraga, N., Imamura, M., Chayama, K., Suzuki, R., Shoji, I., Moriishi, K., Moriya, K., Koike, K. and Matsuura, Y. (2016). "TRC8-dependent degradation of hepatitis C virus immature core protein regulates viral propagation and pathogenesis." Nat Commun 7: 11379.

Akiyama, Y. and Maegawa, S. (2007). "Sequence features of substrates required for cleavage by GlpG, an Escherichia coli rhomboid protease." Mol Microbiol 64(4): 1028-1037.

Antonin, W., Holroyd, C., Fasshauer, D., Pabst, S., Von Mollard, G. F. and Jahn, R. (2000). "A SNARE complex mediating fusion of late endosomes defines conserved properties of SNARE structure and function." EMBO J 19(23): 6453-6464.

Appenzeller-Herzog, C. and Hauri, H. P. (2006). "The ER-Golgi intermediate compartment (ERGIC): in search of its identity and function." J Cell Sci 119(Pt 11): 2173-2183.

Avci, D., Fuchs, S., Schrul, B., Fukumori, A., Breker, M., Frumkin, I., Chen, C. Y., Biniossek, M. L., Kremmer, E., Schilling, O., Steiner, H., Schuldiner, M. and Lemberg, M. K. (2014). "The yeast ER-intramembrane protease Ypf1 refines nutrient sensing by regulating transporter abundance." Mol Cell 56(5): 630-640.

Bai, X. C., Rajendra, E., Yang, G., Shi, Y. and Scheres, S. H. (2015a). "Sampling the conformational space of the catalytic subunit of human gamma-secretase." Elife 4.

Bai, X. C., Yan, C., Yang, G., Lu, P., Ma, D., Sun, L., Zhou, R., Scheres, S. H. W. and Shi, Y. (2015b). "An atomic structure of human gamma-secretase." Nature 525(7568): 212-217.

Bammens, L., Chavez-Gutierrez, L., Tolia, A., Zwijsen, A. and De Strooper, B. (2011). "Functional and topological analysis of Pen-2, the fourth subunit of the gamma-secretase complex." J Biol Chem 286(14): 12271-12282.

Behnke, J., Schneppenheim, J., Koch-Nolte, F., Haag, F., Saftig, P. and Schroder, B. (2011).

"Signal-peptide-peptidase-like 2a (SPPL2a) is targeted to lysosomes/late endosomes by a tyrosine motif in its C-terminal tail." FEBS Lett 585(19): 2951-2957.

Beisner, D. R., Langerak, P., Parker, A. E., Dahlberg, C., Otero, F. J., Sutton, S. E., Poirot, L., Barnes, W., Young, M. A., Niessen, S., Wiltshire, T., Bodendorf, U., Martoglio, B., Cravatt, B. and Cooke, M. P. (2013). "The intramembrane protease Sppl2a is required for B cell and DC development and survival via cleavage of the invariant chain." J Exp Med 210(1): 23-30.

Ben-Sahra, I. and Manning, B. D. (2017). "mTORC1 signaling and the metabolic control of cell growth." Curr Opin Cell Biol 45: 72-82.

Benoff, S. (1997). "Carbohydrates and fertilization: an overview." Mol Hum Reprod 3(7): 599-637.

Bergbold, N. and Lemberg, M. K. (2013). "Emerging role of rhomboid family proteins in mammalian biology and disease." Biochim Biophys Acta 1828(12): 2840-2848.

Bergmann, H., Yabas, M., Short, A., Miosge, L., Barthel, N., Teh, C. E., Roots, C. M., Bull, K. R., Jeelall, Y., Horikawa, K., Whittle, B., Balakishnan, B., Sjollema, G., Bertram, E. M., Mackay, F., Rimmer, A. J., Cornall, R. J., Field, M. A., Andrews, T. D., Goodnow, C. C. and Enders, A. (2013). "B cell survival, surface BCR and BAFFR expression, CD74 metabolism, and CD8- dendritic cells require the intramembrane endopeptidase SPPL2A." J Exp Med 210(1): 31-40.

Berruti, G. and Paiardi, C. (2011). "Acrosome biogenesis: Revisiting old questions to yield new insights." Spermatogenesis 1(2): 95-98.

Beyer, T. A., Sadler, J. E., Rearick, J. I., Paulson, J. C. and Hill, R. L. (1981). "Glycosyltransferases and their use in assessing oligosaccharide structure and structure-function relationships." Adv Enzymol Relat Areas Mol Biol 52: 23-175.

Bieberich, E. (2014). "Synthesis, Processing, and Function of N-glycans in N-glycoproteins." Adv Neurobiol 9: 47-70.

Bolduc, D. M., Montagna, D. R., Seghers, M. C., Wolfe, M. S. and Selkoe, D. J. (2016). "The amyloid-beta forming tripeptide cleavage mechanism of gamma-secretase." Elife 5.

Boname, J. M., Bloor, S., Wandel, M. P., Nathan, J. A., Antrobus, R., Dingwell, K. S., Thurston, T. L., Smith, D. L., Smith, J. C., Randow, F. and Lehner, P. J. (2014). "Cleavage by signal peptide peptidase is required for the degradation of selected tail-anchored proteins." J Cell Biol 205(6): 847-862.

Bonifacino, J. S. and Glick, B. S. (2004). "The mechanisms of vesicle budding and fusion." Cell 116(2): 153-166.

Boyartchuk, V. L., Ashby, M. N. and Rine, J. (1997). "Modulation of Ras and a-factor function by carboxyl-terminal proteolysis." Science 275(5307): 1796-1800.

Bray, S. J. (2016). "Notch signalling in context." Nat Rev Mol Cell Biol 17(11): 722-735.

Brown, M. S., Ye, J., Rawson, R. B. and Goldstein, J. L. (2000). "Regulated intramembrane proteolysis: a control mechanism conserved from bacteria to humans." Cell 100(4): 391-398.

Bukhari, H., Glotzbach, A., Kolbe, K., Leonhardt, G., Loosse, C. and Muller, T. (2017). "Small things matter: Implications of APP intracellular domain AICD nuclear signaling in the progression and pathogenesis of Alzheimer's disease." Prog Neurobiol 156: 189-213.

Capell, A., Grunberg, J., Pesold, B., Diehlmann, A., Citron, M., Nixon, R., Beyreuther, K., Selkoe, D. J. and Haass, C. (1998). "The proteolytic fragments of the Alzheimer's disease-associated presenilin-1 form heterodimers and occur as a 100-150-kDa molecular mass complex." J Biol Chem 273(6): 3205-3211.

Casso, D. J., Liu, S., Biehs, B. and Kornberg, T. B. (2012). "Expression and characterization of Drosophila signal peptide peptidase-like (sppL), a gene that encodes an intramembrane protease." PLoS One 7(3): e33827.

Casso, D. J., Tanda, S., Biehs, B., Martoglio, B. and Kornberg, T. B. (2005). "Drosophila signal peptide peptidase is an essential protease for larval development." Genetics 170(1): 139-148.

Chavez-Gutierrez, L., Bammens, L., Benilova, I., Vandersteen, A., Benurwar, M., Borgers, M., Lismont, S., Zhou, L., Van Cleynenbreugel, S., Esselmann, H., Wiltfang, J., Serneels, L., Karran, E., Gijsen, H., Schymkowitz, J., Rousseau, F., Broersen, K. and De Strooper, B. (2012). "The mechanism of gamma-Secretase dysfunction in familial Alzheimer disease." EMBO J 31(10): 2261-2274.

Chen, C. Y., Malchus, N. S., Hehn, B., Stelzer, W., Avci, D., Langosch, D. and Lemberg, M. K. (2014). "Signal peptide peptidase functions in ERAD to cleave the unfolded protein response regulator XBP1u." EMBO J 33(21): 2492-2506.

Chen, H. J., Anagnostou, G., Chai, A., Withers, J., Morris, A., Adhikaree, J., Pennetta, G. and de Belleroche, J. S. (2010). "Characterization of the properties of a novel mutation in VAPB in familial amyotrophic lateral sclerosis." J Biol Chem 285(51): 40266-40281.

Cheng, W. K. and Oon, C. E. (2018). "How glycosylation aids tumor angiogenesis: An updated review." Biomed Pharmacother 103: 1246-1252.

Cheung, P., Pawling, J., Partridge, E. A., Sukhu, B., Grynpas, M. and Dennis, J. W. (2007). "Metabolic homeostasis and tissue renewal are dependent on beta1,6GlcNAc-branched N-glycans." Glycobiology 17(8): 828-837.

Cho, S., Dickey, S. W. and Urban, S. (2016). "Crystal Structures and Inhibition Kinetics Reveal a Two-Stage Catalytic Mechanism with Drug Design Implications for Rhomboid Proteolysis." Mol Cell 61(3): 329-340.

Chou, A. H., Yeh, T. H., Ouyang, P., Chen, Y. L., Chen, S. Y. and Wang, H. L. (2008). "Polyglutamine-expanded ataxin-3 causes cerebellar dysfunction of SCA3 transgenic mice by inducing transcriptional dysregulation." Neurobiol Dis 31(1): 89-101.

Cox, J., Hein, M. Y., Luber, C. A., Paron, I., Nagaraj, N. and Mann, M. (2014). "Accurate proteome-wide label-free quantification by delayed normalization and maximal peptide ratio extraction, termed MaxLFQ." Mol Cell Proteomics 13(9): 2513-2526.

Cruts, M., Hendriks, L. and Van Broeckhoven, C. (1996). "The presenilin genes: a new gene

family involved in Alzheimer disease pathology." Hum Mol Genet 5 Spec No: 1449-1455.

Cuaranta-Monroy, I., Simandi, Z., Kolostyak, Z., Doan-Xuan, Q. M., Poliska, S., Horvath, A., Nagy, G., Bacso, Z. and Nagy, L. (2014). "Highly efficient differentiation of embryonic stem cells into adipocytes by ascorbic acid." Stem Cell Res 13(1): 88-97.

De Strooper, B. (2014). "Lessons from a failed gamma-secretase Alzheimer trial." Cell 159(4): 721-726.

De Strooper, B., Saftig, P., Craessaerts, K., Vanderstichele, H., Guhde, G., Annaert, W., Von Figura, K. and Van Leuven, F. (1998). "Deficiency of presenilin-1 inhibits the normal cleavage of amyloid precursor protein." Nature 391(6665): 387-390.

Deacon, S. W., Serpinskaya, A. S., Vaughan, P. S., Lopez Fanarraga, M., Vernos, I., Vaughan, K. T. and Gelfand, V. I. (2003). "Dynactin is required for bidirectional organelle transport." J Cell Biol 160(3): 297-301.

Dennis, J. W., Pawling, J., Cheung, P., Partridge, E. and Demetriou, M. (2002). "UDP-N-acetylglucosamine:alpha-6-D-mannoside beta1,6 N-acetylglucosaminyltransferase V (Mgat5) deficient mice." Biochim Biophys Acta 1573(3): 414-422.

Drake, R. R., Ball, L. E. and Abbott, K. L. (2015). Advances in cancer research. Volume 126, Volume 126.

Dulin, F., Leveille, F., Ortega, J. B., Mornon, J. P., Buisson, A., Callebaut, I. and Colloc'h, N. (2008). "P3 peptide, a truncated form of A beta devoid of synaptotoxic effect, does not assemble into soluble oligomers." FEBS Lett 582(13): 1865-1870.

Edbauer, D., Winkler, E., Regula, J. T., Pesold, B., Steiner, H. and Haass, C. (2003). "Reconstitution of gamma-secretase activity." Nat Cell Biol 5(5): 486-488.

Edwards, D. R., Handsley, M. M. and Pennington, C. J. (2008). "The ADAM metalloproteinases." Mol Aspects Med 29(5): 258-289.

Eggert, S., Midthune, B., Cottrell, B. and Koo, E. H. (2009). "Induced dimerization of the amyloid precursor protein leads to decreased amyloid-beta protein production." J Biol Chem

284(42): 28943-28952.

El Hage, F., Stroobant, V., Vergnon, I., Baurain, J. F., Echchakir, H., Lazar, V., Chouaib, S., Coulie, P. G. and Mami-Chouaib, F. (2008). "Preprocalcitonin signal peptide generates a cytotoxic T lymphocyte-defined tumor epitope processed by a proteasome-independent pathway." Proc Natl Acad Sci U S A 105(29): 10119-10124.

Esch, F. S., Keim, P. S., Beattie, E. C., Blacher, R. W., Culwell, A. R., Oltersdorf, T., McClure, D. and Ward, P. J. (1990). "Cleavage of amyloid beta peptide during constitutive processing of its precursor." Science 248(4959): 1122-1124.

Ezkurdia, I., Juan, D., Rodriguez, J. M., Frankish, A., Diekhans, M., Harrow, J., Vazquez, J., Valencia, A. and Tress, M. L. (2014). "Multiple evidence strands suggest that there may be as few as 19,000 human protein-coding genes." Hum Mol Genet 23(22): 5866-5878.

Feng, L., Yan, H., Wu, Z., Yan, N., Wang, Z., Jeffrey, P. D. and Shi, Y. (2007). "Structure of a site-2 protease family intramembrane metalloprotease." Science 318(5856): 1608-1612.

Fleck, D., Voss, M., Brankatschk, B., Giudici, C., Hampel, H., Schwenk, B., Edbauer, D., Fukumori, A., Steiner, H., Kremmer, E., Haug-Kroper, M., Rossner, M. J., Fluhrer, R., Willem, M. and Haass, C. (2016). "Proteolytic Processing of Neuregulin 1 Type III by Three Intramembrane-cleaving Proteases." J Biol Chem 291(1): 318-333.

Fluhrer, R., Grammer, G., Israel, L., Condron, M. M., Haffner, C., Friedmann, E., Bohland, C., Imhof, A., Martoglio, B., Teplow, D. B. and Haass, C. (2006). "A gamma-secretase-like intramembrane cleavage of TNFalpha by the GxGD aspartyl protease SPPL2b." Nat Cell Biol 8(8): 894-896.

Fluhrer, R., Martin, L., Klier, B., Haug-Kroper, M., Grammer, G., Nuscher, B. and Haass, C. (2012). "The alpha-helical content of the transmembrane domain of the British dementia protein-2 (Bri2) determines its processing by signal peptide peptidase-like 2b (SPPL2b)." J Biol Chem 287(7): 5156-5163.

Freeze, H. H. and Elbein, A. D. (2009). Glycosylation Precursors. Essentials of Glycobiology.

nd, A. Varki, R. D. Cummings et al. Cold Spring Harbor (NY).

Friedmann, E., Hauben, E., Maylandt, K., Schleeger, S., Vreugde, S., Lichtenthaler, S. F., Kuhn, P. H., Stauffer, D., Rovelli, G. and Martoglio, B. (2006). "SPPL2a and SPPL2b promote intramembrane proteolysis of TNFalpha in activated dendritic cells to trigger IL-12 production." Nat Cell Biol 8(8): 843-848.

Friedmann, E., Lemberg, M. K., Weihofen, A., Dev, K. K., Dengler, U., Rovelli, G. and Martoglio, B. (2004a). "Consensus analysis of signal peptide peptidase and homologous human aspartic proteases reveals opposite topology of catalytic domains compared with presenilins." J Biol Chem 279(49): 50790-50798.

Friedmann, E., Lemberg, M. K., Weihofen, A., Dev, K. K., Dengler, U., Rovelli, G. and Martoglio, B. (2004b). "Consensus analysis of signal peptide peptidase and homologous human aspartic proteases reveals opposite topology of catalytic domains compared with presenilins." Journal of Biological Chemistry 279(49): 50790-50798.

Fukumori, A., Fluhrer, R., Steiner, H. and Haass, C. (2010). "Three-amino acid spacing of presenilin endoproteolysis suggests a general stepwise cleavage of gamma-secretase-mediated intramembrane proteolysis." J Neurosci 30(23): 7853-7862.

Furuta, N., Fujita, N., Noda, T., Yoshimori, T. and Amano, A. (2010). "Combinational soluble N-ethylmaleimide-sensitive factor attachment protein receptor proteins VAMP8 and Vti1b mediate fusion of antimicrobial and canonical autophagosomes with lysosomes." Mol Biol Cell 21(6): 1001-1010.

Gallagher, J. T. and Hampson, I. N. (1984). "Proteoglycans in cellular differentiation and neoplasia." Biochem Soc Trans 12(3): 541-543.

Golde, T. E., Wolfe, M. S. and Greenbaum, D. C. (2009). "Signal peptide peptidases: a family of intramembrane-cleaving proteases that cleave type 2 transmembrane proteins." Semin Cell Dev Biol 20(2): 225-230.

Gomez-Navarro, N. and Miller, E. (2016). "Protein sorting at the ER-Golgi interface." J Cell

Biol 215(6): 769-778.

Grigorenko, A. P., Moliaka, Y. K., Korovaitseva, G. I. and Rogaev, E. I. (2002). "Novel class of polytopic proteins with domains associated with putative protease activity." Biochemistry (Mosc) 67(7): 826-835.

Guertin, D. A., Stevens, D. M., Thoreen, C. C., Burds, A. A., Kalaany, N. Y., Moffat, J., Brown, M., Fitzgerald, K. J. and Sabatini, D. M. (2006). "Ablation in mice of the mTORC components raptor, rictor, or mLST8 reveals that mTORC2 is required for signaling to Akt-FOXO and PKCalpha, but not S6K1." Dev Cell 11(6): 859-871.

Guyenet, S. J., Furrer, S. A., Damian, V. M., Baughan, T. D., La Spada, A. R. and Garden, G. A. (2010). "A simple composite phenotype scoring system for evaluating mouse models of cerebellar ataxia." J Vis Exp(39).

Haapasalo, A. and Kovacs, D. M. (2011). "The many substrates of presenilin/gamma-secretase." J Alzheimers Dis 25(1): 3-28.

Haass, C. (2004). "Take five–BACE and the gamma-secretase quartet conduct Alzheimer's amyloid beta-peptide generation." EMBO J 23(3): 483-488.

Haass, C. and Selkoe, D. J. (2007). "Soluble protein oligomers in neurodegeneration: lessons from the Alzheimer's amyloid beta-peptide." Nat Rev Mol Cell Biol 8(2): 101-112.

Hamblet, C. E., Makowski, S. L., Tritapoe, J. M. and Pomerantz, J. L. (2016). "NK Cell Maturation and Cytotoxicity Are Controlled by the Intramembrane Aspartyl Protease SPPL3." J Immunol 196(6): 2614-2626.

Hampton, S. E., Dore, T. M. and Schmidt, W. K. (2018). "Rce1: mechanism and inhibition." Crit Rev Biochem Mol Biol 53(2): 157-174.

Hanna, M. G., Peotter, J. L., Frankel, E. B. and Audhya, A. (2018). "Membrane Transport at an Organelle Interface in the Early Secretory Pathway: Take Your Coat Off and Stay a While: Evolution of the metazoan early secretory pathway." Bioessays: e1800004.

Hardy, J. and Selkoe, D. J. (2002). "The amyloid hypothesis of Alzheimer's disease: progress

and problems on the road to therapeutics." Science 297(5580): 353-356.

Hardy, J. A. and Higgins, G. A. (1992). "Alzheimer's disease: the amyloid cascade hypothesis." Science 256(5054): 184-185.

Hemming, M. L., Elias, J. E., Gygi, S. P. and Selkoe, D. J. (2008). "Proteomic profiling of gamma-secretase substrates and mapping of substrate requirements." PLoS Biol 6(10): e257.

Hendrickson, O. D. and Zherdev, A. V. (2018). "Analytical Application of Lectins." Crit Rev Anal Chem 48(4): 279-292.

Hennet, T. (2012). "Diseases of glycosylation beyond classical congenital disorders of glycosylation." Biochim Biophys Acta 1820(9): 1306-1317.

Holtzman, D. M., Morris, J. C. and Goate, A. M. (2011). "Alzheimer's disease: the challenge of the second century." Sci Transl Med 3(77): 77sr71.

Hook, M., Kjellen, L. and Johansson, S. (1984). "Cell-surface glycosaminoglycans." Annu Rev Biochem 53: 847-869.

Hsu, F. F., Yeh, C. T., Sun, Y. J., Chiang, M. T., Lan, W. M., Li, F. A., Lee, W. H. and Chau, L. Y. (2015). "Signal peptide peptidase-mediated nuclear localization of heme oxygenase-1 promotes cancer cell proliferation and invasion independent of its enzymatic activity." Oncogene 34(18): 2360-2370.

Hua, X., Sakai, J., Ho, Y. K., Goldstein, J. L. and Brown, M. S. (1995). "Hairpin orientation of sterol regulatory element-binding protein-2 in cell membranes as determined by protease protection." J Biol Chem 270(49): 29422-29427.

Huang, Y. and Mucke, L. (2012). "Alzheimer mechanisms and therapeutic strategies." Cell 148(6): 1204-1222.

Hutagalung, A. H. and Novick, P. J. (2011). "Role of Rab GTPases in membrane traffic and cell physiology." Physiol Rev 91(1): 119-149.

Huttl, S., Helfrich, F., Mentrup, T., Held, S., Fukumori, A., Steiner, H., Saftig, P., Fluhrer, R. and Schroder, B. (2016). "Substrate determinants of signal peptide peptidase-like 2a

(SPPL2a)-mediated intramembrane proteolysis of the invariant chain CD74." Biochem J 473(10): 1405-1422.

Huttl, S., Klasener, K., Schweizer, M., Schneppenheim, J., Oberg, H. H., Kabelitz, D., Reth, M., Saftig, P. and Schroder, B. (2015). "Processing of CD74 by the Intramembrane Protease SPPL2a Is Critical for B Cell Receptor Signaling in Transitional B Cells." J Immunol 195(4): 1548-1563.

Huttlin, E. L., Ting, L., Bruckner, R. J., Gebreab, F., Gygi, M. P., Szpyt, J., Tam, S., Zarraga, G., Colby, G., Baltier, K., Dong, R., Guarani, V., Vaites, L. P., Ordureau, A., Rad, R., Erickson, B. K., Wuhr, M., Chick, J., Zhai, B., Kolippakkam, D., Mintseris, J., Obar, R. A., Harris, T., Artavanis-Tsakonas, S., Sowa, M. E., De Camilli, P., Paulo, J. A., Harper, J. W. and Gygi, S. P. (2015). "The BioPlex Network: A Systematic Exploration of the Human Interactome." Cell 162(2): 425-440.

Jahn, R. and Scheller, R. H. (2006). "SNAREs–engines for membrane fusion." Nat Rev Mol Cell Biol 7(9): 631-643.

Jung, J. J., Inamdar, S. M., Tiwari, A. and Choudhury, A. (2012). "Regulation of intracellular membrane trafficking and cell dynamics by syntaxin-6." Biosci Rep 32(4): 383-391.

Kilic, A., Klose, S., Dobberstein, B., Knust, E. and Kapp, K. (2010). "The Drosophila Crumbs signal peptide is unusually long and is a substrate for signal peptide peptidase." Eur J Cell Biol 89(6): 449-461.

Kimberly, W. T., LaVoie, M. J., Ostaszewski, B. L., Ye, W., Wolfe, M. S. and Selkoe, D. J. (2003). "Gamma-secretase is a membrane protein complex comprised of presenilin, nicastrin, Aph-1, and Pen-2." Proc Natl Acad Sci U S A 100(11): 6382-6387.

King, M. C., Marks, J. H., Mandell, J. B. and New York Breast Cancer Study, G. (2003). "Breast and ovarian cancer risks due to inherited mutations in BRCA1 and BRCA2." Science 302(5645): 643-646.

Kirkin, V., Cahuzac, N., Guardiola-Serrano, F., Huault, S., Luckerath, K., Friedmann, E.,

Novac, N., Wels, W. S., Martoglio, B., Hueber, A. O. and Zornig, M. (2007). "The Fas ligand intracellular domain is released by ADAM10 and SPPL2a cleavage in T-cells." Cell Death Differ 14(9): 1678-1687.

Kitazume, S., Nakagawa, K., Oka, R., Tachida, Y., Ogawa, K., Luo, Y., Citron, M., Shitara, H., Taya, C., Yonekawa, H., Paulson, J. C., Miyoshi, E., Taniguchi, N. and Hashimoto, Y. (2005). "In vivo cleavage of alpha2,6-sialyltransferase by Alzheimer beta-secretase." J Biol Chem 280(9): 8589-8595.

Kitazume, S., Oka, R., Ogawa, K., Futakawa, S., Hagiwara, Y., Takikawa, H., Kato, M., Kasahara, A., Miyoshi, E., Taniguchi, N. and Hashimoto, Y. (2009). "Molecular insights into beta-galactoside alpha2,6-sialyltransferase secretion in vivo." Glycobiology 19(5): 479-487.

Kitazume, S., Tachida, Y., Oka, R., Nakagawa, K., Takashima, S., Lee, Y. C. and Hashimoto, Y. (2006). "Screening a series of sialyltransferases for possible BACE1 substrates." Glycoconj J 23(5-6): 437-441.

Koonin, E. V., Makarova, K. S., Rogozin, I. B., Davidovic, L., Letellier, M. C. and Pellegrini, L. (2003). "The rhomboids: a nearly ubiquitous family of intramembrane serine proteases that probably evolved by multiple ancient horizontal gene transfers." Genome Biol 4(3): R19.

Krawitz, P., Haffner, C., Fluhrer, R., Steiner, H., Schmid, B. and Haass, C. (2005). "Differential localization and identification of a critical aspartate suggest non-redundant proteolytic functions of the presenilin homologues SPPL2b and SPPL3." J Biol Chem 280(47): 39515-39523.

Kretner, B., Trambauer, J., Fukumori, A., Mielke, J., Kuhn, P. H., Kremmer, E., Giese, A., Lichtenthaler, S. F., Haass, C., Arzberger, T. and Steiner, H. (2016). "Generation and deposition of Abeta43 by the virtually inactive presenilin-1 L435F mutant contradicts the presenilin loss-of-function hypothesis of Alzheimer's disease." EMBO Mol Med 8(5): 458-465.

Kroos, L. and Akiyama, Y. (2013). "Biochemical and structural insights into intramembrane metalloprotease mechanisms." Biochim Biophys Acta 1828(12): 2873-2885.

Kuhn, P. H., Koroniak, K., Hogl, S., Colombo, A., Zeitschel, U., Willem, M., Volbracht, C., Schepers, U., Imhof, A., Hoffmeister, A., Haass, C., Rossner, S., Brase, S. and Lichtenthaler, S. F. (2012). "Secretome protein enrichment identifies physiological BACE1 protease substrates in neurons." EMBO J 31(14): 3157-3168.

Kuhn, P. H., Voss, M., Haug-Kroper, M., Schroder, B., Schepers, U., Brase, S., Haass, C., Lichtenthaler, S. F. and Fluhrer, R. (2015). "Secretome analysis identifies novel signal Peptide peptidase-like 3 (Sppl3) substrates and reveals a role of Sppl3 in multiple Golgi glycosylation pathways." Mol Cell Proteomics 14(6): 1584-1598.

Kuhn, P. H., Wang, H., Dislich, B., Colombo, A., Zeitschel, U., Ellwart, J. W., Kremmer, E., Rossner, S. and Lichtenthaler, S. F. (2010). "ADAM10 is the physiologically relevant, constitutive alpha-secretase of the amyloid precursor protein in primary neurons." EMBO J 29(17): 3020-3032.

Lammers, G. and Jamieson, J. C. (1989). "Studies on the effect of lysosomotropic agents on the release of Gal beta 1-4GlcNAc alpha-2,6-sialytransferase from rat liver slices during the acute-phase response." Biochem J 261(2): 389-393.

Langosch, D., Scharnagl, C., Steiner, H. and Lemberg, M. K. (2015). "Understanding intramembrane proteolysis: from protein dynamics to reaction kinetics." Trends Biochem Sci 40(6): 318-327.

Laudon, H., Hansson, E. M., Melen, K., Bergman, A., Farmery, M. R., Winblad, B., Lendahl, U., von Heijne, G. and Naslund, J. (2005). "A nine-transmembrane domain topology for presenilin 1." J Biol Chem 280(42): 35352-35360.

Lee, J. K., Matthews, R. T., Lim, J. M., Swanier, K., Wells, L. and Pierce, J. M. (2012). "Developmental expression of the neuron-specific N-acetylglucosaminyltransferase Vb (GnT-Vb/IX) and identification of its in vivo glycan products in comparison with those of its paralog, GnT-V." J Biol Chem 287(34): 28526-28536.

Lee, J. R., Urban, S., Garvey, C. F. and Freeman, M. (2001). "Regulated intracellular ligand

transport and proteolysis control EGF signal activation in Drosophila." Cell 107(2): 161-171.

Lee, M. C., Miller, E. A., Goldberg, J., Orci, L. and Schekman, R. (2004a). "Bi-directional protein transport between the ER and Golgi." Annu Rev Cell Dev Biol 20: 87-123.

Lee, S. F., Shah, S., Yu, C., Wigley, W. C., Li, H., Lim, M., Pedersen, K., Han, W., Thomas, P., Lundkvist, J., Hao, Y. H. and Yu, G. (2004b). "A conserved GXXXG motif in APH-1 is critical for assembly and activity of the gamma-secretase complex." J Biol Chem 279(6): 4144-4152.

Lemberg, M. K., Bland, F. A., Weihofen, A., Braud, V. M. and Martoglio, B. (2001). "Intramembrane proteolysis of signal peptides: an essential step in the generation of HLA-E epitopes." J Immunol 167(11): 6441-6446.

Lemberg, M. K. and Freeman, M. (2007). "Functional and evolutionary implications of enhanced genomic analysis of rhomboid intramembrane proteases." Genome Res 17(11): 1634-1646.

Lemberg, M. K. and Martoglio, B. (2002). "Requirements for signal peptide peptidase-catalyzed intramembrane proteolysis." Mol Cell 10(4): 735-744.

Lemberg, M. K., Menendez, J., Misik, A., Garcia, M., Koth, C. M. and Freeman, M. (2005). "Mechanism of intramembrane proteolysis investigated with purified rhomboid proteases." EMBO J 24(3): 464-472.

Levy-Lahad, E., Wasco, W., Poorkaj, P., Romano, D. M., Oshima, J., Pettingell, W. H., Yu, C. E., Jondro, P. D., Schmidt, S. D., Wang, K. and et al. (1995a). "Candidate gene for the chromosome 1 familial Alzheimer's disease locus." Science 269(5226): 973-977.

Levy-Lahad, E., Wijsman, E. M., Nemens, E., Anderson, L., Goddard, K. A., Weber, J. L., Bird, T. D. and Schellenberg, G. D. (1995b). "A familial Alzheimer's disease locus on chromosome 1." Science 269(5226): 970-973.

Li, S. C. and Deber, C. M. (1994). "A measure of helical propensity for amino acids in membrane environments." Nat Struct Biol 1(8): 558.

Li, T., Ma, G., Cai, H., Price, D. L. and Wong, P. C. (2003). "Nicastrin is required for assembly of presenilin/gamma-secretase complexes to mediate Notch signaling and for processing and trafficking of beta-amyloid precursor protein in mammals." J Neurosci 23(8): 3272-3277.

Lichtenthaler, S. F., Haass, C. and Steiner, H. (2011). "Regulated intramembrane proteolysis–lessons from amyloid precursor protein processing." J Neurochem 117(5): 779-796.

Lichtenthaler, S. F., Lemberg, M. K. and Fluhrer, R. (2018). "Proteolytic ectodomain shedding of membrane proteins in mammals-hardware, concepts, and recent developments." EMBO J 37(15).

Lim, S. H., Legere, E. A., Snider, J. and Stagljar, I. (2017). "Recent Progress in CFTR Interactome Mapping and Its Importance for Cystic Fibrosis." Front Pharmacol 8: 997.

Lin, X. (2004). "Functions of heparan sulfate proteoglycans in cell signaling during development." Development 131(24): 6009-6021.

Liu, Y., Liu, H., Liu, W., Zhang, W., An, H. and Xu, J. (2015). "beta1,6-N-acetylglucosaminyltransferase V predicts recurrence and survival of patients with clear-cell renal cell carcinoma after surgical resection." World J Urol 33(11): 1791-1799.

Madala, P. K., Tyndall, J. D., Nall, T. and Fairlie, D. P. (2010). "Update 1 of: Proteases universally recognize beta strands in their active sites." Chem Rev 110(6): PR1-31.

Manolaridis, I., Kulkarni, K., Dodd, R. B., Ogasawara, S., Zhang, Z., Bineva, G., Reilly, N. O., Hanrahan, S. J., Thompson, A. J., Cronin, N., Iwata, S. and Barford, D. (2013). "Mechanism of farnesylated CAAX protein processing by the intramembrane protease Rce1." Nature 504(7479): 301-305.

Martin, L., Fluhrer, R. and Haass, C. (2009). "Substrate requirements for SPPL2b-dependent regulated intramembrane proteolysis." J Biol Chem 284(9): 5662-5670.

Martin, L., Fluhrer, R., Reiss, K., Kremmer, E., Saftig, P. and Haass, C. (2008). "Regulated intramembrane proteolysis of Bri2 (Itm2b) by ADAM10 and SPPL2a/SPPL2b." J Biol Chem

283(3): 1644-1652.

Martoglio, B., Graf, R. and Dobberstein, B. (1997). "Signal peptide fragments of preprolactin and HIV-1 p-gp160 interact with calmodulin." EMBO J 16(22): 6636-6645.

Mayer, C., Adam, M., Glashauser, L., Dietrich, K., Schwarzer, J. U., Kohn, F. M., Strauss, L., Welter, H., Poutanen, M. and Mayerhofer, A. (2016). "Sterile inflammation as a factor in human male infertility: Involvement of Toll like receptor 2, biglycan and peritubular cells." Sci Rep 6: 37128.

Meistrich, M. L. and Hess, R. A. (2013). "Assessment of spermatogenesis through staging of seminiferous tubules." Methods Mol Biol 927: 299-307.

Mentrup, T., Fluhrer, R. and Schroder, B. (2017a). "Latest emerging functions of SPP/SPPL intramembrane proteases." Eur J Cell Biol 96(5): 372-382.

Mentrup, T., Hasler, R., Fluhrer, R., Saftig, P. and Schroder, B. (2015). "A Cell-Based Assay Reveals Nuclear Translocation of Intracellular Domains Released by SPPL Proteases." Traffic 16(8): 871-892.

Mentrup, T., Loock, A. C., Fluhrer, R. and Schroder, B. (2017b). "Signal peptide peptidase and SPP-like proteases - Possible therapeutic targets?" Biochim Biophys Acta Mol Cell Res 1864(11 Pt B): 2169-2182.

Miyoshi, E., Terao, M. and Kamada, Y. (2012). "Physiological roles of N-acetylglucosaminyltransferase V(GnT-V) in mice." BMB Rep 45(10): 554-559.

Moin, S. M. and Urban, S. (2012). "Membrane immersion allows rhomboid proteases to achieve specificity by reading transmembrane segment dynamics." Elife 1: e00173.

Moremen, K. W., Tiemeyer, M. and Nairn, A. V. (2012). "Vertebrate protein glycosylation: diversity, synthesis and function." Nat Rev Mol Cell Biol 13(7): 448-462.

Muller, S. A., Scilabra, S. D. and Lichtenthaler, S. F. (2016). "Proteomic Substrate Identification for Membrane Proteases in the Brain." Front Mol Neurosci 9: 96.

Munter, L. M., Voigt, P., Harmeier, A., Kaden, D., Gottschalk, K. E., Weise, C., Pipkorn, R.,

Schaefer, M., Langosch, D. and Multhaup, G. (2007). "GxxxG motifs within the amyloid precursor protein transmembrane sequence are critical for the etiology of Abeta42." EMBO J 26(6): 1702-1712.

Murakami, T., Kondo, S., Ogata, M., Kanemoto, S., Saito, A., Wanaka, A. and Imaizumi, K. (2006). "Cleavage of the membrane-bound transcription factor OASIS in response to endoplasmic reticulum stress." J Neurochem 96(4): 1090-1100.

Nagae, M., Kizuka, Y., Mihara, E., Kitago, Y., Hanashima, S., Ito, Y., Takagi, J., Taniguchi, N. and Yamaguchi, Y. (2018). "Structure and mechanism of cancer-associated N-acetylglucosaminyltransferase-V." Nat Commun 9(1): 3380.

Niemeyer, J., Mentrup, T., Heidasch, R., Muller, S. A., Biswas, U., Meyer, R., Papadopoulou, A. A., Dederer, V., Haug-Kroper, M., Adamski, V., Lullmann-Rauch, R., Bergmann, M., Mayerhofer, A., Saftig, P., Wennemuth, G., Jessberger, R., Fluhrer, R., Lichtenthaler, S. F., Lemberg, M. K. and Schroder, B. (2019). "The intramembrane protease SPPL2c promotes male germ cell development by cleaving phospholamban." EMBO Rep 20(3).

Noh, J. M., Kim, J., Cho, D. Y., Choi, D. H., Park, W. and Huh, S. J. (2015). "Exome sequencing in a breast cancer family without BRCA mutation." Radiat Oncol J 33(2): 149-154.

Nyborg, A. C., Jansen, K., Ladd, T. B., Fauq, A. and Golde, T. E. (2004). "A signal peptide peptidase (SPP) reporter activity assay based on the cleavage of type II membrane protein substrates provides further evidence for an inverted orientation of the SPP active site relative to presenilin." J Biol Chem 279(41): 43148-43156.

Nyborg, A. C., Ladd, T. B., Jansen, K., Kukar, T. and Golde, T. E. (2006). "Intramembrane proteolytic cleavage by human signal peptide peptidase like 3 and malaria signal peptide peptidase." FASEB J 20(10): 1671-1679.

Oh, Y. S. and Turner, R. J. (2005). "Topology of the C-terminal fragment of human presenilin 1." Biochemistry 44(35): 11821-11828.

Oliveira, C. C., Querido, B., Sluijter, M., de Groot, A. F., van der Zee, R., Rabelink, M. J., Hoeben, R. C., Ossendorp, F., van der Burg, S. H. and van Hall, T. (2013). "New role of signal peptide peptidase to liberate C-terminal peptides for MHC class I presentation." J Immunol 191(8): 4020-4028.

Pang, P. C., Chiu, P. C., Lee, C. L., Chang, L. Y., Panico, M., Morris, H. R., Haslam, S. M., Khoo, K. H., Clark, G. F., Yeung, W. S. and Dell, A. (2011). "Human sperm binding is mediated by the sialyl-Lewis(x) oligosaccharide on the zona pellucida." Science 333(6050): 1761-1764.

Papadopoulou, A. A., Muller, S. A., Mentrup, T., Shmueli, M. D., Niemeyer, J., Haug-Kroper, M., von Blume, J., Mayerhofer, A., Feederle, R., Schroder, B., Lichtenthaler, S. F. and Fluhrer, R. (2019). "Signal Peptide Peptidase-Like 2c (SPPL2c) impairs vesicular transport and cleavage of SNARE proteins." EMBO Rep 20(3).

Paulson, J. C. and Colley, K. J. (1989). "Glycosyltransferases. Structure, localization, and control of cell type-specific glycosylation." J Biol Chem 264(30): 17615-17618.

Polak, P., Cybulski, N., Feige, J. N., Auwerx, J., Ruegg, M. A. and Hall, M. N. (2008). "Adipose-specific knockout of raptor results in lean mice with enhanced mitochondrial respiration." Cell Metab 8(5): 399-410.

Polgar, J., Chung, S. H. and Reed, G. L. (2002). "Vesicle-associated membrane protein 3 (VAMP-3) and VAMP-8 are present in human platelets and are required for granule secretion." Blood 100(3): 1081-1083.

Ponting, C. P., Hutton, M., Nyborg, A., Baker, M., Jansen, K. and Golde, T. E. (2002). "Identification of a novel family of presenilin homologues." Hum Mol Genet 11(9): 1037-1044.

Popot, J. L. and Engelman, D. M. (2000). "Helical membrane protein folding, stability, and evolution." Annu Rev Biochem 69: 881-922.

Praschberger, R., Lowe, S. A., Malintan, N. T., Giachello, C. N. G., Patel, N., Houlden, H., Kullmann, D. M., Baines, R. A., Usowicz, M. M., Krishnakumar, S. S., Hodge, J. J. L.,

Rothman, J. E. and Jepson, J. E. C. (2017). "Mutations in Membrin/GOSR2 Reveal Stringent Secretory Pathway Demands of Dendritic Growth and Synaptic Integrity." Cell Rep 21(1): 97-109.

Prokop, S., Shirotani, K., Edbauer, D., Haass, C. and Steiner, H. (2004). "Requirement of PEN-2 for stabilization of the presenilin N-/C-terminal fragment heterodimer within the gamma-secretase complex." J Biol Chem 279(22): 23255-23261.

Ran, F. A., Hsu, P. D., Wright, J., Agarwala, V., Scott, D. A. and Zhang, F. (2013). "Genome engineering using the CRISPR-Cas9 system." Nat Protoc 8(11): 2281-2308.

Rappsilber, J., Ishihama, Y. and Mann, M. (2003). "Stop and go extraction tips for matrix-assisted laser desorption/ionization, nanoelectrospray, and LC/MS sample pretreatment in proteomics." Anal Chem 75(3): 663-670.

Rawson, R. B., Zelenski, N. G., Nijhawan, D., Ye, J., Sakai, J., Hasan, M. T., Chang, T. Y., Brown, M. S. and Goldstein, J. L. (1997). "Complementation cloning of S2P, a gene encoding a putative metalloprotease required for intramembrane cleavage of SREBPs." Mol Cell 1(1): 47-57.

Rogaev, E. I., Sherrington, R., Rogaeva, E. A., Levesque, G., Ikeda, M., Liang, Y., Chi, H., Lin, C., Holman, K., Tsuda, T. and et al. (1995). "Familial Alzheimer's disease in kindreds with missense mutations in a gene on chromosome 1 related to the Alzheimer's disease type 3 gene." Nature 376(6543): 775-778.

Rowe, T., Dascher, C., Bannykh, S., Plutner, H. and Balch, W. E. (1998). "Role of vesicle-associated syntaxin 5 in the assembly of pre-Golgi intermediates." Science 279(5351): 696-700.

Saito, T., Miyoshi, E., Sasai, K., Nakano, N., Eguchi, H., Honke, K. and Taniguchi, N. (2002). "A secreted type of beta 1,6-N-acetylglucosaminyltransferase V (GnT-V) induces tumor angiogenesis without mediation of glycosylation: a novel function of GnT-V distinct from the original glycosyltransferase activity." J Biol Chem 277(19): 17002-17008.

Saito, T., Suemoto, T., Brouwers, N., Sleegers, K., Funamoto, S., Mihira, N., Matsuba, Y., Yamada, K., Nilsson, P., Takano, J., Nishimura, M., Iwata, N., Van Broeckhoven, C., Ihara, Y. and Saido, T. C. (2011). "Potent amyloidogenicity and pathogenicity of Abeta43." Nat Neurosci 14(8): 1023-1032.

Schachter, H. (2000). "The joys of HexNAc. The synthesis and function of N- and O-glycan branches." Glycoconj J 17(7-9): 465-483.

Schedin-Weiss, S., Winblad, B. and Tjernberg, L. O. (2014). "The role of protein glycosylation in Alzheimer disease." FEBS J 281(1): 46-62.

Schettini, G., Govoni, S., Racchi, M. and Rodriguez, G. (2010). "Phosphorylation of APP-CTF-AICD domains and interaction with adaptor proteins: signal transduction and/or transcriptional role–relevance for Alzheimer pathology." J Neurochem 115(6): 1299-1308.

Scheuner, D., Eckman, C., Jensen, M., Song, X., Citron, M., Suzuki, N., Bird, T. D., Hardy, J., Hutton, M., Kukull, W., Larson, E., Levy-Lahad, E., Viitanen, M., Peskind, E., Poorkaj, P., Schellenberg, G., Tanzi, R., Wasco, W., Lannfelt, L., Selkoe, D. and Younkin, S. (1996). "Secreted amyloid beta-protein similar to that in the senile plaques of Alzheimer's disease is increased in vivo by the presenilin 1 and 2 and APP mutations linked to familial Alzheimer's disease." Nat Med 2(8): 864-870.

Schneppenheim, J., Dressel, R., Huttl, S., Lullmann-Rauch, R., Engelke, M., Dittmann, K., Wienands, J., Eskelinen, E. L., Hermans-Borgmeyer, I., Fluhrer, R., Saftig, P. and Schroder, B. (2013). "The intramembrane protease SPPL2a promotes B cell development and controls endosomal traffic by cleavage of the invariant chain." J Exp Med 210(1): 41-58.

Schneppenheim, J., Huttl, S., Kruchen, A., Fluhrer, R., Muller, I., Saftig, P., Schneppenheim, R., Martin, C. L. and Schroder, B. (2014a). "Signal-peptide-peptidase-like 2a is required for CD74 intramembrane proteolysis in human B cells." Biochem Biophys Res Commun 451(1): 48-53.

Schneppenheim, J., Huttl, S., Mentrup, T., Lullmann-Rauch, R., Rothaug, M., Engelke, M.,

Dittmann, K., Dressel, R., Araki, M., Araki, K., Wienands, J., Fluhrer, R., Saftig, P. and Schroder, B. (2014b). "The intramembrane proteases signal Peptide peptidase-like 2a and 2b have distinct functions in vivo." Mol Cell Biol 34(8): 1398-1411.

Selkoe, D. J. (1991). "The molecular pathology of Alzheimer's disease." Neuron 6(4): 487-498.

Serneels, L., Dejaegere, T., Craessaerts, K., Horre, K., Jorissen, E., Tousseyn, T., Hebert, S., Coolen, M., Martens, G., Zwijsen, A., Annaert, W., Hartmann, D. and De Strooper, B. (2005). "Differential contribution of the three Aph1 genes to gamma-secretase activity in vivo." Proc Natl Acad Sci U S A 102(5): 1719-1724.

Shah, S., Lee, S. F., Tabuchi, K., Hao, Y. H., Yu, C., LaPlant, Q., Ball, H., Dann, C. E., 3rd, Sudhof, T. and Yu, G. (2005). "Nicastrin functions as a gamma-secretase-substrate receptor." Cell 122(3): 435-447.

Sherrington, R., Rogaev, E. I., Liang, Y., Rogaeva, E. A., Levesque, G., Ikeda, M., Chi, H., Lin, C., Li, G., Holman, K., Tsuda, T., Mar, L., Foncin, J. F., Bruni, A. C., Montesi, M. P., Sorbi, S., Rainero, I., Pinessi, L., Nee, L., Chumakov, I., Pollen, D., Brookes, A., Sanseau, P., Polinsky, R. J., Wasco, W., Da Silva, H. A., Haines, J. L., Perkicak-Vance, M. A., Tanzi, R. E., Roses, A. D., Fraser, P. E., Rommens, J. M. and St George-Hyslop, P. H. (1995). "Cloning of a gene bearing missense mutations in early-onset familial Alzheimer's disease." Nature 375(6534): 754-760.

Stanley, P. and Cummings, R. D. (2009). Structures Common to Different Glycans. Essentials of Glycobiology. nd, A. Varki, R. D. Cummings et al. Cold Spring Harbor (NY).

Stanley, P., Schachter, H. and Taniguchi, N. (2009). N-Glycans. Essentials of Glycobiology. nd, A. Varki, R. D. Cummings et al. Cold Spring Harbor (NY).

Steiner, H., Duff, K., Capell, A., Romig, H., Grim, M. G., Lincoln, S., Hardy, J., Yu, X., Picciano, M., Fechteler, K., Citron, M., Kopan, R., Pesold, B., Keck, S., Baader, M., Tomita, T., Iwatsubo, T., Baumeister, R. and Haass, C. (1999). "A loss of function mutation of

presenilin-2 interferes with amyloid beta-peptide production and notch signaling." J Biol Chem 274(40): 28669-28673.

Steiner, H., Fluhrer, R. and Haass, C. (2008). "Intramembrane proteolysis by gamma-secretase." J Biol Chem 283(44): 29627-29631.

Steiner, H., Kostka, M., Romig, H., Basset, G., Pesold, B., Hardy, J., Capell, A., Meyn, L., Grim, M. L., Baumeister, R., Fechteler, K. and Haass, C. (2000). "Glycine 384 is required for presenilin-1 function and is conserved in bacterial polytopic aspartyl proteases." Nat Cell Biol 2(11): 848-851.

Stowell, S. R., Ju, T. and Cummings, R. D. (2015). "Protein glycosylation in cancer." Annu Rev Pathol 10: 473-510.

Strisovsky, K. (2016). "Rhomboid protease inhibitors: Emerging tools and future therapeutics." Semin Cell Dev Biol 60: 52-62.

Strisovsky, K. (2017). "Mechanism and Inhibition of Rhomboid Proteases." Methods Enzymol 584: 279-293.

Strisovsky, K., Sharpe, H. J. and Freeman, M. (2009). "Sequence-specific intramembrane proteolysis: identification of a recognition motif in rhomboid substrates." Mol Cell 36(6): 1048-1059.

Struhl, G. and Adachi, A. (2000). "Requirements for presenilin-dependent cleavage of notch and other transmembrane proteins." Mol Cell 6(3): 625-636.

Sun, L., Li, X. and Shi, Y. (2016). "Structural biology of intramembrane proteases: mechanistic insights from rhomboid and S2P to gamma-secretase." Curr Opin Struct Biol 37: 97-107.

Sykes, A. M., Palstra, N., Abankwa, D., Hill, J. M., Skeldal, S., Matusica, D., Venkatraman, P., Hancock, J. F. and Coulson, E. J. (2012). "The effects of transmembrane sequence and dimerization on cleavage of the p75 neurotrophin receptor by gamma-secretase." J Biol Chem 287(52): 43810-43824.

Takasugi, N., Tomita, T., Hayashi, I., Tsuruoka, M., Niimura, M., Takahashi, Y., Thinakaran, G. and Iwatsubo, T. (2003). "The role of presenilin cofactors in the gamma-secretase complex." Nature 422(6930): 438-441.

Tang, T., Li, L., Tang, J., Li, Y., Lin, W. Y., Martin, F., Grant, D., Solloway, M., Parker, L., Ye, W., Forrest, W., Ghilardi, N., Oravecz, T., Platt, K. A., Rice, D. S., Hansen, G. M., Abuin, A., Eberhart, D. E., Godowski, P., Holt, K. H., Peterson, A., Zambrowicz, B. P. and de Sauvage, F. J. (2010). "A mouse knockout library for secreted and transmembrane proteins." Nat Biotechnol 28(7): 749-755.

Tang, Y. P. and Gershon, E. S. (2003). "Genetic studies in Alzheimer's disease." Dialogues Clin Neurosci 5(1): 17-26.

Teng, F. Y., Wang, Y. and Tang, B. L. (2001). "The syntaxins." Genome Biol 2(11): REVIEWS3012.

Ticha, A., Collis, B. and Strisovsky, K. (2018). "The Rhomboid Superfamily: Structural Mechanisms and Chemical Biology Opportunities." Trends Biochem Sci 43(9): 726-739.

Tomita, T., Watabiki, T., Takikawa, R., Morohashi, Y., Takasugi, N., Kopan, R., De Strooper, B. and Iwatsubo, T. (2001). "The first proline of PALP motif at the C terminus of presenilins is obligatory for stabilization, complex formation, and gamma-secretase activities of presenilins." J Biol Chem 276(35): 33273-33281.

Trimble, W. S., Cowan, D. M. and Scheller, R. H. (1988). "VAMP-1: a synaptic vesicle-associated integral membrane protein." Proc Natl Acad Sci U S A 85(12): 4538-4542.

Tusher, V. G., Tibshirani, R. and Chu, G. (2001). "Significance analysis of microarrays applied to the ionizing radiation response." Proc Natl Acad Sci U S A 98(9): 5116-5121.

Tyndall, J. D., Nall, T. and Fairlie, D. P. (2005). "Proteases universally recognize beta strands in their active sites." Chem Rev 105(3): 973-999.

Urban, S. (2006). "Rhomboid proteins: conserved membrane proteases with divergent biological functions." Genes Dev 20(22): 3054-3068.

Urban, S. (2016). "A guide to the rhomboid protein superfamily in development and disease." Semin Cell Dev Biol 60: 1-4.

Urban, S. and Freeman, M. (2003). "Substrate specificity of rhomboid intramembrane proteases is governed by helix-breaking residues in the substrate transmembrane domain." Mol Cell 11(6): 1425-1434.

Urban, S., Lee, J. R. and Freeman, M. (2001). "Drosophila rhomboid-1 defines a family of putative intramembrane serine proteases." Cell 107(2): 173-182.

Urban, S., Lee, J. R. and Freeman, M. (2002). "A family of Rhomboid intramembrane proteases activates all Drosophila membrane-tethered EGF ligands." EMBO J 21(16): 4277-4286.

Urban, S. and Moin, S. M. (2014). "A subset of membrane-altering agents and gamma-secretase modulators provoke nonsubstrate cleavage by rhomboid proteases." Cell Rep 8(5): 1241-1247.

Urny, J., Hermans-Borgmeyer, I., Gercken, G. and Schaller, H. C. (2003). "Expression of the presenilin-like signal peptide peptidase (SPP) in mouse adult brain and during development." Gene Expr Patterns 3(5): 685-691.

van den Berg, C. W., Elliott, D. A., Braam, S. R., Mummery, C. L. and Davis, R. P. (2016). "Differentiation of Human Pluripotent Stem Cells to Cardiomyocytes Under Defined Conditions." Methods Mol Biol 1353: 163-180.

Varki, A. (2008). Essentials of glycobiology. New York, Cold Spring Harbor Laboratory.

Varki, A., Cummings, R. D., Esko, J. D., Stanley, P., Hart, G. W., Aebi, M., Darvill, A. G., Kinoshita, T., Packer, N. H., Prestegard, J. H., Schnaar, R. L. and Seeberger, P. H. (2017). Essentials of glycobiology.

Varki, A., Esko, J. D. and Colley, K. J. (2009). Cellular Organization of Glycosylation. Essentials of Glycobiology. nd, A. Varki, R. D. Cummings et al. Cold Spring Harbor (NY).

Varki, A. and Freeze, H. H. (2009). Glycans in Acquired Human Diseases. Essentials of

Glycobiology. nd, A. Varki, R. D. Cummings et al. Cold Spring Harbor (NY).

Voss, M. (2014). Signal peptide peptidase-like 3 (SPPL3) is a type II membrane protein-selective sheddase that regulates cellular N-glycosylation. Academic Dissertation, Ludwig-Maximilians-Universität München.

Voss, M., Fukumori, A., Kuhn, P. H., Kunzel, U., Klier, B., Grammer, G., Haug-Kroper, M., Kremmer, E., Lichtenthaler, S. F., Steiner, H., Schroder, B., Haass, C. and Fluhrer, R. (2012). "Foamy virus envelope protein is a substrate for signal peptide peptidase-like 3 (SPPL3)." J Biol Chem 287(52): 43401-43409.

Voss, M., Kunzel, U., Higel, F., Kuhn, P. H., Colombo, A., Fukumori, A., Haug-Kroper, M., Klier, B., Grammer, G., Seidl, A., Schroder, B., Obst, R., Steiner, H., Lichtenthaler, S. F., Haass, C. and Fluhrer, R. (2014a). "Shedding of glycan-modifying enzymes by signal peptide peptidase-like 3 (SPPL3) regulates cellular N-glycosylation." EMBO J 33(24): 2890-2905.

Voss, M., Kunzel, U., Higel, F., Kuhn, P. H., Colombo, A., Fukumori, A., Haug-Kroper, M., Klier, B., Grammer, G., Seidl, A., Schroder, B., Obst, R., Steiner, H., Lichtenthaler, S. F., Haass, C. and Fluhrer, R. (2014b). "Shedding of glycan-modifying enzymes by signal peptide peptidase-like 3 (SPPL3) regulates cellular N-glycosylation." EMBO J.

Voss, M., Schroder, B. and Fluhrer, R. (2013). "Mechanism, specificity, and physiology of signal peptide peptidase (SPP) and SPP-like proteases." Biochim Biophys Acta 1828(12): 2828-2839.

Wang, C. C., Ng, C. P., Lu, L., Atlashkin, V., Zhang, W., Seet, L. F. and Hong, W. (2004a). "A role of VAMP8/endobrevin in regulated exocytosis of pancreatic acinar cells." Dev Cell 7(3): 359-371.

Wang, J., Beher, D., Nyborg, A. C., Shearman, M. S., Golde, T. E. and Goate, A. (2006). "C-terminal PAL motif of presenilin and presenilin homologues required for normal active site conformation." J Neurochem 96(1): 218-227.

Wang, J., Brunkan, A. L., Hecimovic, S., Walker, E. and Goate, A. (2004b). "Conserved

"PAL" sequence in presenilins is essential for gamma-secretase activity, but not required for formation or stabilization of gamma-secretase complexes." Neurobiol Dis 15(3): 654-666.

Wang, T., Li, L. and Hong, W. (2017). "SNARE proteins in membrane trafficking." Traffic 18(12): 767-775.

Wang, Y., Tan, J., Sutton-Smith, M., Ditto, D., Panico, M., Campbell, R. M., Varki, N. M., Long, J. M., Jaeken, J., Levinson, S. R., Wynshaw-Boris, A., Morris, H. R., Le, D., Dell, A., Schachter, H. and Marth, J. D. (2001). "Modeling human congenital disorder of glycosylation type IIa in the mouse: conservation of asparagine-linked glycan-dependent functions in mammalian physiology and insights into disease pathogenesis." Glycobiology 11(12): 1051-1070.

Ward, T. H., Polishchuk, R. S., Caplan, S., Hirschberg, K. and Lippincott-Schwartz, J. (2001). "Maintenance of Golgi structure and function depends on the integrity of ER export." J Cell Biol 155(4): 557-570.

Weggen, S. and Beher, D. (2012). "Molecular consequences of amyloid precursor protein and presenilin mutations causing autosomal-dominant Alzheimer's disease." Alzheimers Res Ther 4(2): 9.

Weihofen, A., Binns, K., Lemberg, M. K., Ashman, K. and Martoglio, B. (2002). "Identification of signal peptide peptidase, a presenilin-type aspartic protease." Science 296(5576): 2215-2218.

Weihofen, A., Lemberg, M. K., Ploegh, H. L., Bogyo, M. and Martoglio, B. (2000). "Release of signal peptide fragments into the cytosol requires cleavage in the transmembrane region by a protease activity that is specifically blocked by a novel cysteine protease inhibitor." J Biol Chem 275(40): 30951-30956.

Wisniewski, J. R., Zougman, A., Nagaraj, N. and Mann, M. (2009). "Universal sample preparation method for proteome analysis." Nat Methods 6(5): 359-362.

Wolfe, M. S. (2009). "Intramembrane-cleaving proteases." J Biol Chem 284(21):

13969-13973.

Wolfe, M. S. (2013). "Toward the structure of presenilin/gamma-secretase and presenilin homologs." Biochim Biophys Acta 1828(12): 2886-2897.

Wolfe, M. S., Xia, W., Ostaszewski, B. L., Diehl, T. S., Kimberly, W. T. and Selkoe, D. J. (1999). "Two transmembrane aspartates in presenilin-1 required for presenilin endoproteolysis and gamma-secretase activity." Nature 398(6727): 513-517.

Wong, P. C., Zheng, H., Chen, H., Becher, M. W., Sirinathsinghji, D. J., Trumbauer, M. E., Chen, H. Y., Price, D. L., Van der Ploeg, L. H. and Sisodia, S. S. (1997). "Presenilin 1 is required for Notch1 and DII1 expression in the paraxial mesoderm." Nature 387(6630): 288-292.

Wongpaiboonwattana, W. and Stavridis, M. P. (2015). "Neural differentiation of mouse embryonic stem cells in serum-free monolayer culture." J Vis Exp(99): e52823.

Wu, C. M. and Chang, M. D. (2004). "Signal peptide of eosinophil cationic protein is toxic to cells lacking signal peptide peptidase." Biochem Biophys Res Commun 322(2): 585-592.

Wyles, J. P., McMaster, C. R. and Ridgway, N. D. (2002). "Vesicle-associated membrane protein-associated protein-A (VAP-A) interacts with the oxysterol-binding protein to modify export from the endoplasmic reticulum." J Biol Chem 277(33): 29908-29918.

Wyles, J. P. and Ridgway, N. D. (2004). "VAMP-associated protein-A regulates partitioning of oxysterol-binding protein-related protein-9 between the endoplasmic reticulum and Golgi apparatus." Exp Cell Res 297(2): 533-547.

Xin, A., Cheng, L., Diao, H., Wu, Y., Zhou, S., Shi, C., Sun, Y., Wang, P., Duan, S., Zheng, J., Wu, B., Yuan, Y., Gu, Y., Chen, G., Sun, X., Shi, H., Tao, S. and Zhang, Y. (2016). "Lectin binding of human sperm associates with DEFB126 mutation and serves as a potential biomarker for subfertility." Sci Rep 6: 20249.

Ye, J., Dave, U. P., Grishin, N. V., Goldstein, J. L. and Brown, M. S. (2000a). "Asparagine-proline sequence within membrane-spanning segment of SREBP triggers

intramembrane cleavage by site-2 protease." Proc Natl Acad Sci U S A 97(10): 5123-5128.

Ye, J., Rawson, R. B., Komuro, R., Chen, X., Dave, U. P., Prywes, R., Brown, M. S. and Goldstein, J. L. (2000b). "ER stress induces cleavage of membrane-bound ATF6 by the same proteases that process SREBPs." Mol Cell 6(6): 1355-1364.

Zahn, C., Kaup, M., Fluhrer, R. and Fuchs, H. (2013). "The transferrin receptor-1 membrane stub undergoes intramembrane proteolysis by signal peptide peptidase-like 2b." FEBS J 280(7): 1653-1663.

Zhou, M., Li, P., Tan, L., Qu, S., Ying, Q. L. and Song, H. (2010). "Differentiation of mouse embryonic stem cells into hepatocytes induced by a combination of cytokines and sodium butyrate." J Cell Biochem 109(3): 606-614.

Zoll, S., Stanchev, S., Began, J., Skerle, J., Lepsik, M., Peclinovska, L., Majer, P. and Strisovsky, K. (2014). "Substrate binding and specificity of rhomboid intramembrane protease revealed by substrate-peptide complex structures." EMBO J 33(20): 2408-2421.

Abbreviations

AD	Alzheimer's disease
ADAM	a disintegrin and metalloproteinase
AICD	APP-ICD
APH-1	anterior pharynx defective-1 protein
APP	amyloid precursor protein
AsA	ascorbic acid
ATF6	activating transcription factor 6
AU	Airy Unit
Aβ	Amyloid β
B3GALT	β3-galactosyltransferase
B3GAT3	β3-glucuronosyltransferase
B4GALT	β4-galactosyltransferase
BACE	β-site of APP cleaving enzyme
BSA	bovine serum albumin
CD74	cluster of differentiation 74
CNS	central nervous system
COP	coat proteins
CRISPR	clustered regularly interspaced short palindromic repeats
CTF	C-terminal fragment
CYB5A	cytochrome B5A
DAPI	4',6-Diamidin-2-phenylindol
DAPT	N-[N-(3,5-Difluorophenacetyl)-L-alanyl]-S-phenylglycine-t-butyl ester
DNA	deoxyribonucleic acid
dsDNA	double stranded DNA
DTT	dithiothreitol
ECL	enhanced chemiluminescence
EGFR	epidermal growth factor receptor signalling
ER	endoplasmic reticulum
ERAD	endoplasmic-reticulum-associated-protein-response
ERGIC	ER-Golgi intermediate compartment
ESC	embryoinic stem cell
EXTL3	exostosin like glycosyltransferase 3
FAD	Familial AD

FasL	Fas ligand
FCS	fetal calf serum
FDR	false discovery rate
FL	full length
Fvenv	foamy virus envelope protein
GAGs	glycosaminoglycans
gDNA	genomic DNA
GlcNAc	N-acetylglucosamine
GnTs	N-acetylglucosaminyltransferases
GnTV	N-acetylglucosaminyltransferase V
GOSR2	Golgi reassembly-stacking protein 2
gRNA	guide RNA
HO-1	heme-oxygenase-1
HSPGs	heparan sulfate proteoglycans
ICD	intracellular domain
I-CLIPs	intramembrane cleaving proteases
IF	Immunofluorescence
IH	Immunohistochemistry
ITM2B	integral membrane protein 2B
JMD	juxtamembrane domain
LFQ	label-free quantification
MEF	mouse embryonic fibroblasts
MHC	major histocompatibility complex
mLIF	mouse leukaemia inhibitory factor
mTORC1	mammalian target of rapamycin complex 1
NK	natural killer cells
NRG1	neuregulin 1
NSF	N-ethylmaleimide-sensitive factor
NTF	N-terminal fragment
OGFOD3	2-oxoglutarate and iron-dependent oxygenase domain-containing protein 3
PCR	polymerase chain reaction
PEN2	presenilin enhancer-2
PFA	paraformaldehyde

PM	plasma membrane
PS	Presenilin
PSA	*Pisum sativum*
PVDF	polyvinylidene fluoride
qPCR	Quantitative Real-Time PCR
RAMP4	ribosome-associated membrane protein 4
Rce1	Ras converting enzyme
RHBDL	rhomboid-like proteins
RIP	regulated intramembrane proteolysis
RNA	ribonucleic acid
RT	room temperature
S1P	site-1 protease
S2P	site-2-protease
SAGE	submerged agarose gel electrophoresis
sAPP	soluble APP
sEXTL3	soluble EXTL3
sGNTV	soluble GnTV
SNAP	soluble NSF attachment protein
SNARE	soluble NSF attachment protein receptor
SNPs	single nucleotide polymorphisms
SP	Signal Peptidase
SPECS	secretome protein enrichment with click sugars
SPP	Signal Peptide Peptidase
SPPL	Signal-Peptide-Peptidase Like
SREBP2	sterol regulatory element-binding protein 2
TCA	Trichloroacetic acid
TfR1	transferrin receptor 1
TGN	*trans*-Golgi network
TM	transmembrane
TMD	transmembrane domain
TNFα	tumour necrosis factor α
TR	T-Rex^{TM}-293
t-SNARE	target-membrane SNARE
UPR	unfolded protein response

VAMP	vesicle associated membrane protein
VAP	vesicle-associated membrane protein-associated protein
v-SNARE	vesicle-membrane SNARE
WB	Western Blot
WGA	Wheat Germ Agglutinin
XBP1u	X-box binding protein 1
XYLT	xylosyltransferase
α-Man I, II	α-mannosidase I, II
$(Z\text{-}LL)_2$-ketone	1,3-di-(N-carboxybenzoyl-L-leucyl-L-leucyl)-amino acetone

Acknowledgements

The whole process of pursuing and completing a PhD thesis is very demanding but also very constructive and rewarding. Approaching the end of this entire task, I came to realize that it is not just the outcome of my personal effort and drive, but I greatly profited from the contribution and support of many important people, including numerous colleagues, friends and family. Many of these people played a very significant role to my scientific advancement and helped me succeed during the years I spent in this wonderful institute. I honestly believe that getting to know and be with those people may even be more valuable than the title I hope to obtain. I would therefore like to express my gratitude to all those who supported me during the past years in making the completion of this thesis not just possible but also a very positive experience.

First and foremost, I would like to thank my supervisor Prof. Dr. Regina Fluhrer for giving me the opportunity to work on such exciting projects and for supporting me with her guidance along the way. She has been a great source of not only knowledge and mentorship, but also of motivation and for that, I am extremely grateful. I am also exceptionally grateful to Prof. Dr. Christian Haass for his support and for choosing me amongst a list of Doctorate applicants and making my dream of performing my PhD in a great institute possible.

Of course, this work would have not been possible without financial support from the Deutsche Forschungsgemeinschaft. Furthermore, I was lucky to be a member of the excellent "International Max Planck Research School (IMPRS) for Molecular Life Sciences". I am very grateful to have received from IMPRS the opportunity to join numerous workshops and funding to join conferences. The coordination office has been a great pleasure to interact with and they truly made my time as a PhD student more fruitful and constructive.

This study has also greatly profited from the work of our collaborators. From the University of Kiel, Prof. Dr. Bernd Schröder, Dr. Torben Mentrup and Johannes Niemeyer contributed to the SPPL2c project. I am grateful to Prof. Dr. Stefan Lichtenthaler and Dr. Stephan Müller for their help with the Mass Spectrometry, as well as, for their helpful suggestions and

discussions. I would also like to thank Dr. Merav Shmueli, without whom the lectin analysis would have been impossible, and Prof. Dr. Artur Mayerhofer who greatly contributed in the phenotypic analysis of the mouse tissues. PD Dr. Reinhard Obst and Dr. Bettina Schmid were extremely kind in contributing to this study with their time and fruitful discussions. This study has greatly profited from the quality antibodies provided by Dr. Regina Feederle.

Numerous members of the Haass department are appreciated for their helpful comments and supportive work environment. Sabine Odoy and Nicole Exner are especially appreciated for keeping the laboratory running and helping with the bureaucracy.

I am truly grateful to the members of Prof. Fluhrer's laboratory: Martina Haug-Kröper, Charlotte Spitz and Christine Schlosser. Martina's technical knowledge and assistance has proved crucial in many occasions. Charlotte has been my laboratory partner for most of my Doctorate study and I would like to thank her for her support and especially for helping with the German translation of my summary. Moreover, what made this experience extremely special, was working in a very friendly and creative atmosphere in the laboratory, where I could feel at home. On that last note, I have to thank my fellow student, Samira Parhizkar, for being with me along this whole process. We met during our PhD interview week, back in March 2014 and since then we have managed to keep company to each other on all major milestones. We planned our happy hour and first TAC meetings together, we had ours papers published at a similar time and had a joined paper-party and we are now privileged enough to hand in our theses together. I could not have asked for a better co-traveler along this journey, thank you!

Last but definitely not least, my family and friends outside the laboratory have always been encouraging and understanding. I would not have made it this far without my mother, Theodora, always being there for me, throughout the years, and the support of my partner in life, Olivier. I would especially like to thank my uncle, Spiros, for his support and advice, and my father, Thanos, for our invaluable discussions that stirred my interest in science.